AD-787 073

HANDBOOK OF CAVITATION EROSION

HYDRONAUTICS, INCORPORATED

PREPARED FOR
OFFICE OF NAVAL RESEARCH

JANUARY 1974

DISTRIBUTED BY:

NTIS
National Technical Information Service
U. S. DEPARTMENT OF COMMERCE

UNCLASSIFIED

SECURITY CLASSIFICATION OF THIS PAGE (When Data Entered)

REPORT DOCUMENTATION PAGE		READ INSTRUCTIONS BEFORE COMPLETING FORM
1. REPORT NUMBER T. R. 7301-1	2. GOVT ACCESSION NO.	3. RECIPIENT'S CATALOG NUMBER AD 787073
4. TITLE (and Subtitle) HANDBOOK OF CAVITATION EROSION		5. TYPE OF REPORT & PERIOD COVERED FINAL
		6. PERFORMING ORG. REPORT NUMBER
7. AUTHOR(s) A. Thiruvengadam		8. CONTRACT OR GRANT NUMBER(s) N00014-73-C-0017
9. PERFORMING ORGANIZATION NAME AND ADDRESS HYDRONAUTICS, Incorporated 7210 Pindell School Road Laurel, Maryland 20810		10. PROGRAM ELEMENT, PROJECT, TASK AREA & WORK UNIT NUMBERS NR 062-293
11. CONTROLLING OFFICE NAME AND ADDRESS Office of Naval Research, Code 438 Department of the Navy Washington, D. C. 20360		12. REPORT DATE January 1974 13. NUMBER OF PAGES 320
14. MONITORING AGENCY NAME & ADDRESS(if different from Controlling Office)		15. SECURITY CLASS. (of this report) UNCLASSIFIED 15a. DECLASSIFICATION/DOWNGRADING SCHEDULE

16. DISTRIBUTION STATEMENT (of this Report)

This document has been approved for public release. Distribution Unlimited.

17. DISTRIBUTION STATEMENT (of the abstract entered in Block 20, if different from Report)

18. SUPPLEMENTARY NOTES

Reproduced by
NATIONAL TECHNICAL
INFORMATION SERVICE
U S Department of Commerce
Springfield VA 22151

19. KEY WORDS (Continue on reverse side if necessary and identify by block number)

Cavitation Damage:
Inception of
Effects of
Mechanisms of
Experimental Facilities for
Material Resistance to
Hydrodynamic Relations with
Protection Against
Procedures for Repair of

20. ABSTRACT (Continue on reverse side if necessary and identify by block number)

This revised Handbook is a completely rewritten and updated version of the original "Handbook of Cavitation Damage" which was published under the auspices of the Office of Naval Research in 1965. This new edition contains the very latest information pertaining to scaling and the effects of fluid properties on Cavitation Erosion, as well as new field experiences with some of the Navy's high performance ships. Again, the scope of this Handbook

DD FORM 1 JAN 73 1473 EDITION OF 1 NOV 65 IS OBSOLETE
S/N 0102-014-6601

UNCLASSIFIED
SECURITY CLASSIFICATION OF THIS PAGE (When Data Entered)

20. ranges from the most basic theoretical cavitation concepts to practical guidance relevant to design, material selection, protection, and field repair procedures.

HYDRONAUTICS, Incorporated

TECHNICAL REPORT 7301-1

Handbook of Cavitation Erosion

by

A. Thiruvengadam

January 1974

This document has been approved for public release;
Distribution Unlimited

DDC
RECEIVED
OCT 17 1974
D

Prepared Under
Office of Naval Research
Department of the Navy
Contract No. N00014-73-C-0017
NR 062-293

ib

DISTRIBUTION STATEMENT A
Approved for public release;
Distribution Unlimited

HYDRONAUTICS, Incorporated

PREFACE

The revised edition of the Handbook of Cavitation Erosion is an outgrowth of several years of research sponsored by the Office of Naval Research. Technical Contract administration was provided by Mr. Stanley W. Doroff as scientific officer of the ONR Fluid Dynamics Program.

A. Thiruvengadam, formerly Head, Materials Sciences Division of HYDRONAUTICS, Incorporated, was primarily responsible for the complete revision of the Handbook. Significant contributions to the revised edition were made by P. Eisenberg, V. E. Johnson, Jr., and A. F. Conn of HYDRONAUTICS, Incorporated.

More recent data relating to the physical properties, corrosion-erosion modeling and adhesion strength of coatings were generated at the Ocean Engineering Laboratory, Institute of Ocean Science and Engineering, The Catholic University of America under contract number N00014-67-A-0377-0008-NR-062-436. Additional data on the erosion resistance of polymers and other non-metallic coatings were developed by the Non-Metallics Division of the Naval Ship Research and Development Center, Annapolis Laboratory by G. Bohlander, H. S. Preiser, and A. Ruffalo.

An attempt has been made to include all points of view emphasizing the practical considerations relevant to the design and material selection process.

ACKNOWLEDGMENTS

The author is grateful to Stan Doroff who was responsible for initiating the Handbook effort as early as 1962. The completion of the Handbook in 1966 and its present revision were made possible through continued support of the Office of Naval Research, Fluid Dynamics Program. Many colleagues both at HYDRONAUTICS, Incorporated and at the Catholic University of America provided significant assistance and contributions to this Handbook at one stage or another. But for their collaboration, assistance and encouragement, the completion of this Handbook would not have been possible.

TABLE OF CONTENTS

Page

LIST OF FIGURES

LIST OF TABLES

NOTATION

A	A constant of proportionality
A_e	Area of erosion
C_i	Cavitation interval
$C_{p,min}$	Minimum pressure coefficient
E_a	Energy absorbed by the material
I	Intensity of cavitation damage
N	Number of cavities
P	Pulse ratio
P_a	Power absorbed by the material
R_o	Maximum radius of the bubble
S_e	Strain energy of the material up to fracture
S_i	Static interval
U	Free stream velocity
U_s	Separated streamline velocity
U_v	Peripheral velocity of a vortex
a	Constant of proportionality
d	Characteristic dimension
f	Frequency of shedding of cavities
g	Acceleration due to gravity
i	Average depth of erosion
ℓ	Length of the cavity
p	Ambient (local) pressure

p_s	Partial pressure of gas inside the cavitation bubble
p_o	Free stream pressure
p_v	Vapor pressure of the liquid
p^*	Critical pressure
r	Radius of the bubble
r^*	Critical radius
t	Duration of test
u	Local velocity
ΔV	Incremental volume loss due to cavitation damage
γ	Surface tension of the liquid-vapor interface
Γ	Circulation
λ	Relative length of cavity
ρ	Density of liquid

The above list of symbols is only a selection of those used in this Handbook. In each chapter specific definitions are given for the symbols used within that chapter.

I. INTRODUCTION

With the advent of high speed naval craft, supercavitating propellers, high performance pumps and turbines, and the requirements for high flow rates in piping systems, the incidence of cavitation and cavitation erosion to vital components has increased. This problem is now regarded as an important design and operational consideration. Recent experiences with full scale systems showed that in some cases even the most resistant material was severely eroded in short operational periods (1). This has motivated several investigators to conduct basic studies with the objective of eventually developing prediction and protection methods. Such methods would aid engineers in dealing with and, to the extent possible, overcoming the problem of cavitation erosion. Developing modeling techniques to scale cavitation erosion by means of laboratory tests seems feasible. There are many problems to be solved, however, before any acceptable modeling technique is established. One is the relation between the resistance of the material used in the laboratory model and that used in the prototype system. The second is the problem of properly simulating the cavitation environment. While continued attention is being paid to these aspects, much new information has been generated since the publication of the first edition of this handbook.

It is now possible to aid the practical engineer with his design and material selection problems in a quantitative manner. Figure 1-1 shows the various engineering aspects of this problem as seen by the designer. The design and material selection process

draws information from basic research and screening tests. Basic research on bubble growth and collapse, material erosion and environmental interaction has generated much needed fundamental knowledge. The relative resistance of many materials has also been catalogued using one of several screening tests. Tests commonly used include: (1) the vibratory test, (2) the rotating disk test, (3) the venturi test, and (4) the jet-impact test. Basic research combined with screening tests has led to several useful protection techniques which include the use of more resistant materials (inlays, overlays, and elastomeric coatings), and the cathodic protection and air injection methods. These protection techniques are successful in some instances but not so useful in other cases. If erosion is serious at the designed operating conditions, operational requirements such as capacity, power, and speed might be reduced. However, if the design is hopeless in terms of erosion intensity, then redesign is generally recommended.

During redesign one would correct obvious mistakes, avoid cavitation if at all possible, and provide air vents at problem areas. It would be highly desirable to verify the redesign (or a preliminary design) with the help of a model test before costly manufacture is initiated. Such model tests would hopefully lead to the necessary modifications to a design so that the erosion intensity levels are within the capability of the candidate material. Attempts to develop such modeling techniques are currently underway. The objective of this revised edition of the Handbook of Cavitation Erosion is to describe these developments in a clear and practical manner which will be useable to designers.

DEFINITION OF CAVITATION, ITS CAUSE AND EFFECTS

In most engineering contexts, cavitation is defined as the process of formation of the vapor phase of a liquid when it is subjected to reduced pressures at constant ambient temperature (2). In general, a liquid is said to cavitate when vapor bubbles are observed to form and grow as a consequence of pressure reduction. When the phase transition is a result of pressure change by hydrodynamic means, a two-phase flow composed of a liquid and its vapor is called a cavitating flow. While these definitions imply a distinction between phase transitions associated with reduction of pressure, on the one hand, and addition of heat (i.e., boiling), on the other, heat-transfer effects may play an important role in many cases of cavitating liquids. Such effects are especially of importance in liquids near their boiling points. From a purely physical-chemical point of view, of course, no distinction need be made between boiling and cavitation, at least insofar as the question of inception is concerned, and many of the basic physical ideas regarding inception, vapor mass transfer, and condensation apply equally (3).

The phenomenon of cavitation produces many effects such as:

(a) damage to boundary materials;

(b) changes in hydrodynamic forces;

(c) vibration and noise.

A very important effect is the problem of cavitation erosion. At the turn of the century, efforts to improve the performance of marine propellers and hydraulic turbines were handicapped by the

severe damage caused by cavitation. In fact, an underlying motive for directing so much attention to the general phenomenon of cavitation was to understand the nature and extent of the resultant erosion to materials of construction. During the past fifty years, since the first systematic investigations were initiated by the Admiralty Sub-Committee (4), several significant advances have been made toward the understanding of the problems associated with this phenomenon of cavitation erosion.

HISTORICAL BACKGROUND

The possibility of the occurrence of cavitation due to pressure changes in a flowing liquid was recognized by Euler as early as 1754 (5). Reynolds (6), in the last decade of the nineteenth century, produced and observed cavitation in a glass venturi tube at room temperature. These dates indicate the early sporadic interest in the problem. However, because of its classical scientific interest and the many sided practical aspects of cavitation damage effects in various fields of endeavor, prominent names such as Rayleigh (7), Parsons (4), Ackeret (8), Föettinger (9), and Hunsaker (10), among others, were associated with this problem right from the turn of the century. Following the work of these early pioneers, several investigators have been devoting major effort to study the details of this fascinating phenomenon over the past fifty years. This handbook summarizes the major contributions of these investigations.

BACKGROUND

Several review articles on cavitation damage have been published over the past twenty-five years, each paper summarizing the significant contributions and progress made up to that time. The more comprehensive critiques were made by Nowotony (11) and Beeching (12) in 1942, Godfrey (13) in 1959, and Eisenberg (14) in 1963. However, these articles were necessarily brief because of their limited scope. In recent years, the rising demand for machines capable of operation at still higher speeds and reduced pressures has brought into focus the need for engineering information on the causes and alleviation of cavitation erosion. Despite the increased interest and need in this area, there existed an information gap among the scientist, the designer and the operator which prevents the effective use of available knowledge on cavitation erosion phenomena. To meet this requirement the First Edition of the Handbook of Cavitation Damage was prepared for the U. S. Office of Naval Research in March 1965 as HYDRONAUTICS Technical Report 233-8. Since then many developments have taken place in this field. The purpose of this revised edition is to increase the usefulness of the Handbook by incorporating this new information about cavitation erosion.

This technical manual attempts to provide, in digested form, the most significant advances toward the solution of problems associated with cavitation erosion damage. In order to reach a wide audience in the scientific community, the scope of this manual includes a state-of-the-art summary, a critical review of the problem

for those in research, and practical information for use by designers and operators.

SPECIFIC CAVITATION PROBLEMS OF THE U. S. NAVY

Cavitation erosion is of critical concern to the Navy. It imposes severe limits to the design and operation of ships and other naval machinery components. Specifically, the erosion of propellers can reach catastrophic proportions in some cases, as discussed in Chapter X. With the advent of higher speed ships, this problem of cavitation erosion is of major concern. Apart from erosion to ship propellers, hull areas and appendages, many other ship components suffer from the effects of cavitation. A few examples can be cited: diesel engine cylinder liner erosion; damage to acoustic communication and detection devices; damage to pump impellers and casings; and erosion of valves and piping sections. The primary aim of this handbook is to assist the scientific and technical personnel of the U. S. Navy in understanding and solving cavitation erosion problems so that the knowledge can be applied toward maintaining the fleet at its optimum performance level.

II. CAVITATION INCEPTION

BASIC PRINCIPLES

The basic principles of cavitation inception may be demonstrated by a simple example of the flow through a Venturi as shown in Figure 2-1. For an ideal case, the velocity and pressure in the throat are controlled by the continuity and Bernoulli equations. It is easily seen that the absolute pressure in the throat depends on upstream velocity and pressure, and the area ratio of the Venturi. For example, the wrong selection of a large area ratio to handle a given flow rate may reduce the throat pressure below the vapor pressure. This may result in the formation of vapor bubbles at the throat, giving rise to the inception of cavitation. Although the above simple example demonstrates the conditions for cavitation inception, the phenomenon of cavitation inception is much more complex. Several additional factors such as the nuclei size and distribution, the surface tension, boundary layer effects and thermodynamic influences are all important in the understanding of the overall phenomenon of cavitation inception. Many contemporary investigators such as Plesset (15), Holl (16), Ripkin (17,18), and Johnson (3) among others have made notable contributions to this understanding. The author has attempted to draw upon this wealth of information; the discussion here is substantially based on the writings of Johnson (3) because of its simplicity and engineering usability.

Generally, cavitation inception in hydraulic systems occurs in three broad categories as follows:

1. unseparated flows,
2. separated flows, and
3. liquids undergoing strong vortex motions.

UNSEPARATED FLOWS

In Figure 2-2 is shown a streamlined body of which the curvatures are sufficiently mild to permit nearly ideal flow; that is, flow without boundary layer separation. The pressure distribution on this body, as obtained from potential flow theory, would be expected to be in good agreement with experimental measurements if the boundary layer displacement thickness is small compared with the body diameter. This condition is usually met if the Reynolds number is sufficiently high to produce a fully developed turbulent boundary layer. For a given body shape, the magnitude of the pressure reduction at the location of minimum pressure can be written as a certain percentage of the total dynamic pressure, $\frac{1}{2}\rho V^2$,

$$p_{min} - p_o = C_{p,min} \frac{1}{2}\rho V^2 \qquad [2\text{-}1]$$

in which $C_{p,min}$ is known as the minimum pressure coefficient. The value of $C_{p,min}$ is not appreciably influenced by p_o or V if the boundary layer satisfies the conditions previously described. In engineering designs, it is generally assumed that cavitation inception occurs when p_{min} becomes equal to the vapor pressure of the liquid. However, it will be helpful to discuss briefly the

physical nature and conditions surrounding the inception of individual cavities which eventually expand and retain their identity during a complex history of growth and collapse; or sometimes coalesce and form a very large, more or less steady cavity.

The Role of Nuclei

In an absolutely pure liquid (all of its constituents in the liquid state) the only way of creating a cavity is by fracturing the liquid; that is, by producing tensile stresses to overcome the molecular cohesive forces. These stresses theoretically may be of the order of several thousand atmospheres. However, experience shows that the critical pressures at which a cavity forms are of the order of a few atmospheres in ordinary engineering liquids. In order to understand the inception of cavitation, it is very helpful to examine the conditions for static stability of a spherical gas volume surrounded by a liquid. Although cavitation is a dynamic phenomenon, the basic principles of inception will be revealed by such a static analysis.

As seen in Figure 2-3, the forces acting on the inside of the bubble are those due to the partial pressure of the gas, p_g, and the partial pressure of the liquid vapor, p_v (3). At the interface (the surface of the bubble) is the surface tension force $2\pi r\gamma$; where r is the bubble radius and γ is the surface tension force per unit length. The surface tension force per unit cross sectional area of the bubble is therefore $2\pi r\gamma/\pi r^2$ or $2\gamma/r$. The term $2\gamma/r$ is often referred to as the surface tension pressure. It should be noted that this surface

tension pressure tends to collapse the spherical bubble. Outside the bubble is the ambient fluid pressure, p. For static equilibrium the following equation must be satisfied.

$$p_v + p_g = p + \frac{2\gamma}{r} \qquad [2\text{-}2]$$

Now if it is assumed that the temperature and weight of the gas in the bubble remains constant as the surrounding fluid pressure is reduced, then the pressure, p_g, for a given weight of gas will vary inversely with the volume of the gas bubble; that is $p_g = A/r^3$, where A is proportional to the number of molecules or to the weight of the gas and r is the radius of the sphere. With the above substitution, Equation [2-2] may be written as

$$p - p_v = \frac{A}{r^3} - \frac{2\gamma}{r} \qquad [2\text{-}3]$$

Now since $r = r_o$ at the free stream pressure, p_o, the value of the constant A in terms of the ambient nuclei size and pressure is

$$A = (p_o - p_v + \frac{2\gamma}{r_o})r_o^3 \qquad [2\text{-}4]$$

Consequently Equation [2-3] becomes (in terms of bubble diameter rather than radius)

$$\frac{p_c - p_v}{p_o - p_v} = \left(\frac{d_o}{d}\right)^3 \left[1 + \frac{4\gamma}{d_o(p_o - p_v)}\left(1 - \frac{d^2}{d_o^2}\right)\right] \qquad [2\text{-}5]$$

Defining the Weber number as $W = \rho U_o^2 d_o/\gamma$ and the vapor cavitation number as $\sigma_v = (p_o - p_v)/\frac{1}{2}\rho U_o^2$, Equation [2-5] may also be written as

$$\frac{p - p_v}{p_o - p_v} = \left(\frac{d_o}{d}\right)^3 \left[1 + \frac{8}{\sigma_v W}\left(1 - \frac{d^2}{d_o^2}\right)\right] \qquad [2\text{-}6]$$

Value of the parameter $(p - p_v)/(p_o - p_v)$ for various values of $\sigma_v W$ as calculated from Equation [2-6] are presented in Figure 2-4. Since the assumptions leading to Equation [2-6] do not allow for additional gas to diffuse into the bubble, Figure 2-4 illustrates that for large values of $\sigma_v W$ all bubbles simply follow a simple isothermal expansion as the pressure is reduced.

The important point to note in Figure 2-4 is that for more reasonable values of $\sigma_v W$ the curves have a minimum and thus the well-known instability or cavitation inception occurs. The critical point for inception in terms of the parameter $\sigma_v W$ may be determined as

$$\left(\frac{d^*}{d_o}\right)_{\text{critical}} = \left[3\left(1 + \frac{\sigma_v W}{8}\right)\right]^{\frac{1}{2}} \qquad [2\text{-}7a]$$

$$\left(\frac{p^* - p_v}{p_o - p_v}\right)_{\text{critical}} = -\frac{2\left(\frac{8}{\sigma_v W}\right)^{3/2}}{3\left(1 + \frac{8}{\sigma_v W}\right)^{\frac{1}{2}}} \qquad [2\text{-}7b]$$

Since the parameter $p^* - p_v$ is a measure of the inaccuracy which results when cavitation inception is assumed to occur at the vapor pressure, the foregoing results may be used to determine the magnitude of inaccuracy (scale effect) which may exist in practical situations. Figure 2-5 is presented in order to demonstrate the variety of observable conditions for cavitation inception which may occur in practical tests. In Figure 2-5, it is assumed that a linearly decreasing pressure exists as a bubble moves from left to right through the pressure field. It is assumed that the true minimum pressure coefficient is .2 and that the observed vapor incipient cavitation number will be .2 if inception occurs at $\frac{p - p_v}{p_o - p_v} = 0$, that is, at the vertical dashed line. Bubbles of initial diameters, .0001, .001, .01, and .05 inches are allowed to pass through the field at free stream velocities corresponding to 30, 60, and 120 fps. The effect of speed on the deviations in inception are caused by the variations in $\sigma_v W$. It should be remembered that the analysis is quasi-steady. The dashed horizontal lines mean that the bubble entering the field is not visible to the naked eye without special lighting. The dots and circles indicate actual bubble sizes except that shaded or black circles indicate that space is not available to show the actual bubble size. The location of instability or cavitation inception is denoted by the starlike symbols. The large velocity scale effect on the .001 inch diameter nucleus should be noted. It should also be noted that the .01 inch diameter nucleus has only a small deviation from inception at the

vapor pressure and then only at the lowest speed. It is also important to observe that the largest bubble, although always reaching its point of true instability at the vapor pressure, has a large observable growth prior to reaching the vapor pressure. Such large bubbles in the flow may be responsible for scale effects in an abnormal sense.

Another important relationship which may be obtained from a static analysis of gas and vapor filled bubbles is the conditions under which a bubble may grow by gaseous diffusion. Although such growth is very slow, it is a process whereby gas bubbles of macroscopic size can be generated and later become unstable at only moderate subpressures. As first stated by Strasberg (19) the condition for bubble growth by gaseous diffusion is simply that the gas within the bubble be in contact with external fluid whose gas partial pressure is greater than that of the gas within the bubble. It can then be shown that the equation defining the inception of gaseous diffusion is

$$\frac{p_c - p_v}{p_o - p_v} = \frac{\bar{p}_s}{\left(1 + \frac{8}{\sigma_v W}\right)}\left[1 + \frac{8}{\sigma_v W}\left(1 - \frac{\left(1 + \frac{8}{\sigma_v W}\right)}{\bar{p}_s}\right)^{2/3}\right] \qquad [2\text{-}8]$$

where

p_c is the critical fluid pressure for incipient gas diffusion and

$\overline{p}_s = \frac{p_s}{p_o - p_v}$, where p_s is the fluid gas saturation pressure.

The conditions for incipient gaseous diffusion as computed from Equation [2-8] and the conditions for cavitation inception (bubble instability) as computed from Equations [2-7] are presented in Figure 2-6. The important point to note from Figure 2-6 is that although the nuclei in an ambient saturated solution may be almost microscopic in size (say .0001 inches), if these bubbles later come to reside in small separated zones along a ship hull where they may be subjected to adequately low sub-ambient pressure, they will grow by gaseous diffusion and can later enter the propeller region with a greatly increased size (several thousandths of an inch). Ripken and Killen (18) suggest that bubble growth through diffusion within the boundary layer of ships or the pipe walls of a conduit or water tunnel will always supply numerous spherical gas bubbles of the order of .001 inch or larger. They have developed an acoustic instrument for determining the size distribution of gas bubbles in water and used it to measure the bubble population in the wake of ships and in water tunnels.

The foregoing discussion on the role of nuclei in cavitation inception indicates that the pressure at which cavitation starts need not necessarily be the vapor pressure. For a given size

nucleus in the fluid, there is a critical pressure, p^*, that will cause nuclei instability and thus cavitation. By establishing p_{min} in Equation [2-1] as equal to p^*, the hydrodynamic conditions for cavitation inception are established as

$$\frac{p^* - p_o}{\frac{1}{2}\rho V_o^2} = C_{p,min} \qquad [2\text{-}9]$$

Thus, if the critical pressure, p^*, and the minimum pressure-coefficients, $C_{p,min}$ are known or can be found either experimentally or theoretically, then Equation [2-9] gives the relationship between the ambient pressure and the stream velocity for which cavitation will commence. Equation [2-9] may be written as

$$\frac{p^* - p_v + p_v - p_o}{\frac{1}{2}\rho V_o^2} = \frac{p^* - p_v}{\frac{1}{2}\rho V_o^2} + \frac{p_v - p_o}{\frac{1}{2}\rho V_o^2} = C_{p,min} \qquad [2\text{-}10]$$

As was discussed previously it is a reasonable assumption that relatively large nuclei will be present in river or sea water and thus the value of p^* is nearly equal to the vapor pressure. Also, for full scale bodies on which cavitation may be expected, the value of V_o is usually high. Thus the term

$$\frac{p^* - p_v}{\frac{1}{2}\rho V_o^2}$$

can often be neglected and Equation [2-10] replaced by

$$\frac{p_v - p_o}{\frac{1}{2}\rho V_o^2} \cong C_{p,min} \qquad [2\text{-}11]$$

The negative of the left side of Equation [2-11] is known as the incipient cavitation parameter, σ_i. This parameter is now universally used for correlating the characteristics of cavitating flows. The value of the parameter

$$\frac{p_o - p_v}{\frac{1}{2}\rho V_o^2}$$

at any condition other than inception is simply denoted without the subscript σ. Thus,

$$\sigma = \frac{p_o - p_v}{\frac{1}{2}\rho V_o^2} \qquad [2\text{-}12]$$

and

$$\sigma_i = \frac{p_o - p_v}{\frac{1}{2}\rho V_o^2} \text{ (at inception)} \cong - C_{p,min} \qquad [2\text{-}13]$$

It should be recognized that Equation [2-13] will not be adequate for small models tested in water which has not been especially treated for the removal of nuclei so that the critical pressure is significantly below the vapor pressure.

There is considerable experimental evidence for the use of the equations and parameters examined herein when the assumptions that are made are justified. That is, the flow must be a good approximation to potential flow with no boundary layer separation and

$$\frac{p^* - p_v}{\frac{1}{2}\rho V_o^2}$$

must be negligible. Obviously, if the flow is separated, $C_{p,min}$ (alone) has little significance as to the location of magnitude of the true minimum pressure in the flow, and if

$$\frac{p^* - p_v}{\frac{1}{2}\rho V_o^2}$$

is not negligible, then σ_i alone cannot be expected to define the conditions for inception.

SEPARATED FLOWS

If the flow about a body is decelerated too rapidly, the boundary layer separates and the pressure distribution along the boundary is no longer a true indication of the minimum pressure in the field. Two examples of separated flow are shown schematically in Figure 2-7. If it is again assumed that

$$\frac{p^* - p_v}{\frac{1}{2}\rho V_o^2}$$

is negligible, cavitation will be incipient when σ_i is the negative of the minimum pressure coefficient in the flow field, $\bar{C}_{p,min}$; the barred symbol being used to distinguish from the minimum pressure coefficient at the boundary, $C_{p,min}$. No exact method of obtaining $\bar{C}_{p,min}$ in terms of the measured boundary pressure is known. However, an examination of the flow field with some assumptions as to its character will permit an approximation to the relationship between $\bar{C}_{p,min}$ and $C_{p,min}$. Because boundary layer separation usually occurs soon after the minimum pressure is reached, the velocity along the separated streamline, v_s, can be approximated from the minimum boundary pressure and the Bernoulli equation as $v_s = V(1 - C_{p,min})$. If it is further assumed that the separated zone may be represented by a forced vortex (rotational) of which the peripheral velocity v cannot exceed v_s; the minimum pressure in the flow field will exist at the core of this rotational vortex and will be given by the approximate equation

$$\bar{C}_{p,min} \cong 2\, C_{p,min}^{-1} \qquad [2\text{-}14]$$

Thus,

$$\sigma_i \text{ (separated flow)}_{max} \cong 1 - 2\, C_{p,min} \qquad [2\text{-}15]$$

Equation [2-15] gives an approximate upper bound to the value of the incipient cavitation index. Actually, the rotational velocity of the vortex is reduced because of shear at the boundary

between the main stream and the separation bubble. If v is taken as $a \cdot v_s$ in which $a \leq 1$, σ_i as given by Equation [2-15] can be modified to a form such as

$$\sigma_i \cong a - (1 + a)C_{p,min} \qquad [2\text{-}16]$$

For the case of a two-dimensional offset in uniform flow, with the offset away from flow, $C_{p,min} = 0$ and, therefore, from Equation [2-16], $\sigma_i = a$. Data obtained in the water tunnel at the U. S. Waterways Experimental Station on such an offset with varying depth is shown in Figure 2-8. In these tests the tunnel water is known to contain large numbers of nuclei with sizes such that the critical pressure is essentially the vapor pressure. Note that σ_i approaches unity as the Reynolds number increases. This particular configuration thus has a critical Reynolds number of approximately 5×10^5, that is, model tests on offsets conducted above such a Reynolds number will produce approximately the correct minimum pressure coefficient in the flow field. Furthermore, if the critical pressure in the model condition is not significantly different from that of the full scale, then scale effects on cavitation inception should not be expected if the model tests are conducted at a Reynolds number greater than the "critical."

Further evidence of the existence of a "critical" Reynolds number and verification of Equation [2-14] is illustrated in Figure 2-9. These results for the incipient cavitation number of a sharp edged disc as influenced by the Reynolds number are reported in

Reference (20). Again, the "critical" Reynolds number for this configuration is approximately 4×10^5 (probably coincidental). The dashed line is the maximum value of the incipient cavitation index predicted by Equation [2-14] using the measured value of the minimum boundary pressure coefficient of -0.44. The predicted maximum inception coefficient of 1.88 is in good agreement with the measured asymptotic value of 2.0. The critical pressure of the model fluid in these experiments is not known. Obviously, the true "critical" Reynolds number for cavitation inception tests is also dependent on a knowledge of the true critical pressure.

In summary, the incipient cavitation number for streamlined bodies with unseparated boundary layers may be approximated by $-C_{p,min}$ if nuclei size effect may be neglected. However, the incipient cavitation number cavitation occurring in separated regions is usually greater than $-C_{p,min}$. The degree to which $\sigma_i \geq -C_{p,min}$ depends on the degree of separation and the Reynolds number but the value of $\sigma_{i,max}$ may be roughly approximated by Equation [2-15].

TIP VORTEX CAVITATION

Another example of cavitation occurring away from the boundary itself and which is particularly important in naval hydrodynamics is tip vortex cavitation. As illustrated in Figure 2-10, the minimum pressure coefficient in the tip vortex depends (for a given loading) on the size of the rotational core of the vortex. Extensive tests carried out by McCormick on tip vortex cavitation (21) show that the core size is highly dependent on the characteristics

of the pressure face boundary layer in the blade tip region. Figure 2-11 illustrates that roughening the suction surface of the blade had no influence on cavitation inception in the tip vortex for positive angles of attack, but at negative angles of attack when the roughness was on the pressure face, the roughness tends to increase the core size and consequently reduce the incipient cavitation number. Thus, reproducing the full scale tip vortex minimum pressure coefficient in a model is difficult and highly Reynolds number dependent. It is not likely that a "critical" Reynolds number exists for such a flow. Basic theoretical and experimental research of the tip vortex flow field should be given very high priority.

Another point related to the tip vortex problem which has been noticed by most experimenters, for example, McCormick (21) and Bindel (22) is that gas bubbles move to the vortex core because of the strong pressure gradients which exist. These bubbles collect in the core regardless of the ambient pressure conditions, and look very much as if the core is cavitating. Thus, as will be discussed in the following section, insuring numerous gas bubbles in the test water in order to establish a critical pressure near vapor pressure may confuse the tip vortex inception problem.

SCALE EFFECTS

The foregoing discussion based on static equilibrium conditions for a bubble will of course be modified by dynamic considerations. However, it was shown in Reference (23) that the

static conditions are quite adequate in most practical cases. Furthermore, it is well known that cavitation can and will occur in the absence of spherical gas bubbles; that is, the nucleus may be a gas particle trapped in a crevice of a foreign particle or of the boundary material itself. However, it is suggested that the critical pressure of such crevice nuclei is very low compared with that of the numerous free gas bubbles which exist in most practical situations, for example, all photographs of full scale ship propeller cavitation show that the water entering the propeller is almost milky white with bubbles. If we operate our water tunnels so as to insure water relatively clear of bubbles in the test section, we should not be surprised when model cavitation data does not agree with those obtained full scale.

The magnitude of the scale effects to be expected in water tunnel cavitation tests is illustrated in Figure 2-12. The ordinate in Figure 2-12 is the ratio of the difference between the ambient pressure and the true critical pressure of the fluid to that of the difference between the ambient and the vapor pressure; it is thus a direct measure of the error to be expected when observed cavitation inception is assumed to occur at the vapor pressure. The abscissa in Figure 2-12 is the size of bubbles existing in the ambient fluid. In the figure $p_o - p_v$ is 1.2 atmospheres; that is, approximately the value 10 feet below the sea surface. The lower curve denoted $U_r = 1$ is assumed to represent full scale conditions and the other curves represent the

same configuration tested in a reduced pressure facility at lower than full scale speeds. The cross hatching on the $U_r = 1$ curve denotes that free gaseous bubbles from .0005 to .002 inches are presumed to be plentiful in full scale. It is very important to note that, in the full scale condition very little error results by assuming that the critical pressure for inception is the vapor pressure. If we assume that the water tunnel water also has free gaseous bubbles in the range of .0005 to .002 inches and we operate at less than full scale speed the error can be extremely large! The use of resorbers to try and drive even smaller bubbles into solution is obviously a mistake if we wish to avoid scaling problems. Figure 2-12 illustrates that if we want to reduce the scale effect due to nuclei size we should try and insure the presence of bubbles of approximately .01 inches in diameter, particularly if the model velocity is less than full scale as is generally the case.

Ripken and Killen (18) have shown that the well-known scale effects of the type shown in Figure 2-13 are largely eliminated if large enough nuclei are present in the fluid. For example, as shown in Figure 2-14, the incipient cavitation index of a 1.5 caliber ogive will increase toward the expected $-C_{p,min}$ value if the free gas content is sufficiently high, in fact the measured cavitation index will exceed $-C_{p,min}$ if bubbles with too large a diameter are entrained in the fluid. These results are certainly not surprising in view of the foregoing analysis.

What is surprising is that more use is not made of the understanding of bubble instability which has been in existence for at least twenty years. We cannot hope to solve model scale effect problems unless we know the true critical pressure of the test water. A very intense effort should be made to develop a reliable instrument for determining the size and distribution of gas bubbles in the tunnel water --- blindly measuring total air content in the hope that it may somewhow be useful is of course not correct. A gross measurement of undissolved air content is not much better. There is some merit in operating very similar models at the same air content if qualitative results at standard conditions are sought.

III. EFFECTS OF CAVITATION

OCCURENCE OF CAVITATION

In Chapter II, the factors governing the inception of cavitation and how one might be able to avoid cavitation in new designs were discussed. This involves both experimental and analytical considerations. It is the overall objective of the designer to avoid inception of cavitation whenever possible. However, it is difficult to design a system which is completely free of cavitation because of practical reasons such as the limitations imposed by size, economic, and manufacturing constraints. When cavitation occurs, because of such unavoidable limitations, the hydrodynamic performance of the system may deteriorate, unacceptable levels of noise and vibration may be produced, and above all the materials used in the system may be eroded, frequently leading to costly repairs or replacements. In this chapter we shall discuss some of the typical effects of cavitation in various systems.

EFFECT ON THE DRAG AND LIFT FORCES OF HYDROFOILS

One of the effects of cavitation is to increase drag and decrease lift on hydrofoils. The cavitation characteristics of a number of foil sections have been reported in several references including Morgan (24). Figure 3-1 shows typical lift and drag coefficients as functions of cavitation number for the Walchner Profile - 7 hydrofoil at an angle of attack of 4 degrees. Since

the lift decreases and drag increases due to cavitation of non-cavitating hydrofoils, the lift-drag ratio decreases significantly, and severely degrades the performance characteristics of the system.

MARINE PROPELLERS

Cavitation is an important problem in marine propellers. The various effects of cavitation on the performance of propellers are fully described by Morgan (24) among others. The important parameters governing the performance of marine propellers are:

Thrust - coefficient $$k_T = \frac{T}{\rho n^2 D^4} ;$$

Torque - coefficient $$k_Q = \frac{Q}{\rho n^2 D^5} ;$$

Advance coefficient $$J = \frac{V_A}{nD} ;$$

Propeller efficienty $$\eta = \frac{T\, V_A}{2\pi n Q} ;$$

Cavitation parameter $$\sigma = \frac{p_o - p_v}{\frac{1}{2}\rho V_o^2}$$ (defined in Chapter II)

where

T = propeller thrust

ρ = density of liquid

n = rate of revolution

D = propeller diameter

Q = propeller torque

V_A = speed of advance

Figure 3-2 shows the effects of cavitation on the performance characteristics of a typical propeller (24). As the advance coefficient increases (higher speeds) the cavitation parameter decreases, producing increasingly severe cavitation. The torque coefficient and the thrust coefficient decrease with a decrease in cavitation parameter. Such deterioration in performance makes the phenomenon of cavitation an important consideration in the design of marine propellers. These effects have led to the invention of super cavitating propellers (25). Such propellers are specifically designed to operate with fully developed cavitation and yet produce the designed thrust, torque, and efficiency. However, material problems such as cavitation erosion, corrosion fatigue, hydrogen embrittlement and stress corrosion cracking still plague these new propeller designs.

PUMPS AND HYDRAULIC TURBINES

The influence of cavitation on the performance of turbomachinery is a very important consideration. Figure 3-3 shows the

decrease in head developed by an axial flow pump as the cavitation in the pump increases. The efficiency of pumps decreases in a similar manner. The parameter governing the degree of cavitation in pumps is the absolute positive suction head above vapor pressure (26). The minimum pressures and hence the cavitation characteristics are related to this suction pressure, H_{sv}:

$$\sigma = \frac{H_{sv}}{\frac{V^2}{2g}}$$

As the net positive suction head decreases, the severity of cavitation increases. These effects are reviewed by Wislicenus (26) and by Wood and Whippen (27).

Similar effects are also noticed in hydraulic turbines. Figure 3-4 shows the deterioration in performance of hydraulic turbines in terms of water flow (28). The efficiency and power are typically affected as shown in Figure 3-5 (29).

In addition to such effects on hydrodynamic performance, unacceptable noise levels may be produced by cavitating hydraulic machinery. For example, 3-6 shows the noise characteristics for cavitating impellers tested in water (27).

CONTROL DEVICES

Cavitation effects in hydraulic control devices such as needle valves, gates, sluice entrances, fuel injection nozzles and butterfly valves are well known (30, 31). The discharge

through valves is greatly affected by cavitation as shown in Figure 3-7. Vibration, noise, and material erosion are also produced by cavitation.

Figure 3-8 shows the typical influence of cavitation on the coefficient of discharge of mouthpices. It is interesting to note the hysteresis effect caused by cavitation and the resulting decrease in the coefficient of discharge (32).

OTHER DEVICES

There are many other components and devices such as deisel liners, aircraft engines, sonar domes, jet nozzles, and bearings that are affected by cavitation. The following chapters outline the mechanics of this phenomenon and how one might protect these systems in service.

IV. DYNAMICS OF CAVITIES

As described in the earlier chapters, it is clear that the phenomenon of cavitation is undesirable from the point of view of hydrodynamic performance, mechanical vibrations, noise pollution and material erosion. In high-speed liquid flow systems this phenomenon imposes a serious limitation. The avoidance and minimization of this problem depends upon an understanding of the various complex aspects of the phenomenon of cavitation, which involves the formation, growth and collapse of cavitation bubbles. A group of cavitation bubbles are called cavities. There are many types of cavities observed in practice. The terminology describing the types of cavities is vast, and sometimes confusing. The following classification, based on a rational application of hydrodynamic principles, is mainly due to Eisenberg (2, 14).

TYPES OF CAVITATION

To illustrate the "types" of cavitation that may occur, it will be sufficient to consider the phenomena from an elementary point of view. In steady, irrotational flow of an incompressible fluid, the pressure equation may be written (neglecting effects of gravitational acceleration):

$$p = p_o + \tfrac{1}{2}\rho(V^2 - v^2) \qquad [4\text{-}1]$$

where

p = the local pressure,

p_o = free stream pressure,

v = the local velocity,

V = free stream velocity, and

ρ = the mass density of the fluid.

In dealing with cavitating flows, the pressures must be referred to the absolute scale.

Familiar examples of cavitation in flows which obey Equation [4-1] on individual streamlines are shown in Figures 4-1, 4-2 and 4-3. Figure 4-1 shows the cavitation developed in a venturi section; as the flow proceeds through the constricted section, the speed is increased and the pressure reduced, resulting in cavitated regions near the boundaries with the liquid jet still intact in the center. Figures 4-2 and 4-3 illustrate two types of cavitation on the suction sides of marine propeller models. In Figure 4-2 a fully-developed, or "steady", cavity exists near the tip, while in Figure 4-3, cavitation has occurred in the form of discrete bubbles which grow in regions of low pressure and collapse as they proceed into high pressure regions where they eventually disappear; cavitation of this latter type may be termed "transient" and we shall be mainly concerned with such cavitation in connection with the mechanism of cavitation erosion. The fluid dynamics of transient and steady cavities will be discussed in detail in a subsequent section.

Another type of flow in which low pressures occur is the vortex flow associated with lifting surfaces as in hydraulic machines. The equation of motion for a simple vortex approximating such real flows is

$$\frac{1}{\rho}\frac{\partial p}{\partial r} = \frac{v^2}{r} \qquad [4\text{-}2]$$

which on integration and evaluation at the center of the vortex gives the pressure

$$p_c = p - \frac{\rho \Gamma^2}{4\pi r_1^2} \qquad [4\text{-}3]$$

where

p_c = the pressure at the center of the vortex,

Γ = the circulation (related to the lift of the blades on a propeller, for example),

r = the radial distance from the center of the vortex, and

r_1 = the radius of the vortex core.

Here, again, the pressure may fall to very low values depending upon the strength of the vortex. In the case of lifting surfaces, the conditions in the tip vortices, whose strengths are related to the lift distribution, may be described approximately by Equation [4-3]. An example of such a flow is shown in Figure 4-4, in which the tip vortices of a model propeller are clearly delineated.

Finally, in Figure 4-5 is shown the cavitation cloud produced in the acoustic field of a barium titanate transducer in a beaker of water at a frequency of about 20,000 cycles per second. These photographs have a magnification of 17 and are silhouettes taken with a xenon spark having a duration of about ½ microsecond. A description of the barium titanate apparatus, developed by A. T. Ellis (33) for producing accelerated cavitation erosion, will be found in the section on laboratory methods for accelerated damage experiments.

To complete the picture of the role of the hydrodynamics of such flows in the damage process, we will first examine some details of the dynamics of the "transient" cavitation bubbles and then discuss the so-called "steady" cavities in terms of the phenomena which may be associated with damage in the latter flows.

DYNAMICS OF "TRANSIENT" CAVITATION BUBBLES

To understand the origin of the theories and evidence that cavitation erosion is associated with mechanical effects, it is necessary to examine the pressures that might be generated in a cavitating flow. As will be seen, it is theoretically possible to produce pressures many times that required for local failure of metals; however, a number of circumstances may arise in real fluids that tend to reduce these pressures by orders of magnitude --- thus accounting for an essential reason why the mechanical damage hypothesis has been questioned in the past. We will trace through the basic results first and then point out the various influences that tend to attenuate the maximum possible pressures.

Spherical Collapse

The motions and pressures associated with the collapse of a spherical cavitation bubble have been treated in varying detail by a number of writers. The classical solution for a perfectly empty cavity was first given by Rayleigh (7); for an incompressible fluid the pressures at final collapse become infinite, and a number of modifications and refinements to the theory have been carried out to investigate the effect of the properties of real fluids. Surface tension tends to increase the rate of collapse; viscous effects, compressibility effects, and the effects of entrained air (or vapor which cannot dissolve rapidly enough to follow the collapsing bubble walls and therefore acts as a permanent gas) all tend to slow down the motion (Figure 4-6) and, hence, to reduce the maximum attainable pressures. Such studies have been made by Flynn (34), Trilling (35), Gilmore (36), and Poritsky (37), to cite only a few who have considered some of these aspects. (A more exhaustive bibliography will be found in Reference 38.) An intensive review of bubble dynamics was made by Plesset (15), Hickling and Plesset (39). Ivany and Hammitt (40), and Noltingk and Neppiras (23) have more recently discussed these effects at great length.

Because of the extreme complexity of the behavior of cavitation bubbles, it is not possible to state unequivocally either the maximum pressures developed or the pressure history during the motion and collapse of such bubbles. Many estimates have been made --- with as many answers as estimates depending upon

the initial assumptions concerning the influence of the properties of the liquid and the contents of the bubbles. Such estimates range from pressures that are too low for damage because a high air content was assumed to be present in the bubbles (but with the accompanying high temperatures associated with the compression of the gas) to values that are more than sufficient for stressing materials beyond their yield points. Such computations will be found in papers starting with Rayleigh (7) and proceeding through many variations by Ackeret (8, 39), Silver (41), and Beeching (12), among others, to the more modern refinements of the authors cited above (33, 34, 35, 36). For spherical bubbles, results based on the Rayleigh model but including surface tension effects (as worked out by Beeching, for example) give pressures of the order of hundreds of tons per square inch. This result may be compared with Silver's analysis which gives pressures of the order of tens of tons per square inch when the velocity of bubble collapse is assumed to be limited by the rate at which the vapor phase can be condensed. These pressures are sufficient to account for fatigue failure of most metals. On the other hand, Ackeret, assuming that the vapor of air in a bubble obeys a polytropic equation of state, found maximum pressures of the order of only tens of atmospheres with an accompanying temperature rise in the gas of the order of thousands of degrees Centigrade. Such high temperatures were attributed to causing luminescence (42) in cavitation regions due to the possible dissociation of the gas when heated during compression.

While all of the results cited above refer to spherical bubbles, it is known that most bubbles do not collapse spherically because of impressed pressure gradients and instabilities that arise for a number of reasons. The important point is that the pressures developed under non-spherical collapse may be orders of magnitude less than those mentioned above. Attempts to directly measure the actual pressures in cavitated regions have been fraught with difficulty since the rise of pressure to its maximum value occurs in a time of the order of a microsecond and over a very small area. Instrumentation in early experiments lacked sufficient resolution to obtain results consistent with the theoretical computations and usually gave pressures that were only of the order of a few tons per square inch (43, 44, 45, and 46). Consequently, adherents of the mechanical damage hypothesis inferred from experiments on actual damage of materials that the pressures must indeed be high enough for failure to occur either by direct stressing or fatigue.

More recently, experiments have been made with equipment capable of response sufficiently rapid to enable the measurement of pressures during single bubble collapse, and with some degree of confidence that the above difficulties could be avoided or at least accounted for. Measurements by Vennard and Lomax (47) showed maximum pressures as high as 30,000 atmospheres, but the methods used in data reduction have been subject to criticism. Sutton (43) using a photoelastic technique, reported stresses as high as 200,000 pounds per square inch in CR-39, a thermosetting

polymer of allyldiglycol carbonate, which was used as the photoelastic specimen. Careful measurements under controlled conditions by Jones (44, 14) (subsequently confirmed in an independent set of experiments [45, 14]) resulted in peak pressures of at least 12,000 atmospheres. All of these experiments were carried out in deaerated water (although the actual entrained air in the collapsing cavity is not known, of course). In general, the pressures in both aerated and deaerated water are so high that shock waves should be formed, and Mundry and Güth (46) have successfully taken Schlieren photographs of the radiated shock waves associated with collapsing cavities. The obvious conclusion from these results is that collapsing cavities of the type discussed here can develop pressures sufficiently high for mechanically produced damage to materials. In fact, the question that should be at the forefront of investigations concerning cavitation damage is that of the importance of non-mechanical mechanisms and of the interaction of mechanical with other mechanisms, and this view is beginning to permeate much of the research now in progress.

Nonspherical Collapse

Recent attention has been directed toward an understanding of nonspherical collapse. However, interest in the formation of liquid jets arising out of nonspherical collapse may be traced to early investigators. For example, Eisenberg (2, 48) as early as 1950, hypothesized the formation of liquid jets caused by the "unsymmetrical collapse of cavitation bubbles in a pressure

gradient." Kornfeld and Suvorov (49) and Naude and Ellis (50) observed experimentally the formation of such jets during the later stages of bubble collapse. Naude and Ellis (50) photographed such jets and the indentations caused by these jets. Hancox and Brunton (51) and Thiruvengadam et al. (52) have shown that multiple impacts by water jets can cause erosion even at impact speeds in the range of 100 fps. More recently, Benjamin and Ellis (53), Tulin (54), Mitchell and Hammitt (55), and Plesset and Chapman (56) have all contributed to the understanding of the jet impact mechanism. It is interesting to note that the theoretical prediction of the microjet formation in front of the primary jet (Figure 4-7) is very similar to the experimental "Monroe Jet" observations of Bowden and Brunton (57).

HYDRODYNAMICS OF "STEADY" CAVITIES

It is characteristic of some cavitating flows that the cavity appears as a large, smooth, stationary surface. Such cavities often appear to be filled only with vapor or air (or both). On the other hand, a cavitating region made up entirely of small, transient cavities may exhibit the properties of a "steady" cavity in that the average envelope of such a region does not vary with time. In large cavities of this type, the liquid flows along the boundary of the cavity and re-enters at the downstream end. Depending on a number of factors not yet completely understood, the re-entering fluid may fill the cavity completely and cause it to collapse, whereupon the cycle of growth, filling, and collapse

reoccurs. When the velocities are high enough, and presumably when the rate of entrainment of the re-entering liquid becomes great enough, the entrained liquid is swept out of the "cavity" region, the re-entrant jet has insufficient momentum to refill the cavity, and the cavity then remains essentially filled only with vapor and air diffused from the proximate liquid. The re-entrant jet still appears but is dissipated before it can fill the cavity again. Under these conditions, the trailing end of the cavity exhibits quite an unstable motion leading to oscillating forces that are of rather low frequency and certainly not of sufficient magnitude to cause damage in the sense considered here. Such oscillations may, however, induce rather severe vibrations in adjacent structures.

An illustration of such cavities is shown in Figure 4-8; here a cavity is formed behind a disk supported from the downstream side. In this photograph, taken at a high frame rate, the very rough appearance of the cavity wall is seen clearly. A number of small, "transient" cavities may be seen traveling along the boundary of the cavity wall. The appearance is characteristic of cavities in which the re-entrant liquid still can fill the cavitating region and cause oscillations of the type described above. Such cavities have been studied by Eisenberg and Pond (58), Shal'nev (59), and Knapp (60). These investigators among others describe the cavity shapes, cavity dimensions, and the unsteady behavior of some of these so-called "steady" cavities.

V. REVIEW OF CAVITATION EROSION MECHANISMS

The history of the evolution of thoughts on the mechanisms of cavitation erosion is very interesting. Although Reynolds (6) was the first to conduct laboratory experiments on cavitation in a Venturi tube, the first critical investigation of the mechanism of erosion was initiated by the Cavitation Subcommittee appointed by the British Admiralty in 1915 (4). Since their motivation came from the erosion of ship propellers in seawater, they were preoccupied with the corrosive influence of seawater on propeller materials. However, the calculations of Cook (4) and Rayleigh (7) greatly influenced some of the members of the Committee who believed that the mechanism of erosion was primarily mechanical deformation and fracture of material particles from the surface. The very same controversy (whether corrosion or erosion) still persists even today. Table 5-1 gives the various mechanisms proposed since the early work of the Admiralty Committee (61).

The water-hammer pressure theory, as it was called in those days, was based on the calculations of Cook (4) and Rayleigh (7), who computed the magnitude of the collapse pressures on the surface of the material. Föettinger (9) in Germany showed that even glass could be eroded by cavitation bubbles. de Haller (62) built a jet impact machine and produced erosion similar to cavitation erosion by the direct impact of water on the material. The first attempt to measure the high pressures predicted by Rayleigh was made by de Haller himself. He was able to record

300 atmospheres by means of piezo-electric pressure transducers. Then Boettcher (63) suggested the idea of surface fatigue and repeated stressing. Beeching (12) realized the importance of corrosive environments in such repeated stressing and suggested the influence of a mechanism similar to that of corrosion fatigue as it is called today.

The mechanical theory itself had many variations. For example, Poulter (64) thought that high pressure liquid may penetrate into the pores of the material and tear microscopic particles from the surface. He argued that even the most perfect material contained microscopic pores. Knapp (65) conducted some experiments with soft annealed aluminum, observed individual spherical dents and determined through high speed photography that only one bubble in every 30,000 produced a dent.

Metallographic observations by Kerr (66), Mousson (67), Nowotny (11), Rheinghans (68), Leith (69), Plesset and Ellis (70), Gould (71), Woodford (72), and Price (73), among others, indicate that different materials exhibit different microstructural changes depending on the material and the intensity of erosion of their experiment. Some of these observations are noted in the following chapters where they are pertinent.

In the year 1948, Petracchi (74) observed that cathodic protection reduced erosion significantly. He explained this with a mechanism of electro-chemical corrosion produced from the electric current generated by the localized strains resulting from the collapse of bubbles. Since then Wheeler (75), Plesset (76), Preiser

and Tytell (77), Nechleba (78) and Waring, et al (79), among others, have observed similar effects. Wheeler (80) noted that cavitation erosion in corrosive liquids takes place in two parts. The first part was dissolved in the test liquid in the form of soluble corrosion products and the second part remained as undissolved eroded particles. He showed that the cathodic protection stops only the corrosive part of the erosion.

There is another school of thought which attributes the corrosion to the chemical activity of the gasses caused either by high temperatures or by electric discharges taking place in the 'atmosphere' of the cavities at the moment of formation (81). Plesset and Ellis (70) conducted some experiments using chemically inert toluene with a chemically inert helium atmosphere and produced erosion on several materials in a short exposure period. They also used the x-ray diffraction technique to locate the plastic deformation occurring on the metals tested. However, Wheeler (75) did notice an increased rate of erosion in salt water after a prolonged exposure as compared to the toluene experiments. The present consensus among contemporary investigators is that corrosion does play an active role in corrosive environments and contributes to the mechanical erosion process.

Another school of thought believes that the erosion is caused by the melting of the metal due to the very localized high temperatures produced by the adiabatic compression of the bubble. Wislicenus (26) noted that the "most promising explanation is that based on the simple thermodynamic consideration that the high

impact pressure may lead locally to very high temperatures. Although the impact pressures may not be sufficient to destroy the material at room temperature, they may very well cause such destruction at the high temperature produced by the impact." To support this view, he cited the use of 18/8 Cr. steel; this steel exhibits good cavitation erosion resistance as well as high temperature strength. Crewdson (82) thought that the major part of the energy available for the erosion was stored in the bubbles and not in the surrounding water. Cavitation bubbles filled with water vapor may be compressed adaibatically in a field of water and at its maximum compression, the bubble may contain highly superheated steam at substantial pressure. Such superheated steam would attack the metal surface. In any case, the resulting temperature gradients in the metals attacked may produce thermoelectric effects leading to electrolytic attack, especially in corrosive liquids. Thus, mechanical action combined with chemical and thermal effects lead to the erosion process in practical environments.

VI. EXPERIMENTAL FACILITIES AND TECHNIQUES

EXPERIMENTAL FACILITIES

The experimental facilities that have been used for investigations of cavitation erosion may be grouped into two categories: those that depend on inducing low pressures as a result of high velocities in flowing liquids or motion through a stationary liquid; and those that produce cavitation by means of local, periodic accelerations in an otherwise stationary liquid. The first group includes devices such as venturi tubes and rotating discs while the second depend on alternating pressure fields such as are produced by acoustic or other acceleration producing devices. In addition to such equipment, other types of "impact" producing devices used in the past include liquid jets impinging on specimens and single shock waves in a bar in contact with the liquid.

The relative merits of these equipment will be evident from their description. The question of the relations between the results in different devices and extrapolation of results from one to another, as well as to field conditions, will be considered in connection with the discussion of methods of analysis.

Venturi Tubes

Venturi sections were among the first flow devices used in the study of cavitation erosion. These are simply convergent-divergent nozzles of the type shown in Figure 4-1. Such Venturi

sections are made part of a closed system in which the liquid is pumped around the circuit. The pressure in the test section is then controlled by the velocity through the test section and the ambient pressure imposed on the entire closed system (see Equation [4-1]). The pressure along the test section will drop as the liquid is accelerated through the position of minimum area and increase as it proceeds into the diffusing section where the area is increasing. Cavitation then occurs when the pressure drops to the order of the vapor pressure, and the extent of the cavitating zone will be increased in length as the speed increases, or the ambient pressure is lowered, and the vapor pressure is reached by points further and further along the section. The cavitation zone collapses in the diffuser where the pressure increases; it is just at this position and in the wall of the venturi that test specimens are placed so as to be exposed to the collapsing cavities. Very often, the cavitation zone will surround a central core of liquid that cannot be fully vaporized during its passage through the length of the low pressure region. In this case, there will be agitation due to turbulent mixing of the "jet" with the condensed liquid in addition to the violent action of the collapsing cavity. Further discussions of the cavitating flow in such nozzles and their use in damage experiments will be found in References (9), (14), and (67).

Since many machines operate under conditions of high velocity flow similar to those described here, the venturi section is considered to be quite representative of these field conditions.

However, as in the field, measurable damage proceeds at rates that require long periods of exposure (sometimes of the order of hours as in the tests reported by Mousson). Consequently, emphasis on laboratory equipment has been directed toward simpler methods of producing more rapid and reproducible data.

Cavitation Tunnels

Cavitation damage tests have also been performed in large cavitation tunnels which operate on principles similar to the venturi section described above. However, these may take a number of different forms including closed sections in which the section flows full (as in the case above), open sections in which a high speed jet discharges into a water-filled section maintained at low ambient pressure, and free jets in which a high speed jet discharges into an evacuated space. It is beyond the scope of our discussion to describe the details of such tunnels and the methods whereby they are operated and controlled. It is only necessary to point out that for cavitation erosion tests, the test specimen is mounted on a body of revolution or a hydrofoil, on which cavitation is produced by the combination of high tunnel speeds, low ambient pressures, and high velocities induced on the test body as a result of its particular shape. Descriptions of some typical cavitation tunnels will be found in References (83) and (84), and a description of cavitation damage experiments carried out in recent years in such a tunnel in Reference (60).

Such tunnels are seldom used for erosion tests because of the expense of operation, the relatively complicated procedures required in installing experiments, and the length of time they must operate to obtain measurable weight loss.

However, specialized water tunnels have been constructed to perform certain experiments. One such example is the high speed water tunnel that has been specifically designed and built for cavitation erosion studies. These studies include the response of elastomeric coatings to cavitation bubble collapse and adhesion failures under the combined action of hydrodynamic forces and bubble collapse impacts.

Although considerable effort has been made to screen elastomeric coatings for applications in hydrofoils, practically no basic research has been initiated with the primary objective of studying bubble collapse dynamics and how these affect the coating response and cause adhesion failures. This situation has led to apparent anomalies in which some coating systems behave extremely well during laboratory screening tests conducted at relatively higher velocities but fail rapidly in field applications at much lower velocities.

Recently, a high speed water tunnel has been used to study the response of coatings on actual hydrofoils (85). The facility consists of a test section, a contraction, a diffuser, and a pump as shown in Figure 6-1. The size of the test section is 2 by 3 by 18 in. with a maximum speed capability of 90 knots (46 m/s,

150 fps). Since this is a closed loop system, the pressure can be varied from 0 to 200 psig independent of velocity. The entire test section is made of plexiglas so that the cavity formation, collapse, and coating failure phenomenon can be photographed with a high speed movie camera. Typical coating failures produced in this facility are shown in Figure 6-2.

Rotating Disks

A device that has been used in recent years for studies of cavitation erosion is a rotating disk on which cavitation is induced in a separated flow regime. We have already discussed how cavitation occurs in such regions in connection with inception of cavitation. Basically, such devices consist of a disk with holes at the periphery, rotated at high speeds in a chamber in which the ambient pressure can be controlled. Because of the unstable flow within the hole, a separated region is formed and a cavitating wake is shed downstream of the opening. The test specimen is placed in this wake so that the cavitating zone collapses at the position of the specimen. Such devices have been used and described by Rasmussen (86) and by Lichtman, et al (87). A sketch of the disk used by Rasmussen is shown in Figure 6-3. The test chamber is normally designed with fixed stilling vanes on either side of the disk to damp the induced circulation of the liquid. Rotation speeds as high as 3200 rpm have been used (87) with a disk 12-inches in diameter. Figure 6-4 shows an overall view of this apparatus (87).

Rotating Foil Apparatus

Although the vibratory cavitation facility is a compact and convenient tool for the study of basic erosion processes and the screening of materials, it is difficult to relate the results to hydrodynamic systems such as hydrofoils or propellers. For this reason a new facility called the rotating foil apparatus has been developed, based on the idea of rotating a cavitating body in a relatively stationary liquid. Rasmussen (86) was the first to develop the rotating disk facility, which was further improved by Lichtman, et al (87) and Thiruvengadam (61). Cavitation erosion was produced in the wake of a circular hole drilled in a disk rotated in a stationary liquid. The flow pattern behind the hole was so complex that a basic understanding of the phenomena involved seemed difficult; thus, the idea of attaching two symmetrical hydrofoils at diametrically opposed locations on a rotating disk was initiated. Since then much effort has been devoted toward developing this facility into a scientific apparatus. A detailed description of this apparatus as well as its calibration is given in Reference (88).

Briefly, the apparatus (Figure 6-5) consists of a cylindrical steel chamber capable of withstanding internal pressures up to 215 psia, and an 18-in. diameter, 7/8-in. thick rotating disk mounted between two variable-height stilling vane assemblies separated from the chamber wall by an adjustable gap ring (Figure 6-5a and 6-5b). The drive system consists of a 50-hp electric motor, pulleys, a timing drive belt, and a 90-deg gear

box. The foil speed can be varied by suitable combinations of the pulleys. Temperature of the test liquid in the chamber is controlled by means of a plate coil heat exchanger which is affixed to the chamber's removable cover. Some additional control is provided by a cooling jacket that surrounds the chamber. The effectiveness of the stilling vanes in stopping the rotation of the liquid within the chamber was verified by actual pitot tube measurements. The core velocity was less than 6 percent of the foil velocity (88).

Typical erosion produced on a hydrofoil in this apparatus is shown in Figure 6-6. The equipment has been used extensively in our studies on the effect of velocity, pressure, and size of the foil on cavitation erosion. A maximum speed of 200 ft/s has been achieved.

Careful observations and analysis of results indicate that secondary flows caused by centrifugal forces affect the bubble collapse pattern. There are also restraints on the model size and weight due to structural strength requirements and geometrical confines.

High Velocity Cavitating Water Jet Apparatus

In order to explore the possibilities of harnessing the destructive forces of cavitation erosion in ocean engineering applications, a high speed cavitating jet facility has been developed (Figure 6-7). A positive displacement pump driven by a 100-hp motor delivers 80 gpm at 2000 psi to a $\frac{1}{4}$-in. nozzle,

producing a cavitating jet of water at velocities close to 500 fps. The velocity can be controlled by means of a bypass valve. A 30-in. diameter by 7-ft resorber system is used to remove the free bubbles in the water before it re-enters the pump. Low gas content is important for effective erosion. Figure 6-8 shows the severe erosion produced on various materials. This facility is useful in screening materials quickly and in optimizing various techniques of drilling on different materials under water (89).

Hydraulic Jets

Although the impact of water drops is not a cavitation damage testing device, the use of such impact tests was important in early examinations of the mechanism of cavitation damage and is therefore mentioned here. In order to examine the question of whether the mechanism of cavitation damage was associated with mechanical erosion, de Haller (62) ran experiments in which small rods, fastened to the periphery of a wheel rotating at a high rate of speed, were passed through a high speed water jet. While he could not account for the pressures thought necessary for such damage in either type of experiment, and was puzzled by the fact that damage was observed in all cases as long as enough impacts were sustained, he did conclude that the damage in a cavitation test is of the same nature as that observed in the drop impact tests. Thus, as was discussed earlier, he came to the view that cavitation damage is primarily mechanical in nature.

Vibrating Cavitation Erosion Apparatus

The expensive and time consuming experiments that result with the types of equipment discussed so far have led to the development of laboratory devices for simpler experiments. Of these, the most important has been the vibrating apparatus, which is still the most widely used device and therefore merits rather detailed description. This apparatus possesses the attributes of compactness, precise control, comparatively low initial cost, and economy of operation.

The observation that cavitation is produced at the end of a piston vibrating in liquids was effectively used to screen cavitation erosion resistant materials in the laboratory as early as 1932 (90). In this apparatus, the test specimen is vibrated along its longitudinal axis in a test liquid, Figure 6-9. The test parameters include the frequency, the amplitude, the size of the specimen, the size of the liquid container, and the depth of immersion of the test specimen.

Basically, the apparatus consists of either a laminated nickel stack or a piezo-electric transducer that produces the vibrations (Figure 6-9). The strain is amplified by means of a specially designed transition component, known as a velocity transformer, which transmits the vibrations from the transducer to the test specimen. The other essential components of this equipment are an audio oscillator, an amplifier, and a stabilized power supply. The displacement amplitude is monitored by means of an oscilloscope display of the voltage developed by a pickup

coil. The resonant frequency can be controlled by the length of the velocity transformer. Both exponential and double-cylinder velocity transformers have been used for these investigations.

In 1955, the American Society of Mechanical Engineers standardized the test parameters (91); however, since then their test conditions have become obsolete. Plesset (92) used an exponential horn to amplify the displacement amplitude following the work of Mason (93). Hammitt, et al (94) have recently reported on an interlaboratory test made under ASTM auspices.

Based on this round robin testing, the ASTM has now adopted a new standard for the vibratory test method (95). Basic researchers may be inclined to vary all the parameters in this test method. However, an accepted standard procedure and standard parameters would be very helpful in screening materials. Adherence to this method will permit a better understanding and correlation of the test results of various investigations. It would also help in establishing rational specifications and in procurement of materials.

Figure 6-10 shows the important parameters of the vibratory test facility as recommended in the 1972 ASTM standard. The schematic and overall views of a typical piece of equipment are shown in Figures 6-9 and 6-11. A standard commercially available 800 ml low form glass beaker is used to contain the test liquid. The test liquid is generally at least 600 ml of distilled water, meeting specifications for "non-referee reagent water" given by ASTM specification D1193 or other clearly defined distilled water.

A cooling bath or cooling coil will be necessary to maintain the temperature of the test liquid at 72 ± 2° F. (22°±1°C). The test specimen diameter is 0.625 ± 0.002 in (15.88 ±0.05mm). The test surface should be machined plane and square to the transducer axis within an indicator reading of 0.001 in (0.127 mm). Unless otherwise required, the test surface is prepared and polished according to the procedure outlined in the ASTM manual on fatigue testing.

In order to check the operation of the machine periodically and to insure the accuracy of test procedure, it is recommended that commercially pure (99.98%) annealed nickel of hardness HRB 25 to HRB 30, such as the INCO nickel 270 used in the ASTM round robin test (94), be tested from time to time. The approximate range of test results to be expected for this material, under the conditions here specified, is shown in Figure 6-12 based on the results reported in the round robin test.

A clean specimen is carefully weighed on an accurate and sensitive balance (0.1 mg accuracy and sensitivity) before the test. The specimen is immersed to a depth of at least one-eighth in. (3.2mm) and not more than one-half inch (12.7mm). A dummy test specimen should be vibrated in the test liquid for 15 min before the liquid is used for testing a given material, in order to stabilize the gas content of the test liquid. The test may be conducted at normal atmospheric pressure on the free surface of the test liquid unless otherwise specified.

The frequency of oscillation of the test specimen is 20 kHz ±1% (one kHz = 1000 cycles per second). The peak-to-peak displacement amplitude is 0.002 in. (0.051 mm). This amplitude must be maintained throughout the test within ±5% tolerance. Some sensor is provided to detect the displacement amplitude and is calibrated with a filar microscope or a photonic sensor. The amplitude is generally monitored within a tolerance of ±5% throughout the test.

The loss due to cavitation erosion may be periodically determined by interrupting the test at suitable intervals, removing, and carefully cleaning, drying, and weighing the specimen again. It is well known that the rate of mass loss varies with exposure time. The intervals between measurements must be such that a curve of cumulative mass loss versus cumulative exposure time can be established with reasonable accuracy. The duration of these intervals, therefore, depends upon the test material and its erosion resistance, and cannot be rigorously specified in advance. (Suitable intervals may range from about 15 minutes for aluminum alloys, through 1 hour for pure nickel and 2 or 3 hours for 316 stainless steel, or 8 or 10 hours for stellite 6B. This is only a rough guide.)

It is recommended that the testing of each specimen shall be continued <u>at least</u> until the rate of erosion has reached a maximum and begins to diminish. It is also recommended that when several materials are to be compared, all materials be tested until they reach comparable mean depths of erosion. The mean depth of erosion, for the purpose of this test method, may

be calculated on the basis of the full area of the test surface of the specimen, even though generally a narrow annular region at the periphery of the test surface remains virtually undamaged. The specified area, based on the diameter of the test specimen is 0.307 in^2 (1.98 cm^2).

Fatigue failure of the threaded portion of the specimens made of relatively weaker materials may become a problem. Using a threaded stud made of stronger material such as titanium and reducing the mass of the specimen are recommended as possible remedies. Very careful cleaning and drying of specimens before each weighing is recommended. For porous (cast) materials, a vacuum desiccator may be used. The specimen must be tightly secured to the horn to ensure good energy transmission. Some experimenters use silicone grease while others rely on very good matching between mating surfaces. Heating of the horn and unusual noise are indications of either fatigue failure or improper tightening of the specimen.

The report may contain the following for each material tested: available identification, specification, heat treatment, composition, and mechanical properties of the test material; mechanical properties listed include hardness, as measured on the specimen or the stock from which it came; method of preparing test specimens and test surface, preferably including initial surface roughness measurement. The number of specimens tested should be indicated, with a tabulation of cumulative mass losses, rate of loss, the corresponding cumulative exposure time

for each specimen; also cumulative mean depth of erosion versus cumulative exposure time for each specimen, and the rate of erosion versus cumulative exposure time are plotted. The specific details of the test liquid (distilled water for the standard) should also be given.

Another type of acoustic field generator, operating at frequencies from 400 to 1000 kHz has been used in experiments by Lichtman, et al (87). This equipment produces a high-frequency vibration of a piezo-electric ceramic transducer bowl comprising part of a liquid container. Cavitation is generated at the focal point in the coupling fluid. In spite of the higher powers used in this apparatus, the rate of damage is evidently much lower than that in the barium titanate system designed by Ellis (33).

INTENSITY OF CAVITATION DAMAGE

Early Notions of Intensity

The term "intensity" has long been used in a vague sense by many previous investigators. It was characterized by the following measurements:

(i) Weight loss
(ii) Volume loss
(iii) Number of pits produced
(iv) Loss of radioactive coating materials.

It was realized as early as 1935 by Schumb, et al (96) that weight loss can be a misleading parameter characterizing intensity since the strength and density can vary independently. In

spite of this fact, weight loss continues to be used for comparing various materials by many investigators, even to date. Knapp (97) proposed the method of measuring the number of pits per unit time per unit area on a given material to represent the "intensity or damage potential" of a particular device. However, this measure can only represent the rate and density with which the bubbles are collapsing and not the energy of collapse of the bubbles. The loss of radioactive coating materials is not generally favored because of its inherent procedural complexity and further it is only an indirect measure of weight loss. By far the best and simplest measure of the total energy absorbed by the material is the volume loss for a given material. However, the gross volume loss cannot represent the intensity because it would vary with size or area.

All of the above discussions represent only the "output" intensity of erosion as experienced by the material. Evidently this "output" is related to the pressures produced and to the rate at which such pressures are applied. Furthermore, these pressures are related to some "input" intensity which causes the bubbles to collapse and radiate these pressures. A successful attempt has been made to formulate the definition of intensity of erosion based on the "output" parameters discussed above (98). However, an important aspect is the effect of the test duration itself on the rate of damage. This effect will be fully discussed later in this handbook. Neglecting this effect for the moment, we may formulate a definition of intensity of erosion as follows:

Present Definition of Intensity

It is generally accepted that a portion of the total bubble collapse energy is absorbed by the test material causing final fracture and volume loss. The energy absorbed by the material, E_a, is given by

$$E_a = \Delta V \cdot S_e \qquad [6\text{-}1]$$

where, ΔV is the volume loss and S_e is the strain energy which is defined as the energy absorbed per unit volume of the material up to complete fracture*. Hence, the power absorbed by the material is given by

$$P_a = \frac{\Delta V \cdot S_e}{\Delta t} \qquad [6\text{-}2]$$

where, $\Delta V/\Delta t$ is the volume loss per unit time (rate). In order to take into consideration the effect of size of the system, the power absorbed per unit eroded area is defined as the intensity of cavitation erosion of the device (98). Then,

$$I = \frac{P_a}{A_e} = \frac{\Delta V \cdot S_e}{A_e \cdot \Delta t} \qquad [6\text{-}3]$$

*The logic behind using the strain energy and the limitations are discussed in detail in Chapter VII.

or,

$$I = \frac{\Delta y \cdot S_e}{\Delta t} \qquad [6\text{-}4]$$

where

I is the intensity of cavitation erosion,

A_e is the area of erosion, and

$\Delta y = \Delta V/A_e$ is the mean depth of erosion.

The value of I can easily be computed if we know the average depth of erosion per unit time and the energy absorbed by the unit volume of the material up to fracture by this type of loading. While the average depth of erosion per unit time can be accurately measured by actual test on a material, the value of S_e is not precisely known at present. This difficulty was overcome by using the strain-energy (area of the stress-strain diagram) obtained from a simple tensile test as a first approximation (99).

Estimation of Intensities of Various Test Devices

The value of the intensity of cavitation erosion, I, for various test devices was estimated from the published data using one of the five materials for which the strain energy values are known as given in Reference (98). At least one of these five materials has been used by each one of the investigators. Table 6-1 gives the value of the parameters used for computing the intensity of each equipment as published along with the

values of intensity in watts per square meter. The reason why these five materials were specifically used for this analysis is because the strain-energy for other materials used by various investigators has not been published.

Comparison of Intensities of Various Devices

Table 6-1 presents an interesting comparison of intensities of cavitation erosion of sixteen devices for which quantitative data have been published in the literature. It so happens that the device No. 1 (A.S.M.E. Standard Magnetostriction Device) is not only an arbitrarily defined standard device but it can also be considered as a unit intensity device since its intensity is about one watt per square meter. It is a matter of coincidence that the intensity level of the rotating disk device (Device No. 16) used by Thiruvengadam (61) is also approximately one watt/meter^2. It can be seen from Table 6-1 that the most intense device so far used is the rotating disk device of Rasmussen (Device No. 14). This result shows that the so-called accelerated devices (vibratory apparatus) are not more intense than the rotating disk devices. Further it will be noted that the intensities of Device Nos. 8, 10 and 12 are just a tenth of the intensity of the A.S.M.E. Standard Magnetostriction Device (Device No. 1).

There is a general feeling that the intensities of actual field systems would be very much lower that the intensity of vibratory devices. The present analysis shows that this

contention may not be a general case applied to field devices. The term "accelerated device" is rather misleading from this point of view.

The second interesting result that emerges from the analysis is that the devices used by advocates of the chemical and electrochemical damage mechanisms have possessed very low intensities. It is understandable why Petracchi (74) attributed no weight loss to the mechanical part of the mechanism because the device used by him (Device No. 9) was one thousand times less intense than the standard A.S.M.E. device. Similarly, the device used by Wheeler (75) (Device No. 5) was 250 times less intense than the A.S.M.E. Standard Device.

METHODS OF MEASUREMENT, ANALYSIS AND CORRELATION

Some of the special methods that are of particular interest, especially in two respects, will be examined in detail: first, the question of stresses and damage actually induced by cavitation during both the incubation period and the post-incubation period when material losses occur; and, second, the question of the meaning of certain measurements in relation to the problems of comparison of one situation with another, and of extrapolation and prediction of damage rates for field installations from laboratory results. The latter problem is of interest also in determining whether imposed protective systems should be used and, if so, in deciding upon specifications for such systems, e.g., air injection. Consequently, it will be recognized that

the selection of some of the methods to be discussed in connection with the first question was made on the basis of their relevancy to the second.

Some Special Methods in Cavitation Erosion Experiments

a. Weighing and pit counting

The most widely used criterion of cavitation erosion is, of course, the rate at which material is removed from the test specimen. As mentioned previously, this rate of damage is clearly time dependent. While the rate of weight-loss can give some measure of the rate of erosion following the incubation period, very soft metals such as lead and pure aluminum are pitted readily under cavitation attack long before actual weight loss is observed. Consequently, some attempts have been made to characterize erosion and obtain an "index" of erosion rate by counting the pits or depressions formed during this period. Some observations of this type are those of Knapp (97), who tested soft aluminum and compared the rate of formation of pits with the velocity of the fluid in his experiments. It is clear that this technique is applicable only to the very soft metals. Furthermore, to relate the rate of erosion on such materials to the damage rates on hard materials would obviously be a most formidable task.

All of the attempts to characterize cavitation erosion for purposes of extrapolation and prediction must be related somehow to the "intensity" of the cavitation produced in the laboratory and occurring in the field. These investigations have

generally sought to find a relation between weight loss (100, 87) or erosion rates (65, 101) and the flow velocity or the amplitude of vibration of magnetostriction oscillators and to discover a "threshold" for the onset of measurable loss. The details of such investigations and the significance of the observations will be discussed in Chapter VIII.

b. Radioactive tracers

Another method of measuring the intensity of cavitaion erosion makes use of radioisotopes applied to a test sample or to a part of a machine in the region of cavitation. Details have been given by Rosenberg (102), who is evidently the first to develop a specific method, and by Kerr and Rosenberg (103). Rosenberg's method consists of using a radioactive paint prepared with 5 grams of radioactive arsenic (As 76), having a total activity of 750 mC, in a vehicle of Manila copal cement used as the base for a coating material. Other details of the composition of the final coating material, as well as of the techniques and precautions to be observed in actual application, are given in Reference 103. This development was motivated particularly by a need for a simple method to be used in field installations.

To determine the effects of cavitation, the activity of the coating is measured as a function of time. The decrease in activity, corrected for the natural decay in radioactivity, is then taken as a measure of the cavitation intensity. An example of the data obtained by Rosenberg on turbine blades is shown in

Figure 6-13 in which the measured radioactivity in micro-curies per hour, used as the cavitation erosion index, is plotted as a function of the axial velocity at the runner.

c. Electrical resistance change

By measuring the change in electrical resistance of a material with change in physical dimensions as it is corroded or eroded, it is possible to obtain a measure of the rate of damage. Such methods have been in use for some time as detectors of chemical and electrochemical corrosion (104), and recently have been used (105) for measuring the weight loss in cavitation erosion. The method consists simply in measuring the change in electrical resistance of one arm of a bridge, which is the exposed specimen, as the specimen loses material. In the instruments, now in use as corrosion detectors, an insulated arm is used as the reference and for temperature compensation. The successful application to weight loss detection in cavitation erosion should provide a more convenient and accurate method than weight loss measurements in field experiments.

It would also be interesting to examine the use of such methods in determining the events during the incubation period. If the electrical properties of metals vary sufficiently with the amount of hardening and stress application, such changes may be detectable during an actual cavitation experiment and would give a measure of the rate of damage during the incubation period.

d. Photoelastic methods

The great difficulties associated with measurement of the pressures produced in a cavitating zone, evident from our previous discussions, led Ellis (106) to study the possibilities of using photoelastic techniques to study this question. The advantage of a successful photoelastic method lies in the fact that the actual stress produced would be measured rather than an integrated pressure as obtained with standard piezo-electric transducers. Additionally, with simultaneous use of high-speed photography, it might be possible to identify the relations between bubble motions and position relative to a specimen and the resulting strain waves. Both the latter measurements and the measurements and observations of the strain waves require ultra-high-speed photography and such photographic methods have also been developed by Ellis, particularly in this connection. The principal feature which allows the very short exposure time in Ellis' system is a Kerr cell electro-optical shutter with which he has obtained exposure times of the order of 10^{-7} second. Using a rotating mirror driven by an air turbine, he has obtained sequences of as many as 700 pictures at a rate of a million frames per second. Details of this development and of the principles of operation of the Kerr cell shutter, as well as the lighting problems, will be found in Reference 106. Of particular interest here is the development of the photoelastic technique which was carried out in detail by Sutton (43). Ellis and Fourney have increased this capability of 1½ million frames per second using a laser beam as a light source (107).

The essential problem in developing a satisfactory photoelastic technique arose from the little known dynamic characteristics of ordinary photoelastic materials. Consequently, the dynamic properties (Poisson's ratio, internal damping, stress wave speed) of a common photoelastic plastic CR-39, mentioned previously, were studied in some detail. CR-39 is a thermosetting polymer of allyl-diglycol carbonate; the method of manufacture is described in Reference (43). Sutton found that this plastic exhibits strain birefringence (rather than stress birefringence) and that its strain-optic constant is independent of the rate of loading. Consequently, together with the high speed photographic techniques previously developed, it was possible to study the strain waves produced by cavitation. It was with this type of material that Sutton deduced that cavitation may produce stresses as high as 200,000 psi. It was estimated that the duration of the pressures in his experiments was about 2 microseconds and the area affected by the cavitation pressure had a diameter of about 0.001 inch. Further development of such techniques will be useful in obtaining quantitative information on the input intensity of cavitation damage.

VII. PROPERTIES OF MATERIALS AND THEIR CAVITATION EROSION RESISTANCE

METALS

It is now generally accepted that the bubble collapse energy produces indentations on the metal as shown in Figure 7-1. The indentations may be produced on the material either by shock waves (7) or by impingement of jets (14), Figure 4-7. The evidence in support of these methods of dent formation is abundant in the literature. In the absence of corrosion, it is quite reasonable to proceed on the assumption that these dents, formed by mechanical means, are the main cause of fracture and loss of metal.

When such repeated, indenting forces or blows act upon a metallic surface, the material response would depend upon the intensity of impact as follows:

i. There may not be any permanent deformation, even after a relatively long period of exposure (threshold of erosion);

ii. The metal may deform after a certain number of repetitive blows (incubation of erosion);

iii. A permanent deformation may develop at the onset of the first blow (single impact erosion); or

iv. The metal may flow plastically as a result of high strain rates during the first blow itself or after a certain number of repetitions (high intensity of erosion) (108).

These possibilities can be readily understood from Figure 7-2, which shows schematically the variation of the internal friction of metals with strain amplitude in the case of repeated loadings (109). The response of metals to a given spectrum of repeated strains can be qualitatively represented by an equivalent indentation fatigue diagram as shown in Figure 7-3. Accordingly, the response of a metal to a cavitation erosion test is dependent upon the order of magnitude of the strain. In Figure 7-3 three regions have been designated to point out the possible material responses to indentations discussed previously. Photographs of the metallic surfaces which exhibited typical response in each region are also shown.

With the above physical picture in mind, let us pose the question: What is the characteristic property of a metal that controls the eroded volume as a result of this mechanical process? Obviously this property must be in some way related to the energy absorbing capacity per unit volume of the metal up to fracture when subjected to the repeated overlapping indentations. At the present state of knowledge, there is no way to determine this quantity exactly. For this reason, several investigators have tried to correlate this quantity with most of the commonly known mechanical properties of metals. These correlations are discussed here in detail.

Mechanical Properties

a. Hardness

Hardness has been shown to be an important factor in cavitation erosion resistance. In general, materials with greater hardness, as measured by the Brinell hardness scale for example, have better resistance to damage than softer materials. However, certain materials do not fall into this general pattern; in Table 7-1 are shown the erosion rates of a series of cast stainless steels as determined by Rheingans (68), using a vibratory apparatus. The order of resistance generally follows the order of hardness except for a few cases. Another example of the correlation of erosion resistance with hardness is given in Table 7-2, abstracted from the results of Mousson (67) on materials tested in a Venturi apparatus. The first four specimens in Table 7-2 basically have the ferritic type of grain structure, while the last three show an austenitic matrix. While the groups show correlation within themselves of increasing resistance with increasing hardness, there is clearly another factor which influences the comparative losses between groups. This may be attributed to grain structure and cold working properties and will be discussed subsequently.

As a final example of the role of hardness, the experiments of Plesset and Ellis (70) on a number of different materials may be cited. Their results are summarized in Table 7-3. The criterion of damage was the depth to which a small hole was drilled by a focused cavitation cloud such as that shown in Figure 4-5.

They point out, in addition, that nickel and brass show plastic deformation after a few seconds of exposure to cavitation, while a similar amount of deformation takes several minutes for vanadium, approximately an hour for molybdenum, and several hours for tungsten.

b. Work Hardening

The original hardness of materials before cavitation attack does not in itself constitute a unique correlation parameter although it may be overriding for many materials. There is clear evidence that resistance to erosion is dependent upon the ability of a metal to be work hardened under repeated impact. This is well illustrated by a comparison of stainless steels which shows the excellent properties of the austenitic steels. In Table 7-4 are shown some results from tests by Mousson (67) in substantiation of this conclusion. Although the original hardness of the austenitic stainless (18-8 chromium-nickel) steel was lower than that of the stainless 17-percent chromium steel, the resistance of the former is far superior over the duration of the experiments. (These tests were made in Device No. 8, Table 6-1, at lower rates of damage than occurs in magnetrostriction oscillators.) The other austenitic stainless steels also exhibit similar beneficial effects of the work hardening properties of such metals. Mousson also measured the change in hardness of various metals after exposure to cavitation damage and found large increases in the zones of exposure (67) as would be expected on the basis of our previous discussion of plastic deformation accompanying cavitation erosion.

c. Ultimate Tensile Strength

It is difficult to distinguish between the importance of tensile strength and hardness since these properties are usually closely correlated for most metals. In general, materials with high ultimate tensile strength tend to exhibit high resistance to cavitation erosion as indicated in Table 7-3 for example.

In this connection, it is of interest to refer again to the results of Plesset and Ellis summarized in Table 7-3. It was noted that, in these experiments, plastic deformation appeared almost immediately in the soft specimens, nickel, brass, and pure titanium. These materials have ultimate tensile strengths on the order of 50,000 psi: it may therefore be concluded that the stresses induced by cavitation in this apparatus were at least of this magnitude. Since, however, erosion developed very slowly for materials such as titanium 150-A and tungsten, which have ultimate tensile strengths of the order of 130,000 psi, it might be inferred that the cavitation-induced stresses were below this value for this case.

d. Strain Energy

The above discussion indicates that the attempts to relate erosion resistance with individual properties such as yield strength, ultimate strength, ultimate elongation, hardness and modulus of elasticity were not too successful. This is mainly because it is possible to select several materials with

the same yield strength with different ultimate strengths or elongation or hardness or modulus. In such a case, a material with lower yield strength and hardness seems to erode less if it has higher ultimate strength and elongation. Such observations showed that the erosive forces have to do more work to fracture the same volume of material because the material is capable of absorbing more energy before it fractures. Careful experimentation with different materials indicated that the strain energy of the material, as given by the area under the stress-strain curve up to fracture, may be more representative of the energy absorbing capacity of the material when exposed to erosion than some of the more conventional material properties such as yield strength and ultimate strength (61, 108). (See Figures 7-4 through 7-9.)

A detailed investigation (110) showed the following correlation factors for each of the properties:

Mechanical Property	Correlation Factor, r'	Figure
Strain Energy	0.91	7-4
Ultimate Strength	0.79	7-5
Yield Strength	0.65	7-6
Brinell Hardness	0.51	7-7
Modulus of Elasticity	0.49	7-8
Ultimate Elongation	0.48	7-9

The correlation factor, r', for two variables, x and y, was calculated from the following formula:

$$r' = \frac{n\sum xy - \sum x \sum y}{[n\sum x^2 - (\sum x)^2]\,[n\sum y^2 - (\sum y)^2]}$$

where

n = the number of points in an x, y plane.

According to this investigation, strain energy appeared to be the most significant parameter. Further evidence to support this finding came from the studies of Young and Johnston (111) on steel and some of the super alloys in liquid sodium at 800°F. as shown in Figure 7-10. However, one of the materials tested by them, Stellite 6B, did not agree with the strain energy correlations. More recently Gould (112, 113) and Woodford (72) have made some additional investigations on Stellite and found out that Stellite 6B undergoes a phase change as it is exposed to erosion. This effect, discussed below in detail, probably accounts for its anomalous behavior.

e. Ultimate Resilience

Hobbs (114) argued that a material can absorb the energy released by the collapsing cavity in three ways: 1) by elastic deformation, 2) by plastic deformation, and 3) by fracture. He investigated the relative contributions of these factors and concluded that the ultimate resilience [expressed as $\frac{1}{2}$(tensile strength)^2/elastic modulus)] correlated fairly with

the erosion resistance of materials as shown in Figure 7-11. Hammitt, et al (115) have subsequently found some supporting evidence for Hobb's conclusion.

f. Erosion Strength

The foregoing disagreements and difficulties associated with the attempts to correlate the erosion resistance with other mechanical properties become understandable from a review of similar attempts being made to relate the fatigue strength of materials with their mechanical characteristics (116). However, in many practical applications the designer needs some numerical value of a property that represents the erosion resistance of a material. In order to accomplish this objecti e, Thiruvengadam (108) suggested a concept of erosion strength and outlined a procedure to determine the erosion strength with the help of standard screening tests.

The procedure to determine the erosion strength makes use of the definition of the intensity of erosion given by Equation [6-4]. For example, in a vibratory cavitation erosion test the intensity of erosion is given by the reciprocal of the slope of correlating line, Figure 7-4, divided by the eroded area, if we assume that the erosion strengths for these materials are identically the same as their strain energies. The same group of materials, or one among this group, or an entirely new group such as the one used by Young and Johnston (111), Figure 7-10, may be used to determine the intensity of erosion of a given

test device under a set of test conditions. We may call this procedure the calibration of the test device, wherein we obtain the numerical value of the intensity of erosion of the screening test. Once such a calibration is accomplished, the erosion strength of any material may be experimentally determined by measuring the rate of depth of erosion with this calibrated test device from Equation [6-4]. This procedure is feasible with any type of erosion, whether it is cavitation, liquid-impact, or solid-impact. It may even be extended to wear of materials due to friction.

g. Relative Erosion Resistance

Another approach to characterizing erosion resistance as a property in its own right is to compare the relative resistance of materials with a "standard" material. In the field of cavitation erosion, such attempts have been made over the years. For example, Beeching (12) during the period 1937 to 1942 used a material called admiralty propeller bronze as a standard material and tabulated his "figure of merit" for 25 alloys. More recently, Heymann (117, 118) has suggested a similar scale called "normalized erosion resistance" which is scaled relative to 18-8 stainless steel (170 DPH hardness) (Figure 7-12). This approach is quite useful in material selection for practical designs.

However, the advantage of using an erosion strength scale (in preference to a figure of merit scale) is that the strength

(force per unit area) multiplied by the rate of depth of erosion (length per unit time) will give an intensity scale (power per unit area) which can be used in a chart such as the one shown in Figure 7-13. In addition, it may be helpful in theoretical developments. In related fields such as metal cutting (119) and rock drilling (120), it is called specific work or energy (work required to remove a unit volume of material).

Metallurgical Aspects

The foregoing discussion highlighted the relation between mechanical properties of metals and their resistance to erosion. However, the mechanical properties as well as the resistance depend on the metallurgical structure of the metals and alloys. Both macroscopic aspects such as grain size, orientation and boundaries and microscopic factors such as the lattice structure, phase distribution and phase transformation all play important roles. Several investigators have noted the increase in erosion resistance with decreasing grain size (67, 11, 121). Mousson's (67) results (Table 7-5) show that nonferrous alloys (brasses), which have almost the same mechanical properties, hardness, yield strength and hardenability, possess considerably different erosion resistances.

According to Mousson (67), inclusions in the form of impurities or undissolved alloy constituents tend to affect erosion resistance. Adding sulphur to a stainless steel to improve its machinability adversely affects its erosion resistance. Similar

effects were observed in forged stainless steels. Presence of free graphite is cited as one of the reasons for the poor erosion resistance of cast iron (67). Mousson observed increased resistance to damage (Table 7-6) by successive additions of molybdenum and nickel to chromium stainless steels. The primary effect was associated with decreasing grain sizes obtained with the addition of these alloying constituents.

More recently, Gould (112, 113) used electron microscopy to follow the various stages of erosion. He found that the cobalt alloy Stellite 6B has a steady state rate of volume loss an order of magnitude less than many titanium- and iron-based alloys of comparable hardness. He attributed this result to the fact that Stellite 6B and other cobalt alloys undergo a stress-induced phase transformation during cavitation erosion. Although it was well known that the face centered cubic (fcc) phase of stellite may transform to hexagonal closed pack (hcp) the work of Gould demonstrated a close association between the progress of cavitation erosion and the phase transformation. Woodford (72) followed this investigation further and found that transformable (fcc) alloys do have high erosion resistance relative to non-transformable (fcc) alloys. However, he concluded that, although many erosion resistant materials undergo a surface transformation during erosion, there is a lack of correlation between erosion resistance and any simple quantitative measure of transformation.

Criteria for the Threshold of Erosion

Boettcher (63) as early as 1936 realized the importance of surface fatigue due to repeated bubble collapse. Later Mueller (122) suggested the possibility of a threshold velocity of erosion for each material, similar to the fatigue limit. Beeching (12) understood the importance of corrosive environments in such repeated stressing and suggested the possibility of corrosion fatigue. It is becoming increasingly common to observe a threshold parameter such as the threshold intensity of cavitation erosion, the threshold amplitude of oscillation, the threshold velocity of flow, the threshold impact velocity, and so forth, in erosion problems such as cavitation erosion, steam erosion, rain erosion and sand erosion.

An understanding of the threshold conditions wherein the impact stresses reach a limiting value just sufficient to initiate detectable erosion is important in the selection of materials for erosion free systems. The difference between the prediction of threshold of erosion and erosion rate is schematically illustrated in Figure 7-14. According to this figure one can arrive at two types of problems. The first one is the understanding of the threshold conditions wherein the impact stresses reach a limiting value just sufficient to initiate detectable erosion either at the first blow or after repetitive blows. The second problem is the prediction of the amount of erosion if the erosive forces are above the threshold for the material.

There have been some recent investigations twoard establishing threshold criteria for designs (108, 52). In the case of liquid impact erosion, one could estimate the impact stresses on the material and relate these stresses to some material properties. For example, the dynamic stress caused by a cylindrical liquid column impinging on a material produces a dynamic stress (108), given by

$$\sigma_I = \frac{\rho_\ell C_\ell U_I}{1 + \frac{\rho_\ell C_\ell}{\rho_m C_m}}$$

where

σ_I = the impact stress,

U_I = the impact velocity,

ρ_ℓ = the density of liquid,

ρ_m = the density of material,

C_ℓ = the sound speed in liquid, and

C_m = the sound speed in material.

For most practical cases of liquids and materials involved, the ratio $\rho_\ell C_\ell / \rho_m C_m$ is small, and may be neglected; in which case the impact stress becomes

$$\sigma_I \cong \rho_\ell C_\ell U_I$$

Table 7-7 shows that the dynamic yield strength and the fatigue endurance limit of various materials are closely related to the threshold impact stress. More recently investigations by Thiruvengadam, et al (52), using a liquid impact erosion facility and a high frequency fatigue technique (123, 124) have shown that there is close correlation between the fatigue strength and calculated threshold impact stress. For example, Figure 7-15 shows the relationship between the impact velocity and number of impacts at which visible erosion is observed (52). The threshold impact stresses were calculated for each velocity for the data shown in Figure 7-15. The impact stresses were multiplied by a constant factor for each material (for example, by three for nickel) and plotted as a function of number of impacts in Figure 7-16. In the same figure, the high frequency fatigue stresses are also plotted as a function of number of cycles to failure. This lends support to the early speculations of Boettcher (63) and Mueller (122) that fatigue failure of the surface particles is the primary mechanism of erosion. This sort of correlation for candidate materials would provide engineering data for designs.

In the case of cavitation erosion, an attempt was made to relate the threshold velocity of erosion in a rotating disk apparatus with the yield strength of materials (61) as shown in Figure 7-17. The ratio between the yield strength and the hydrodynamic pressure was found to be linearly proportional to the cavitation inception parameter (Figure 7-18). The relationship

is easily understood from the analysis of hydrodynamic parameters discussed in the following chapter.

More recently (125), the definition of intensity of erosion was used instead of the threshold velocity. Using a vibratory cavitation erosion apparatus, the intensity of erosion was determined as a function of amplitude of vibration (126). In the steady state erosion period, the cavitation erosion is proportional to the square of the displacement amplitude. Furthermore, these experiments showed that there is a minimum displacement amplitude for each metal below which there will be no cavitation erosion. This minimum amplitude is called the threshold amplitude and the corresponding intensity of erosion is designated as the threshold intensity of erosion. The threshold intensity of erosion for six metals is shown in Figure 7-19, as a function of the high frequency fatigue strength at one billion cycles. The datum for SAE 1020 steel shows the influence of corrosion on the threshold intensity of erosion.

PROTECTIVE COATINGS

Protection against cavitation erosion may be considered from several points of view: a) elimination of the problem at the source by hydrodynamic design --- model tests are important in this case; b) use of highly resistant materials in zones of expected cavitation attack; c) use of artificial means such as cathodic protection and air injection. In the past, several repair procedures and protection methods have been highly successful in some cases, while the same methods were not so successful

in other situations. An important example is the use of elastomeric coatings to protect marine systems against corrosion as well as cavitation erosion.

The superior erosion resistance of elastomeric coatings is illustrated in Figures 7-20 and 7-21. In a rotating disk screening test, common propeller materials such as manganese bronze, manganese nickel bronze and nickel aluminum bronze erode at a rate of about 1/16-inch in 72 hours at a speed of 150 fps (Figure 7-20). This corresponds to an erosion rate of 8 ipy. At the same intensity of erosion of the rotating disk screening test, elastomeric coatings such as neoprene offer remarkable erosion resistance as shown in Figure 7-21. This figure shows the performance of neoprene coating at 150 fps after 72 hours of exposure in the rotating disk apparatus (127, 128).

Although elastomeric coatings offer excellent resistance to erosion in a laboratory screening test, their success in service applications is rather limited. Some coating systems behaved extremely well in the screening test at relatively higher velocities, whereas the same coating system failed rapidly in field applications at much lower velocities (Figure 7-22). Adhesion failure of these coatings in service is still a mysterious problem. Considerable effort has been spent in screening elastomeric coatings for hydrofoil applications (128); however, further basic research is necessary to understand how these coatings respond to the dynamic pressures created by the cavitation bubble collapse and how they fail to adhere to the substrate. Understanding

of the mechanism of adhesion failures and the development of coating systems with adequate adhesion strength will eventually enhance the operating life of hydrodynamic systems to a great extent

Mechanism of Cavitation Erosion in Viscoelastic Materials

The behavior of the viscoelastic materials depends upon their response to the repeated dynamic indenting forces produced by the collapse energy of the cavitation bubbles and the cumulative absorption of this energy by the material in each cycle (Figure 7-23). Since the dynamic response of these materials is different from that of metals, the mode of damage in these materials needs some further explanation. The following mechanism was given by Chatten and Thiruvengadam (129) for viscoelastic materials. The initiation of failure in an elastomeric material may take place along the grain direction as shown in Figure 7-24 in contrast to the dents produced in lead as shown in Figure 7-25. Figures 7-26 and 7-27 further suggest that the propagation of tear, due to continued accumulation of energy, may result in gross removal of relatively large pieces, especially if the adhesive bond to the substrate material is marginal. When the adhesive bond to the substrate is adequate, the material may be torn away in small particles. It appears that the energy of tear propagation is the primary factor controlling the mechanism of cavitation damage in viscoelastic materials. This hypothesis is based on observations of cavitation damage of elastomeric coatings both in laboratory tests and in field trials on ships' underwater appendages.

Since the energy transfer to the viscoelastic material from the cavitation bubble collapse is a repeated process, the tearing mechanism may take place in either of two ways: (a) if the time for one cycle, i.e., the duration between two consecutive stress pulses, is less than the relaxation time of the material, then it behaves like a brittle material producing conchoidal fracture in some cases. Lichtman (130) photographed this type of failure in an epoxy-polysulfide compound, Figure 7-27; (b) if, however, the time for one cycle is greater (lower frequency) than the relaxation time of the viscoelastic material, then the energy of collapse transmitted to the material is partly released (elastically) and partly dissipated and absorbed or conducted as heat. Still there always remains a residual strain energy and this strain energy will be accumulated in the material. When this accumulated energy exceeds the energy of tear propagation, the material fails by tearing.

Rheingans (68) tested a thiokol rubber compound using a magnetrostriction apparatus and showed that the compound exhibited high resistance to cavitation erosion. Kerr and Leith (131) conducted a few additional experiments with neoprene coatings. Extensive data on the relative resistance of viscoelastic coating materials have been accumulated and published by the U. S. Navy Applied Science Laboratory (128, 87, 132). Coatings tested by Lichtman, et al, at the above laboratory include neoprene, urethane, polyurethane, polysulphide, polysiloxane, and Hypalon. These coatings have been classified into three orders of merit.

Table 7-8 shows the mechanical properties of the coatings possessing the first order of merit. Figure 7-28 shows a few typical coatings possessing the first order of merit performance. Similarly Tables 7-9 and 7-10 show the second and third order of merit coatings while Figures 7-29 and 7-30 show the typical performance of these types of coatings.

Based on these investigations, elastomeric compounds may be screened as possible erosion resistant materials for service in a cavitating environment by evaluating their physical properties.

Physical Properties

a. Tear Strength

To illustrate the relative importance of the various properties, Chatten and Thiruvengadam (129) tested six compounds specifically designed to exhibit some properties as maximum and some others as minimum. They found significant correlation between the tear strength of the polymer material and the volume loss due to cavitation erosion for two velocities, Figure 7-31. According to the mechanism outlined earlier, the energy absorbed by the material which produces the volume loss should be inversely proportional to the tear propagation energy; this was supported by data as shown in Figure 7-31.

b. Strain Energy

Further, it is known that the area under the stress-strain curve (strain energy or rupture energy) is proportional to the tear propagation energy (tear "strength") required

to create the new surface (133). The tear propagation energy is determined by twice the force necessary to initiate tearing, divided by the film thickness and therefore has the dimension of energy per unit area (134). The relationship between tear energy and the strain energy as experimentally obtained by Chatten and Thiruvengadam (129), for six compounds mentioned earlier (Figure 7-32). As in the case of metallic materials, the strain energy is also a significant parameter for visco-elastic coatings.

c. Ultimate Tensile Strength

The correlation between ultimate tensile strength and the cavitation damage resistance of elastomers was found to be somewhat less significant (129). However, coatings with higher ultimate tensile strength generally exhibit better damage resistance. This same view is expressed by Lichtman and others (87).

d. Ultimate Elongation

No satisfactory correlation could be established between ultimate elongation and cavitation damage resistance (129). This finding is confirmed by Kallas and Lichtman (128), who cited the poor performance of the caulking type polysulfide.

e. Elasticity and Hysteresis

Chatten and Thiruvengadam (129) state that many elastomeric materials are much more resistant than metals even though they exhibit markedly lower strain energies. They

attribute this behavior to the viscoelastic nature of the former materials, particularly their resistance to the repeated dynamic indenting forces produced by the collapse energy, and by the lower rate of cumulative absorption of strain energy. Lichtman, et al (87), observed that the highly damage-resistant elastomeric coatings have generally low hysteresis as indicated by the almost complete recovery of these materials after hardness indentation tests.

Dynamic Response and Adhesion Failure of Protective Coatings

Although considerable effort has been spent in screening elastomeric coatings and in developing erosion resistant coatings that exhibit an order of magnitude superior erosion resistance in the laboratory test at relatively more severe erosion conditions, service applications of these coatings have not been very successful (127). The primary reason is that the adhesion failure of the protective coatings precedes the erosion failure in many service applications (128). Some recent investigations on the phenomenon of adhesion failure of coatings have emphasized the importance of the dynamic response of elastomeric coatings, consisting of a coating, adhesive, and substrate. The collapse of a bubble on a layered medium (Figure 7-33) sets into action a complex sequence of stress wave propagation, reflection, and interaction. The study and understanding of these events, depicted schematically in Figure 7-33, was initiated by Thiruvengadam during the sixties and much progress has been made since then by Conn (135, 136, 137). As a result of these studies, fundamental understanding of the failure mechanisms has been achieved.

An apparatus called the split Hopkinson pressure bar was used to study several candidate coating materials. The technique is based on the measurement of the elastic strain waves transmitted through a system consisting of two long pressure bars which have a test specimen sandwiched between them. A schematic of this configuration is given in Figure 7-34. A projectile impacts the first elastic bar, known as the input bar, creating the incident strain pulse, ϵ_I. Upon reaching the specimen, this incident pulse is partially reflected, as shown by ϵ_R in Figure 7-34. The second pressure bar, the output bar, receives a transmitted strain pulse, ϵ_T. Each strain wave component is measured by strain gages placed fore and aft of the specimen. From the two strain-time histories recorded by these gages, the strain, stress and strain rate in the test specimen can be calculated.

Assuming negligible radial inertia forces in the specimen, and with a small coefficient of friction between the faces of the specimen and load bars, it can be shown that the following relationships may be used:

$$\sigma_s = \frac{EA}{2A_s} (\epsilon_I - \epsilon_R + \epsilon_T)$$

$$\epsilon_s = \frac{c_o}{L_s} \int_o^t (\epsilon_I + \epsilon_R - \epsilon_T)\, dt$$

$$\dot{\epsilon}_s = \frac{c_o}{L_s} (\epsilon_I + \epsilon_R - \epsilon_T)$$

where

σ_s = average stress in specimen,

ϵ_s = average strain in specimen,

$\dot{\epsilon}_s$ = average strain rate in specimen,

L_s = original length of specimen,

A_s = original area of cross section of specimen,

A = area of cross section of pressure bars,

E = elastic modulus of pressure bars,

c_o = elastic bar velocity in pressure bars, and

t = time.

In these equations all signs relating to tension, compression, and wave directions have been accounted for, so that absolute values of each strain wave component may be used.

An overall view of the HYDRONAUTICS, Incorporated split Hopkinson pressure bar facility is shown in Figure 7-35. The components shown in this figure include the air gun with pressure chamber and barrel, the furnace chamber, two oscilloscopes with their associated plug-in units for signal amplifications and integration, cameras, and the velocity measuring system consisting of a photoelectric velocity measuring unit and time interval counter. A schematic of the apparatus is seen in Figure 7-36.

The air gun used to accelerate the cylindrical projectiles has a 104-in.-long barrel with a 0.4975-in.-bore diameter.

Operating pressures up to 100 psi may be used. A typical projectile, made of either aluminum or titanium alloy, is 10-in. long, with a slightly rounded impact face to minimize undesirable elastic vibrations in the pressure bars. The furnace chamber may be used to heat the specimen and pressure bars up to 500°F. for measurement of dynamic property variations due to elevated temperature. Each set of pressure bars was made of the same material as the projectiles, either 7075-T6 aluminum alloy or Ti-7Al-4Mo titanium alloy. The pressure bars were 30-in. long and 0.500-in. in diameter. The bars were supported on pairs of teflon holders and could move freely in the axial direction.

Strain versus time histories in the pressure bars were obtained from foil strain gages, mounted in pairs on each bar at positions 14-in. from the ends which contact the test specimen. The gages were placed in series to cancel voltage changes due to flexural strain components, and operated in a potentiometer-type dynamic circuit, with calibration provided by an electronic chopper and precision calibration resistors.

Two Tektronix Type 561A oscilloscopes were used to display the strain gage output signals. The test traces were photographed with Type K-5 Oscillotron cameras with Polaroid film pack backs. The oscilloscopes were operated in the single sweep mode and were triggered externally when the projectile struck the input bar.

Making use of this apparatus, Conn and his coworkers (136, 137) have experimentally determined the stress-strain relationships at high strain rate compressive loadings for several elastomeric coating materials. Typical curves for the highly resistant coatings such as neoprene and polyurethane are shown in Figure 7-37. A few other materials commonly used in erosion research are also compared in Figure 7-38 (136). Such high strain rate data led to the realistic prediction of impact stresses encountered by different materials during raindrop collision (Figures 7-39 and 7-40). These investigations also highlighted the important role played by the dynamic impedance of different materials in erosion phenomenon; such a role was foreseen by Thiruvengadam as early as 1964. Conn (137) for the first time correlated several rain erosion screening test data with the dynamic stress data and the high frequency fatigue results as shown in Figure 7-41. Figure 7-42 shows an experimental demonstration of the applicability of the uniaxial stress, elastic-plastic stress wave theory to describe rain erosion observations. Morris (138) has tried to make calculations based on shock wave theory (uniaxial strain theory), which predicts stresses in a coated substrate that are larger than the stresses predicted for direct water impact on bare substrate. Conn's work has shown that the use of shock wave theory may not lead to realistic understanding of practical failure problems at currently encountered speeds whereas it may be useful at higher impact velocities. A practical and useful correlation between the

impact velocity and the number of impacts to failure for two polyurethane materials has been made by Conn and Rudy (137) as shown in Figure 7-43.

The investigations currently carried out by Conn and his coworkers, Springer and Baxi (139) and Engle and coworkers (140) would hopefully lead to meet the following primary long range objectives:

a. To understand the dynamic response of the best available erosion resistant coatings and to learn the parameters that give rise to the resistance of the impact forces.

b. To analyze the stress wave (shock wave) propagation and reflection in a coating-adhesive-substrate system as a whole and to derive improved theories to predict the dynamic failures in practical coating systems.

c. To predict the desirable parameters of any future coating systems and to guide the development of such coatings.

Stability in a Marine Environment

All the properties discussed above, including adhesion, tend to deteriorate in a marine environment. Hence, it is essential to understand the behavior of a coating system in a long term marine operation even if the coating system has been successful in a laboratory test. This aspect will be again emphasized when we discuss service trials.

Structural Plastics

In spite of their high tensile strengths, the structural plastics (such as Fiberglas) behave poorly in terms of cavitation erosion resistance (141). Lichtman, et al (141), attribute this behavior to their very low ultimate elongation. One possible exception is the case of pressure molded nylon which behaved as well as the elastomeric coatings. Table 7-11 shows the order of merit of a few structural plastics tested at the U. S. Navy Applied Science Laboratory (132, 141) along with their mechanical properties. Figure 7-44 shows a pictorial rating of this order of merit.

CERAMICS (POROUS VITREOUS AND CRYSTALLINE MATERIALS AND AGGRAGATES)

One of the early experiments conducted by Föttinger (9) showed that even glass can be eroded by cavitation. This was used as a good argument against the purely electrochemical hypothesis of damage. However, it is only very recently that some systematic studies of cavitation damage on ceramic materials have been started.

Concrete

Price and Wallace (142) concluded that while compressive strength of concrete is the primary property representing cavitation erosion resistance, even the best concrete will not resist the forces of cavitation for prolonged periods. Thiruvengadam (143) also confirmed that the most significant property controlling cavitation damage was the compressive strength, Figure 7-45. However, even concrete has a certain minimum intensity of damage below

which it will be strong enough to withstand the forces of bubble collapse.

Stone

It has been found that compressive strength of stones again is a significant property to represent cavitation damage resistance (143). Polishing the stones had a marked effect in reducing initial damage. However, polishing affords only a temporary remedy (143).

Inorganic Coatings and Paints

Lichtman and Weingram (132) also studied the behavior of inorganic coatings and paints. Unfused ceramic and metallic coatings have relatively low cavitation erosion resistance. They state that this is probably due to the heterogeneity of the coating as contrasted to fused coatings (glasses and fused metallics). They found that the hardness of the coatings was an important parameter. Table 7-12 lists some of the non-elastomeric coatings tested at the U. S. Navy Applied Science Laboratory (128, 132), their properties, and their order of merit of cavitation damage resistance. Figure 7-46 gives a qualitative picture of this order of merit.

Electroplating and Anodizing

Electroplated nickel, chromium, and platinum offer substantial resistance both to corrosion and erosion. Stainless steel and Stellite overlays have also been used occasionally to protect against cavitation erosion (144). Anodizing seems to improve the life of components made of aluminum alloys.

VIII. RELATION BETWEEN HYDRODYNAMIC PARAMETERS AND CAVITATION EROSION INTENSITY

So far we have discussed the general principles of cavitation, its effects, mechanisms of erosion, and material response. An important consideration in all of these aspects is the dynamics of the bubble, its growth and collapse. Since the recognition and identification of cavitation as a serious problem, much effort has been devoted to these areas. Most significant among them are the early investigations of Rayleigh (7). More recently, Plesset and coworkers (15, 56, 145) and Hammitt and coworkers (38, 40, 146) have considered various aspects of bubble dynamics extensively. Increasing attention is being paid to the asymmetrical collapse of the bubble first pointed out by Kornfeld and Suvorov (147) and Eisenberg (2, 14). Naude and Ellis (50) demonstrated experimentally for the first time that such an asymmetrical collapse produced high speed jets which could deform the metal. Following them, several investigators [Shutler and Mesler (148), Hammitt (146), Benjamin and Ellis (53), and Tulin (54)] have made contributions. Excellent review of all aspects of bubble collapse have been made by Daily, Hammitt, and Knapp (38) and Eisenberg (48).

Much effort has been devoted to understanding the various aspects of bubble dynamics, the mechanism of material removal, the interaction of various physical and chemical properties of the liquid and the relative performance of materials. However, only recently has there been encouraging progress made in the

important task of converting the basic research into practical data which will benefit the designer. Knapp (60, 65) made the pioneering effort to relate laboratory experiments with field results. He realized the importance of defining the intensity of erosion in such an attempt and remarked as follows (65): "However, at this point, the investigator finds himself on the brink of an abyss gazing out over completely unknown territory since no satisfactory method has been developed for measuring the absolute intensity of cavitation, either in the laboratory or in the field...Future work on the relative resistance of materials to damage should be correlated with studies of mechanics of damage. An important step would be the development of a definition of intensity of cavitation and some rational measure of it which could be used both in hydraulic machines and structures and in equipment employed for determining relative resistance."

Knapp measured the number of pits per unit area per unit time on an ogive body made of soft annealed aluminum at various speeds in a water tunnel (Figure 8-1). He found that the number of pits per unit area per unit time (which he called the intensity) varied as the sixth power of the velocity at a selected cavitation parameter. He compared these laboratory data with his measurements in a full scale hydraulic turbine operating in the field and discovered that the field measurements at one velocity agreed well with his laboratory measurements at the same velocity in spite of the different geometry and size of the

field system (Figure 8-1). From these investigations, Knapp concluded that the intensity is solely a function of speed and does not depend upon the size or shape of the flow system.

Following Knapp, Kerr and Rosenberg (103) measured the decay of a radioactive paint in an actual turbine and found it to vary as the sixth power of the velocity. Rasmussen (86) measured the erosion produced on a circular cylinder placed in the throat of a two-dimensional venturi (the axis of the circular cylinder was normal to the direction of flow). He found that the rate of erosion increased with increasing velocity, reached a maximum and then decreased with further increases in velocity. In the same paper (86) he described another set of experiments in a rotating disk apparatus. Circular holes were drilled in a disk and rotated in a chamber containing water. Rasmussen found that the rate of erosion increased linearly with the peripheral speed. Recently, Thiruvengadam (149) found that the rate of erosion behind a circular hole on a rotating disk depended on the peripheral speed as shown in Figure 8-2. In contrast to most of the previous investigators' results, the rate of erosion increased with velocity to a maximum and then decreased with increasing velocity. Wood, et al (150), observed that the relationship between the rate of erosion and the velocity was not unique. The significant point in all of these experiments is that these investigators failed to consider the effect of the cavitation parameter on erosion. The cavitation parameter was an uncontrolled variable.

The first systematic attempt to study the effect of cavitation parameter on erosion was made by Shalnev (151). Using a circular cylinder with its axis normal to the direction of flow in a two-dimensional venturi, Shalnev found that the rate of erosion on lead depended very much on the cavitation parameter (Figure 8-3). His use of lead as the test material was questionable because of its tendency to flow and deform excessively before being removed from the surface. These results were further confirmed by Thiruvengadam using aluminum as the test material (61).

Kohl (89) conducted extensive experiments at speeds ranging from 100 fps to 500 fps using a high speed cavitating jet in connection with the development of a rock drill utilizing cavitation erosion. Kohl found that there was an optimum distance between the nozzle and the specimen at which the erosion was a maximum.

The maximum intensities of erosion observed by these various investigators using different geometrical systems at different velocities are shown plotted against the corresponding velocities in Figure 8-4. The rate of depth of erosion was measured and reported by each of these investigators in the respective references shown in Figure 8-4. The erosion strength of soft annealed lead used by Shalnev was assumed to be 500 psi. The soft annealed aluminum used by Rasmussen, Thiruvengadam and Kohl was assumed to be 2000 psi. The solid line in Figure 8-4 is the sixth power line. It is indeed very interesting that the

maximum intensity of erosion varies as the sixth power of the velocity according to the data of these particular investigators. However, there were several questions that arose in connection with this important result. The data of Wood, et al (150), Shalnev (151) and Thiruvengadam (149) questioned the sixth power law. Moreover, the conclusion that the intensity of erosion is independent of the size and shape of the flow system needed further experimental verification.

The rotating foil apparatus fully described in Chapter VI was specifically developed for these studies. Figure 6-5 shows an overall view of this facility. Systematic experiments were conducted on NACA 16-021 hydrofoils using this apparatus. Two sizes of the foil (3 inches and 1½ inches in chord length) were tested. The rate of erosion was determined as a function of exposure time for each set of test conditions, lasting over cumulative exposure periods ranging from 10 hours to 70 hours depending upon the intensity of erosion. A typical plot of rate of erosion as a function of exposure period is shown in Figure 8-5. Both velocity and pressure were varied independently; these experimental results have been reported in References 152 and 153.

These investigations clearly established that the rate of erosion depended greatly on the exposure time, clarifying some of the controversies on this aspect of the phenomenon (154). There was an incubation period during which there was no measurable weight loss. Following the incubation period, there was a period of accelerating erosion rates. After reaching a

maximum value, the rate of erosion decreased with a tendency toward a steady state. The maximum rate of erosion was highly dependent on the cavitation number at a given velocity. The erosion rate increased with decreasing cavitation number, reached a maximum value and then decreased with further reduction in the value of cavitation number as shown in Figure 8-6. The intensity of erosion represented by the ordinate of this figure is given by

$$I_e = \frac{\Delta y}{\Delta t} S_e \qquad [7\text{-}1]$$

where Δy is the average depth of erosion over the eroded area in a given exposure interval of Δt, and S_e is the erosion strength (108).

The results shown in Figure 8-6 demonstrate that the intensity of cavitation erosion depends upon the velocity and the size of the foil in addition to the cavitation number. For example, the three inch foil at 175 fps has a peak intensity of 1.2 w/m^2 which occurs at a cavitation number of 0.30; whereas the peak intensity is only 0.6 w/m^2 at a cavitation number of 0.36, for the 1½ inch foil at the same velocity. The maximum rates corresponding to the optimum cavitation numbers are plotted against velocity in Figure 8-7. The solid line in this figure corresponds to Knapp's sixth power law. An understanding of these results is very crucial in the overall objective of solving erosion problems in service.

As discussed previously in this handbook, the understanding of the roles played by the hydrodynamic parameters becomes increasingly important as a result of recent experiences with full scale naval craft; in these instances, the erosion intensity was so severe that no known protection method could withstand the erosion intensity (127). This necessitated hydrodynamic redesign and better operational procedures. These experiences brought forth the desirability of developing modeling techniques to predict erosion intensities.

However, the feasibility of such model tests depends both upon economic aspects and technical considerations. For example, the cost of the test facility depends upon its size, which in turn governs the auxiliary machinery components such as pump and motor. Model size and test speed determine the capacity and cost of these components. Similarly, operating costs are governed by testing time and model costs.

In technical terms, the feasibility of model testing depends upon the knowledge of the following three important scaling parameters in addition to several other considerations: i) time scale, ii) velocity scale, and iii) size scale. The technical considerations dealing with these scales are discussed in the following sections.

SELECTION OF MODELING MATERIALS TO SCALE LONG TERM EROSION OF PROTOTYPE COMPONENTS

Usually prototype components are required to operate erosion free for a long time, typically in the range of thousands of

hours. However, model tests must necessarily simulate such long term erosion in a shorter time in the laboratory test. This makes it essential to develop scaling techniques with which one could shorten the test duration for the model test.

It is now well established that the rate of erosion is a non-linear function of the exposure time. It was known to hydraulic engineers that cavitation erosion decreased with repeated exposure of the hydraulic structures to floods (155). Thiruvengadam (143, 61) noticed the decreasing trend in erosion with continued exposure. Hobbs (156) as early as 1962 reported this effect. Investigators (157) working on the problem of steam erosion noticed the non-linear dependency with exposure time as early as 1957. These evidences led Thiruvengadam and his co-workers (126, 153, 98) to conduct a series of systematic experiments on these effects. The essential conclusion was that is is important to consider these effects both in comparing different materials and in extrapolating the laboratory experience to field systems. These studies stimulated an intensified research activity in this area. Hobbs (114), Plesset and Devine (154), Heymann (158), Hammitt and his co-workers (159), Ripken (160), Rao, et al (161), Tichler (162), and Canavelis (163) among others have made significant contributions in understanding the various aspects of this phenomenon.

The erosion history may be divided into four periods*, Figure 8-8, as follows:

1. Incubation period
2. Acceleration period
3. Deceleration period
4. Steady period

Several exceptions to this general trend are reported in the literature. For example, Hammitt and Garcia (159) reported that there are in fact two acceleration periods in some cases. Hobbs (114) found that there is a steady period in between the acceleration period and the deceleration period. The experiments on 4340 steel by Plesset and Devine (154) as well as the experiments by Tichler (162) on chromium steel show that this is indeed the case. However, in all of the vibratory experiments using a wide range of materials** (including 1100-F aluminum, 2024 aluminum, tobin bronze, commercially pure nickel, monel, 316 stainless steel and SAE 1020 steel) a truly steady period was not found in between the acceleration and deceleration periods (126). This is also true in experiments with liquid sodium at various temperatures (164). For some stronger materials such as 316 stainless steel and 4340 steel, the transition from the

*These terms correspond to the recently developed definitions by the ASTM Sub-Committee headed by Dr. Robert Hickling.

**It is important to note that these materials include two pure metals, one carbon steel, one stainless steel and three different alloys.

acceleration period to the deceleration period takes place over a longer time interval and one could approximate it to be a steady period for the purpose of analyses.

Except for these variations, it is now generally accepted by most investigators that these effects are indeed true and important. Figure 8-9 shows a log-log plot of erosion rates versus exposure periods for several materials. According to this figure, the erosion rates as well as the exposure times to cover all four periods vary over two orders of magnitude. If we include more resistant materials such as stellites, then the range of erosion rates and erosion times would vary over three orders of magnitude as pointed out by Heymann (117).

If the relationship between various materials during the four erosion periods, extending over such a wide range, can be quantitatively established, then it is indeed possible to conduct experiments in the laboratory in a shorter period of time using a weaker material and to infer the behavior of more resistant material in the field. This is precisely the objective of this section. An attempt has been made to use the erosion theory recently developed by Thiruvengadam (165, 168) to accomplish this objective. The usefulness as well as the limitations of this approach are also discussed.

CORRELATION OF EXPERIMENTAL DATA WITH THE ELEMENTARY THEORY

The experimental data shown in Figure 8-9 are all reduced in a non-dimensional form first introduced by the author in

1967 (165). The experimentally determined erosion rate (in any form such as rate of weight loss, rate of volume loss, and rate of mean depth of erosion) is divided by the peak rate of erosion to get the relative rate of erosion. The relative rate of erosion is the same as the relative intensity of erosion if we assume that the area of erosion as well as the erosion strength of the material remains constant during a given test. Even if one does not believe in any theory, this non-dimensional plot is physically significant since one can compare the relative behavior of different materials at a given intensity of erosion as well as the behavior of the same material at different intensities. The discussion by Hammitt and Garcia (159) contains an idea similar to this. This is an important step toward quantitative correlations. The relative erosion rate is plotted against the relative exposure time in Figure 8-10. The relative exposure time is obtained by dividing the exposure time by the characteristic time, t_1, corresponding to the peak rate.

There is a certain amount of subjective decision involved in selecting the peak erosion rate and the characteristic time. However, standard numerical techniques with the aid of modern computers may be used in determining the erosion rates more rationally. One such method* is the five point averaging technique described by Hildebrand (166) which leads to a more objective determination of the peak rate and the characteristic exposure time.

*The author is grateful to Dr. A. F. Conn of HYDRONAUTICS, Incorporated for suggesting this method.

Figure 8-10 shows that the relationship between the relative erosion rate (and, hence the relative intensity of erosion) and the relative exposure time is very nearly the same for all the materials considered in this study. For example, the erosion rates on all these materials would reduce to almost 40 percent of the peak rate after exposing them for a relative exposure time of about five. If we can relate the peak rates and the corresponding exposure times for a modeling material as well as the prototype material, then we will be able to estimate the performance of the prototype material from the behavior of the modeling material at a corresponding intensity of erosion. More than anything else, this is where we need a quantitative theory that would correlate with experimental data as shown in Figure 8-10.

There have been several attempts to explain the erosion history quantitatively, the foremost being that of Heymann (158) followed by Thiruvengadam (165) and Mok (167). For the purpose of this book, we will make use of the elementary theory developed by Thiruvengadam (165). In this theory, the intensity of erosion is defined as

$$I_e = S_e \frac{dr}{dt} \qquad [8\text{-}1]$$

where

I_e = the intensity of erosion,

$\frac{dr}{dt}$ = the instantaneous rate of erosion, at any time, t,

S_e = is the erosion strength, and

r = the mean depth of erosion as measured from the original surface of the material. Furthermore, the following two assumptions are made:

The intensity of impact on the surface is assumed as

$$I_i = \frac{A^n I_c}{(r + r_c)^n} \qquad [8\text{-}2]$$

where

I_i = the intensity of impact,

I_c = the intensity of collapse or collision,

A = a proportionality constant, with dimension of length,

n = the attenuation exponent, and

r_c = the distance between the original surface of material and the center of bubble.

The second assumption is

$$I_e = \eta I_i \qquad [8\text{-}3]$$

where η is a material property governing the efficiency of energy absorption and varies with the exposure time. Combining Equations [8-1], [8-2], and [8-3], we can derive the differential equation of erosion

$$\frac{dI_e}{dt} + \frac{KI_e^{(2n+1)/n}}{(\eta)^{1/n}} - \frac{I_e}{\eta}\frac{d\eta}{dt} = 0 \qquad [8\text{-}4]$$

where

$$K = \frac{n}{S_e(A^n I_c)^{1/n}} \qquad [8\text{-}5]$$

This equation can be normalized with respect to the parameters corresponding to the maximum intensity of erosion.

At $t - t_1$; (t_1 is called the characteristic time.)

$$\begin{cases} I_e = I_{max} \\ \dfrac{dI_e}{dt} = 0 \\ \eta = \eta_1 \end{cases}$$

Then relative exposure time, $\tau = \dfrac{t}{t_1}$,

relative intensity of erosion, $\bar{I} = \dfrac{I}{I_{max}}$,

relative efficiency, $\eta = \eta/\eta_1$, and

relative rate of erosion $= \dfrac{\dot{r}}{\dot{r}_{max}}$

where the dot represents the derivative with respect to time.

Using these normalized values, Equation [8-4] becomes

$$\frac{d\bar{I}}{d\tau} + \frac{\bar{K}\,\bar{I}^{\frac{(2n+1)}{n}}}{(\bar{\eta})^{1/n}} - \frac{I}{\eta}\frac{d\bar{\eta}}{d\tau} = 0 \qquad [8\text{-}6]$$

where

$$\bar{K} = \frac{K\, I_{max}^{\frac{n+1}{n}}\, t_1}{(\eta_1)^{1/n}} = \frac{d\bar{\eta}}{d\tau} \quad \text{at } \tau = 1$$

The general solution of this normalized equation is given by

$$\bar{I} = \frac{\bar{\eta}}{\left[1 + 3/2\ \bar{K} \int_1^{\tau} \frac{\bar{\eta}}{\eta} d\tau\right]^{2/3}} \qquad [8\text{-}7]$$

where n = 2.

Again if we assume that η is of the Weibull type of probability distribution functions, then

$$\eta = 1 - \exp\left[(-\tau)^{\alpha}\right] \qquad [8\text{-}8]$$

$$\eta_1 = \frac{e - 1}{e} = 0.635 \qquad [8\text{-}9]$$

$$\bar{\eta} = 1.58\ [1 - \exp\ (-\tau)^{\alpha}], \text{ and} \qquad [8\text{-}10]$$

$$\bar{K} = 0.58\alpha \qquad [8\text{-}11]$$

The cumulative depths of erosion at any exposure time may be derived as follows:

$$\bar{I} = \frac{I_e}{I_{max}} = \frac{S_e}{I_{max}} \cdot \frac{dr}{dt} \; ; \; I_{max} = S_e \cdot \left(\frac{dr}{dt}\right)_{max}$$

at $$t = t_1, \; r = r_1 \; ; \; \bar{r} = \frac{r}{r_1} \; ; \; \tau = \frac{t}{t_1} \; .$$

Then $$\bar{I} = \frac{S_e}{I_{max}} \frac{r_1}{t_1} \frac{d\bar{r}}{dt} \; , \text{ and}$$

$$\frac{S_e \; r_1}{I_{max} \; t_1} \bar{r} = \int_0^{\tau} \bar{I} \; d\tau \qquad [8\text{-}12]$$

Again at t_1, $\tau = 1$ and $\bar{r} = 1$

$$\frac{S_e \; r_1}{I_{max} \; t_1} = \int_0^{1} \bar{I} \; d\tau \qquad [8\text{-}13]$$

Then

$$\bar{r} = \frac{\int_0^{\tau} \bar{I} \; d\tau}{\int_0^{1} \bar{I} \; d\tau} \qquad [8\text{-}14]$$

Considering Equations [8-7] through [8-11], the function $\bar{I} \; d\tau$ is solely dependent on the shape parameter, α. The definite integral in Equation [8-13] is a constant for a given value of α.

$$\int_0^{\tau} \bar{I}\, d\tau = C_1(\alpha) \qquad [8\text{-}15]$$

The values of $C_1(\alpha)$ are shown in Figure 8-11.

Using Equations [8-5] and [8-8] through [8-11], we get

$$\frac{2}{(A^2 I_c)^{\frac{1}{2}} S_e} = \frac{I_{max}^{-3/2} \left(\frac{e-1}{e}\right)^{\frac{1}{2}} \alpha}{t_1 (e-1)} \qquad [8\text{-}16]$$

Simplifying and rearranging:

$$S_e = \frac{0.33\, A^2 I_c\, \alpha^2}{t_1^2 (\dot{r}_{max})^3} \quad , \text{ and}$$

$$\dot{r}_{max} = \frac{r_1}{t_1 C_1} \qquad [8\text{-}17]$$

Then $$S_e = \frac{0.33\, A^2 I_c\, \alpha^2 C_1^3\, t_1}{r_1^3} \qquad [8\text{-}18]$$

According to this theory, the erosion rates and the exposure times are also normalized with respect to the conditions at the peak rate of erosion. Equation [8-7] gives the relative intensity of erosion (and hence relative rate of erosion) as a function of the relative exposure time. Using a value of 2 for the attenuation exponent and assuming Weibull type

distributions* for the efficiency function, the relative intensity of erosion can be calculated. Figure 8-12 shows this relationship for various values of the shape parameter (165, 168). By inspection, it is found that the data in Figure 8-10 best fit the curve corresponding to the shape parameter, $\alpha = 1.5$.

Now that we have determined the value of α, we can proceed further to make use of the theoretical equations to determine the peak rates and the corresponding times. The relationship between the erosion strength and the other parameters is given by Equation [8-18]

where

α = the shape parameter,

C_1 = a constant given by Equation [8-15] and depends only on α,

r_1 = the cumulative mean depth of erosion corresponding to the peak rate of erosion,

t_1 = the exposure time corresponding to the peak rate of erosion and is called the characteristic time, and

$A^2 I_c$ = a constant for a given input intensity of erosion governed by the bubble collapse energy.

For practical purposes, let us assume that the value of the shape parameter is a constant for the materials considered in Figure

*The use of Weibull type distributions is questioned by Heymann both in private discussions and in the discussion of Reference (52) which contains complete details. It must be pointed out that this controversy does not limit the use of this theory for practical applications.

8-10. Later on we shall consider the variations in the shape parameter. From Equation [8-15], C_1 is solely a function of α and is a constant if α is a constant. According to the original assumption represented by Equation [8-2], the value of $A^2 I_c$ represents the intensity of the bubble cloud and is constant for a given test condition.

At this juncture, it is useful to review some of the experimental facts concerning the cumulative mean depth, r_1. Heymann (169) in 1965 reported the results of Hobbs at the National Engineering Laboratory and of Pearson at CEGB Marchwood Engineering Laboratories, both in the United Kingdom; the total volume loss per unit eroded area up to the start of the attenuation period was the same for all metals tested by them. In other words, the cumulative mean depth (which is total volume per unit eroded area divided by the density of the material) corresponding to the peak was a constant. This result seemed to be significant and indicated that a certain mean depth of erosion caused the attenuation in all the metals. An analysis of our results confirms the earlier British work. Table 8-1 shows that r_1 (the cumulative mean depth of erosion corresponding to the peak rates) for the seven materials considered in this paper remains constant with a maximum deviation of 13 percent. Based on these evidences, we can conclude that r_1 is a constant. Now then, the only variable in Equation [8-18] is the characteristic time, t_1. According to Equation [8-18], the characteristic time, t_1, should be directly proportional to the erosion strength, S_e.

The controversies about the erosion strength and the attempts to relate it with other mechanical properties were discussed in the previous chapter. Without going into these details again, it is adequate here to point out that the characteristic time, t_1, is somewhat related to the strain energy of these materials as shown in Figure 8-13. Each data point is enclosed in a shaded area which represents the scatter zone both for t_1 and for strain energy. Since both are experimental quantities, they do vary over a range represented by the shaded area. Figure 8-13 shows a general trend which is good enough for practical purposes. However, one may find a better correlation by taking into account the variations in the shape parameter, α. For example, the shape parameter for SAE 1020 steel is nearly 2 whereas that for 2024 aluminum is about 1. According to Equation [8-18], the erosion strength depends both on α^2 and on $C_1^3(\alpha)$. The functions $C_1(\alpha)$ and $\alpha^2 C_1^3(\alpha)$ are plotted in Figure 8-11.

These correlations do indicate that the strain energy is a good material parameter for at least a few commonly used materials. However, it may not be a unique property that represents the erosion resistance of all materials. In fact, it need not be. It is enough if it serves as the basis for a few calibrating materials. The same argument holds well for any other property such as ultimate resilience and tensile strength. The combination of mechanical properties will complicate the dimensional balance of the equations. With these few remarks,

let us leave it to the personal preference of the investigator to choose his scale for the erosion strength. Equation [8-18] lends itself to a free choice of the erosion strength which will determine the value of $A^2 I_c$ for given test equipment and test parameters.

MODEL-PROTOTYPE CORRELATIONS

In order to apply these ideas for correlating a model and its prototype, one would start testing the model material and the prototype material in a standard screening apparatus such as a vibrating apparatus. From such a test, the values of S_e, α and C_1 for both materials will be known. Then the model test may be carried out from which the values of r_1, t_1, and hence, $A^2 I_c$ can be determined. Since the model is supposed to simulate the cavitation environment, the value of $A^2 I_c$ would be the same both for model and prototype. Using Equation [8-18] we can calculate the value of t_1 for the prototype material, assuming r_1 to be the same for both. From Equation [8-17], we can calculate the maximum intensity of erosion. Once we know the values of I_{max}, t_1, and α, we can generate the entire erosion curve for the prototype material using this theory. While these ideas offer exciting possibilities, the success of this approach has yet to be demonstrated by actual model prototype experience.

The data discussed so far were collected at an intensity level of about one watt/meter^2. Even the stainless steel is

eroded substantially in about 50 hours. However, if a prototype system were to operate for 10,000 hours or more, the intensity should be less than a hundredth of a watt/meter^2. There is a need for a systematic study of such low intensities of erosion. Hammitt (101) pioneered work in this area as early as 1962 using a Venturi cavitation apparatus in the laboratory. However, such studies should be coordinated with prototype performance in the field over a long exposure period.

In addition, the operating conditions (such as speed, load, and depth or pressure) of the prototype may vary during its life either systematically or at random depending on the prototype's mission. This is an important limitation to any quantitative approach. The experience and judgment of the designer plays a very important role in this case.

The selection of materials for the model will be governed by several requirements such as structural strength, environmental effects such as corrosion, reproducibility of results, and techniques employed in the manufacture of the models, in addition to the considerations involving test duration.

For systems operating at a fairly high intensity of erosion (consequently short-life systems), it is economical and convenient to use the actual prototype material in the model. This is justified because the model life as well as the prototype life will be short at high intensities of erosion.

HYDRODYNAMIC MODELING OF EROSION INTENSITY

In the previous section, we discussed considerations involving selection of the model material to allow short-term model tests to be extrapolated to long-term prototype operations. The next step is the simulation of model speed and model size. The velocity scale and size scale are governed by the mechanics of bubble formation and collapse which in turn depends to a great extent on the hydrodynamic aspects of cavitation. In this section we will consider these aspects leading to the derivation of a few hydrodynamic scaling laws for cavitation erosion.

Hydrodynamic Scaling Laws For Cavitation Erosion

Spherical Collapse

It is now generally accepted that high pressures caused by the collapse of bubbles produce deformation and material failure. As early as 1917, Rayleigh (7) attempted to show that such high pressures are possible during bubble collapse. Rayleigh's analysis of an empty bubble collapsing in an incompressible liquid predicted infinite bubble wall velocities and collapse pressure (Figure 4-6). He obviated this difficulty by introducing a perfect gas obeying Boyle's law in the bubble. Furthermore, he knew that a satisfactory theory should take into account the compressibility of the liquid. Realizing the importance of compressibility effects in bubble collapse, several investigators including Hickling and Plesset (170) and

Ivany and Hammitt (171) considered this effect in their calculations. While surface tension tends to increase the rate of collapse, compressibility, viscosity and non-condensible gas in the bubble tend to slow down the collapse rate (172). The influence of viscosity on collapse rate is negligible except for large bubbles.

Nonspherical Collapse

Recent attention has been directed toward an understanding of nonspherical collapse. However, interest in the formation of liquid jets arising out of nonspherical collapse may be traced to early investigators. For example, Eisenberg (2), as early as 1950, hypothesized the formation of liquid jets caused by the "unsymmetrical collapse of cavitation bubbles in a pressure gradient". Kornfeld and Suvorov (147 and Naude and Ellis (50) observed experimentally the formation of such jets during the later stages of bubble collapse. Naude and Ellis (50) photographed such jets and the indentations caused by these jets. Hancox and Brunton (173) and Thiruvengadam, et al (52), have shown that multiple impacts by water jets can cause erosion even at impact speeds in the range of 100 fps. More recently, Benjamin and Ellis (53), Tulin (54), Mitchell and Hammitt (55), and Plesset and Chapman (56) have all contributed to the understanding of the jet impact mechanism. It is interesting to note that the theoretical prediction of the microjet formation in front of the primary jet (Figure 8-14) is very similar to the experimental Monroe Jet observations of Bowden and Brunton (57) .

Indentation and Rate of Erosion

If the stress caused by the collapse of the bubble exceeds the yield strength of the material, a permanent dent may be produced by a single impact. However, even if the collapse stress is less than the yield strength, a dent may still be produced after several collapses due to fatigue failure of the material. The actual fracture of a particle from the surface of the material may be produced from overlapping indentations caused by the collapse of many bubbles. For a single impact, the depth of indentation, $\Delta y'$, may be approximately related to the strength of the material, S_e, the impact pressure, P_i, and the size of the shock or jet, R, by the following relationship*

$$\Delta y' \cdot S_e \propto P_i \cdot R \qquad [8\text{-}19]$$

*The sign $\propto$ means "is proportional to". All the constants of proportionality are omitted in the following derivations since we are interested only in nondimensional ratios.

For a sufficiently shallow indentation of predominantly plastic character, the diameter of indentation, d, is proportional to $\sqrt{R \cdot \Delta y'}$. This result, when used with conventional relationships for hardness, will lead to relation [8-19]. Ideal plasticity is assumed. If the impact stress is much larger than the yield strength of the material, deep craters and associated plastic flow are produced on the surface of the material. This analysis is mainly applicable to materials that are neither too soft nor too strong, i.e., with yield strengths of the same order of magnitude as the impact stress.

If we use the simple analogy of a hardness test, the strength, S, corresponds to the appropriate hardness of the material (Figure 8-14). For the case of multiple impacts with a frequency of f, the rate of indentation may be approximated by

$$\frac{\Delta y}{\Delta t} \cdot S_e \propto P_i \cdot R \cdot f \qquad [8\text{-}20]$$

The left side of relation [8-20] represents the intensity of erosion, as given by relation [6-4], whereas the right side is the intensity of bubble collapse. The genesis of these ideas may be traced to References (61, 99). The details of the derivations for relations [8-19] and [8-20], and the following result, including assumptions and limitations, are contained in Reference (174).

The intensity of bubble collapse depends upon three parameters, namely the impact pressure, P_i, the size of the bubble or jet, and the frequency of impact. The approach is to relate these three parameters to hydrodynamic characteristics such as velocity, pressure, and size of the system. As shown in Figure 8-14, we can classify the bubble collapse mechanisms into three categories, spherical collapse, macrojet impact, and microjet impact. Rayleigh (7) and several other investigators considered the spherical collapse in detail. Plesset and Chapman (56) among others have considered the macrojet and microjet.

Spherical Collapse

The collapse pressure due to spherical collapse, P_c, is given by

$$P_c \propto P_o \left(\frac{R_o}{R_c}\right)^3 \qquad [8\text{-}21]$$

where P_o and R_o correspond to initial pressure and radius and R_c is the final collapse radius. If the center of collapse is of the order of the initial radius, the impact pressure, P_i, is given by

$$P_i \propto P_o \left(\frac{R_o}{R_c}\right)^2 \qquad [8\text{-}22]$$

allowing for a (1/radius) attenuation (175). The relative radius, R_o/R_c, depends upon many factors including surface tension, noncondensible gas, heat transfer effects and compressibility of the liquid (176). For example, the influence of noncondensible gas obeying Boyle's law was given by Rayleigh (7) as

$$\frac{R_o}{R_c} \propto \exp\left(\frac{P_o}{Q_o}\right)^{1/3} \qquad [8\text{-}23]$$

where Q_o is the partial pressure of the gas at the beginning of the collapse. Similarly, other effects may also be evaluated (176).

Jet Impact

The pressure caused by the jet may be classified into two categories: (1) the stagnation pressure developed by a long jet acting for a large duration, and (2) the water hammer pressure resulting from a short jet of small duration. According to Plesset and Chapman (56), velocity of the jet is proportional to $\sqrt{P_o}$. Then the stagnation pressure is proportional to P_o, whereas the water hammer pressure is proportional to $C\sqrt{\rho P_o}$; C is the sound speed and ρ is the density of the liquid;

$$P_i \propto P_o \quad \text{(for the case of stagnation pressure)} \qquad [8\text{-}24]$$

$$P_i \propto C\sqrt{\rho P_o} \quad \text{(for the case of water hammer pressure)} \qquad [8\text{-}25]$$

Growth of Bubbles

The initial size of the bubble at the beginning of the collapse is related to the time available for growth and the pressure difference between the inside and the outside of the bubble (15), Figure 8-15. The growth time, τ_g, is directly proportional to the length of travel of the bubble and inversely proportional to the translational velocity of the bubble. The travel length is proportional to the cavity length which is proportional to the model length at a given cavitation number. Experimental observations by Ivany, Hammitt and Mitchell (177) show that the bubbles move at approximately the same speed as

the liquid. The pressure causing growth is related to the difference between the vapor pressure, p_v, and the minimum pressure, p_{min}. The surface tension is neglected, but is is possible to account for it. These relationships may be written as follows:

$$R_o \propto \tau_g \sqrt{\frac{\Delta p}{\rho}} \qquad [8\text{-}26]$$

$$\tau_g \propto \frac{\ell}{V_o} \qquad [8\text{-}27]$$

$$\Delta p \propto p_v - p_{min} \qquad [8\text{-}28]$$

Combining these equations and using the relations for the cavitation number, σ, and the minimum pressure coefficient, $C_{p,min}$, given by Equation [2-12]:

$$\sigma = \frac{p_o - p_v}{\frac{1}{2}\rho V_o^2} \qquad [8\text{-}29]$$

and [2-9]:

$$C_{p,min} = \frac{p_{min} - p_o}{\frac{1}{2}\rho V_o^2} \qquad [8\text{-}30]$$

and assuming that σ_i, the cavitation inception number is

$$\sigma_i = - C_{p,min} \text{ [See Johnson (3)]} \qquad [8\text{-}31]$$

we get

$$R_o \propto \ell \, (\sigma_i - \sigma)^{\frac{1}{2}} \qquad [8\text{-}32]$$

Moreover, the radius of the jet, R_j, is assumed as:

$$R_j \propto R_o \qquad [8\text{-}33]$$

Frequency of Bubble Growth and Collapse

As discussed earlier, the rate of erosion is related to the number of bubbles collapsing per unit time at a given location. The number of bubbles that collapse is related to the number of bubbles that become unstable and grow. Some of the parameters that affect the bubble instability are:

1. Nuclei size,
2. Surface tension,
3. Velocity,
4. Pressure, and
5. Size of the model.

Johnson (3) considered these parameters and demonstrated that bubbles smaller than the critical size do not grow under a given set of flow conditions (Figure 2-5). For example, bubbles of the order of 10^{-4}-in. in diameter may not grow at speeds less than 60 fps whereas they may become critical at a speed of 120 fps, as shown in Figure 2-5.

If n_o is the cumulative number of nuclei that pass a given point in a given time interval, then one can plot a distribution of sizes of these bubbles as shown in Figure 8-16. The relative nuclei size is $d/\bar{d}$ where $\bar{d}$ is the mean diameter and n is the cumulative number corresponding to the diameter d. As of now, there are no systematic measurements of such distributions in practical flow systems. However, if we assume that the nuclei size is governed by a Weibull type of distribution, then

$$\frac{n}{n_o} = \exp\left[-\left(\frac{d}{\bar{d}}\right)^{\alpha}\right] \qquad [8\text{-}34]$$

where α is the Weibull shape parameter. It is easily recognized that the Weibull distribution gives the simple exponential distribution when $\alpha = 1$, the Rayleigh distribution when $\alpha = 2$, and approximates the normal distribution when $\alpha = 3.57$ (178).

According to Johnson (3),

$$d^* = \frac{8\gamma}{3(p_v - p_{min})} \qquad [8\text{-}35]$$

where

d^* = the critical diameter of the nucleus, and

γ = the surface tension of the liquid.

If n^* corresponds to d^*, and a simple exponential distribution is assumed for the nuclei size, one obtains (174):

$$n^* \propto \frac{V_o}{\bar{d}} \exp \left[\frac{-2.67}{W(\sigma_i - \sigma)} \right] , \qquad [8\text{-}36]$$

where $W = \frac{1}{2}\rho V_o^2 \bar{d}/\gamma$ is the Weber number.

Scaling Laws for Cavitation Erosion

So far, we have discussed the relationships governing the impact pressure, the size of the bubble or the jet, and the number of bubbles collapsing per unit time. We also showed in this section that the intensity of bubble collapse is the product of these parameters. For example, the jet impact case reduces to

$$I_e \propto P_i \cdot R_j \cdot f; \quad P_i \propto p_o$$

$$\propto p_o \ell (\sigma_i - \sigma)^{\frac{1}{2}} \frac{V_o}{\bar{d}} \exp \left[\frac{-2.67}{W(\sigma_i - \sigma)} \right] \qquad [8\text{-}37]$$

Again,

$$p_o - p_v = \sigma \tfrac{1}{2}\rho V_o^2$$

But

$$p_v \ll p_o \quad \text{for practical cases of erosion.}$$

Then

$$p_o \approx \sigma \tfrac{1}{2}\rho V_o^2$$

Hence

$$I_e \propto \tfrac{1}{2}\rho V_o^3 \frac{\ell}{d} \sigma(\sigma_i - \sigma)^{\frac{1}{2}} \exp\left[\frac{-2.67}{W(\sigma_i - \sigma)}\right] \qquad [8\text{-}38]$$

Rearranging [8-43] in non-dimensional groups, we obtain,

$$\Theta = \frac{\sigma}{\delta} (\Delta\sigma)^{\frac{1}{2}} \exp\left[-\frac{2.67}{W(\Delta\sigma)}\right] \qquad [8\text{-}39]$$

as an expression for the erosion number, Θ, for the jet impact case; where

$$\Theta = \frac{I_e}{\frac{1}{2}\rho V_o^3} \quad - \text{ Erosion number} \qquad [8\text{-}40]$$

$$\delta = \frac{\bar{d}}{\ell} \quad - \text{ Relative nuclei size} \qquad [8\text{-}41]$$

$$W = \frac{\frac{1}{2}\rho V_o^2 \bar{d}}{\gamma} \quad - \text{ Weber number} \qquad [8\text{-}42]$$

$$\sigma = \frac{p_o - p_v}{\frac{1}{2}\rho V_o^2} \quad - \text{ Cavitation number} \qquad [8\text{-}43]$$

$$\sigma_i = \frac{p_i - p_v}{\frac{1}{2}\rho V_o^2} \quad - \text{ Cavitation inception number} \qquad [8\text{-}44]$$

$$\Delta\sigma = (\sigma_i - \sigma) \quad - \text{ Degree of cavitation} \qquad [8\text{-}45]$$

Similar results for the water hammer pressure produced by microjets and for spherical shocks produced by spherical collapse are summarized in Table 8-2.

If we examine the case of water hammer pressure, then

$$\textcircled{H} = \frac{\sigma}{\delta M} (\Delta\sigma)^{\frac{1}{2}} \exp\left[\frac{-2.67}{W(\Delta\sigma)}\right] \qquad [8\text{-}46]$$

where

$$M = V_o/C = \text{Mach number},$$

and

$$C = \text{the speed of sound in the liquid.}$$

For the case of spherical shock, we get

$$\textcircled{H} = \frac{\sigma}{\delta} (\Delta\sigma)^{\frac{1}{2}} \exp\left[\frac{2}{3}\left(\frac{p_o}{Q_o}\right) - \frac{2.67}{W(\Delta\sigma)}\right] \qquad [8\text{-}47]$$

where Q_o is the partial pressure of noncondensible gas in the bubble at the start of collapse.

Surface tension, compressibility and thermal effects may also be included for the case of spherical collapse. A discussion of these effects is available in Reference (176).

In essence, this section leads to some of the important scaling laws governing the phenomenon of cavitation erosion. It is necessary to verify these scaling parameters with carefully planned experiments. In the meantime, an attempt has been made to see if these scaling laws would explain the available experimental results.

According to the experimental results shown in Figure 8-6, the intensity of erosion increases with increasing cavitation number, reaches a maximum and then decreases to a negligible

value at the cavitation inception number. Similar behavior is seen in Figure 8-17 which shows a plot of the computed value of $\Theta \cdot \delta$ (product of the erosion number and the relative nuclei size) as a function of cavitation number for various values of the cavitation inception number. These values are computed from the relationship [8-39] for a particular value of the Weber number. The trends of computed results are in agreement with the experimental results and reinforce the explanation given in Reference (153).

The experimental results in Figure 8-6 further show that the size of the hydrofoil has an influence on the intensity of erosion as well as on the cavitation number at which the maximum intensity occurs. The maximum intensity for the 3-in. chord hydrofoil at 175 fps is about one half that of 1½-in. chord hydrofoil at the same speed. Changing the size of the foil changes both the relative nuclei size, δ, and the cavitation inception number, σ_i, thereby affecting the degree of cavitation, $\Delta\sigma$. If we neglect the change in $\Delta\sigma$, then the intensity is proportional to the model size when all the other parameters are held constant.

Furthermore, experimental observations show that the intensity of erosion is proportional to $(V_o)^e$. The value of the exponent, e, has been reported to vary anywhere from 3 to 10 (151, 143, 150). This variation in the velocity exponent can also be understood by plotting $\Theta\delta/\sigma(\Delta\sigma)^{\frac{1}{2}}$ as a function of Weber number for various values of $\Delta\sigma$, from Equation [8-39],

as shown in Figure 8-18. For nuclei sizes on the order of 10^{-5} ft. in water, for a speed range of 100 to 200 fps, the Weber number would be on the order of 20 to 80. For most of the experiments the degree of cavitation ($\Delta\sigma$) was close to 0.05. Keeping δ, σ, and $\Delta\sigma$ constant, we see in the shaded region in Figure 8-18, that the following approximate relation exists:

$$\Theta \propto W^{1.5}$$

As derived in Figure 8-18, we find

$$I_e \propto V_o^6 \qquad [8\text{-}48]$$

which seems to agree with Knapp's sixth power relation for the dependence of erosion on velocity. Similarly, the other values of velocity exponents can be obtained depending upon the range of W and $\Delta\sigma$ for each specific experiment. Table 8-3 shows the range of nuclei size, velocities, and Weber numbers that are of interest in model-prototype correlations. As shown in Figure 8-18, the erosion number, Θ, becomes independent of Weber number for $W > 1000$.

Assumptions and Limitations

The discussions above have attempted to probe into some of the important experimental results in terms of the scaling parameters suggested so far. The analysis seems to explain the roles played by cavitation number, velocity, and size of the system. However, the phenomenon of cavitation erosion is a very

complex process. The discussions and analyses outlined in this chapter are only a first step, and much more remains to be understood. Many assumptions have been made to simplify the complexity of the analyses. For example, the phenomenon of bubble collapse is statistical in nature. Similarly, the fracture of solid particles from the surface of the material is also a statistical process. Assigning a strength value or an energy value to the resistance of the material in this context is controversial, to say the least. The author's approach, represented by relation [8-20] is one of many different approaches, concepts and ideas that are forthcoming from several contemporary investigators.

As discussed earlier, the inception of cavitation depends both on free nuclei as well as on surface nuclei (179). Only the case of free nuclei has been considered in this report. However, it is possible to extend the same approach to the surface nuclei case. It is also necessary to investigate different nuclei distribution functions. For example, Figure 8-19 shows the influence of the Weibull shape parameter for a given degree of cavitation; the shape parameter has no appreciable influence for Weber numbers greater than 30, which is the practical range. Similar to the statistical distribution for bubble growth, there is likely to be another distribution for the number of bubbles collapsing near the material surface. Future investigations may have to take this aspect also into consideration.

Summary Remarks

The necessity for developing model tests to determine the intensity of erosion of full scale systems is being recognized by all concerned. Time scale, velocity scale, and size scale are among the important scales in modeling cavitation erosion. The technical feasibility of scaling these parameters was discussed in this cahpter. Time scaling may be accomplished by using a weaker (less resistance to erosion) material in the model. However, the selection of a modeling material will be governed by several factors including corrosion and structural strength.

The set of non-dimensional numbers discussed here seems to shed some light on the feasibility of scaling velocity and size. The erosion number represents the efficiency of erosion. It depends upon the cavitation number, the degree of cavitation and the relative nuclei size at a given Weber number. For given values of the relative nuclei size, the cavitation number and the degree of cavitation, the erosion number varies as an exponential function of the Weber number. At large values of the Weber number, the erosion number becomes independent of the Weber number. These results tend to agree with some of the available experimental observations. For example, Knapp's sixth power relation, observed contradictions to this relation, effect of cavitation number, and effect of size of the model are among the results that agree reasonably well with this approach.

These investigations indicate that it is feasible to model cavitation erosion; they also provide some guidelines in the selection of the velocity scale, the model size scale, the nuclei size scale, the required surface tension of the test liquid, and the degree of cavitation during the planning stage of a model test program. As pointed out earlier, there are several limitations to this approach. Further carefully planned experimental research is needed for demonstrating the practicality of model tests.

IX. RELATION BETWEEN LIQUID PARAMETERS AND CAVITATION EROSION INTENSITY

The function of the liquid in the mechanism of erosion is twofold: (1) the dynamics of the bubble is controlled by the physical properties of the liquid; (2) the corrosive environment is provided by the chemical properties of the liquid. The purpose of this chapter is to discuss these two aspects in detail.

ROLE OF PHYSICAL PROPERTIES

Temperature Effects

In examining the effects of the temperature of the liquid on the erosion process, account must be taken of all the physical properties of the liquid that become affected by a change in the temperature. The effects of temperature have been studied by Kerr (66), Rheingans (68), Nowotny (11), Mousson (67), Wilson and Graham (180), Leith and Thompson (100), Bebchuk (181, 182), and Devine and Plesset (183), among others. The results of experiments by several investigators are reproduced in Figure 9-1 as typical of the behavior generally observed. The occurrence of the peak in the damage curves may be explained as follows. At the lower temperatures, the vapor pressure is relatively low but the capacity of the liquid for solution and entrainment of gases is relatively high. Thus, the high air content provides permanent gas for "cushioning" of bubble collapse and erosion is relatively slight. As the temperature is increased, gas is driven off but the vapor pressure is still not high enough to provide

any cushioning effect. In fact, the higher vapor pressure may provide additional unstable nuclei and, consequently, more cavitation bubbles will be available for erosion. As a result, erosion is rapidly increased. Finally, as the temperature continues to increase, the vapor pressure reaches high enough values to provide considerable cushioning for the collapsing bubbles and damage is again reduced.

Vapor Pressure

The effects of vapor pressure on the damage process was demonstrated strikingly by Nowotny (11) in experiments on pure aluminum in water, benzene, benzol (octane-nonane mixture), and ethyl ether. He compared damage in water at 20°, 60°, and 90°C with damage in the other liquids at approximately 26°C. The vapor pressures for water at the three temperatures cited are 17, 150, and 525 mm Hg, while the vapor pressures of n-octane, benzol, and ethyl ether at the test temperature were about 16, 100, and 500 mm Hg, respectively. The damage obtained at the corresponding vapor pressures was very nearly the same. He observed further that in the ether no damage could be observed even after long exposure to attack; this behavior is typical of water near the boiling point and in highly volatile liquids in general, and was an important piece of circumstantial evidence in substantiation of the mechanical damage hypothesis for many years.

Surface Tension

Other factors remaining constant, the expected effect of surface tension, based on the conclusions from dynamics of transient cavities, would be an increase in damage with increasing surface tension (since collapse pressures would be higher with higher surface tension). This is indicated in Nowotny's (11) experiments. Nowotny's results are shown in Figure 9-2 where the weight loss of a pure aluminum specimen has been plotted as a function of surface tension; in these experiments, the vapor pressure was held approximately constant. Recent experimental data are compared with Nowotny's data in Figure 9-3. The experiments by Plesset (184) and Thiruvengadam (185) were conducted at a test frequency of 15 kHz as compared to 8 kHz used by Nowotny (11).

Viscosity

Since cavity collapse pressures in liquids of low viscosity tend to be higher than in liquids of high viscosity, greater cavitation damage of a mechanical nature would be expected in the former. This conclusion is also borne out by experiments. We cite, in particular, the results of Wilson and Graham (180), which are reproduced in Figure 9-4. Using mineral oils of different viscosities and glycerine-water mixtures of different composition and therefore different viscosity, they conducted experiments in two ways. In experiments on a silver-plated surface, the energy input (to a magnetrostriction oscillator) was held constant and the viscosity varied. As would be expected, the erosion decreased with increasing viscosity. To

further check this effect, experiments were carried out on an aluminum surface with the energy input increased to compensate for the increase in damping of the cavitation bubbles as the viscosity of the liquid was increased. Approximately constant erosion was obtained in this way and this result further confirms the role of mechanical effects in cavitation damage. More recent experiments by Thiruvengadam (176) using polymer additives, Figure 9-5, confirm the findings of Wilson and Graham (180).

Compressibility and Density

Wilson and Graham's (180) experiments on the effects of compressibility and density, separately, showed generally the trends that would be expected on the basis of the behavior of collapsing transient cavities, i.e., increasing erosion with increasing density and decreasing compressibility, although the scatter in data is rather large. Reasoning from the approximate Rayleigh theory of bubble collapse with account for the compressibility of the liquid, they correlated their results on the basis of the product of sound velocity and density. The results for experiments on silver surfaces in a variety of liquids are reproduced in Figure 9-6. Not only are these results of interest in connection with the mechanism of cavitation erosion, but they will be of some interest in practical cases where a knowledge of the relative effects of various liquids will assist in design or in extrapolation of experimental results from one liquid to another.

Discussion of the Role of Physical Properties of the Liquids

Plesset (184) conducted extensive experiments using several liquid mixtures. His experimental data are shown in Figures 9-7 (a), (b), and (c). He suggested that the reduction in erosion rates was mainly due to the reduction in corrosive influence by the addition of the second liquid. Considering the fact that he used soft aluminum and his experiments lasted at the most 15 minutes, it was very difficult to attribute all of the reduction in erosion rate to corrosion. Realizing this, Tung and Thiruvengadam (186) extended the analysis outlined in Chapter VIII and derived the following relationships for the intensity of erosion of the vibratory erosion apparatus.

For the case of spherical collapse, assuming isothermal compression of the gas inside the bubble,

$$I_e \propto \rho^{\frac{1}{2}} c U_o \, (P_v - P_o)^{\frac{1}{2}} \exp\left(\frac{2}{3}\frac{P_o}{Q} - \frac{2.67}{P_v}\frac{\gamma}{d}\right) \qquad [9\text{-}1]$$

where

$U_o = \omega\xi$ = maximum velocity of vibration,

ω = angular frequency of vibration,

ξ = the maximum amplitude of vibration,

c = the sound speed in liquid,

ρ = the density in the liquid,

$P_o = \rho c U_o$ = the acoustic pressure,

P_v = the vapor pressure of the liquid

Q = the partial pressure of air in the bubble,

γ = the surface tension of the liquid, and

$\bar{d}$ = the mean radius of the nuclei.

Assuming adiabatic compression, the intensity of erosion for the case of spherical collapse is given by:

$$I_e \propto \rho^{\frac{1}{2}} c U_o (P_v - P_o)^{\frac{1}{2}} \left(\frac{P_o}{Q}\right)^2 \exp\left(\frac{-2.67\gamma}{P_v \bar{d}}\right) \qquad [9\text{-}2]$$

Similarly the intensity of erosion for the case of macrojet may be derived as:

$$I_e \propto \rho^{\frac{1}{2}} c U_o (P_v - P_o)^{\frac{1}{2}} \exp\left(\frac{-2.67\gamma}{P_v \bar{d}}\right) \qquad [9\text{-}3]$$

For the case of a microjet, it is given by

$$I_e \propto \rho^{\frac{1}{2}} C^{3/2} U_o (P_v - P_o)^{\frac{1}{2}} \exp\left(\frac{-2.67\gamma}{P_v \bar{d}}\right) \qquad [9\text{-}4]$$

Let Subscript 1 represent pure water and 2 represent other concentrations of test liquid. Then the ratio of the intensity of erosion of the test liquid and pure water is given by:

$$\frac{I_2}{I_1} = \left(\frac{P_2}{P_1}\right)^{\frac{1}{2}} \left(\frac{c_2}{c_1}\right) \left(\frac{P_{v_2} - P_{o_2}}{P_{v_1} - P_{o_1}}\right)^{\frac{1}{2}} \exp\left\{\left[\frac{2}{3}\left(\frac{P_o}{Q}\right)_2 - \frac{2}{3}\left(\frac{P_o}{Q}\right)_1\right]\right.$$

$$\left. + \frac{2.67\gamma_1}{P_{v_1}\,\bar{d}_1}\left(1 - \frac{\gamma_2}{\gamma_1}\,\frac{\bar{d}_1}{\bar{d}_2}\,\frac{P_{v_1}}{P_{v_2}}\right)\right\} \qquad [9\text{-}5]$$

The last term in the exponential function involves the ratio of mean diameter of nuclei, and it is given by:

$$\frac{\bar{d}_1}{\bar{d}_2} = \frac{\gamma_1}{\gamma_2}\left(\frac{\frac{P_{v_2}}{P_a} - 1}{\frac{P_{v_1}}{P_a} - 1}\right) \qquad [9\text{-}6]$$

Then equation [9-5] becomes:

$$\frac{I_2}{I_1} = \left(\frac{\rho_2}{\rho_1}\right)^{\frac{1}{2}} \left(\frac{c_2}{c_1}\right)\left(\frac{P_{v_2} - P_{o_2}}{P_{v_1} - P_{o_1}}\right) \exp\left[\frac{2}{3}\left[\left(\frac{P_o}{Q}\right)_2 - \frac{2}{3}\left(\frac{P_o}{Q}\right)_1\right.\right.$$

$$\left.\left. + \frac{2.67\,\gamma}{P_{v_1}\,\bar{d}_1}\left(1 - \frac{\left(1 - \frac{P_a}{P_{v_2}}\right)}{\left(1 - \frac{P_a}{P_{v_1}}\right)}\right)\right] \qquad [9\text{-}7]$$

Similarly for adiabatic compression, we have:

$$\frac{I_2}{I_1} = \left(\frac{\rho_2}{\rho_1}\right)^{\frac{1}{2}} \left(\frac{c_2}{c_1}\right) \left(\frac{P_{v_2} - P_{o_2}}{P_{v_1} - P_{o_1}}\right)^{\frac{1}{2}} \left[\left(\frac{P_o}{Q}\right)_2 \Big/ \left(\frac{P_o}{Q}\right)_1\right]^2$$

$$\exp\left[\frac{2.67\,\gamma_1}{P_{v_1}\,\bar{d}_1}\left(1 - \frac{\left(1 - \frac{P_a}{P_{v_2}}\right)}{\left(1 - \frac{P_a}{P_{v_1}}\right)}\right)\right] \qquad [9\text{-}8]$$

for the spherical collapse;

$$\frac{I_2}{I_1} = \left(\frac{\rho_2}{\rho_1}\right)^{\frac{1}{2}} \left(\frac{c_2}{c_1}\right) \left(\frac{P_{v_2} - P_{o_2}}{P_{v_1} - P_{o_1}}\right)^{\frac{1}{2}} \exp\left[\frac{2.67\,\gamma_1}{P_{v_1}\,\bar{d}_1}\left(1 - \frac{\left(1 - \frac{P_a}{P_{v_2}}\right)}{\left(1 - \frac{P_a}{P_{v_1}}\right)}\right)\right]$$

[9-9]

for the macrojet; and,

$$\frac{I_2}{I_1} = \left(\frac{\rho_2}{\rho_1}\right)^{\frac{1}{2}} \left(\frac{c_2}{c_1}\right)^{3/2} \left(\frac{P_{v_2} - P_{o_2}}{P_{v_1} - P_{o_1}}\right)^{\frac{1}{2}}$$

$$\exp\left[\frac{2.67\gamma_1}{P_{v_1}\,\bar{d}_1}\left(1 - \frac{\left(1 - \frac{P_a}{P_{v_2}}\right)}{\left(1 - \frac{P_a}{P_{v_1}}\right)}\right)\right] \qquad [9\text{-}10]$$

for the microjet.

The calculated results from these relationships are compared with experimental results using water alcohol mixtures in Figure 9-8. The above analysis seems to explain the role of the various physical properties such as density, sound speed, vapor pressure, surface tension, and gas content. This analysis also successfully predicts the role of ambient temperature of the test liquid in cavitation erosion as shown in Figure 9-9. The assumption of adiabatic collapse seems to be more realistic than the assumption of isothermal collapse. Furthermore, the above analysis seems to indicate the role played by various physical properties of the liquids in cavitation erosion (186).

INFLUENCE OF CORROSIVE ENVIRONMENT

A number of mechanisms for cavitation erosion have been proposed at various times which involve almost all aspects of electrochemical phenomena including, thermogalvanic effects,

stress-induced galvanic effects, oxygen concentration cells, ion concentration cells and so on. Largely these speculations have been based on the observed effects of applied cathodic protection rather than direct observation and analysis. None of these postulates are in conflict with the mechanical model of cavitation erosion if one keeps in mind the intensity of cavitation erosion under which some of these phenomena may have occurred. The conjoint action of mechanical and electrochemical effects, with the consequent increase in an accelerated rate of attack is a common occurrence in corrosion fatigue, stress corrosion cracking, jet impingement, velocity corrosion, sand abrasion, fretting corrosion, and wire drawing to name just a few.

We shall first consider the evidence on which these various postulates are based and then discuss recent research on the mechanism of cathodic protection as it relates to these postulates. It should be kept in mind that our discussion refers to electrochemical effects associated specifically with phenomena occurring during or directly from the cavitation process and not with the more familiar galvanic effects arising with dissimilar metals in an electrolyte, for example. The fact that galvanic effects of the latter type are often present simultaneously in practical situations has complicated and obscured the cavitation erosion mechanism and account of these effects must be taken separately.

Thermogalvanic Postulates

Thermogalvanic postulates require that electrochemical effects associated with temperature changes be brought about by the presence or creation of high temperatures as the primary mechanism inducing the flow of corrosive currents in a metal. The possibility of high stresses concurrent with or responsible for such high temperatures is assumed to have only a secondary effect on the corrosion process. Two sources of high temperature are generally identified in support of such theories: (1) the high temperatures that are possible momentarily in the collapsing bubbles due to compression of the contained gas, and (2) possible high temperatures associated with the momentary stressing of the metal at the position of bubble collapse. The idea of thermogalvanic effects has been advanced by Krenn (187) on the basis of the heat flow between corroded parts and adjacent power generating equipment in machines and by Foltyn (188) and Nechleba (78) on a more rational assumption of a heat potential generated by increase of temperature of the metal due to local stressing or due to high temperatures in the cavitation bubbles themselves. Owing to this local heating, a temperature gradient is created between the heated spot and the surrounding material which causes an electric current to flow (in a conducting medium). The electrolytic corrosion presumably caused by such current flow will be directly proportional to the current. To test this hypothesis, Foltyn carried out experiments using impressed cathodic currents in which the counter current was adjusted to be just equal to the

electrolytic current measured during an independent cavitation experiment. While he was able to report considerable reduction in erosion, he was not able to completely eliminate the loss of material. The explanation offered for the ameliorating effects of such cathodic protection is that the potential of the specimen cathode is raised above the potential level induced at the attacked point. It is interesting to note that both Foltyn and Nechleba were able to achieve reduction in damage by means of cathodic protection only with very smooth surfaces, while very little, if any, protection was observed on roughened surfaces. This is not surprising, however, since at constant applied current the cathodic current density will decrease with surface roughness.

Mechanically-Induced Electrochemical Effects

A number of suggestions have been made to account for cavitation erosion or cavitation-associated erosion which, in one way or another, relies on a primary mechanism of electrolytic corrosion induced or accelerated by the concurrent cavitation activity. These range from very simple postulates which require that the stirring action produced by cavitation in water in which polarization has occurred assists in removing hydrogen layers (which tend to inhibit electrolytic processes) from the cathode surface, to more sophisticated corrosion mechanisms associated with mechanical stresses. Since ordinary electrolysis attack is very slow compared with observed cavitation erosion, any effects of the former type cannot play a very important role.

Another suggestion is based on electrolytic corrosion associated with fluctuations in the boundary between the metal, liquid, and atmosphere.

Stress-induced galvanic effects

Closely related to the idea of the mechanism of thermogalvanic effects of the type described above is that of stress-induced galvanic effects between adjacent crystals accompanying the high local stresses associated with collapsing cavitation bubbles. This hypothesis was first announced by Petracchi (189), who also admits the possibility of secondary thermal effects of the type described above. The arguments and alternatives are approximately as follows. Deformation of the microcells increases their e.m.f. by altering the internal energy of the small surfaces which constitute the electrodes. Alternatively, the polarization of the microcells might be slowed down or impeded by the varying stresses. Finally, even microcells with very low e.m.f. values can give rise to appreciable effects since the corrosive effects are localized in the most highly stressed areas and in turn increase the stresses.

Petracchi assumed that the suggested mechanism is somehow related to the mechanism of corrosion fatigue and that, by the use of cathodic protection which can retain in a corrosive medium the fatigue properties of a metal in air, for example, he would be able to improve cavitation erosion resistance. His experiments (189) show considerable protective effect similar to the tests cited in the foregoing.

The cathodic current densities he employed were on the order of 1 ma/cm^2 whic. is 25 to 50 times larger than that required for normal cathodic protection applications. He also showed that by making the specimens anodic at moderate current densities of 0.02 ma/cm^2 ($\sim$20 ma/ft^2) he was able to produce in several metals a considerable increase in cavitation erosion. In light of new evidence, Petracchi's results are easily understood since the intensity of his device was on the order of 10^{-3} watts/meter^2 (See Chapter VI). Also the cathodic current densities he employed certainly would have resulted in the evolution of hydrogen gas at the cathode, which provides an additional cushioning effect (refer to section on cathodic protection in the latter part of this chapter).

Film rupture

It has been shown by Ffield, Mosher, and O'Neil (190) that materials such as bronze in water form a protective film that may be cathodic to the underlying material; they report that such films have been observed both in their laboratory experiments and on ship propellers. They postulate that rupturing this film will create a galvanic cell between the bare metal and the surrounding film. In view of the highly localized action of mechanical cavitation erosion, it is concluded that the area relationship between anode and cathode will be favorable for very high galvanic corrosion rates. Thus, their thesis assumes that the mechanical aspects of cavitation is only the trigger which sets off a violent electrochemical effect. They

point out further that, if this is a primary cause of cavitation erosion, the galvanic effect should be eliminated by applying cathodic protection which would immediately heal the mechanically damaged areas.

Although Ffield et al (190) did not believe they were inducing cavitation erosion in their rotating disk apparatus, actually in one case where they simulated roughness by locating 1/4-inch rivet heads and 1/8-inch depression holes spaced 90° apart on the periphery of the disc, they succeeded in getting a substantial erosion damage pattern on the disc downstream of the rivet heads. By applying cathodic protection in the order of 250 ma/sq ft to the discs rotating at peripheral velocities of 200 fps, they succeeded in eliminating the erosion. In view of the understanding of the effects of cathodic protection (amplified further at the end of this chapter), we find that this result is perfectly feasible in light of the mechanical erosion hypothesis when it is realized that the intensity of erosion of Ffields device is in the order of 10^{-2} watts/meter^2. It should be pointed out, however, that this low intensity is presumably due to air entrainment since other rotating devices discussed earlier produced much higher intensities of erosion.

Strain-produced anodic corrosion

This mechanism, which evidently embodies some of the features of corrosion fatigue and is somewhat related to the ideas set forth by Petracchi (189) has been discussed in detail by Wheeler (75). It is based on the expectation that strained

portions of a metal, in which the crystal structure is distorted, will be unstable electrochemically, and the observation that cold worked iron exhibits a solution rate very much greater than annealed iron. Thus, if a previously annealed specimen is subjected to repeated plastic deformation with the formation of associated strain centers, anodic areas will be continuously created. Where the metal is stressed but not permanently deformed, the electrode potential shift will be transitory and varying with the stress. These anodic areas, adjacent to the undisturbed metal, will give rise to electrolytic corrosion if the surface is in contact with an electrolyte, and corrosion will continue until polarization prevents further flow of current or until the anodic areas are etched away. A previously cold-worked material, or a material in which adjacent grains have different electrode potentials (heterogeneous materials), will be immediately attacked electrolytically when placed in an electrolyte and such attack will be accelerated in the above manner when subjected additionally to cavitation erosion.

However, according to Tomashov (191), cold working of metals undergoing extreme plastic deformation produce only minor shifts in potential. One case cited was that of a chromium-nickel stainless steel undergoing 71 percent compression by rolling which produced a cathodic potential shift equivalent to 1.5 - 2.5 mv. In general, even though it is feasible that localized instability can be much greater for individual atoms in sharp corners of a crack formed by impact stresses, the changes in

potential are generally too insignificant to account for extremely accelerated corrosion. Other mechanisms, such as discontinuity in protective films, probably acting in concert, can substantially influence the development of an accelerated corrosion process. Cathodic protection should prove to be of value in stifling this type of corrosion mechanism.

Interfacial potential fluctuations

Based on observations of the greatly increased cavitation erosion of cast iron in synthetic sea water as compared with fresh water, Shal'nev (192) attributed the cavitation erosion process entirely to electrochemical corrosion associated with potential fluctuations in the metal-liquid-atmosphere interface. According to his hypothesis, the movement of the liquid-vapor (or gas) interface across the surface of the metal during cavitation erosion results in momentary electrode potentials which are orders of magnitude greater than that caused by an unbroken contact between liquid and electrolyte and produces electrochemical corrosion at tremendously high rates. He cites the irregular shape of attacked regions in a vibratory apparatus as evidence that such electrochemical attack is associated with different modes in the growth and collapse of the cavitating mass and the irregular shape of unstable transient cavities locally. However, an explanation of the irregularities of the erosion patterns in such an experiment, associated with hydrodynamic instabilities, has recently been given, and a method for completely eliminating them has been devised. Furthermore, such

a mechanism cannot, of course, account for the damage to materials which are not as active as cast iron nor to erosion in non-corrosive media, although such a mechanism as a source of additional damage in some cases probably cannot be ruled out at the present time. Also, it must be remembered that cast iron is a matrix of graphite and iron in which graphite is dispersed in discrete particles. It is conceivable that the high potentials postulated for this mechanism are due to the unpolarized (momentary electrolytic contact) galvanic couple of clean iron and active graphite. This type of matrix segregation is not prevalent in most other alloys in general.

The Role of Impressed Cathodic Currents (Cathodic Protection)

Although we shall later discuss cathodic protection as a means of reducing or eliminating cavitation erosion, it is worthwhile to mention here the results of research which explains the protective nature of the cathodically applied currents cited in substantiation of many of the postulated mechanisms of damage discussed in the foregoing. It is clear that cathodic protection in a corrosive medium will assist in delaying the highly damaging effects of cavitation simply by preventing electrolytic corrosion associated with purely galvanic activity. However, in no case has it been demonstrated that the currents required for prevention of such galvanic action are sufficient to prevent cavitation erosion where high intensities are involved.

It has been suggested that the mechanism of cathodic prevention of cavitation erosion in water is associated with currents sufficiently high to result in hydrogen evolution (see, e.g., References 193 and 194); the hydrogen gas then acts to form a "cushion" to reduce the high pressures of the collapsing cavities. In a series of experiments, Plesset, et al (195, 196) have essentially confirmed the validity of this explanation. Their results may be summarized as follows. Tests with various materials in a solution of salt in water showed a reduction in weight loss for all of the materials when the test specimen was made the cathode of an electrolytic cell and when the conditions were such that gas was evolved at the surface of the specimen. This protective effect against cavitation erosion increased with increasing magnitude of the cathodic current. Similar protection was obtained when the specimen was made the anode in a test liquid of buffered distilled water. In the latter case, the gas evolved at the specimen surface is oxygen. Plesset found additional evidence for the protective effect of such gas layers in a series of experiments in which the voltage applied to the cell was reduced to a level at which no gas was evolved on the surface of the specimen; there was then no protective effect with the specimen cathodic or anodic. The results reported in these experiments were taken at an arbitrary constant time interval of cavitation erosion.

In view of these results, it is questionable whether the protective effect of cathodic currents may be used in evidence for the importance of thermogalvanic and mechanically-induced

electrochemical effects as sources of erosion in the cavitation process. However, as will be developed later, the intensity of cavitation erosion is related to the protective effects offered by cathodic protection. In quite another connection, however, cathodic protection of an active metal in an electrolytic environment should show significant reduction in the rate of cavitation erosion in view of fatigue properties. It has been demonstrated that the resistance of metals to cavitation erosion is closely related to fatigue properties because of the mechanical effects in the erosion processes. Consequently, the rate of erosion should be increased in a corrosive environment, since the corrosion fatigue limit is so much lower than the limit for fatigue in air. Thus, by applying cathodic protection to prevent electrolytic activity, it would be expected that the fatigue limit achieved in air can be restored. In this way, too, the erosion rates in a cavitating system should be reduced proportionately. This aspect will be discussed in more detail in a later section in this chapter.

Chemical Corrosion

Concurrent chemical attack has been observed during many experiments on cavitation erosion. This has been explained variously on the bases of straightforward chemical activity in highly corrosive media and of chemical activity induced or accelerated by the production of high temperatures which either produce chemically active products in the liquid environment or render the metal itself more active.

Strictly speaking, corrosion in electrolytes is generally considered electrochemical in nature (that is, reactions associated with the passage of current); while corrosion attack in non-electrolytes or dry gases is considered to be chemical in nature (subject purely to the basic laws of chemical kinetics of heterogeneous reactions). Cavitation erosion in liquid metals is an example of concurrent chemical attack.

Chemically-corrosive environments

Among the earliest observations of direct chemical corrosion during cavitation attack were those of Spannhake (197) and Schröter (198), and effects similar to those reported by them have been found by subsequent investigators; see, e.g., Nowotny (11). In tests in venturi tubes, after long exposure to cavitation, pronounced tarnish has been noted on brass specimens as well as various steels. Nowotny reports that, in tests carried out by Spannhake (unpublished), it was found that steel subjected to a short test had a loosely adhering film of oxide or hydroxide which was of a thickness to produce a blue interference color. However, he attributes this discoloration at least in part to the high local temperatures which are hypothesized as occurring during the collapse of cavitation bubbles. After long exposures, these films became very strong and anchored themselves into the metal. In one exceptional case, the oxide film was so thick as to cause an increase in the weight of the specimen. Such films are subsequently removed by the mechanical erosion of the primary, mechanical attack. A secondary chemical effect

is associated with the provision of localized micropores by mechanical attack which then act as seats for direct chemical action. Such corrosion is conducive to corrosion fatigue under continued stressing by the forces of the collapsing cavities. However, in most cases the mechanism of corrosion fatigue has been ascribed as electrochemical. Nevertheless, from an analysis of the particles actually removed during tests of aluminum, zinc, and cadmium in water, Nowotny found that this residue was in each case composed mostly of pure metal with only a very small remainder of oxide. Tests by Rheingans (68) of steels and various nonferrous metals in sulphuric acid and hydrochloric acid also showed very little effect of the corrosive medium in comparison with distilled water in exposures of two hours. In fact, most of his results indicate less damage in the acids than in the water. Here, however, account must be taken of the effect of passivity of certain metals to acid environments.

To reduce the contributing factors associated with chemical activity, and in some cases electrochemical activity, corrosion inhibitors have been tried and used with increasing frequency. These will be summarized in connection with our discussion of methods of reducing cavitation damage.

High temperature chemical activity

The sources of temperature rise which have been postulated to result in locally increased chemical activity are (1) conversion of mechanical energy into heat energy during the deformation

of the material by the forces of collapsing cavities, and (2) heating of the gases or vapor entrained in the cavitation bubbles when compressed during bubble collapse. On the basis of the explanation of work hardening as formulated by Taylor and Quinney (199), Wheeler (75, 80) proposes that sufficient heat is generated to increase significantly the chemical reactivity between iron and water, for example. According to Taylor and Quinney, 85 percent or more of the work during deformation of metal by the slip process is converted into heat and the remainder into potential energy of internal stress. Work hardening is then explained by the internal stress due to very small centers of strain located at grain boundaries (or "sessile" dislocations). It is the heat formed during this process that Wheeler postulates as the source of increased chemical activity; from estimates of the amount of work done in pitting metals during cavitation attack, he estimates that momentary temperature increases of several hundred degrees Centigrade can occur, depending upon the hardness of the metal.

As already mentioned above, chemical activity observed in cavitation erosion experiments has also been attributed to the production of very high temperatures in the gases within the cavities themselves. While the evidence for such temperatures in cavitation experiments where bubbles occur only once and then disappear, their place to be taken by others, is only indirect, the existence of high temperatures is bubbles in an ultrasonic field seems well documented. A number of investigations by

Griffing, et al (200, 201), have demonstrated that bubbles in resonance with an ultrasonic field evidently produce temperatures that are of the order of hundreds and even thousands of degrees. These conclusions are based on the chemical reactions obtained, e.g., the production of H_2O_2 in irradiated water, and the observation of luminescence. Much remains to be done before it can be definitely stated whether such effects are of importance in engineering applications where damage occurs. It is not clear whether the reactions take place inside the bubbles or at the bubble walls, whether the bubble oscillation frequency is important in producing high temperatures, and whether such phenomena can occur in all liquids of engineering interest. These questions will have to be answered before the role of such phenomena in the damage process can be clearly delineated.

Also, some mention should be made of cavitation erosion studies in high temperature alkali liquid metals (202, 203, 204). Here the chemical activity of mass transfer, or differential solubility of metals due to thermal gradients in the heated liquid could be appreciable and affect the ultimate erosion rate considerably (205).

Some Recent Experiments on the Role of Corrosion in Cavitation Damage Erosion

Pulsing Technique

Plesset (206) introduced a relatively new laboratory procedure known as the pulsing technique in which cavitation damage is produced in an intermittent manner. This technique consists

of a cavitating interval, C_i, and a static interval, S_i, in which the specimen r mains stationary in the liquid. The pulse ratio P is defined as

$$P = \frac{C_i}{S_i + C_i}$$

Using this technique, Plesset showed that the materials less resistant to corrosion in a corrosive medium exhibited greater cavitation damage rates in pulsed cavitation than the more resistant materials.

Effect of testing time

The experiments conducted by Waring, et al (79), with 1020 SAE steel in a 3 percent NaCl solution showed that the corrosive environment does not essentially change the existence of the four zones of damage with respect to time observed in relatively non-corrosive environments.

Effect of amplitude

It has been shown experimentally that the cavitation erosion rate in distilled water at 80°F varies as the second power of the displacement amplitude when testing with a vibratory apparatus in the steady state period. This result has been confirmed with seven metals, namely: 1100-0 aluminum, 304-L stainless steel, 410 stainless steel, molybdenum, cast iron, Inco-300M, and 1020 SAE steel (126). The same relationship is shown in Figure 9-10 for 1100-F aluminum in distilled water and in NaCl solutions of different concentrations up to 9 percent by weight (79). However,

when 1020 SAE steel is tested in NaCl solutions of various concentrations, the relationship between the cavitation erosion rate and amplitude continually changes as shown in Figure 9-11. The erosion rate varies as the second power of the amplitude in distilled water and this power relationship becomes modified to a linear relationship as the NaCl concentration is increased (79) gradually.

Estimation of electrochemical corrosion

The following methods were employed to estimate the rate of loss of material due to electrochemical corrosion so that its relative role can be properly understood (79).

Polarization Measurements.

(1) Static measurements

(2) Dynamic measurements

Pulsing Techniques.

(1) Short pulses

(2) Long pulses

a. Polarization Measurements

An attempt was made to determine the polarization curves for SAE steel specimens in 3 percent NaCl solution in distilled water by means of an applied current technique. Static anodic and cathodic polarization curves were first obtained. The specimen was then cavitated at a double amplitude of 1.5×10^{-3} inch and another set of anodic and cathcdic polarization curves were obtained. The current and potential values were recorded

after 5-minute intervals for each increase in current. Calculations with the Stern-Geary equation (210) yielded a static corrosion rate of 2×10^{-3} mg/min and a dynamic corrosion rate of 15×10^{-3} mg/min.

b. Estimation by pulsing technique

For a particular pulse ratio of P = 1/20, Plesset (206) obtained the cavitation damage of SAE steel (BHN = 150) in 3-percent NaCl solution. He obtained similar data for steady (non-pulsing) cavitation also. From these data, the corrosion rate during the static interval, S_i, was estimated to be of the order of 20×10^{-3} mg/min.

Plesset showed that the rate of erosion depended upon the pulse ratio P. However, the erosion rate not only depends on P but also on the actual value of S_i since the corrosion rate itself is time dependent. A few experiments were conducted by Waring, et al (79), in which C_i was chosen to be 30 minutes instead of 12 milliseconds as selected by Plesset. In this case the value of S_i was of the order of hours. These experiments showed that the corrosion products accumulated during the static interval S_i were removed during the following cavitation interval C_i giving rise to a higher rate of weight loss. However, these rates reach the steady state value if the cavitation interval C_i is long enough. It should also be noted that for similar pulse ratos but different cavitation intervals, the erosion rate can be altered markedly. The rate of corrosion estimated by this technique is of the order of 7×10^{-3} mg/min.

Table 9-1 shows the relative role of electrochemical corrosion in cavitation erosion of 1020 SAE steel in 3-percent NaCl solution under various testing conditions as obtained from the above investigations. It can be seen from this table that the cavitation erosion rate is of the order of 90 x 10^{-3} mg/min in distilled water whereas it is 260 x 10^{-3} mg/min in 3-percent NaCl solution. As shown in Figure 9-6, the contribution to this increased erosion rate from the change in physical properties of the liquid is negligible. However, the rate of electrochemical corrosion as estimated from the above methods can account for only on the order of 10 x 10^{-3} to 20 x 10^{-3} mg/min. Hence, it seems highly probably that the major contribution to the increased weight loss in a corrosive liquid comes from the corresponding deterioration of mechanical properties in a corrosive environment.

Corrosion fatigue

Figure 9-12 shows the fatigue results of SAE 1020 steel in 3-percent NaCl solution along with the results obtained in distilled water (123). These results were obtained in the same vibratory apparatus used for cavitation erosion. The high frequency corrosion fatigue results show that it is the corrosive weakening of the surface that contributes to the major part of the increased rate of damage.

The change in the relationships between damage rate and amplitude for distilled water and for NaCl solutions can also be explained in terms of the fatigue results shown in Figure 9-12.

As the stress levels are decreased the corrosion component of weight loss becomes comparable to the mechanical erosion.

Leith (69) has compared the length of incubation time with the corrosion fatigue limits of four metals as given in the Corrosion Handbook (210), Figure 9-13.

Cavitation Erosion-Corrosion Modeling in an Ocean Environment

The problem of scaling exposure periods in model-prototype correlations was discussed in detail in Chapter VIII. It was also pointed out that the interacting influence of corrosion on their problem is very important. Recently, McGuiness and Thiruvengadam (208, 209) conducted erosion experiments using steels (HY 80, HY 130, and SAE 1020) aluminum alloys and copper alloys in synthetic seawater as well as in distilled water at various intensities of erosion using the ASTM standard vibratory apparatus. The normalized erosion rates are plotted as a function of relative exposure periods in Figures 9-14 through 9-18. A corrosive environment increased the maximum erosion rates, decreased the exposure period needed to attain the maximum erosion rates and decreased the erosion strength of the material. In addition, it also changed the shape of the normalized erosion curves, with the shape parameter, α, increasing systematically with increasing intensity of erosion. This increase in the shape parameter was related to the materials ranking on the galvanic series in sea water (Table 9-2).

X. INTENSITIES ENCOUNTERED IN FIELD DEVICES

Ever since the discovery of the serious erosion of marine propellers, hydraulic turbines, and other major hydraulic structures, there have been several attempts to relate quantitatively the erosion occurring in field installations to that observed at the laboratory. These attempts were handicapped by the lack of an acceptable definition of intensity of erosion which can be readily computed for field devices as well as for laboratory devices.

Furthermore, the field experiences were mostly reported in a qualitative manner rather than in specific quantities such as depth of erosion, area of erosion, physical and chemical properties of materials and liquids used, hydrodynamic characteristics of the device, time of operation, time during which the most serious damage occurred. The reason for the lack of quantitative information is the obvious difficulty in obtaining such data. In fact, such detailed information is not available even for the research devices used in the laboratory.

As a result of this situation, there has been a general impression among the various investigators that the intensity of cavitation erosion (although no quantitative definition of the intensity of cavitation erosion was available until recently) experienced in field installations is very low when compared to the laboratory test devices, e.g., vibratory apparatus. It is for this reason that tests conducted in such devices have been

called "accelerated" tests. In addition, this reasoning led to the question of the suitability of the test method for screening materials for use in field installations operating under so called "real time" erosion conditions.

In the past, several repair procedures and protection methods have been highly successful in some cases, while the same methods have failed badly in other applications. Perhaps this could have been explained or anticipated if there were some quantitative way of determining intensity ranges in which a given method proved to be successful. Furthermore, in certain cases, hydrodynamic redesign coupled with a superior material selection helped to reduce or completely eliminate cavitation erosion. Such successes have gone unnoticed because of the lack of quantitative correlations between the remedy applied and successful performance.

These considerations bring forth the necessity for a new approach toward quantifying the field experience rationally in terms of some acceptable and at the same time easily obtainable parameters and to compare them with laboratory experience. This would lead to an overall perspective of the problem of cavitation erosion from the points of view of researchers, designers, and operators. Such is the aim of this chapter which is based on Reference 125.

DEFINITION OF INTENSITY OF CAVITATION EROSION

One of the approaches to the problem of cavitation erosion is to define the intensity of cavitation erosion in a rational

manner and to compute its value for various field installations. The definition of the intensity of cavitation erosion is discussed in Chapter VI. (See Equation [6-4].)

FIELD INSTALLATIONS AFFECTED BY CAVITATION EROSION

The above intensity parameter is estimated for the field devices that have been affected by cavitation erosion in the past so that one can get a relative idea of how serious the cavitation erosion problem is in relation to the various types of installations (125). The installations that have experienced serious cavitation damage may be listed as follows:

(1) Ship underwater appendages, hydrofoils, struts, rudders, hull, etc.,

(2) Ship propellers,

(3) Hydraulic turbines,

(4) Pumps,

(5) Valves, regulators, sluice gates,

(6) Diesel engine cylinder liners,

(7) Bearings,

(8) Civil engineering hydraulic structures such as baffle piers, stilling basins, spillways, intake structures, penstocks, and tunnels,

(9) Underwater sound transmission and detection devices, and

(10) Nuclear and space technology equipment such as liquid metal handling equipments, cryogenic liquid handling equipments.

This classification is by no means complete. An attempt will be made to discuss some of the above cases for which some quantitative information is available.

CAVITATION EROSION INTENSITY ESTIMATOR AND MASTER CHART

A nomogram (Figure 10-1) called a cavitation erosion intensity estimator has been prepared using Equation [6-4] with three aims in mind. It provides a visual idea of the range of intensities encountered in actual practice within the ranges of the depth of erosion, material used, and time of operation. It also provides a quick and easy method of estimating the intensity of erosion for a given installation. This would be particularly useful for operators. Lastly, the selection of better materials, if available is easily made.

The procedure in using this estimator is as follows:

1. To determine the intensity of erosion, if the depth of erosion, the erosion strength of the material, and the duration of erosion are available, draw a straight line connecting the depth of erosion and the erosion strength. This line will intersect the pivot line (second line from the left without any scale). Join this point of intersection with the duration of erosion by means of another straight line which will intersect the intensity scale, thus giving the intensity for this case.

2. To determine the depth of erosion after a given operating time on a given material, if the intensity of the system is known, draw a straight line connecting the duration

of operation and the intensity so as to intersect the pivot line. A straight line joining this point of intersection and the erosion strength of the material would intersect depth of erosion scale, indicating the depth of erosion for these conditions. This procedure is the reverse of the previous operation.

3. To determine the erosion strength of the material required to give a certain depth of erosion after a given duration of operation in a system of given intensity, draw a straight line joining the intensity and the time of operation intersecting the second line from the left. Another straight line connecting the point of intersection and the depth of erosion would cut the erosion strength scale at the required value.

4. Similarly one can find the duration of operation for a given system of known intensity, fabricated from a given material, if a criterion for the allowable depth of erosion is set.

The estimator should be a convenient design tool for engineers. The usage of the proper units as shown in the nomogram for each parameter would yield the intensity in watts per square meter. The following conversion would give the intensity in American Engineering units

$$\text{Watt/Meter}^2 = 1.25 \times 10^{-4} \text{ H.P./Foot}^2.$$

Figure 7-13 shows the intensity of erosion plotted against rate of depth of erosion for various materials ranging from soft lead to very highly resistant stellites. The range of intensities typical of practical machines varies from 10^3 - 10^4 in.-lb_f/year-in.^{2}. The screening tests such as the vibratory test and rotating disk test operate at intensity levels on the order of 10^5 in.lb_f/year-in.^{2} (1 watt/m^2). The depth of erosion is generally in the range of a fraction of an inch per year. Chemical corrosion rates on steel are in the range of 10^{-3} - 10^{-2} inch per year (ipy) (210, 211). Erosion rates on the order of 1 ipy represent serious erosion which may warrant operational limitation or redesign.

INTENSITY ENCOUNTERED IN FIELD INSTALLATIONS

Ship Hulls and Appendages

It is known that ship hulls and other appendages may be seriously eroded by cavitation. However, very little data are reported. For one case of a destroyer, the armor hull plates above the propeller were pierced by a hole of dimensions of about one square foot after the destroyer had operated for several hours at maximum speed (212). If we assume the thickness of the armor plate as one inch, the time as 10 hours and the erosion strength as 50,000 psi, we would obtain the intensity as approximately 250 watts/meter^2. This intensity is surprisingly high since it is 125 times that of the standard ASTM vibratory erosion device. One can easily conclude that no material can resist this intensity for a prolonged period

of operation and this would form a basis in suggesting a change in the hydrodynamic design and operational limits.

Lichtman, et al (213), made a detailed survey of cavitation erosion encountered in U. S. Navy vessels and attributed certain cavitation erosion ratings, Table 10-1. However, no information as to the depth of erosion, material used, and time of operation was given. Cavitation erosion is a serious problem in some of the modern hydrofoil boats. In one case of the PC (H) PETROL craft hydrofoil boat of the U. S. Navy, $\frac{1}{4}$-inch thick HY-80 plate was completely eroded by cavitation in less than one-half hour at top speed during service trial (214). The intensity of erosion for this case was estimated to be about 50 watts per square meter. Similar estimates for Tucumcari and Flag Staff give an intensity of erosion in the range of 0.1 to 1 watt per square meter (215).

Ship Propellers

Cavitation erosion in some of the early designs of ship propellers was so serious that they had to be discarded after their maiden voyages. Neville (216) reported that for the case of the Bremen, the propeller blades were eroded up to 4 3/4 inches deep within two round trips across the Atlantic Ocean. Similarly, several more instances may be cited from the literature. Actual data were collected for a few modern destroyers of the U. S. Navy which have experienced significant cavitation erosion* (Table 10-2). The intensities ranged from 10^{-1}

*These data were kindly furnished by Mr. J. Hill of U. S. Bureau of Ships, Department of the Navy (212).

watt/meter^2 to 250 watts/meter^2 as compared to two watt/meter^2 for the ASTM vibratory erosion apparatus. In one case (DDG-15), the ship cruised at 20 knots for 20 hours and its intensity was of the order of 40 watts/meter^2, whereas for the other propellers, the exact duration of cavitation erosion is not known. However, the number of hours of operation and the corresponding speed ranges were available in some cases. It is most likely that the major portion of damage occurred at speeds higher than 30 knots.

In view of the importance of knowing this information, future attempts must be made to collect quantitative data. Such detailed information was available (212) for one case of the propeller of a destroyer, USS HIGBEE. Figure 10-2 shows a typical field inspection data sheet from which the intensity could be computed in the range of 2 - 50 watts/meter^2 depending upon the speed at which most of the damage was done. This destroyer had steamed for 9 hours at full ahead and 3 hours at full astern. Most steaming has been at 15 - 20 knots. Figure 10-3 shows the damage on the suction face of blade No. 3 of this propeller. More recent observations of the propellers of the PC (H) hydrofoil boat of the U. S. Navy have indicated an intensity of erosion experienced by the propeller blades in the range of 1 to 2 watts per square meter. The supercavitating propeller blades used in the Flag Staff hydrofoil boat of the U. S. Navy are also experiencing this magnitude of erosion. The maximum erosion rates are observed during "take-off" and "landing" at a speed of around 20 knots (215). This field observation supports the laboratory results obtained in the rotating foil apparatus as

shown in Figure 8-6. According to these observations, the erosion intensity increases with increasing speed, reaches a maximum and then decreases with further increase in speed. This is an important finding most useful in design and operation of critical systems.

Valves

The present survey shows that very serious erosion may occur in valves controlling liquid flow. Borland and Stiles (31) reported that a 316 stainless steel needle valve failed in 10 minutes of operation (Figure 10-4). The maximum intensity for this case has been estimated to be as much as 3000 watts/meter^2. Table 10-3 shows the details and intensities for a few more cases.

Diesel Engine Cylinder Liners

Another case where cavitation damage seems to be important is in Diesel engine cylinder liners (218, 219, 220). As shown in Table 10-4, the damage intensity in certain specific cases can be as much as one watt/meter^2.

Hydraulic Turbines and Pumps

Almost parallel with the detection of cavitation erosion in ship propellers, erosion was also discovered in hydraulic turbines and pumps. However, it is much more difficult to extract quantitative data for turbines and pumps except for some early cases of severe erosion. In recent literature, the erosion is described only qualitatively. Despite this limitation, some

quantities have been estimated from photographs and other descriptions as shown in Table 10-5. In two cases for pumps, quantitative information was available and are included in Table 10-6. Both cases are examples of liquid metal handling pumps.

Since the operational times are total hours of operation and since cavitation erosion occurs most likely during a part of this time, the intensities estimated in Reference (125) would generally be lower than the actual intensities by a factor of at least ten.

Other Devices

Similar estimates of the intensity of erosion could be made for any machine which has experienced cavitation erosion. Since there is not much information available for other devices, no estimates are presented herein. However, this kind of estimation of intensity would form a guide for selecting suitable protection methods based on the experience with other devices.

GENERAL DISCUSSION

What has been presented in this chapter is only a preliminary step toward more rational approaches that are to come by a coordinated effort in the laboratory as well as in the field. Because of the approximate nature of the data available, the whole analysis is necessarily approximate. The intensities estimated herein would vary depending upon the depth of erosion. In most cases the maximum depth of erosion is reported and it would indicate the maximum intensity. This is unavoidable unless more detailed observations are reported in the future.

Again, the property of the material characterizing its erosion resistance is not readily available. Even the use of the strain energy (as given by the area of the stress-strain diagram from a simple tensile test) may not be justified for strain-rate sensitive materials. However, the strain energy seems to be adequate at least for the most common metals which do not exhibit strain rate sensitivity.

The third important parameter is the time during which the erosion took place. This is very difficult to determine, particularly for field installations. Since the operating hydrodynamic parameters would be varying over a period of time and since the output intensity of erosion as estimated in this chapter would also be varying along with input hydrodynamic parameters, the intensities reported herein are essentially approximate in most cases. However, this kind of analysis brings forth the possibility of a quantitative approach for future guidance along with some a priori conclusions.

The intensities of the case histories reported herein apply only to specific cases where significant cavitation has occurred and should not be generalized, at this stage, for the purposes of design.

SOME REMARKS ON THE RANGE OF INTENSITIES FOR THE POSSIBLE APPLICATION OF KNOWN PROTECTION METHODS

It is interesting to compare the intensity ranges for each of the field installations considered with the intensities of the laboratory test devices reported in Chapter VI. As pointed

out earlier, the erosion intensities of certain valves have been estimated to be as much as 3000 watts/meter^2 and certain propeller erosion intensities as great as 250 watts/meter^2 compared to two watt/meter^2 of the ASTM standard vibratory erosion apparatus. As more and more data become available, a statistical distribution of the occurrence of intensities for each type of installation will be possible.

Some Remarks on Protection Methods

From the discussion of threshold intensities in Chapter VII, it is clear that the level of threshold intensities for various metals are of the order of 10^{-1} watt/meter^2 at the most. Elimination of cavitation erosion by substituting one metal for another is possible only up to this level of intensity. For this reason, the usefulness of cathodic protection also seems to be limited at this level. If one is prepared to tolerate some erosion and periodic maintenance, then the materials selection coupled with cathodic protection can possibly extend the allowable intensity levels up to 1 watt/meter^2. However, if the intensity levels are higher than these values, then the above protection methods may not work. In such cases, hydrodynamic redesign, air injection, and specifying limits for operation are the alternate remedial possibilities. These considerations are pictorially represented in Figure 10-5. Further field and laboratory investigations are needed to confirm these ideas.

XI. METHODS OF PROTECTION AGAINST CAVITATION EROSION

TYPES OF PROTECTION

Protection against cavitation erosion may be considered from several points of view: (1) elimination of the problem at the source; (2) use of highly resistant materials in regions of expected cavitation attack; (3) use of artificial means in which protective methods are employed as adjuncts to the system; and, (4) combinations of the latter two methods. Elimination of the problem at the source and the use of specially resistant materials either in the primary structure or as coatings for the primary structure may be considered as methods of reducing the effects of cavitation by primary design. The use of methods which are essentially added or imposed on the system as adjuncts following the basic design but are not part of the structure itself may be considered as imposed protection. Thus, we shall consider the various methods of protection in these terms.

PRIMARY DESIGN

Hydrodynamic Design

A detailed discussion on the factors governing the inception of cavitation appears in Chapter II. Hydrodynamic considerations leading to the prediction and elimination of cavitation have been described therein. It is essential to avoid low pressure regions where the pressures may fall to levels required for cavitation inception; in general, this means regions of high velocity and low ambient pressure. However, the efficient operation of many

machines depends just on this ability to induce high velocities at low pressures; requirements for weight saving and small size in hydraulic machinery also imply operation at high velocities and low pressures. In addition to these factors, which are usually considered in some detail in the design of hydraulic machines, a number of other flow conditions may exist that are conducive to low pressures and the onset of cavitation. Of particular importance are separated flows in which the local turbulent pressure fluctuations and the low pressures induced in the vertical flow associated with such regions may lead to cavitation at ambient pressures higher than would be expected for cavitation inception. Examples of such situations are stalled rotors in hydraulic machinery and the flow about roughness elements on a surface that otherwise has pressures nowhere low enough to cause cavitation to occur.

Very often, for reasons of efficiency or weight reduction, or because a machine must operate under cavitating conditions for only limited periods during its life, it may actually be advantageous to allow operation with cavitation and try to reduce the adverse effects by structural design or imposed protective systems.

Materials for Primary Structures

From the examination of correlations between material properties and resistance to erosion, certain characteristics are desirable for primary structures which must withstand the effects of cavitation. Without regard to other requirements that a

material must possess, such as machinability, the most highly resistant materials are those with a tough, homogeneous, fine-grained structure, a high tensile strength, high elongation, high hardness, good work hardening properties, and high fatigue and corrosion fatigue limits. The stainless steels generally possess these properties in a good measure as do aluminum bronzes. An outstanding material is stellite, but its poor machining qualities (because of great hardness) and high cost make it unattractive for many applications. Materials such as molybdenum, tungsten, and titanium alloys possess very attractive properties but have not yet come into full engineering use in this application. The relative merits of other metals and alloys will be found in Chapter VII.

Where materials are used for primary structures that are not particularly suitable for erosion resistance, it has become a growing practice to use overlays of highly resistant metals or other coatings.

Special Coatings

In an attempt to reduce the destructive effects of cavitation either in a new machine or when repairing eroded surfaces, several metallic and nonmetallic materials have been investigated for use as coatings. These take the form of welded overlays, sprayed metallic or nonmetallic coatings, and nonmetallic coatings applied by special techniques including bonding.

Welded overlays of stainless steel or aluminum bronze are excellent for protection as might be expected from their general

behavior under cavitation erosion. There are a number of other welding alloys that are suitable and have good erosion resistance qualities (see e.g., Rheingans [221]); selection of such materials will, however, be governed by their machining, grinding, and finishing properties as well as their cavitation erosion resistance.

Sprayed metal coatings are attractive because of the ease of application and low cost. However, difficulties may be encountered unless the sprayed metal is also fused to the base metal. Rheingans (221) has given data on the characteristics of various sprayed metal coatings both fused and unfused; his data from laboratory damage tests are reproduced in Table 11-1. He points out that the resistance of unfused coatings is not very good, because of the difficulty of obtaining a good bond between the coating and the base metal. The fused metallic coating shown in Table 11-1 was prepared by spraying on a specially prepared base and then heating to 1850°F. Rheingans remarks that although these coatings exhibit good resistance qualities they are limited in usefulness by high cost and by the distortion produced in the base metal during fusion.

Among the nonmetallic materials that have been tested as coatings are natural and synthetic rubbers and a number of plastics. Examples of materials tested for this purpose are thiokol rubber, neoprene, nylon, phenolic resin, and teflon. Neoprene and polyurethane coatings appear to have exceptionally good resistance (see Chapter VII). Plastics generally exhibit poor resistance characteristics compared with neoprene. These results

are discussed in detail in Chapter VII. Major difficulties with such coatings arise because of poor bonding between coating and base material; the entire coating may be torn away from the base material by the violent action of cavitation before the coating itself is eroded. Such adhesion failures of these coatings in service is still a mysterious problem. Some coating systems behaved well for about 72 hours in a laboratory rotating disk screening test at a speed of 150 fps, whereas the same coating system failed badly in field applications at speeds lower than 75 fps in a shorter time (222, 214). Experiments were recently conducted (223, 224, 225) measuring the adhesion strength of candidate coatings for U. S. Naval hydrofoil boats before and after exposure to cavitation erosion. Cavitation was induced on specimen plates by the ASTM vibratory apparatus. Adhesion was measured using a Hesiometer (223) and a modified universal testing machine (225). The effects of varying coating thickness and different substrate materials were investigated.

Among the two commercial polyurethane coating systems, Astrocoat 8006 and Laminar X500, test results showed that the softer of the two polyurethanes retained adhesion strength if the coatings applied were greater than 5 mils and were applied with sufficient care to eliminate air bubbles and other "holidays". In general, it was found that erosion resistance is proportional to coating thickness in the range of thicknesses tested. Theoretical predictions concerning adhesion strength as a function of the ratio of acoustic impedance of substrate and coating were borne out in these investigations.

IMPOSED PROTECTION

Air Injection

Perhaps the earliest method of artificially protecting hydraulic machinery against cavitation damage was the use of small amounts of air injected into the cavitating region. It is unlikely that the idea originated from the observation that cavitation damage is reduced in large turbines during seasons when the air content of the reservoir water is high. Ackeret (226) was perhaps the first to point out on theoretical grounds that a permanent gas in cavitation bubbles would greatly reduce the collapse pressures (although he also decided that the temperature of such gas must increase greatly). In any event, air injection has been used with success in reducing or even eliminating cavitation erosion (155, 227), and the mechanism of its protective action is clearly the "cushioning" effect produced during compression by the collapsing cavitation bubbles. As pointed out in a previous part of this chapter, the fact that such air injection does reduce or eliminate cavitation erosion also substantiates the observations that cavitation erosion is primarily a mechanical effect.

Experimental observations of the effectiveness of air injection have been recorded by Mousson (67) and Rasmussen (228, 86). Some results of Mousson on a copper bus bar in a venturi apparatus are shown in Figure 11-1a; the effect of air injection on the damage sustained by an aluminum alloy in experiments by Rasmussen using a rotating disk apparatus is shown in Figure 11-1b. The air

content in Mousson's experiments is given in percent of discharge (volumetric flow rate) while that of Rasmussen's experiments is given in parts per thousand. In each case the ameliorating effects of relatively small quantities of air is strikingly demonstrated.

It is of interest to note that the introduction of air does not seem to produce adverse effects on most metals as far as corrosion is concerned --- the reduction of primary mechanical damage being so much greater than any adverse chemical effects. Only in one case has there been observed such adverse chemical effects. In Rasmussen's experiments on cast iron, the increase in chemical corrosion was just about balanced by the protective action of the air bubbles. The reduced pressures of the bubbles were still sufficiently large or the water motion great enough to remove the oxide layers formed on the iron.

Cathodic Protection and Hydrogen Evolution

There has been much controversy and conjecture concerning the application of cathodic protection to prevent cavitation erosion so that it is worth devoting some detail to the understanding of this subject. From the foregoing discussions in Chapter IX much evidence has been presented to show that under certain favorable conditions the corrosive influence of the environment can radically affect the cavitation erosion sustained by some metals. It also follows that where the corrosive influence is large in the cavitation erosion process any method of mitigating the effects of corrosion should effect an improvement

in the cavitation resistance of the metal in the specific environment. In general, overall corrosion processes are slow when compared to the mechanical rate of destruction of materials undergoing cavitation erosion. However, the intensity of erosion appears to be the key factor in determining the role of corrosion in the cavitation erosion process at low intensities (see Chapter IX); the rate of mechanical damage due to cavitation is low and therefore the damage contributed by corrosion could be a substantial portion of the total damage. It appears that for cavitation erosion intensities below 0.1 watt/meter^2 in a corrosive environment marked improvement in resistance to erosion can be gained by the application of corrosion control methods, such as cathodic protection.

It has been shown by numerous investigators such as Krenn (187), Preiser et al (229), Ffield et al (190), Higgins (230). Duff (231), and others that the application of cathodic protection at reasonable current densities (under 250 ma/ft^2) can effectively reduce cavitation erosion in specific instances (turbine runners and ship propellers).

It has also been pointed out in Chapter IX that where corrosion fatigue of metal seriously impairs its mechanical strength, then substantial increases in damage rate can be expected when the metal is cavitating in a corrosive environment as compared to a non-corrosive one. Here again, the application of cathodic protection to stifle the relatively small amount of electrochemical corrosion, which in turn has a large effect on the fatigue properties of the metal, can show a large improvement in its resistance to cavitation erosion.

The same gains could be expected for metals which exhibit stress corrosion cracking. In these cases, the mechanical weakening influence of the corrosive environment, could be stopped or reduced by the proper application of cathodic protection.

Some precautionary remarks should be made regarding the use of cathodic protection. Cathodic reaction on certain amphoteric materials such as zinc, magnesium, and aluminum could accelerate the corrosion process by the formation of alkali deposits on the cathode (cathodic corrosion) and therefore the current density requirements for protection need to be defined carefully.

Also, certain metals, such as some of the stainless steels and titanium materials, exhibit a weakening of its lattice structure by the uptake of hydrogen sometimes associated with the cathodic process. This phenomenon is known as hydrogen embrittlement. Again, care must be exercised to delineate the correct current density for corrosion protection without introducing undesirable side effects. Discussions of the problems of hydrogen embrittlement in steel from the viewpoint of basic mechanisms and the application of cathodic protection for prevention of normal electrolytic corrosion will be found in References 232 and 233.

Cathodic protection at moderate current densities can be a powerful protection method for alleviating the considerable corrosive influence of low intensity cavitation erosion to susceptible materials in aggressive environments. Materials

which do not show marked reduction of endurance limits in corrosive environments or materials which exhibit a high degree of passivity are not usually benefited in the cavitation erosion resistance by the application of cathodic protection (moderate current densities). However, cathodic protection at high current densities (above 1 ampere/ft^2) can have considerable effect because the accompanying evolution of hydrogen gas at the cathode can indeed provide a cushioning effect which reduces the mechanical impact of cavitation bubble collapse similar to that produced by air injection described previously.

Plesset and his colleagues (195, 196) performed a series of experiments in a vibratory apparatus in which the cavitation erosion rates on a 4340 steel and a high purity copper were determined as a function of applied cathodic current.

Results of the experiments on 4340 steel are shown in Figure 11-2. The effect of large impressed cathodic currents is clearly demonstrated. Tests were also made on copper of high purity in order to compare the above results with those for relatively inactive metal. Figure 11-2 is the summary of the average results for the latter experiments as reported by Plesset (196). Thus, similar trends were found for both the steel and copper specimens. It is emphasized that in all of the experiments in the salt solution hydrogen evolution was observed on the specimen surface even at the lowest cathodic current of 1 milliamp which corresponds to current density of 1 ampere/ft^2. Considering the range of materials tested, these results indicate that the protective effect against cavitation erosion is

associated with the cushioning provided by the evolved hydrogen. Further substantiation of this conclusion is the result that the weight loss decreases monotonically with increasing rate of hydrogen evolution (or increasing cathodic current). Full protection was not obtained over the range of currents used and this fact is attributed to the removal of the hydrogen gas layer through agitation produced in the cavitated zone.

In further substantiation of the conclusion that this protection is associated with the cushioning effects of evolved gas, a series of experiments was performed by Plesset (196) in which the specimen was the anode of an electrolytic cell but in such a way that, at the same time, gas evolved at the specimen surface. This was done by using stainless steel in distilled water buffered to pH 8. One electrode of the cell was again platinum, and the other 17-7 PH stainless steel. Two sets of experiments were performed. In the first, the specimen was the cathode of the cell, and erosion was determined for cathodic currents of 20, 50, and 100 milliamps corresponding to current densities of 20, 50, and 100 amp/ft^2, respectively; for all of these values, hydrogen gas was observed to be evolved at the specimen. The results are summarized in Figure 11-3a. In the second series, the specimen was made the anode of the cell and erosion was measured for anodic currents of 40, 100, and 200 milliamps. The gas evolved in the latter case is oxygen with a valence twice that of hydrogen, so that double the current is required to evolve comparable amounts of gas for purposes of direct comparison. A summary of the latter results is shown in

Figure 11-3b. A comparison of the results of the two types of experiments shows that the protective effect in each case is of the same order of magnitude; this result would be expected if the protection provided is indeed attributable to the cushioning effects of evolved gas.

A final series of tests made by Plesset is of interest in this connection. An attempt was made to observe the damage at current levels so low that no gas was evolved. This was not possible with the cathodic specimen in salt, since gas was evolved at the lowest currents practicable. However, in the case of both the cathodic and anodic specimens in buffered water, no observable gas evolution occurred at a current of 2 milliamps. Under these conditions, no protective effect against cavitation damage could be obtained.

It is clear from these experiments that the application of large cathodic current densities, resulting in hydrogen gas evolution, can effectively reduce cavitation erosion in electrolytes. This method should find application for the protection of components with relatively small area, e.g., propellers and hydrofoils, subjected to high intensity cavitation erosion. The additional benefits of cathodic protection achieved simultaneously by this method are probably small, but it is an added bonus.

The application of cathodic protection to cavitating systems in poor electrolytes is not practical or particularly beneficial. The choice of these protective methods is clearly dictated by the

intensity of cavitation erosion, size of structure and the economics of applying the protective current at suitable current densities. The practical design of such systems for ships has been made (234).

Corrosion Inhibitors

The employment of corrosion inhibitors for prevention of cavitation erosion in diesel cylinder liners has been partially successful in field installations particularly where the correct concentrations were used (235). Corrosion inhibitors derive their protective influence by their retarding action on anodic and cathodic processes associated with the dissolution of metal in an electrolyte. There are two types of inhibitors: anodic inhibitors which are primarily inhibitors of oxidizing action; cathodic inhibitors, which suppress the corrosion rate by reducing the effectiveness of the cathodic process or by reducing cathode area. They can be inorganic or organic in chemical composition. Organic inhibitors generally absorb on the metal cathodes and increase the hydrogen overpotential; or in some cases on the metal anodes they stifle the anodic process. It is apparent that inhibitors affect the electrochemical processes of corrosion similar to that of cathodic or anodic protection and therefore should only be effective for low intensity cavitation damage situations in corrosive environments which are usually obtained in diesel cylinder liners exposed to jacket cooling water. The higher intensity cavitation damage associated with magnetostriction devices tends to mask the effectiveness of inhibitors as observed by Rheingans (68) and Speller and Laque (236).

Inhibitors can act as corrosion stimulators if not used in the proper concentration. Anodic inhibitors (oxidants) act as good depolarizers and therefore accelerate the cathodic process while simultaneously tending to passivate the anodic process. Therefore, as in the case of chromates, insufficient concentration would reduce the anodic sites in the corrosion process and at the same time accelerate the cathodic processes. As a result, the remaining active anodes now bear the full corrosion load and therefore tend to corrode faster producing localized pits. Only when all the anodes are passivated (increasing concentration) does the inhibitor become effective.

The same applies to cathodic inhibitors such as sodium sulphate or calcium bicarbonate, however, here insufficient concentration only results in partial protection. However, in certain cases, partial absorption of oxygen by a cathodic inhibitor can activate a passive metal such as stainless steel and stimulate pitting.

It follows from this discussion that if inhibitors are employed in proper concentration to stifle electrochemical corrosion, then at low intensity levels of cavitation damage, where this suppression of corrosion is effective, the resistance of the material can be markedly improved.

XII. FIELD REPAIR PROCEDURES AND SERVICE TRIALS

WELDING

Overlay

One of the most popular remedial measures to repair damaged parts is overlay welding. Detailed procedures vary with the practical situation and other requirements. However, it is the general practice to machine or grind the surface suitably for the particular type of welding. Some practices of the hydraulic turbine industry and the U. S. Navy in propeller repair will be reviewed herein. Some procedures of the hydraulic turbine industry in surface preparation are (237):

1. Chip the pitted area. This is not generally recommended if it would otherwise damage the blades.

2. Where pitting is shallow, simply grind prior to welding.

3. An oxygen gouging flame or electri-arc gouging flame may be used.

After preparation of the surface, welding with one of the following procedures follows:

1. Strenge (238) reports that the Lincoln-ferro weld has been successful for cast runners where damage is shallow. Where deeper pits are found in cast iron runners, it has been their practice to use a Lincoln bronze Aerris weld rod for the first pass and to follow this with a layer of Lincoln strain weld A-6(18-8) lime-coated rod.

2. Sherwood (239) recommends welding with Eutectic No. 280, Eutectic Xyron No. 2-24, or AmpCo No. 10 electrodes for bronze runners of hydraulic turbines. For cast steel runners, mild steel electrodes have been successfully used for shallow damages. Where the damage is intense, the pits are filled by use of the mild steel electrode except for the last two passes. The next to the last pass is filled with 25-20 stainless steel and the final layer is made with a 17-7 stainless electrode.

3. Alexander (240) states that no difficulties have been observed for different coefficients of thermal expansion of cast steel and 17-7 stainless steel. However, when several passes of stainless have been applied, the underlying passes have on occasion been peened to reduce residual stresses and reduce any possible distortion to a minimum. Both hand welding with a stick electrode and semi-automatic shielded inert-gas metallic arc welding with a consumable wire electrode are used.

Alexander (240) recommends that these welded overlays must be finished with exactness and care to the optimum contours for a successful repair. Deskin (241) adds that a highly polished surface is most resistant to cavitation erosion. However, Strenge (238) does not find any adverse effects from lack of fine finishing and polishing.

Some practices of the U. S. Navy in propeller repair by means of welding are described in Reference (242). The repair procedure is selected with regard to the propeller material and

type of erosion. In general the welding procedure must meet three qualifications (242):

1. Tensile test specimens shall exhibit minimum tensile strength of the base metal.

2. Side bend test specimens (MIL-STD-418) developing a crack 1/8-inch long in any direction shall be considered as having failed.

3. Macro-etch test shall show no slag or lack of fusion over 1/8-inch in length.

Some recommended welding processes are briefly outlined below:

On manganese bronze propellers repairs to heavy sections should be made by means of shielded metal-arc welding or the inert-gas, metal-arc welding process. Gas welding should be limited to repair of the edges. Major repairs to manganese bronze propellers are made with the flow welding process. This process requires a preheat to 500°F - 600°F and a stress-relief treatment.

On nickel aluminum bronze propellers, repairs are made by means of the inert-gas metal-arc welding process with consumable electrodes.

On nickel manganese bronze propellers, inert-gas tungsten metal-arc process is used.

On Superston 40 bronze propellers, either metal-arc or inert-gas metal-arc welding processes are used with consumable electrodes.

In each case discussed above the filler metal is specified (242). Directions are also specified for preheat treatment, furnace stress relief and local stress relief.

Inserts

Another method of field repair that is currently receiving consideration is the welding of an insert of a more resistant material in place of the damaged material. In this technique, a material is selected by means of the cavitation estimator described in Chapter X which will resist the known field intensity of erosion for the required time. This material is then cut in thin plate form and bonded by means of a special proprietary pressure welding process, to a substrate of material similar to the rest of the component (e.g., a propeller). This insert is then welded onto a properly prepared recess from which the damage material was removed. This process is not fully developed as yet since several problems remain:

1. The adhesion of the bond between the resistant metal and substrate of the insert.
2. Edge preparation for welding.
3. Galvanic effects of dissimilar materials.
4. Thermal expansion of different materials during welding.

ELASTOMERIC COATINGS AND INLAYS

Lichtman and Weingram (132) of the U. S. Navy Applied Science Laboratory reported on the extensive experience gained from

attempts to protect against cavitation erosion with elastomeric coatings and inlays. These included liquid, pre-cured sheets and in situ cured and bonded materials of different basic polymer types. Three specific cases of application of this procedure to ship's structures are reported:

1. Application to the foils, struts, rudders, and flaps of HIGH POINT [PC(H)-1].

2. Application to the propeller of USNS AMERICAN EXPLORER (T-Ao-165).

3. Application to the propeller of USS STORMES (DD 780).

Application Procedures

The metallic surfaces have to be cleaned thoroughly before the coatings are applied either by sandblasting or by disk grinding. Further cleaning and degreasing may be done by trichloroethylene. When the coating is to be applied on a surface that is already damaged by cavitation erosion, it is a good practice to weld the eroded area, finish the surface, and then apply the coating. After these preparations, the coating system with proper adhesives is applied. For two cases, a PC(H)-1 hydrofoil boat and the propeller of the USNS AMERICAN EXPLORER (T-Ao-165), a neoprene coating MIL-C-570, developed by the U. S. Naval Applied Science Laboratory, was applied (132).

Another case in which an elastomeric inlay [MIL-C-663 (SBR-1500) of the U. S. Naval Applied Science Laboratory] was applied and cured in 1/8-inch deep machined recesses in the root

areas of the suction faces of three of the four blades of each propeller of USS STORMES (Figure 12-1). The inlays were fitted to the dovetailed recesses and were cured under heat and pressure.

SERVICE TRIALS

Careful observations were made on service trials of the above three cases and the following conclusions are reported by Lichtman (132):

Adhesive Strength

Deficiencies in adhesive strength have contributed to every service failure described (See Figures 12-2, 12-3, and 12-4). Tests of the actual adhesive strength of overlays or inlays in service trials should be made to confirm laboratory tests. Until non-destructive procedures are developed, destructive methods may be used, patching the test areas with neoprene trowelling compound.

Adhesion processes providing higher adhesive strengths than those now available are required.

Erosion Resistance

The erosion resistance of MIL-C-663 (SBR 1500) inlays was inadequate, Figure 12-4. Variability and inadequate control of cure in the in situ field applications probably contributed to this inadequacy.

The erosion resistance of the neoprene coating system MIL-C-570 was not indicated by the service trials because of adhesion failures, Figure 12-5.

Field Inspection of Tucumcari and Flag Staff Hydrofoil Boats

Field observations (243) of the Tucumcari and Flag Staff hydrofoil boats indicated that the failures of these coatings were localized in contrast to the gross failure observed earlier by Lichtman (132) for the case of HIGH POINT [PC(H)-1] hydrofoil boat. These localized failures may be generally classified into adhesion failures, failures due to cavitation erosion, marine fouling, and corrosion of substrates. The adhesion failures generally occur at leading edges, trailing edges, strut-pod intersections, flap-foil intersections (in the case of Tucumcari), panel joints, rivet and bolt heads, and any at local surface roughness. Possible causes include improper application of coatings at difficult locations (including difficulties in preparing the sharp corners before the application and in the curing conditions and procedures), high local hydrodynamic shear stresses at critical locations, cavitation bubble collapse forces and substrate corrosion (including crevice corrosion), and galvanic effects caused by water permeation at localized areas. Cavitation erosion was more pronounced at local areas where boundary layer separation may be expected. The critical speeds for erosion were different at different locations. During take-off and landing, each of these areas experience cavitation for periods ranging from 30 seconds to 3 minutes. The fact that critical

cavitation erosion depends upon operational speeds was demonstrated by the serious erosion of the supercavitating propellers in 2 hours at 17 - 18 knots operation.

CONCLUDING REMARKS

Additional quantitative data are being generated from more recent service trials. The intensities of erosion experienced by hydrofoils, propellers, turbine blades, and diesel engine liners are well documented and the successful protection techniques already exist. These successes have been primarily due to the coordinated effort both in laboratory experimentation and in the service trial experience. The intensity of cavitation erosion is a very useful parameter in understanding and solving the erosion problems encountered in service through proper utilization of laboratory data. Consistent with this approach, attempts have been made in the laboratory to delineate the ranges of intensities for which specific protection methods may be successful as indicated in Figure 10-5. This figure has considerably aided the selection of specific field repair and protection methods. It appears that there are no effective protection methods, neither changing the materials nor the techniques such as welding and coating, beyond the intensity range of one watt/square meter for long term operation. Ever stellite is known to be eroded above this intensity. Beyond this intensity range the designer should be prepared to live with erosion or he must redesign his system so as to reduce the intensity range, through proper hydrodynamic means and model tests. There seems

to be ample scope for research in this area. More insight is being gained into the role of liquid parameters and hydrodynamic parameters in the mechanism of the cavitation erosion process. Experimental investigations are in progress for understanding and defining the non-metallic material response to cavitation erosion. The design and material selection process is being aided greatly through such understanding.

REFERENCES

1. Thiruvengadam, A., "Cavitation Erosion," Applied Mechanics Reviews, Vol. 24, No. 3, 245-253, March 1971.

2. Eisenberg, P., "On the Mechanism and Prevention of Cavitation," The David W. Taylor Model Basin, Washington, D.C., Report No. 712, 3, July 1950 and "Mechanics of Cavitation." in Handbook of Fluid Dynamics, Streeter, Victor L., ed., McGraw Hill Book Co., Inc., New York, 1961.

3. Johnson, V. E., Jr., "Cavitation Inception and Damage," Schiffstechnik, Bd. 13, 19-26, Heft 65, 1966.

4. Parsons, C. A., and Cook, S. S., "Investigations into the Causes of Corrosion or Erosion of Propellers," Engineering, Vol. 107, 515-519, 1919.

5. Euler, L., "More Complete Theory of Machines Driven by Hydraulic Reaction," (in French), Histoire de Academie Royale des Sciences et Belles Lettres, Classe de Philosophie Experimentale, 227-295, Mem 10, 1754, Berlin, 1756.

6. Reynolds, O., "Experiments Showing the Boiling of Water in an Open Tube at Ordinary Temperatures," British Assoc. Adv. Sci. Report, 564, 1894, see also Scientific papers, 578-587.

7. Rayleigh, Lord, "On the Pressure Developed in a Liquid During the Collapse of a Spherical Cavity," Phil. Mag., Series 4, Vol. 34, 94-98, 1917.

8. Ackeret, J., "Kavitation," Handbuch der Experimentalphysik, leipeing, Vol. 4, Part I. 461-468, 1926: David Taylor Model Basin Translation 22, 0-22, June, 1933.

9. Föttinger, H., "Studies of Cavitation and Erosion in Turbines, Turbopumps, and Propellers," (in German), Hydraulische Probleme, 14-64, 107-110, 1926.

10. Hunsaker, J. C., "Cavitation Research at the Massachusetts Institute of Technology," Mech. Eng., Vol. 57, No. 4, 211-216, April 1935; see also Trans, Am. Soc. Mech. Engrs., Vol. 57, No. 7, 423-424, October 1935.

11. Nowotny, H., "Destruction of Materials by Cavitation," VDI-Verlag, Berlin, 85, 1942. (Reprinted by Edwards Brothers, Inc., Ann Arbor, Michigan, 1946.) English translation as ORA Report No. 03424-15-I, Nuclear Engineering Department, University of Michigan, 1962.

12. Beeching, R., "Resistance to Cavitation Erosion," Trans. Inst. Engrs. and Shipbuilders, Scotland, Vol. 85, 210-276, 1942.

13. Godfrey, D. J., "Cavitation Damage - A Review of Present Knowledge," Admiralty Materials Laboratory, Holton Heath, Poole, Dorset, June 6, 1959.

14. Eisenberg, P., "Cavitation Damage," HYDRONAUTICS, Incorporated Technical Report 233-1, Laurel, Md., 110, 1963.

15. Plesset, M. S., "Bubble Dynamics in Cavitation in Real Fluids," (Robert Davis, Ed.) pp. 1-18, Elsevier Publishing Company, Amsterdam, 1964.

16. Holl, J. W., "Limited Cavitation," Cavitation State of Knowledge, ASME, 26-64, 1969.

17. Ripkin, J. F., "A Study of the Influence of Gas Nuclei in Cavitation Scale Effects in Water Tunnel Tests," St. Anthony Falls Hydraulic Lab., Univ. of Minn., Proj. Report No. 58, February, 1958.

18. Ripkin, J. F., and Killen, J. M., "A Study of the Influence of Gas Nuclei on Scale Effects and Acoustic Noise for Incipient Cavitation in a Water Tunnel," St. Anthony Falls Hydraulic Lab., Univ. of Minn. Tech. Paper No. 27, Series B, September, 1959.

19. Strasberg, M., "Undissolved Air Cavities as Cavitation Nuclei," Cavitation in Hydrodynamics (Proc National Phys. Lab. Symp.), Paper No. 6, H. M. Stationary Office, London, 1956.

20. Kermeen, R. W., McGraw, J. T., and Parkin, B. R., Trans. of ASME, Vol. 77, 533-541, 1955.

21. McCormick, B. W., Jr., "On Cavitation Produced by a Vortex Trailing from a Lifting Surface," ASME Paper No. 61-WA-100, December 1961.

22. Bindel, S., and Lombardo, R., "Influence de la Vitesse et de la Teneur en Air de L'Eau Sur L'Apparition de la Cavitation Sur Modele," Assoc. Technique Maritime et Aeronautique, 1964.

23. Noltingk, B. E., and Neppiras, E. A., "Cavitation Produced by Ultrasonics," Proc. Phys. Society 63B, 674-685, 1950; AMR 5 (1952), Rev. 1760.

24. Morgan, W. B., and Lichtman, J. Z., "Cavitation Effects on Marine Devices," ASME Symp. on Cavitation State of Knowledge, 195-241, 1969.

25. Tulin, M. P., "Supercavitation Propellers - History, Operating Characteristics, Mechanism of Operation," Proc. of the Fourth ONR Symposium on Naval Hydrodynamics, U. S. Government Printing Office ACR-92, 239-286, 1962.

26. Wislicenus, G. F., "Fluid Mechanics of Turbomachinery," Dover Edition.

27. Wood, G. M., and Whippen, W. G., "Cavitation Effects in Turbomachinery," ASME Symp. on Cavitation State of Knowledge, 148-165, 1969.

28. Ishii, T., "The Two Types of the Runaway State of Propeller Turbine Under Cavitation," Paper No. B-5, Proceedings of IAHR Symposium on Cavitation and Hydraulic Machinery, Sendai, Japan, 1962.

29. Nechleka, Miroslav, "Hydraulic Turbines," Constable and Co., Ltd., London WC2, p. 235, 1957.

30. Warnock, J. E., "Experiences of the Bureau of Reclamation," Cavitation in Hydraulic Structures - A Symposium, Proc. Am. Soc. Civil Engrs., Vol. 71, No. 7, 1044-1046, Sept. 1945.

31. Borland, B. B., and Stiles, G. F., "Cavitation as Related to Control Valves," Fisher Sales Meeting, May 24, 1960, Fisher Governor Company, Marshalltown, Iowa, 1960.

32. Thiruvengadam, A., Unpublished research.

33. Ellis, A. T., "Production of Accelerated Cavitation Damage by an Acoustic Field in a Cylindrical Cavity," Jour. Acous. Soc. Amer., Vol. 27, No. 5, 913-921, September, 1955.

34. Flynn, H. G., "Collapse of a Transient Cavity in a Compressible Liquid, Part I, An Approximate Solution," Harvard University Acoustic Research Lab. Tech. Memo 38, 1957.

35. Trilling, L., "The Collapse and Rebound of a Gas Bubble," Jour. Applied Phys. 23, 14-17, 1952; AMR 6 (1953), Rev. 214.

36. Gilmore, F. R., "The Growth or Collapse of a Spherical Bubble in a Viscous Compressible Liquid," Calif. Inst. Tech. Hydrodynamics Lab. Rept. 26-4, April, 1952.

37. Poritsky, H., "The Collapse or Growth of a Spherical Bubble or Cavity in a Viscous Fluid," Proc. First U. S. Natl. Congr. Applied Mech. (ASME), 813-821, 1952; AMR 7 (1954), Rev. 3623.

38. Daily, J. W., Hammitt, F. G., and Knapp, R. T., "Cavitation," McGraw Hill Book Company, 1970.

39. Hickling, R., and Plesset, M. S., "Collapse and Rebound of a Spherical Bubble in Water," Physics of Fluids 7, 7-14, 1964; AMR 17, (1964), Rev. 5963.

40. Ivany, R. D., and Hammitt, F. G., "Cavitation Bubble Collapse in Viscous Compressible Liquids - Numerical Analysis," Jour. Basic Engineering, Trans. ASME Series D 87, 977-985, 1965; AMR 19 (1966), Rev. 3684.

41. Silver, R. S., "Theory of Stress Due to Collapse of Vapor Bubbles in a Liquid," Engineering, Vol. 154, 501-502, December 25, 1952.

42. Chambers, L. A., "Emission of Visible Light from Cavitated Liquids," Jour. of Chemical Physics, Vol. 5, No. 5, 290-292, May, 1937.

43. Sutton, G. W., "A Photoelastic Study of Strain Waves Caused by Cavitation," Jour. Applied Mech., Vol. 24, No. 3, 340-348, September 1957.

44. Jones, I. R., "The Measurement of the Pressure Due to the Collapse of Cavities in Liquids," Unpublished Thesis, University of Wales, Aberystwyth, England, 1958.

45. Private Communication from Dr. Ieuen R. Jones, California Institute of Technology, July 24, 1959.

46. Mundry, E., and Guth, W., "Kinematographische Untersuchungen der Schwingungskavitation," Acustics, Vol. 7, 241-250, 1957.

47. Vennard, J. K., and Lomax, C. C., Jr., "Experimental Research on Cavitation Collapse Pressures," Stanford University Dept. Civil Eng. Rept., Office of Naval Research Contract N6-ONR-25118, December 15, 1950.

48. Eisenberg, P., "Mechanics of Cavitation," in Handbook of Fluid Dynamics, Streeter, Victor L., ed., McGraw Hill Book Co., Inc., New York, 1961.

49. Kornfeld, M., and Suvorov, L., "On the Destructive Action of Cavitation," Jour. App. Phys. Vol. 15, 495, 1944.

50. Naude, C. F., and Ellis, A. T., "On the Mechanism of Cavitation Damage by Nonhemispherical Cavities Collapsing in Contact with a Solid Boundary," Trans. ASME, Vol. D83, Jour. Basic Eng., 648, 1961.

51. Hancox, N. L., and Brunton, J. H., Phil. Trans. Roy. Soc. London, Series A. Math. Phys. Sciences 260, 121, 1966.

52. Thiruvengadam, A., Rudy, S. L., and Gunasekaran, M., "Experimental and Analytical Investigations on Liquid Impact Erosion," ASTM STP 474, 249-287, 1970.

53. Benjamin, T. B., and Ellis, A. T., "The Collapse of Cavitation Bubbles and the Pressures Thereby Produced Against Solid Boundaries," Phil. Trans. Roy. Soc. London, Series A, Math. Phys. Sciences 206A, 221-240, 1966.

54. Tulin, M. P., "On the Creation of Ultra-jets," L. I. Sedov 60th Anniversary Volume, Problems of Hydrodynamics and Continuum Mechanics, Moscow, 1969.

55. Mitchell, T. M., and Hammitt, F. G., "Collapse of a Spherical Bubble in a Pressure Gradient," ASME Cavitation Forum, May, 1970.

56. Plesset, M. S., and Chapman, R. B., "Collapse of an Initially Spherical Vapor Cavity in the Neighborhood of a Solid Boundary," Rep. 85-49, Cal. Inst. of Tech., Div. of Engr. and Appl. Science, June, 1970.

57. Bowden, F. P., and Brunton, J. H., "The Deformation of Solids by Liquid Impact at Supersonic Speeds," Proc. Roy. Soc. London, Series A, Math. Phys. Sciences 263m,433-450, 1961.

58. Eisenberg, P., and Pond, H. L., "Water Tunnel Investigations of Steady State Cavities," David Taylor Model Basin Report 668, October 1948.

59. Shal'nev, K. T., "The Structure of the Cavitation Region," (in Russian), Isvestia Akad, Nauk, SSSR, Div. of Tech. Sci., No. 5, 120-146, 1954.

60. Knapp, R. T., "Recent Investigations of the Mechanics of Cavitation and Cavitation Damage," Trans., ASME, Vol. 77, No. 7, 1045-54, October 1955.

61. Thiruvengadam, A., "Prediction of Cavitation Damage," PhD Thesis, Dept. of Hydraulic Engr., Indian Institute of Science, Bangalore, India, 1961.

62. de Haller, P., Scheweitzer Bauzeitung 101, 243-246, and 260-264, 1933.

63. Boettcher, H. N., "Failure of Metals due to Cavitation Under Experimental Conditions," Trans. ASME, Vol. 58, 355-360, 1936.

64. Poulter, T. C., "The Mechanism of Cavitation Erosion," Jour. Appl. Mech., A-31--A-37, March, 1942.

65. Knapp, R. T., "Accelerated Field Test of Cavitation Intensity," Trans. ASME, Vol. 80, No. 1, 91-102, January 1958.

66. Kerr, S. L., "Determination of the Relative Resistance to Cavitation Erosion by the Vibratory Method," Trans. ASME, Vol. 59, 373-397, 1937.

67. Mousson, J. M., "Pitting Resistance of Metals Under Cavitation Conditions," Trans. ASME, Vol. 59, 399-408, 1937.

68. Rheingans, W. J., "Accelerated Cavitation Research," Trans. ASME, Vol. 72, No. 5, 705-719, July, 1950.

69. Leith, W. G., "Cavitation Damage of Metals," The Engineering Journal, March, 1959.

70. Plesset, M. S., and Ellis, A. T., "On the Mechanism of Cavitation Damage," Trans. ASME, Vol. 77, No. 7, 1055-1064, October 1955.

71. Gould, G. C., "Some Observations on Erosion by Cavitation and Impingement," ASTM STP 474, 182-211, 1970.

72. Woodford, D. A., "Cavitation Erosion Induced Phase Transformations in Alloys," Metallurgical Transactions, Vol. 3, 1137-1145, May 1972.

73. Vejas, B., and Price, C. M., "Cavitation Induced Deformation of Aluminum," ASTM Symposium on Erosion, Wear and Interfaces with Corrosion, June 1973 (in press).

74. Petracchi, G., "Investigation of Cavitation Corrosion," Engineering Digest, Vol. 10, 314, September 1949.

75. Wheeler, W. H., "Mechanism of Cavitation Erosion," Cavitation in Hydrodynamics (Proc. National Phys. Lab. Symp.), H. M. Stationery Office, paper No. 21, London 1956.

76. Plesset, M. S., "On Cathodic Protection in Cavitation Damage," Calif. Inst. Tech. Engineering Division Report 85-12, July 1959. See also Jour. Basic Engr., Trans. ASME, Vol. 82, 809, 1960.

77. Preiser, H. S., and Tytell, B. H., "The Electrochemical Approach to Cavitation Damage and its Prevention," Corrosion, Vol. 17, 535-549, November 1961.

78. Nechleba, M., "Das Problem der Kavitation," Maschinenbautechnik, Vol. 2, 81-88, February 1955.

79. Waring, S., Preiser, H. S., and Thiruvengadam, A., "On the Role of Corrosion in Cavitation Damage," HYDRONAUTICS, Incorporated Technical Report 233-4, February 1964.

80. Wheeler, W. H., "Indentation of Metals by Cavitation," Jour. Basic Eng., Paper No. 59-Hyd-15, ASME Hydraulic Conf., April 13-15, 1959.

81. Foltyn, V., "Kathodicka Ochrana Proti Kavitacni Korosi," (Cathodic Protection Against Cavitation Corrosion), Strojirenstvi, Vol. 2, No. 9, 402-408, Czechoslovakia, September 1952.

82. Crewdson, E., "Cavitation," Engineer, Vol. 195, 122, 1953.

83. Robertson, J. M., "Water Tunnels for Hydraulic Investigations," Trans. ASME, Vol. 78, No. 1, 95-104, January 1956.

84. Wright, E. A., "Some International Aspects of Ship Model Research," David Taylor Model Basin Report 1220, April 1958.

85. Thiruvengadam, A., and Conn, A. F., "Some Recent Techniques for the Study of the Behavior of Ocean Engineering Materials," Materials Research and Standards, ASTM, Vol. 12, No. 3, 24-30, March 1972.

86. Rasmussen, R. E. H., "Some Experiments on Cavitation Erosion in Water Mixed with Air," Cavitation in Hydrodynamics, (Proc. National Phys. Lab. Symp.), Paper No. 20, H. M. Stationery Office, London 1956.

87. Lichtman, J. Z., Kallas, D. H., Chatten, C. K., and Cochran, E. P., Jr., "Study of Corrosion and Cavitation - Erosion Damage," Trans. ASME, Vol. 80, No. 6, 1325-1339, August 1958.

88. Kohl, R. E., "Experimental Studies to Establish Scaling Laws for Modeling Cavitation Damage," HYDRONAUTICS, Incorporated Technical Report 233-12, June 1968.

89. Johnson, V. E., Jr., Thiruvengadam, A., and Kohl, R. E., "Rock Tunneling with High-Speed Water Jets Utilizing Cavitation Damage," ASME paper 68-FE-42, May 1968, (also HYDRONAUTICS, Incorporated Technical Report 713-1, June 1968).

90. Gaines, N., "A Magnetrostriction Oscillator Producing Intense Audible Sound and Some Effects Obtained," Physics, Vol. 3, No. 5, 209-229, 1932.

91. Robinson, L. E., Holmes, B. A., and Leith, W. C., "Progress on Standardization of the Vibratory-Cavitation Test," Trans. ASME, Vol. 80 No. 1, 102-107, January 1958.

92. Plesset, M. S., "On Cathodic Protection in Cavitation Damage," Jour. Basic Engr., Trans. ASME, Vol. 82, 809, 1960.

93. Mason, W. P., "Internal Friction and Fatigue in Metals at Large Strain Amplitude," The Jour. Acous. Soc. America, Vol. 28, No. 6, 1207-1218, 1956.

94. Hammitt, F. G., Chao, C., Kling, C. L., Mitchell, T. M., Rogers, D. O., "ASTM Round Robin Test with Vibratory Cavitation and Liquid Impact Facilities of 6061-T6511 Aluminum Alloy, 316 Stainless Steel, and Commerically Pure Nickel," Materials Res. and Standards, ASTM, Vol. 10, 16-24, October 1970.

95. Standard Method of Vibratory Cavitation Erosion Test, Am. Soc. Testing Materials Standards, Designation G-32-72, 1972.

96. Schumb, W. C., Peters, H., and Milligan, L. H., "New Method for Studying Cavitation Erosion of Metals," Metals and Alloys, Vol. 8, 126-132, May 1937.

97. Knapp, R. T., "Accelerated Field Test of Cavitation Intensity," Trans. ASME, Vol. 80, No. 1, 91-102, January 1958.

98. Thiruvengadam, A., "A Comparative Evaluation of Cavitation Damage Test Devices," HYDRONAUTICS, Incorporated Technical Report 233-2; see also Proc. Symp. Cavitation Research Facilities and Techniques, ASME, New York, 1964.

99. Thiruvengadam, A., "A Unified Theory of Cavitation Damage," Jour. of Basic Eng., Trans. ASME, Vol. 85, Series D, No. 3, 365-376, September 1963.

100. Leith, W. C., and Thompson, A. L., "Some Corrosion Effects in Accelerated Cavitation Damage," ASME, Annual Meeting, paper No. 59-A-52, November 29 - December 4, 1959.

101. Hammitt, F. G., "Observations on Cavitation Damage in a Flowing System," Trans. ASME, Vol. 85, Series D, No. 3, Jour. Basic Engr., 347-359, September 1963.

102. Rosenberg, K., "Wear of Francis Turbines Due to Cavitation Effects During Operation by Means of Radioisotopes," Fifth World Power Conference, Paper 192H/44, Vienna, 1956.

103. Kerr, S. L., and Rosenberg, K., "An Index of Cavitation Erosion by Means of Radioisotopes," Trans. ASME, Vol. 80, No. 6, 1308-1311, August 1958.

104. Marsh, G. A., and Schaschl, E., "Laboratory Method for Corrosion Inhibitor Evaluation," Corrosion, Vol. 12, 534-538, November 1956.

105. Canavelis, R., "The Investigation of Cavitation Damage by Means of Resistance Gages," Proc. Symp. on Cavitation Research Facilities and Techniques, Am. Soc. Mech. Engrs., New York, 136-145, 1964.

106. Ellis, A. T., "Techniques for Pressure Pulse Measurements and High-Speed Photography in Ultrasonic Cavitation," Cavitation in Hydrodynamics, (Proc. National Phys. Lab. Symp.), Paper No. 8, H. M. Stationery Office, London 1956.

107. Ellis, A. T., and Fourney, M. E., "Application of a Ruby Laser to High Speed Photography," Proc. IEEE, Vol. 51, No. 6, June 1963.

108. Thiruvengadam, A., "The Concept of Erosion Strength," ASTM STP 408, 22-36, 1967 (originally HYDRONAUTICS, Incorporated Technical Report 233-9, December 1965).

109. McLean, D., "Mechanical Properties of Metals," John Wiley and Sons, New York, First Edition, 51-52, 1962.

110. Thiruvengadam, A., and Waring, S., "Mechanical Properties of Metals and Their Cavitation Damage Resistance," Jour. Ship Research, Vol. 10, No. 1, 1-9, 1966 (originally HYDRONAUTICS, Incorporated Technical Report 233-5, June 1964).

111. Young, S. G., and Johnson, J. R., "Accelerated Cavitation Damage of Steels and Superalloys in Sodium and Mercury," Erosion by Cavitation or Impingement, ASTM STP 408, Am. Soc. Testing Materials, 186-212, 1967.

112. Gould, G. C., "Some Observations on Erosion by Cavitation and Impingement," ASTM STP 474, 182-211, 1970.

113. Gould, G. C., "The Cavitation Erosion of Stellite and Other Metallic Materials," Proc. International Conf. on Rain Erosion and Allied Phenomena, Roy. Aircraft Est. Farnborough, England, 1970.

114. Hobbs, J. M., "Experience with a 20-kc Cavitation Erosion Test," Erosion by Cavitation or Impingement, ASTM STP 408, 159-185, 1970.

115. Hammitt, F. G., et al, "A Statistically Verified Model for Correlating Volume Loss Due to Cavitation or Liquid Impingement Characterization and Determination of Erosion Resistance," Am. Soc. Testing Materials, ASTM STP 474, 1970.

116. Manson, S. S., "Fatigue: A Complex Subject - Some Simple Approximations," The William M. Murray Lecture, Experimental Mechanics, Vol. 5, No. 7, 193-226, July 1963.

117. Heymann, F. J., "Toward Quantitative Prediction of Liquid Impact Erosion," ASTM STP 474, 212-244, 1970.

118. Heymann, F. J., "Frosion by Liquids - The Mysterious Murderer or Metals," Machine Design, 118-124, December 10, 1970.

119. Shaw, M. C., "Metal Cutting Principles," Third Ed., M.I.T. Press, Cambridge, Mass. (1960).

120. Maurer, W. C., "Novel Drilling Techniques," Pergamon Press, New York (1968).

121. Schwarz, M. V., and Mantel, W., "Zerstörung Metallischer Werkstoffe durch Wasserschlag," Zeit. Ver. Deut. Ing., Vol. 80, No. 28, 863-867, July 1936.

122. Mueller, H., "Anfressungen durch Hohlsog und Tropfenschlag," Stahl und Eisen, Vol. 58, 881-888, 1938.

123. Thiruvengadam, A., "High Frequency Fatigue of Metals and Their Cavitation Damage Resistance," Trans. ASME, Jour. of Engineering for Industry, Vol. 88, Series B, No. 3, August 1966 (originally HYDRONAUTICS, Incorporated Technical Report 233-6, December 1964).

124. Thiruvengadam, A., and Conn, A. F., "On High Frequency Fatigue and Dynamic Properties at Elevated Temperatures," Experimental Mechanics, Vol. 11, 315-320, 1971

125. Thiruvengadam, A., "Intensity of Cavitation Damage Encountered in Field Installations," ASME Symp. on Cavitation in Fluid Machinery, 32-46, 1965 (originally HYDRONAUTICS, Incorporated Technical Report 233-7, February 1965).

126. Thiruvengadam, A., and Preiser, H. S., "On Testing Materials for Cavitation Damage Resistance," Journal Ship Research, Vol. 8, No. 3, 39-56, December 1964 (originally HYDRONAUTICS, Incorporated Technical Report 233-3, December 1963).

127. Thiruvengadam, A., "Prevention and Cure of Cavitation Erosion," Naval Research Reviews, Vol. XXV, No. 5, 10-27, May 1972.

128. Kallas, D. G., and Lichtman, J. Z., "Cavitation Erosion," Environmental Effects on Polymeric Materials, Vol. 1, Chap. 2, Interscience, New York, 1968.

129. Chatten, C. K., and Thiruvengadam, A., "Cavitation Erosion Resistance Tests for Polymers," Testing of Polymers, Vol. III, (Ed. J. V. Schmidt), Interscience Publishers, New York, In Press (1965).

130. Lichtman, J. Z., "Possible Contributions of Reentrant Flow to Cavitation Erosion," ASME Paper 62-HYD-3, May 1962.

131. Kerr. S., and Leith, W. C., "A Review of Cavitation Damage by the Vibratory Method at the Dominion Engineering Works, Ltd.," Milwaukee Cavitation Committee Meeting, ASME, November 1955.

132. Lichtman, J. Z., and Weingram, E. R., "Cavitation Design Handbook," Final Report, Lab. Project 9300-17, NR 062-314, P. O.-3-0079, U. S. Naval Applied Science Laboratory, September 1964.

133. Rivlin, R. S., and Thomas, A. G., "Rupture of Rubber I, Characteristic Energy for Tearing," Jour. Poly. Science, Vol. 10, 291-318, 1953.

134. Bueche, F., "Physical Properties of Polymers," First Edition, Interscience Publishers, New York, 323-331, 1962.

135. Conn, A. F., and Thiruvengadam, A., "Dynamic Response and Adhesion Failures of Rain Erosion Resistant Coatings," Journal of Materials, Vol. 5, 698-718, 1970.

136. Conn, A. F., "Prediction of Rain Erosion Resistance from Measurements of Dynamic Properties," Third International Conference on Rain Erosion and Associated Phenomena, Hampshire England, August 1970.

137. Conn, A. F., and Rudy, S. L., "The Effects of Fatigue and Dynamic Recovery on Rain Erosion," presented at ASTM Annual Meeting, June 1973 (to be published in an ASTM STP).

138. Morris, J. W., Jr., "Supersonic Rain and Sand Erosion Research - Part II - Mechanistic Investigation of Rain Erosion," Technical Report AFML-TR-69-287, Part II, Textron's Bell Aerosystems Co., Buffalo, New York, September 1969.

139. Springer, G. S., and Baxi, C. B., "A Model for Rain Erosion of Homogeneous Materials," Univ. of Michigan Technical Report AFML-TR-72-106, June 1972.

140. Engel, O. G., and Piekutowski, A. J., "Investigation of Composite-Coating Systems for Rain-Erosion Protection," Univ. of Dayton Final Report UDRI-TR-71-47, November 1971.

141. Lichtman, J. Z., Kallas, D. G., Chatten, C. K., and Cochran, E. P., "Cavitation Erosion and Behavior of Materials," 17th Annual Conference National Association of Corrosion Engineers, March 1961.

142. Price, W. H., and Wallace, G. B., "Resistance of Concrete and Protective Coatings to Forces of Cavitation," Jour. Amer. Concrete Inst., Vol. 21, No. 2, 109-120, October 1949.

143. Thiruvengadam, A., "Cavitation and Cavitation Damage," Masters Thesis, Indian Institute of Science, Bangalore, India, 1959.

144. Rheingans, W. J., "Resistance of Various Materials to Cavitation Damage," Report of 1956 Cavitation Symposium, Am. Soc. Mech. Engrs., New York, 1956.

145. Plesset, M. S., "Shock Waves from Cavitation Collapse," Phil. Trans. Royal Society (London), A-260, 241-244, 1966.

146. Hammitt, F. G., "Damage to Solids Caused by Cavitation," Phil. Trans. Royal Society (London), A-260, 245-255, 1966.

147. Kornfeld, M., and Suvorov, L., "On the Destructive Action of Cavitation," Jour. Appl. Physics, Vol. 15, 495-506, 1944.

148. Shutler, N. D., and Mesler, R. B., "A Photographic Study of the Dynamics and Damage Capabilities of Bubbles Collapsing Near Solid Boundaries," Trans. ASME, 87, Series D, Jour. Basic Enginerring, 511-517, 1965.

149. Thiruvengadam, A., Unpublished Results, Materials Laboratory, New York Naval Shipyard, 1963.

150. Wood, G. M., Knudsen, L. K., and Hammitt, F. G., "Cavitation Damage Studies with Rotating Disk," Trans. ASME, Jour. Basic Engr. Vol. 89, No. 1, Series D, 98-110, 1967.

151. Shal'nev, K. K., "Experimental Study of the Intensity of Erosion Due to Cavitation," Proc. Symp. on Cavitation in Hydrodynamics, (N. P. L. 1955), H. M. S. O. 1956.

152. Kohl, R. E., "Experimental Studies to Establish Scaling Laws for Modeling Cavitation Damage," HYDRONAUTICS, Incorporated Technical Report 233-12, June 1968.

153. Thiruvengadam, A., "Effect of Hydrodynamic Parameters on Cavitation Erosion Intensity," HYDRONAUTICS, Incorporated Technical Report 233-14, 1970.

154. Plesset, M. S., and Devine, R. E., "Effect of Exposure Time on Cavitation Damage," Trans. ASME, Jour. Basic Engr., Vol. 88, No. 4, Series D, 691-705, December 1966.

155. "Cavitation in Hydraulic Structures: A Symposium," Proc. Amer. Soc. Civ. Engr. Vol. 71, No. 7, September 1945.

156. Hobbs, J. M., "Vibratory Cavitation Erosion Testing: Proceedings of a Meeting on 13 June 1963," NEL Report 149, National Engineering Laboratory, England, 1964.

157. Baker, D. W. C., Jolliffe, K. H., and Pearson, D., "Resistance of Materials to Impact Erosion Damage," Phil. Trans. Royal Soc., Series A, No. 1110, Vol. 260, 193-203, 1966.

158. Heymann, F. J., "On the Time Dependence of the Rate of Erosion Due to Impingement or Cavitation," ASTM STP 408, 70-110, 1967.

159. Garcia, R., Hammitt, F. G., and Nystrom, R. E., "Correlation of Cavitation Damage with Other Material and Fluid Properties," Erosion by Cavitation or Impingement, ASTM STP 408, Am. Soc. Testing Materials, 239, 1967.

160. Ripken, J. F., "A Test Rig for Studying Impingement and Cavitation Damage," ASTM STP 408, 3-18, 1967.

161. Syamala Rao, B. C., Rao, N. S. L., and Seetharamiah, K., "Cavitation Erosion Studies with Venturi and Rotating Disk in Water," Jour. Basic Engineering, Trans. ASME Series D, Vol. 92, 563-579, 1970.

162. Tichler, J. W., Van der Elsen, J. B., and de Gee, A. W. J., "Resistance Against Cavitation Erosion of 14 Chromium Steels," Jour. Lub. Tech., Trans. ASME Series F, Vol. 92, 228-242, 1970.

163. Canavelis, R., "Jet Impact and Cavitation Damage," Jour. Basic Engr., Trans. ASME, Vol. 90, Series D, 355-366, September 1968.

164. Thiruvengadam, A., Couchman, C., III, and Preiser, H. S., "Cavitation Damage Resistance of Materials in Liquid Sodium," Jour. Space Craft and Rockets, Vol. 2, No. 2, March - April 1965 (also see HYDRONAUTICS, Incorporated Technical Reports 235-1, July 1964; 467-Final, November 1965).

165. Thiruvengadam, A., "Theory of Erosion," Proc. Second Meersburg Conference on Rain Erosion, Roy. Aircraft Est., Farnborough, England, 1967 (originally HYDRONAUTICS, Incorporated Technical Report 233-11, March 1967).

166. Hildebrand, F. B., Advanced Calculus for Applications, Prentice-Hall, Inc., New Jersey, 1962.

167. Mok, C. H., "On the Erosion of Solids by Impingement at Low Velocities," Presented at the Symposium on Characterization and Determination of Erosion Resistance, ASTM Annual Meeting, Atlantic City, New Jersey, June 1969.

168. Thiruvengadam, A., "On the Selection of Modeling Materials to Scale Long Term Erosion Behavior of Prototype Systems," Proc. of the Third International Conference on Rain Erosion and Allied Phenomena, Royal Aircraft Est.,Farnborough, England, 1970.

169. Heymann, F. J., "Report on a Trip to British Erosion Laboratories," Westinghouse Electric Corp., Lester, Pa., June 28, 1965.

170. Hickling, R., and Plesset, M. S., "Collapse and Rebound of a Spherical Bubble in Water," Physics of Fluids 7, 7-14, 1964; AMR Vol. 17 (1964), Rev. 5963.

171. Ivany, R. D., and Hammitt, F. G., "Cavitation Bubble Collapse in Viscous Compressible Liquids - Numerical Analysis," Jour. Basic Engineering, Trans. ASME Series D 87, 977-985, 1965; AMR Vol. 19 (1966), Rev. 3684.

172. Poritsky, H., "The Collapse or Growth of a Spherical Bubble or Cavity in a Viscous Fluid," Proc. First U. S. National Congr. Applied Mech. (ASME), 813-821, 1952; AMR Vol. 7 (1954), Rev. 3623.

173. Hancox, N. L., and Brunton, J. H., Phil. Trans. Roy. Soc. London, Series A, Math. Phys. Sciences, Vol. 260, 121, 1966.

174. Thiruvengadam, A., "Scaling Laws for Cavitation Erosion," Proc. of the Symp. on Flow of Water at High Speeds, Leningrad, USSR, International Union of Theoretical and Applied Mechanics, June 22-26, 1971 (also HYDRONAUTICS, Incorporated Technical Report 233-15, December 1971).

175. Hickling, R., "Some Physical Effects of Cavity Collapse in Liquids," Trans. ASME, Jour. Basic Engr., Series D, Vol. 88, No. 1, 229-235, 1966.

176. Thiruvengadam, A., "On Modeling Cavitation Damage," Jour. Ship Research, Vol. 13, 220-233, 1969; AMR Vol. 23 (1970), Rev. 4549.

177. Ivany, R. D., Hammitt, F. G., and Mitchell, R. M., "Cavitation Bubble Collapse Observations in a Venturi," Trans. ASME, Jour. Basic Engr., Vol. 88, No. 3, Series D, 649-657, 1966.

178. A Guide for Fatigue Testing and the Statistical Analysis of Fatigue Data (supplement to Manual on Fatigue Testing, STP No. 91) ASTM Special Technical Publication No. 91-A, Second Edition, 1963.

179. Holl, J. W., "Limited Cavitation," Cavitation State of Knowledge, ASME, 26-64, 1969.

180. Wilson, R. W., and Graham, R., "Cavitation of Metal Surfaces in Contact with Lubricants," Conference on Lubrication and Wear, The Institution of Mechanical Engineers, London, October 1957.

181. Bebchuk, A. S., "The Problem of Cavitational Damage to Solid Bodies," Soviet Physics-Acoustics, Vol. 3, No. 1, January - March 1957.

182. Bebchuk, A. S., "On the Problem of the Mechanism of Cavitation Damage to Solid Bodies," Soviet Physics-Acoustics, Vol. 3, No. 4, October - December 1957.

183. Devine, R. E., and Plesset, M. S., "Temperature Effects in Cavitation Damage," Report No. 85-27, Division of Engineering and Applied Science, California Institute of Technology, Pasadena, April 1964 (also see Jour. Basic Engr., Trans. ASME, Series D, Vol. 94, 559-566, 1972).

184. Plesset, M. S., "Cavitation Erosion in Non-Aqueous Liquids," Jour. Basic Engr., Trans. ASME, Vol. 92, Series D, 807-818, December 1970.

185. Thiruvengadam, A., Unpublished Discussion of Ref. 184, December 1970.

186. Tung, S., and Thiruvengadam, A., "Role of Physical Properties of Liquids in Cavitation Erosion," Proc. South-Eastern Conference on Theoretical and Applied Mechanics, The Catholic University of America, March 1974.

187. Krenn, H., "Wärmefluss als Korrosionsursache," Maschinenbau und Wärmewirtschaft, 81-87, 1948.

188. Foltyn, V., "Kathodicka Ochrana Proti Kavitacni Korosi," (Cathodic Protection Against Cavitation Corrosion), Strojirenstui, Vol. 2, No. 9, 402-408, Czechoslovakia, September 1952.

189. Petracchi, G., "Intorno All'interpretazione del Processo di Corrosions per Cavitazione," La Metallurigia Italiana, Vol. 41, No. 1, 1-6, January - February 1949.

190. Ffield, P., Mosher, L. M., and O'Neill, A. J., "Some Aspects of Propeller Deterioration and its Prevention," Soc. of Naval Arch. and Marine Engineers, New England Section, May 1956.

191. Tomoshov, N. D., "Theory of Corrosion and Protection of Metals," translated and ed. by Tytell, B. H., Geld, I., and Preiser, H. S., The Macmillan Co., (1965).

192. Shal'nev, K. K., "Resistance of Metals to Cavitation Corrosion in Fresh Water and Sea Water," (in Russian), Doklady Acad., Nauk., (SSSR), Vol. 95, No. 2, 229-232, 1954.

193. Eisenberg, P., "Modern Developments in the Mechanics of Cavitation," Applied Mechanics Reviews, Vol. 10, No. 3, 85-89, March 1957.

194. Plesset, M. S., "Physical Effects in Cavitation and Boiling," Discussion by P. Eisenberg of Paper, Proc. Symp. on Naval Hydrodynamics, U. S. National Academy of Sciences - National Research Council Publication No. 515, Washington, D. C., 321, 1957.

195. Plesset, M. S., Bass, B. C., and Hickling, R., "Cathodic Protection in Cavitation Damage -- Tests of Mild Steel in a Salt Solution," California Inst. Tech. Engineering Division Report No. 85-10, November 1958.

196. Plesset, M. S., "On Cathodic Protection in Cavitation Damage," California Inst. Tech. Engineering Division Report No. 85-12, July 1959 (also see Jour. Basic Engr., Trans. ASME, Vol. 82, 809, 1960).

197. Spannhake, W., "Kavitationsversuche am Massachusetts Institute of Technology und ihre Deutung," Zeit. angew. Math. und Mech., Vol. 14, 374-378, 1931.

198. Schröter, H., "Korrosion durch Kavitation in einem Diffusor," Zeit. Ver. Deut. Ing., Vol. 76, 511-512, 1932.

199. Taylor, G. I., and Quinney, H., "The Latent Energy Remaining in a Metal After Cold Working," Proc. Royal Soc. London, Series A, Vol. 143, 1933-34.

200. Griffing, V., and Sette, D., "Luminescence Produced as a Result of Intense Ultrasonic Waves," Jour. of Chemical Physics, Vol. 23, No. 3, 503-509, March 1955.

201. Fitzgerald, M. E., Griffing, V., and Sullivan, J., "Chemical Effects of Ultrasonics -- 'Hot Spot' Chemistry," Jour. of Chemical Phys., Vol. 25, No. 5, 926-933, November 1956.

202. Preiser, H. S., Thiruvengadam, A., and Couchman, C. E., "Cavitation Damage in Liquid Sodium," HYDRONAUTICS, Incorporated Technical Report 235-1, April 1, 1964.

203. Couchman, C. E., Preiser, H. S., and Thiruvengadam, A., "Cavitation Damage in Liquid Metals," HYDRONAUTICS, Incorporated Technical Report 467-1, March 10, 1965.

204. Thiruvengadam, A., Preiser, H. S., and Rudy, S. L., "Cavitation Damage in Liquid Metals," HYDRONAUTICS, Incorporated Technical Report 467-2, April 28, 1965.

205. Amateau, M. F., "The Effect of Molten Alkali Metals on Containment Metals and Alloys at High Temperatures," DMIC Report 169, Defense Metals Information Center, Battelle Memorial Institute, Columbus, Ohio, May 28, 1962.

206. Plesset, M. S., "The Pulsation Method for Generating Cavitation Damage," Trans. ASME, Jour. Basic Engr., Vol. 85, Series D, No. 3, 360-364, 1963 (see also Corrosion, Vol. 18, No. 5, 181-188, 1962).

207. Thiruvengadam, A., and Preiser, H. S., "On Testing Materials for Cavitation Damage Resistance," HYDRONAUTICS, Incorporated Technical Report 233-3, December 1963 (see also Jour. Ship Research, Vol. 8, No. 3, 39-56, December 1964).

208. McGuinness, T., "Cavitation Erosion-Corrosion Modeling in An Ocean Environment," Ph.D. Thesis, Catholic University of America, 1973.

209. McGuinness, T., "Cavitation Erosion-Corrosion Modeling in an Ocean Environment," ASTM Symp. on Erosion, Wear and Interfaces with Corrosion, ASTM STP (in press) 1974.

210. Uhlig, H. H., "Corrosion Handbook," John Wiley and Sons, New York, (1948).

211. LaQue, F. L., "Materials Selection for Ocean Engineering," Ocean Engineering (Brahtz, ed.,) Chap. 16, John Wiley and Sons, Inc., 1968.

212. Data obtained by H. S. Preiser and S. Waring of HYDRONAUTICS, Incorporated from John Hill of U. S. Bureau of Ships, Department of Navy, USA, 1964.

213. Lichtman, J. Z., Kallas, D. H., Chatten, C. K., and Cochran, E. P., Jr., "Study of Corrosion and Cavitation Erosion Damage," Trans. ASME, Vol. 80, No. 6, 1325-1339, August 1958.

214. Watson, F. B., "Protective Coatings - Foil System, PC(H)-1 HIGH POINT," Code Indent. No. 81205, D2-133600-1, Contract Nobs-4838, The Boeing Co. Seattle, Wash., August 1966.

215. Bohlander, G., Preiser, H. S., Kelly, J., and Thiruvengadam, A., "Field Inspection of Erosion Intensities Encountered in U. S. Navy Hydrofoil Boats," NSRDC, Annapolis Laboratory Project Report, 1973.

216. Neville, H., Discussion of the Paper by R. Beeching (Ref. 12), 241, 1942.

217. Borland, B. B., and Stiles, G. F., "Cavitation as Related to Control Valves," Fisher Sales Meeting, May 24, 1960, Fisher Governor Company, Marshalltown, Iowa, 1960.

218. Ride, R. N., Symposium on Corrosion (Melbourne University), 267, esp. 269, 1955-56; see also Evans, U. R., "The Corrosion and Oxidation of Metals: Scientific Principles and Practical Applications," First Edition, Edward Arnold (Publishers) Ltd., London, 752, 1961.

219. Speller, F. N., and LaQue, F. L., "Water Side Deterioration of Diesel Engine Cylinder Liners," Corrosion, Vol. 6, No. 7, 209-215, 1950.

220. Collins, H. H., "Pitting of Diesel Cylinder Liners," The Oil Engine and Gas Turbine," February and March 1960; see also British Cast Iron Research Association, External Report 418, 1960.

221. Rheingans, W. J., "Selecting Materials to Avoid Cavitation Damage," Materials in Design Engineering, 102-106, September 1958.

222. Kallas, D. H., and Lichtman, J. Z., "Cavitation Erosion," Environmental Effects on Polymeric Materials, Vol. I, Chap. 2, Interscience, New York, 1968.

223. Bohlander, G., and Preiser, H. S., "Hydrofoil Coatings Research," NSRDL Report, 1973.

224. Thiruvengadam, A., and Kenkeremutt, D., "Influence of Cavitation Erosion on Adhesion Strength of Elastomeric Coatings," Sea Technology, 30-32, July 1973.

225. Ryans, M., "Deterioration of Adhesion Strength of Elastomeric Coatings as a Result of Cavitation Erosion," Masters Thesis, Catholic University of America, 1974.

226. Ackeret, J., "Experimentelle und Theoretische Untersuchungen über Hohlraumbildung (Kavitation) in Wasser," Tech. Mech. und Thermodyn., Vol. 1, 1930.

227. Mousson, J. M., "Cavitation Problems and Their Effects upon the Design of Hydraulic Turbines," Proc. Second Hydraulics Conf., State Univ. of Iowa Bull. 27, Iowa City, Iowa, 146-170, June 1942.

228. Rasmussen, R. E. H., "Experiments on Flow With Cavitation in Water Mixed With Air," Trans. Danish Academy of Technical Sciences, No. 1, 3-60, 1949.

229. Preiser, H. S., and Tytell, B. H., "The Electrochemical Approach to Cavitation Damage and Its Prevention," Corrosion, Vol. 17, 535-549, November 1961.

230. Higgins, R. I., British Cast Iron Research Association Journal of Research, Vol. 7, 1957.

231. Duff, M. G., Corrosion Technology, 250, August 1958.

232. Graham, D. P., Cook, F. E., and Preiser, H. S., "Cathodic Protection in the U. S. Navy: Research - Development - Design," Trans. Soc. Nav. Arch. and Mar. Eng., Vol. 64, 241-290, 1956.

233. Schuetz, A. E., and Robertson, W. D., "Hydrogen Absorption, Embrittlement, and Fracture of Steel," Corrosion, Vol. 13, 33-54, July 1957.

234. Preiser, H. S., "Corrosion - Erosion - Cavitation Protection for Marine Propellers," U. S. Pat. No. 3,049,479.

235. Margulis, W., McGowan, J. A., and Leith, W. C., "Cavitation Control Through Diesel-Engine Water Treatment," Trans. Soc. Automotive Eng., Vol. 65, 331-336, 1957.

236. Speller, F. N., and LaQue, F. L., "Water Side Deterioration of Diesel Engine Cylinder Liners," Corrosion, Vol. 6, No. 7, 209-215, 1950.

237. Winternitz, W. A. L., Discussion on Session 6, Proc. Symp. "Cavitation in Hydrodynamics," National Phys. Lab., London, H. M. Stationary Office, H p-2, 1956.

238. Strenge, K. O., Proc. Symp., "Cavitation in Hydrodynamics," National Phys. Lab., London, H. M. Stationary Office, 10, 1956.

239. Sherwood, H. L., Proc. Symp., "Cavitation in Hydrodynamics," National Phys. Lab., London, H. M. Stationary Office, 10, 1956.

240. Alexander. J. L., Proc. Symp., "Cavitation in Hydrodynamics," National Phys. Lab., London, H. M. Stationary Office, 10, 1956.

241. Deskin, A. J., Proc. Symp., "Cavitation in Hydrodynamics," National Phys. Lab., London, H. M. Stationary Office, 11, 1956.

242. NAVSHIPS 344-0041, "Repair of Bronze Ship Propellers Straightening and Welding," Bureau of Ships, Navy Department, Washington 25, D. C.

243. Bohlander, G., and Thiruvengadam, A., "Field Inspection of Cavitation Erosion Problems Encountered in Tucumcari and Flag Staff Hydrofoil Boats," NSRDL, Annapolis, 1973.

TABLE 5-1. Mechanisms of Cavitation Erosion

No.	Year of Publication	Author and Reference	Details of the Mechanism Proposed
1	1917	Lord Rayleigh Phil. Mag. Vol. 34, pp. 94-98	Calculated the energy of collapse of the bubble and showed the possibility of high pressures.
2	1919	Sir Charles Parsons and S. S. Cook, Engineering Vol. 107, pp. 515-519	Conducted the famous nose cone experiment demonstrating water hammer pressures and were the first to propose the mechanical action theory. Cook calculated the pressure due to collapse earlier than Rayleigh.
3	1926	H. Föettinger Hydrauliche Probleme (Berlin) Section 27	Supported mechanical action theory by producing damage on glass.
4	1932	J. Ackeret Hydromechanische Probleme der Schiffsantriebs, Hamburg	First to suggest the effect of flow velocity on the intensity of erosion. Based on this fact he discarded the corrosion theory and supported the mechanical action theory.
5	1933	P. de Haller Schweitzer Bauseitung, Vol. 101, p. 243	First to attempt the experimental observation of high pressure pulses due to cavity collapse. The oscillograms obtained by him showed the impulse pressures of the order of three hundred atmospheres.

TABLE 5-1 (continued)

6	1935	H. N. Boetcher Trans. ASME, Vol. 58 pp. 355-360	Introduced the idea of "surface fatigue" of "cavitation fatigue" and recommended materials of high corrosive fatigue strength. Found correlation between damage and hardness.
7	1936	J. Ackeret and P. de Haller Schweitzer Bauzeitung Vol. 108, p. 105	They used a precussion wave to produce superficial damage on various metals. Advanced the drop-impact theory.
8	1937	M. Vater Z.V.D.I., Vol. 81, p. 1305	Suggested "periodic strains."
9	1938	H. Mueller Stahl und Eisen, p. 884	First to suggest the concept of threshold velocity for each material similar to fatigue limit. Suggested that the mechanical action depends upon the corrosive influence of the testing liquid.
10	1940	J. Frenkel Acta Physiocochimica Vol. 12, p. 317	Suggested chemical action upon the surface of the material by the gases contained in the cavity. The chemical activity was attributed either to the high temperatures by adiabatic compression of the bubble or to the electric discharges taking place within the "atmosphere" of the cavities.

TABLE 5-1 (continued)

11	1942	R. Beeching Trans. Inst. Ship Builders Scot., Vol. 85, p. 210	Agreed with the mechanical action concept and attributed the influence of corrosion to its influence on fatigue limit.
12	1947	T. C. Poulter Frontier, Vol. 10(2), p. 728	Suggested liquid penetration through crevices and shattering of the particles out from the material by the liquid momentarily under high pressure.
13	1947	G. F. Wislicenus Fluid Mech. of Turbo Machinery, McGraw Hill Inc., New York, p. 74	Suggested local melting of the material due to increase in temperatures caused by adiabatic compression of the bubble.
14	1949	G. Petracchi La Melatturgica Italiana Vol. 41(1), p. 1.	Noticed an influence of cathodic protection and attributed the mechanism of damage due to corrosion produced by electrolytic currents due to local mechanical stresses.
15	1955	M. Nechleba Machinenbautechnik, Vol. 2, p. 81	Generation of corrosive currents to a thermocouple action resulting from local heating of the metal by the temperature rise of the collapsing cavity. Supported Poulter's view.
16	1955	M. S. Plesset and A. T. Ellis, Trans. ASME, Vol. 77, p. 1055	First to show plastic deformation by X-ray diffraction patterns. They demonstrated clearly that corrosive effects are of secondary importance, at least in non-corrosive liquids.

TABLE 5-1 (concluded)

17	1955	R. T. Knapp N.P.L. Symposium on "Cavitation in Hydrodynamics," (Teddington) Paper 19	Suggested that at the instant of collapse minute regions of high intensity "water hammer" pressures are produced. The stored energy radiates from the collapse center as a spherical shock wave whose intensity decreases rapidly as its radius increases.
18	1955	W. Gueth Ibid. Appendix I, Paper I	First to photograph the shock wave radiated from the bubble by means of Schlieren's method.

TABLE 6-1

Intensities of Various Laboratory Test Devices
[Thiruvengadam (98)]

Device* No.	Material	Strain Energy kgm/cm^2	Density gms/cm^3	Weight Loss mgs.	Time seconds	Area of Erosion cm^2	Average Depth of erosion $cm \times 10^3$	Intensity $watts/meter^2$
1	Commercial Brass	800	8.5	150	120 × 60	1.6	11.00	1
2	1100-0-Aluminum	80	2.7	1.5	10 × 60	1.6	0.11	0.01
3	Commercial Brass	880	8.5	31.1	90 × 60	1.6	2.3	0.4
4	Commercial Brass	880	8.5	53.5	90 × 60	0.8	7.9	1
5	Mild Steel	230	7.9	0.8	120 × 60	0.8	0.13	0.004
6	Copper	700	8.3	30	30 × 60	1.6	6	2.5
7	1100-0-Aluminum	80	2.7	6.5	60	1.6	1.5	2
8	18-8 Cr.St.Steel	2750	7.8	11.8 × 7.8	16×60×60	7	1.7	0.1
9	Commercial Brass	880	8.5	4.0	20×60×60	4	0.12	0.001
10	Lead	20	13	-	60 × 60	-	18	0.1
11	Commercial Brass	880	8.5	1.0	60 × 60	1.0	0.12	0.03
12	1100-0-Aluminum	80	2.7	4.0	60	20	0.07	0.1
13	304 St.Steel	2750	7.8	-	150×60×60	-	0.006	0.00003
14	1100-0-Aluminum	80	2.7	260	30 × 60	1.0	96	4
15	1100-0-Aluminum	80	2.7	220	3.5×60×60	1.5	54	0.34
16	1100-0-Aluminum	80	2.7	2.5	60	1.5	0.62	1

*See Reference 98 for a description of these devices.

TABLE 7-1

Cavitation Damage Resistance of Cast Stainless Steels
(After Rheingans - Reference 68)

Chrome (percent)	Brinell Hardness Number	Rate of Loss (mg. per min. in last 30 min. of test)	Total Loss (mg. in 120 min.)
12	302	0.20	20
13	302	0.26	25
13	235	0.43	49
13	241	0.39	51
12	225	0.55	54
13	229	0.46	57
13	207	0.51	70
12	167	0.73	141

TABLE 7-2

Cavitation Damage Resistance of Plain and Alloyed Cast Irons
(After Mousson - Reference 67)

Alloy	Chemical Composition (percentage)							Tensile Strength (p.s.i.)	Brinell Hardness Number	Cavitation Loss in 16 hrs. ($mm.^3$)
	C[a]	Mn	Si	Ni	Cr	Cu	Note			
Cast Iron	3.18	.50	2.13				1	25,000	171	636
Cast Iron with Casting Skin	3.20	.50	2.00				2	25,000	200	396
Nickel-Tensyleran	2.54	.76	2.51	1.05			1	56,000	235	376
5 percent Nickel Cast Iron	2.93	.50	1.36	4.81			1	35,000	303	269
Ni Cu Cast Iron	3.10	1.50	2.00	15.00	1.00	7.00	2	18,000	107	837
Ni Cr Cu Iron	2.77	1.00	1.86	14.48	1.88	6.00	1	25,000	116	247
Ni Cr Cu Cast Iron	2.95	1.00	1.89	14.36	3.95	6.00	1	35,000	161	109

Notes: (1) Actual analysis. (2) Estimated analysis. (a) Total C.

TABLE 7-3

Cavitation Damage Resistance of Various Metals
(After Plesset and Ellis -- Reference 70)

Material (arranged in order of increasing hardness)	Composition percent	Hardness (Brinell)	Ultimate tensile strength (psi x 10^3)	Modulus of elasticity (psi x 10^6)	Depth of Cavitation Damage Hole in microns (10^{-4} cm)						
					10 sec	1 min	15 min	30 min	1 hr	2 hrs	3 hrs
Aluminum(soft)		16	16	10	10	80					
Titanium (annealed)		58	79	16			43	78			
Nickle		90	50	30			80	115			
Molybdenum		120	57	50				10	25	60	100
Brass	Cu 70,Zn 30	123	56	13		1	35	128			
Stainless Steel	Cr 18,Ni 8	163	102	29			15	28			
Titanium 75-A		203	80	16					30	66	
Steel (4130)		258	130	30					32	55	
Tungsten		350	597	51				0	0	3	
Titanium 130-A	Ti 92,Mn 7.9	351	130	16				0	3	16	
Colmonoy		400	61					0	3	18	34
Titanium 150-A	Ti 96,Cr 2.7, Fe 1.3	437	150	16				0	0	3	26
Stellite	Co 55 Cr 33, W 6	495	100	36				0	3	14	

TABLE 7-4

Comparison of Cavitation Resistance of Some Stainless Steels
(From Mousson -- Reference 67)

Material	Tensile Strength (p.s.i.)	Yield Point (p.s.i.)	Brinell Hardness	Loss in 16 hrs (mm^3)
Stainless 17% Cr. Steel	85,000	40,000	201	67.0
Stainless Steel 18-8 Cr. Ni	75,000	30,000	145	8.8
Stainless Steel 24-12 Cr. Ni	196,000	96,000	139	8.6
Stainless Steel 26-13 Cr. Ni	-	-	161	4.1

TABLE 7-5

Comparison of Damage Resistance of Two Nonferrous Alloys
(After Mousson -- Reference 67)

Alloy	Chemical Composition (percents)						Tensile Strength (p.s.i.)	Yield Point (p.s.i.)	Brinell Hardness	Loss in 16 hrs (mm^3)
	Cu	Zn	Mn	Ni	Fe	Al				
Hy-ten-sl Bronze No. 4	68	22	4	-	3	3	85,000	40,000	165	43.3
Turbine Metal	56	36	2	2	1	1	80,000	40,000	166	80.2

TABLE 7-6

Effect of Alloy Constituents on Damage Resistance
(From Mousson - Reference 67)

Alloy	Chemical Composition (percentages)								Tensile Strength (psi)	Brinell Hardness	Loss in 16 hrs (mm^3)
	C	Mn	P	S	Si	Ni	Cr	Mo			
Stainless 12 percent Cr. Steel	.06	.43	.015	.028	.38	.17	12.88	-	99,000	206	24.6
Stainless 12 percent Cr.Ni Steel	.08	.49	.016	.021	.48	1.53	12.44	-	126,250	281	6.3
Stainless 13 percent Cr.Mo Steel	.10	.47	.014	.027	.33	.12	12.88	.58	123,750	275	9.5
Stainless 14 percent Cr.Ni Steels	.06	.39	.016	.021	.33	.98	14.72	-	-	238	85.5
	.05	.32	.016	.021	.35	1.14	14.48	-	-	302	32.0
	.05	.36	.018	.019	.31	2.02	14.30	-	-	321	12.9
	.07	.35	.016	.015	.40	3.36	14.30	-	-	352	9.8

TABLE 7-7

Threshold Criteria (108)

Water-Hammer theory $\frac{\sigma_e}{\rho_\ell C_\ell U_I} \cong 2$; Engel's theory $\frac{\sigma_e}{U_I \rho_\ell^{1/2} E_m^{1/2}} \cong \frac{1}{\beta}$; $\frac{1}{\beta} = 2\left(\frac{K_\ell}{E_m}\right)^{1/2}$

E_m = Young's modulus of material

K_ℓ = Bulk modulus of liquid

No.	Material	Liquid	Threshold Impact Velocity, U_ℓ, ft/sec	Density of Liquid, ρ_ℓ, slugs/ft^3	Velocity of Sound, C_ℓ, ft/sec	Dynamic Yield Strength, Y_D, psi	Modulus of Elasticity, E_m, psi	Endurance Limit σ_e, psi	$\frac{\sigma_e}{\rho_\ell C_\ell U_I}$	$\frac{\sigma_e}{U_I \rho_\ell^{1/2} E_m^{1/2}}$	$\frac{1}{\beta}$
1	Copper	water	99 (30 m/sec)	value of $\rho_\ell C_\ell U_I$ = 5750 psi (= 4 kg/mm^2)		21 500 (15 kg/mm^2)	16×10^6	12 000	1.85	0.25	0.26
2	Steel	water	295 (90 m/sec)	$\rho_\ell C_\ell U_I$ = 17 100 psi (=12 kg/mm^2)		72 000 (50 kg/mm^2)	30×10^6	36 000	2.1	0.18	0.20
3	Chromium Steel	water	400	1.94	4800	---	30×10^6	50 000	1.9	0.19	0.20
4	Stellite 6	water	600	1.94	4800	---	36×10^6	80 000	2	0.20	0.20
5	Stellite	water	1100	1.94	4800	---	36×10^6	80 000	1	0.10	0.18
6	Chromium Steel	water, single impact	800 to 900	1.94	4800	100 000	30×10^6	---	2	0.4	0.20
7	Stellite 6	water, single impact	1100 to 1200	1.94	4800	150 000	36×10^6	---	2	0.2	0.18

TABLE 7-8

First Order of Merit Coatings
[Lichtman and Weingram (132)]

Material Type	Sample Code	Ultimate Tensile Strength PSI	% Elongation	Hardness	Tear Strength PLI	Tensile Hysteresis %
Neoprene	I-1A	2065	1180	-	79.5	-
	I-2A	2250	350	Sh A 67	44	31
	I-3A (60mil)	1590-2180	410-550	ShA 57-70	25-41	37
Urethane	II-1A	4900	430	ShA 80	300	42
	II-1B	5300	600	ShA 85	310	68.6
	II-1F	2930	545	-	137	-
	II-2A	4900	530	ShA 80	300	42
	II-2B	5185	475	ShD 45	132	51
	II-2E	4625	650	ShA 97 ShD 43	171	38.4
	II-2I	2840	375	ShA 69	55	33
Butadiene Polymers and Copolymers	VIII-2A	2270	380	ShA 73	175	22.6
	VIII-2B	2700	860	ShA 64	280	-
	VIII-2D	3110	430	-	-	-
	VIII-2E	3530	550	-	-	-
	VIII-3C	2155	255	ShA 81	44	38
	VIII-3E	760	519	ShA 56	23	62
	VIII-3F	540	443	ShA 56	19	-
	VIII-3G	2645	1000	ShA 64	128	42
	VIII-3H	2700	856	ShA 64	118	40
	VIII-3I	2918	628	ShA 62	47	12
	VIII-3J	3470	727	ShA 62	57	20
	VIII-3K	619	643	ShA 55	21	45
	VIII-3N	3360	550	ShA 72	48	32
Natural Rubber	IX-2B	4450	650	-	123	34
	IX-2C	4000	630	-	235	30
	IX-2F	1600	750	ShA 75	48	-
	IX-2G	4000	700	ShA 60	42	-
	IX-3A	4450	650	ShA 65	123	34
	IX-3E	4360	595	ShA 66	122	21

TABLE 7-9

Second Order of Merit Coatings
[Lichtman and Weingram (132)]

Material Type	Sample Code	Ultimate Tensile Strength PSI	% Elongation	Hardness	Tear Strength PLI	Tensile Hysteresis %
Neoprene	I-1C (30mil)	1890	860	ShA 80	160	60
	I-1G	2205-2405	510-1075	ShA 80	140-173	66-74.1
	I-2C	1530	595	ShA 55	15	75.3
	I-2D	2370	430	-	23	23.7
	I-3A (10-40 mil)	1590-2180	410-550	ShA 57-70	25-41	37
	I-3B	-	-	ShA 60(2)	-	-
Urethane	II-1E	730	135	ShA 80	15	34
	II-1O	3490	460	-	-	-
	II-2F	4000	400-500	ShA 80-85	>150	-
	II-2G	4715	700	ShA 88	173	30.1
Butadiene Polymers and Copolymers	VIII-2C	-	-	ShA 79	-	-
	VIII-3D	2700	283	ShA 81	42	55
	VIII-3M	3375	464	ShA 72	48	31
Natural Rubber	IX-2A	1950	645	ShA 47	55	23.2
	IX-2D	3400	930	ShA 60	47	-
	IX-2E	3350	750	ShA 60	44	-
	IX-3B	3980	660	ShA 60	121	-
	IX-3C	3530	640	ShA 58	71	-
	IX-3F	4000	630	ShA 63	235	-
	IX-3G	3118	260	ShA 87	-	-

TABLE 7-10

Third Order of Merit Coatings
[Lichtman and Weingram (132)]

Material Type	Sample Code	Ultimate Tensile Strength PSI	% Elongation	Hardness	Tear Strength PLI	Tensile Hysteresis %
Neoprene	I-1B	555	520	ShA 45-55	-	-
	I-1C (10mil)	1890	860	ShA 80	160	60
	I-1E	2885	760	-	66	63.4
	I-1F	2545	840	-	57	54.0
	I-1H	1760	560	-	55	65.4
	I-2B	1400	270	-	38-60	32.9
	I-3A (5 mil)	1590-2180	410-550	ShA 57-70	25-41	37
Urethane	II-1C	440	130	ShA 60	17.6	66.2
	II-1P	2670	590	ShA 85	-	-
	II-1S	1260	230	ShA 80	75	66
	II-2C	9940	170	ShD 56	101	59.8
	II-2D	5240	575	ShA 86	130	33.2
	II-2H	3315	795	ShA 77	125	23.6
	II-2J	1590	100	ShA 89	68	53
Poly-sulfide	III-1A	115	180	ShA 60	42.9	47
	III-1B	375	275	ShA 60	6	37
	III-1C	210	360	ShA 18	23.3	-
Poly-siloxane	IV-1A	390	90	ShA 65	8	37
Hapalon	V-1A	245	255	-	50	-
Butyl	VII-2A	1000	570	ShA 57	94	60
Butadiene Polymers and Copolymers	VIII-3A	1900	540	-	29.9	27
	VIII-3B	1000	540	-	20.	-
	VIII-3L	500	700	ShA 55	23	14.4
Natural Rubber	IX-1A	460	40	-	0	-
	IX-2H	2700	250	ShA 85	30	-
	IX-3D	407	205	ShA 56	21	-
Glyamine Resins	XII-1A	2165	45	ShA 84	145	-
	XII-1B	1900	75	ShA 85	65	-

TABLE 7-11

Structural Plastics
[Lichtman and Weingram (132)]

Sample Code, Material Type	Order* of Merit	Ultimate Tensile Strength PSI	Ultimate Elongation %	Mod. of Elasticity PSI in Tension	Hardness (3)(4)	Impact Strength Izod, Notch Energy Absorbed Ft. Lb./In.
A, Polyamide (unfilled)	1	11,500 (1) 11,000 (2)	60 (1) 300 (2)	4.20×10^5 (1) 2.05×10^5 (2)	ShD 79(1) 70(2)	0.9-2.0 (1) -
B, Polyamide, FRP	2	30,000	2.0	-	ShD 87(1)	5.0 (1)
L, Acetal	2	8,000	40	-	ShD 85 Rm 76	1.1 (notched) 20 (un-notched)
M, Acetal	2	10,000	15	-	ShD 87 Rm 94	1.4 (notched) 20 (un-notched)
N, Polyimide	3	13,000	6-8	4.3×10^5	ShD 81 Rh 83-89 Rm 112	0.7-1.1
C, Polycarbonate	4	6,920	97	3.2×10^5	ShD 85	2.0
D, Polycarbonate	4	6,825	90-125	$2.8\text{-}3.2 \times 10^5$	ShD 83 Rm 75	2-3
E, Polycarbonate FRP	5	20,000	1.4	13×10^5	ShD 90 Rm 95	4.0
F, Poly Vinyl Chloride	5	6,000-9,000	1-5	-	ShD 87 Rr 110-120	0.4-1.0
G, Poly Vinyl Chloride	5	6,000-9,000	1-5	-	-	0.4-1.0
K, Styrene-Acrylonitrile	6	10,000-12,000	1.0-3.2	5.2×10^5	ShD 77 Rm 30-55	0.3-0.55
H, Epoxy GRP	7	20,000-60,000			ShD 93	11-26
I, Epoxy GRP	7	20,000-60,000	2.5	-	ShD 93	11-26
J, Polymethyl Methacrylate	8	8,000-14,300	2-7	$3.5\text{-}5.0 \times 10^6$	ShD 85-88 Sh 90-100	0.4-0.5

Notes* 1: highest erosion resistance, 8: lowest erosion resistance,
(1) 0.2% H_2O, (2) 2.5% H_2O, (3) Sh: Shore, (4) R: Rockwell

TABLE 7-12

Non-Elastomeric Coatings
[Lichtman and Weingram (132)]

Material Type	Sample Code	Order of Merit*	Ultimate Tensile Strength-PSI	Ultimate Elongation Percent	Hardness	Tear Strength PLI
Anti-Corrosive and Anti Fouling	VII-D	1	2100	920		325
	VII-E	1	2390	1000		250
Metallic	VIII-A	1	440	< 10	ShA 87	-
Glass	IX-B	1	-	-	Rc 65 Mohs scale	-
	IX-D	1	-	-	6-7	-
Nylon	IV-A	2	1730	0	ShD 73	-
	IV-B	2	-	-	ShD 82	-
Epoxy	I-A	3	1000	< 10	ShD 90 pts	-
	I-B	3	-	-	ShD 85 pts	-
	I-D	3	1530	< 10	ShD 88 pts	-
	I-H	3	3056	< 10	ShD 93	-
	I-I	3	-	-	ShD 88	-
	I-J	3	6900	10	ShD 78	-
	I-K	3	2720-1700	50-55	ShA 87	65
	I-L	3	-	-	ShD 8C	-
	I-N	3	-	-	ShD 75	-
Flurocarbon	VI-A	3	3200	290	ShD 78	-
	VI-B	3	4200	330	-	90
Glass	IX-A	3	-	-	Rockwell Superficial 15N-94,30N-82, Rc 58	-
Epoxy	I-C	4	1810	< 10	ShD 93 pts	20
	I-E	4	3400	-	ShA 60	-
	I-F	4	1100	20	ShA 75 pts	22
	I-G	4	560	0	ShD 75	-
	I-M	4	2450	< 5	ShD 85	-
Polyester-glass flake	II-A	4	3970	1.0	ShD 89 pts	-
Silicone Resin	III-A	4	-	-	ShD 90	-
Chlorinated Polyester	V-A	4	6050	85	ShD 78	-
Anti-Corrosive and Anti-Fouling	VII-A	4	440	< 10	ShA 87	-
	VII-B	4	350	< 10	-	-
	VII-C	4	290	< 10	-	-
	VII-F	4	1240	< 10	-	-
Zinc-Rich	X-A	4	70	0	ShA 90 pts	-
	X-B	4	-	-	ShA 85 pts	-
	X-C	4	220	0	-	-

NOTE: * 1: highest erosion
4: lowest erosion

TABLE 8-1

Cumulative Mean Depth of Erosion Corresponding to
The Peak Rate of Erosion

Material	Total Volume Loss up to peak rate of erosion, cm^3	Cumulative Mean Depth of erosion, cm	Percent Derivation from Mean
1100-F Aluminum	10.80×10^{-3}	6.9×10^{-3}	-1
2024 Aluminum	11.70×10^{-3}	7.4×10^{-3}	+5
Tobin Bronze	10.21×10^{-3}	6.5×10^{-3}	-8
Nickel	12.06×10^{-3}	7.6×10^{-3}	+9
Monel	11.71×10^{-3}	7.4×10^{-3}	+5
1020 Steel	11.38×10^{-3}	7.2×10^{-3}	+2
316 Stainless Steel	9.59×10^{-3}	6.1×10^{-3}	-13

TABLE 8-2

Summary of Scaling Parameters

	Jet Impact		Spherical Collapse
	Stagnation Pressure (Macro-jet)	Water Hammer Pressure (Micro-jet)	
	$\Theta = \frac{\sigma}{\delta}\,(\Delta\sigma)^{\frac{1}{2}} \exp\left[\frac{-2.67}{W(\Delta\sigma)}\right]$	$\Theta = \frac{J}{\delta_M}(\Delta\sigma)^{\frac{1}{2}} \exp\left[\frac{-2.67}{W(\Delta\sigma)}\right]$	$\Theta = \frac{\sigma}{\delta}\,(\Delta\sigma)^{\frac{1}{2}} \cdot \exp\left[\frac{2}{3}\,\alpha - \frac{2.67}{W(\Delta\sigma)}\right]$
Erosion number	$\Theta = \frac{I_e}{\frac{1}{2}\rho V_o^3}$	Same	Same
Relative nuclei size	$\delta = \bar{d}/\ell$	Same	Same
Weber Number	$W = \frac{\frac{1}{2}\rho V_o^2 \bar{d}}{\gamma}$	Same	Same
Cavitation number	$\sigma = \frac{p_o - p_v}{\frac{1}{2}\rho V_o^2}$	Same	Same
Cavitation inception number	$\sigma_i = \frac{p_i - p_v}{\frac{1}{2}\rho V_o^2}$	Same	Same
Degree of cavitation	$\Delta\sigma = \sigma_i - \sigma$	Same	Same
Mach number	None	$M = V_o/C$	None
Damping number	None	None	$\alpha = P_o/Q_o$

TABLE 8-3

Range of Nuclei Size, Velocity and Weber Number
for Laboratory Experiments and for Prototype Operations

$\rho = 1.98$ slugs/ft^3

$\gamma = .005$ lb/ft

Mean Nuclei Size $\bar{d}$, ft	Velocity V_o, fps	Weber Number $W = \frac{\frac{1}{2}\rho V_o^2 \bar{d}}{\gamma}$
10^{-5}	50	5
	100*	20*
	200*	80*
10^{-4}	50	50
	100	200
	200	800
10^{-3}	50	500
	100**	2000**
	200**	8000**
10^{-2}	50	5000
	100	20000
	200	80000

*Range of values likely for experiments in the laboratory.

**Range of values likely for prototype operation.

TABLE 9-1

Relative Role of Corrosion in Cavitation Damage
Material: SAE 1020 Steel

[Waring et al (79)]

Test Method	Liquid	Double Amplitude (inches)	Frequency kcs	Rate of Weight Loss mg/min
1. Total Cavitation Damage	Distilled H_2O	1.5×10^{-3}	15	90×10^{-3} (2.36 ipy)
2. Total Cavitation Damage	3% NaCl solution	1.5×10^{-3}	15	260×10^{-3} (6.84 ipy)
3. Static Polarization Measurements	3% NaCl solution	—	—	*2×10^{-3} (.052 ipy)
4. Dynamic Polarization Measurements	3% NaCl solution	1.5×10^{-3}	15	*15×10^{-3} (.395 ipy)
5. Pulsing Technique (Plesset)	3% NaCl solution	2.0×10^{-3}	14.2	*20×10^{-3} (.525 ipy)
6. Pulsing Technique (Waring)	3% NaCl solution	1.5×10^{-3}	15	*7×10^{-3} (.184 ipy)

* Estimated corrosion

TABLE 9-2. Galvanic Series of Metals In Flowing Sea Water

ANODIC OR LEAST NOBLE

Magnesium and magnesium alloys
Cb 75 aluminum anode alloy
Zinc
B605 aluminum anode alloy
Galvanized steel or galvanized wrought iron
Aluminum 7072 (cladding alloy)
Aluminum 5456
Aluminum 5086
Aluminum 5052
Aluminum 3003, 1100, 6061, 356
Cadmium
Aluminum 2117 rivet alloy
Mild steel
Wrought iron
Cast iron
10% chromium steel type 410 (active
17% chromium steel type 430 (active)
18-8 stainless steel type 304 (active)
18-12-3 stainless steel type 316 (active)
Ni-resist
Lead
Tin
Muntz metal
Manganese bronze
Naval brass (60% copper, 39% zinc, 1% tin)
Yellow brass (65% copper, 35% zinc)
Copper
Silicon bronze
Red brass (85% copper, 15% zinc)
Aluminum brass
Composition G bronze
Composition M bronze
Admiralty brass
90% copper, 10% nickel
70% copper, 30% nickel
Nickel
INCONEL alloy 600 (78% nickel, 13.5% chromium, 6% iron)
Nickel aluminum bronze
Silver
Titanium
18-8 stainless steel type 304 (passive)
INCONEL alloy 625
HASTELLOY alloy C
MONEL alloy 400
Type 316 stainless steel (passive)
INCOLOY alloy 825
Graphite
Platinum

CATHODIC OR MOST NOBLE

TABLE 10-1

Damage Ratings of Ship's Underwater Appendages
[Lichtman et al (213)]

Vessel	Shafts	Rating of Removal of Coating[a]			Skegs	Average Rating	Rating of Degree of Corrosion of Bared Metal[a]					Average Rating
		Struts	Rudders	Barrels			Shafts	Struts	Rudders	Barrels	Skegs	
DD 853	1	3	8	4	2	3.6	7	6	2	4	6	5.0
DDR 807	3	5	7	4	4	4.6	4	6	5	6	6	5.4
DDR 830	4	6	7	7	6	6.0	4	5	5	6	6	5.2
DDE 859	1	3	5	2	4	3.0	2	6	4	3	6	4.2
DDE 860	1	1	8	1	5	3.2	3	1	1	1	7	2.6
DDE 858	1	1	7	6	9	5.4	2	5	2	4	7	4.0
DD 865	2	5	6	6	4	4.6	3	5	4	4	7	4.6
DD 850	4	5	8	10	9	7.2	4	4	3	5	6	4.4
DE 447	1	1	-	9	-	-	3	5	-	3	-	-
DD 821	1	7	6	10	8	6.4	3	5	4	6	7	5.0
DD 841	4	3	9	6	9	6.2	3	5	2	4	8	4.4
CVS 32	1	5	1	8	1	3.2	2	5	2	4	4	3.4
DE 532	1	3	-	9	-	-	1	5	-	6	-	-
CVA 39	1	7	4	9	3	4.8	0	5	3	5	5	3.6
DE 538	-	-	-	-	-	-	7	7	7	5	7	6.6
PCE 880[b]	1	3	3	1	4	2.4	0	1	2	2	2	1.4
PCE 894[b]	1	1	1	0	3	1.2	0	0	1	0	1	0.4
Total	28	62	81	92	71	61.4	49	76	47	66	85	60.6
Average	1.8	3.8	5.8	5.8	5.1	4.4	2.9	4.5	3.1	4.0	5.7	4.0

[a] Rating 10 = maximum, 0 = minimum damage.

[b] Operated in fresh water.

TABLE 10-2

Intensity of Cavitation Damage on Some Ship Propellers
[Thiruvengadam (125)]

Designation	Ship Velocity (Knots)	Time of Operation (Hours)	Maximum Depth of Erosion (Inches)	Material Used	Strain Energy (psi)	Intensity $\frac{\text{watts}}{(\text{meter})^2}$	Location of Damage	Area of Damage	Remarks
Bremen		500 - (2 round trips across Atlantic	4-3/4"	Al-Bronze (Assumed)	16,500	8			Metal not given.
DDG-15	20	20	7/8	Mn Bronze	18,000	36			
DD-779 Douglas H. Fox	>30	5-1/4	3/16	Superston	22,600	40	6" from hub	6" x 1-1/2"	All four blades showed similar damage
	25-30	120	3/16			2			
	0-25	2105	3/16			10^{-1}	9" from hub	7" x 1/2"	
DD-7o Massey	25-30	~ 100	1/2	Mn Bronze	18,000	5			
DD-806 Higbee	15-20	~ 150	1/2	Mn Bronze	18,000	3	Suction side, 12"-18" from leading edge	18" x 3"	3000 miles traveled
DD-888 Stickell	< 25	2013	1/4	Mn Bronze	18,000	10^{-1}		5" x 2-1/2"	Port side more pitted than Starboard
	25-30	53	1/4			4			
	> 30	6	1/4			37			
DD-876 Rogers	< 25	529	3/16	Superston	22,600	4×10^{-1}			Damage on all four blades
	25-30	10	3/16			20			
	> 30	8	3/16			26			
	> 30	128	3/16			2	Pressure side	4" x 2"	Test run
DD-838 Small	< 25	1935	1/2	Superston	22,600	3×10^{-1}			Starboard - less damage
	25-30	139	1/2			4			
	> 30	25	1/2			22			
DD-851 Rupertus	< 25	1289	1/8	Superston	22,600	10^{-1}	3" from leading edge		
	25-30	42	1/8			3			
	> 30	8	1/8			17			
DD-875 Truber	< 25	1220	3/4	Stainless Steel	35,000	10^{-1}	6" from trailing edge; 6" from hub		On all blades
	25-30	12	3/4			110			
	> 30	6	3/4			220			
DD-836 McKenzie	> 25	1458	1/8	NALAB Bronze	17,000	10^{-1}			Scattered pits over 50% at 6" radius from hub
	25-30	26	1/8			4			
	> 30	10	1/8			10			

TABLE 10-3

Intensity of Cavitation Damage on Valves *
[Thiruvengadam (125)]

Type	Hydraulic Details	Time of Operation	Depth of Erosion	Material	Strain Energy (psi)	Intensity watts/m^2
6" Cast Iron Test Valve	200 psig → 0 psig	3 or 4 wks.	Say 1/2"	Cast Iron	10,000	5×10^{-1}
Feed Water Bypass regulator.	2800-300 psi 600 fps 2" x 3/4"	6 to 9 hrs.	1/2 to 1"	316 St. Steel.	40,000	200
Control Valve	——	Few hrs. Assume 10 hrs.	Say 1/2"	18-8 St. Steel with harder overlay	35,000	100
Control Valve	2000 psi pressure difference	10 min.	1/4"	316 St. Steel	40,000	3000
Needle Valve	145 ft. head 72" diameter	1 month	1/2"	Steel	15,000	5×10^{-1}
Needle Valve	52" conduit	One flood. Assume 1 wk.	1-1/4"	Steel	15,000	6
Sluice Gate	10'x9-1/2' size Discharge of ≅ 5000 cu. secs.	1500 hrs.	3/4"	Steel	15,000	3×10^{-1}
Sluice Gate		75 hrs.	1/4"	Steel	15,000	2

* These are some specific cases where cavitation damage data are available.

TABLE 10-4

Intensity of Cavitation Damage on Diesel Engine Cylinder Liners*
[Thiruvengadam (125)]

Horsepower	Time of Operation	Material Used	Maximum Depth inches	Strain Energy	Intensity
	300 hours	Cast Iron	1/2	10,000	1
River Barge Diesel Engine	3 weeks	not given Assumed Cast Iron	1/16	10,000	10^{-1}
	900 hours	Cast Iron	5/16	10,000	10^{-1}
	one year	Cast Iron	3	10,000	10^{-1}
	1000 hours	Cast Iron	1/10	10,000	5×10^{-2}

* These are some specific cases where cavitation damage data are available.

TABLE 10-5

Intensity of Cavitation Damage on Hydraulic Turbines*
[Thiruvengadam (125)]

Type	Time of Operation	Depth of Erosion	Material Used	Strain Energy	Intensity
Francis Turbine	3 years	"So Badly" Assume 1"	Cast Steel	15,000	3×10^{-2}
Francis Turbine	4 years	"Hole Through" Assume 1"	Cast Steel	15,000	2×10^{-2}
Francis Turbine	3 years	1/64"	Bronze	18,000	10^{-3}
Francis Turbine	"Few Weeks" say 10 wks.	1"	Bronze	18,000	5×10^{-1}
Kaplan Turbine	4 years	3"	Not Given Assume Bronze	18,000	10^{-1}
Peltor. Wheel	Two weeks	2"	—	20,000	7

* These are some specific cases where cavitation damage data are available.

TABLE 10-6

Intensity of Cavitation Damage on Pumps*
[Thiruvengadam (125)]

Detail	Liquid Pumped	Time of Operation	Depth of Erosion inches	Material Used	Strain Energy	Intensity
Liquid Potassium Pump	Liquid Potas-sium	300 hrs.	50×10^{-3}	Stainless Steel	Assume 15,000	10^{-1}
Sodium and Salt Fused Pump	Liquid Sodium at $1200^{\circ}F$	2500	0.34	Inconel	Assume 18,000	10^{-1}

* These are some specific cases where cavitation damage data are available.

TABLE 11-1

Cavitation Damage Resistance of Sprayed Coatings

[After Rheingans -- Reference 221]

Alloy	Weight Loss in 2 hrs. - mg
UNFUSED	
High Chromium Stainless Steel (Metcoloy 2)	72
18 Cr-8 Ni stainless steel (Metcoloy 1)	98
13 percent Cr stainless steel	192
Molybdenum	358
FUSED	
65 to 75 Ni-15 to 20 Cr-2.7 to 4.7 percent B(Colmonoy 6)	8
75 to 85 Ni-8 to 14 Cr-2 to 3 percent B (Colmonoy 4)	30

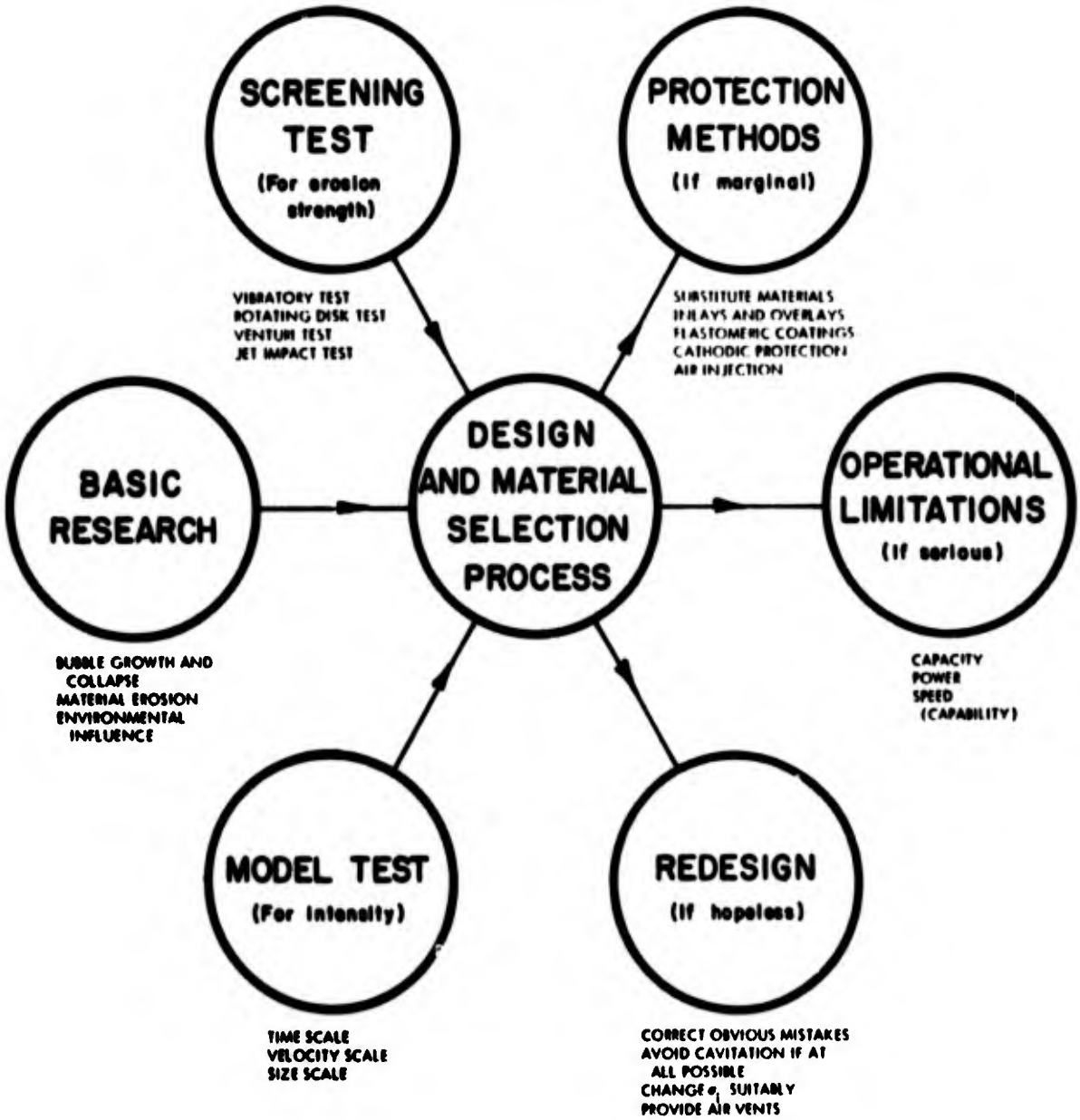
SCREENING TEST
(For erosion strength)
VIBRATORY TEST
ROTATING DISK TEST
VENTURI TEST
JET IMPACT TEST
PROTECTION METHODS
(If marginal)
SUBSTITUTE MATERIALS
INLAYS AND OVERLAYS
ELASTOMERIC COATINGS
CATHODIC PROTECTION
AIR INJECTION
BASIC RESEARCH
BUBBLE GROWTH AND COLLAPSE
MATERIAL EROSION
ENVIRONMENTAL INFLUENCE
DESIGN AND MATERIAL SELECTION PROCESS
OPERATIONAL LIMITATIONS
(If serious)
CAPACITY
POWER
SPEED
(CAPABILITY)
MODEL TEST
(For intensity)
TIME SCALE
VELOCITY SCALE
SIZE SCALE
REDESIGN
(If hopeless)
CORRECT OBVIOUS MISTAKES
AVOID CAVITATION IF AT ALL POSSIBLE
CHANGE σ_i SUITABLY
PROVIDE AIR VENTS

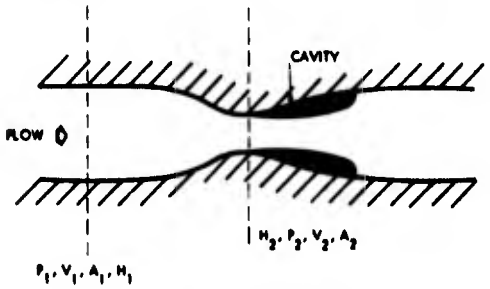

$$V_1A_1 = V_2A_2$$

$$\frac{V_1^2}{2g} + H_1 = \frac{V_2^2}{2g} + H_2$$

$$H_2 = H_1 - \frac{V_1^2}{2g}\left[\left(\frac{A_1}{A_2}\right)^2 - 1\right]$$

CONDITION FOR CAVITATION INCEPTION
H_2 ≤ VAPOR PRESSURE OF THE LIQUID

FIGURE 2-1 - SIMPLE CASE OF CAVITATING VENTURI SHOWING THE CONDITIONS FOR CAVITATION INCEPTION

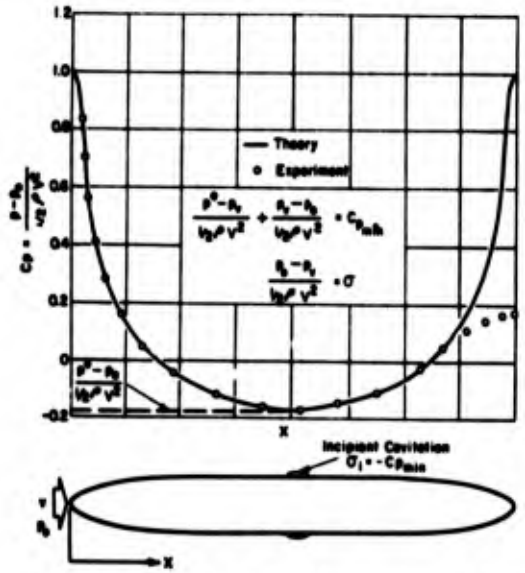

FIGURE 2-2 - PRESSURE DISTRIBUTION ON STREAMLINED BODY

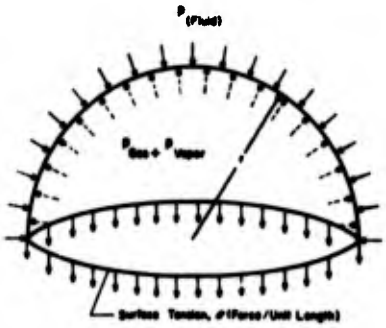

$$\sum F = 0 = \pi r^2 (P - P_g - P_v) + 2\pi r\sigma$$

$$\therefore P - P_v = P_g - \frac{2\sigma}{r} = (P_o - P_v) - \left(\frac{2\sigma}{r} - \frac{2\sigma}{r_o}\right)$$

FIGURE 2-3 - STATIC FORCES ON A SPHERICAL BUBBLE

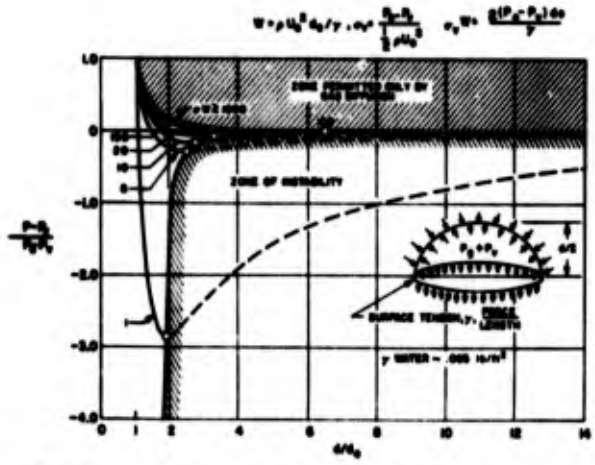

FIGURE 2-4 - THE QUASI-STEADY GROWTH OF SPHERICAL GAS BUBBLES IN A LIQUID

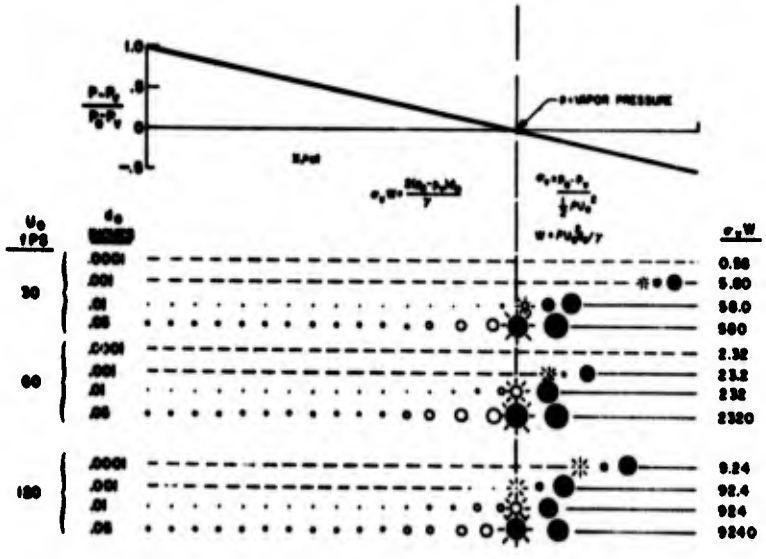

FIGURE 2-5 - SPHERICAL GAS BUBBLE GROWTH $\sigma_v = 0.2$

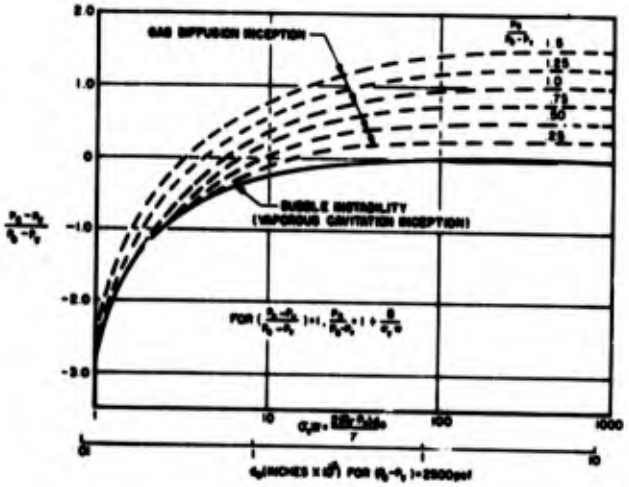

FIGURE 2-6 - CRITICAL PRESSURES FOR BUBBLE INSTABILITY AND GAS DIFFUSION

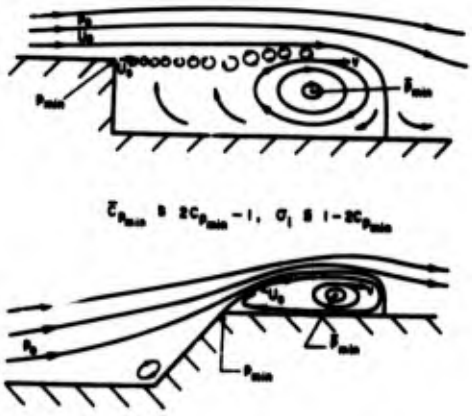

FIGURE 2-7 - EXAMPLES OF SEPARATED FLOW

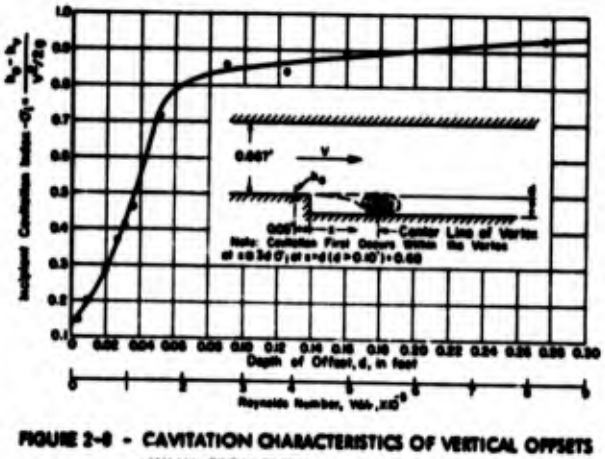

FIGURE 2-8 - CAVITATION CHARACTERISTICS OF VERTICAL OFFSETS AWAY FROM FLOW

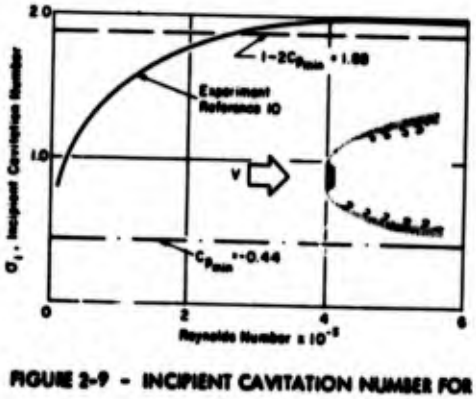

FIGURE 2-9 - INCIPIENT CAVITATION NUMBER FOR DISCS

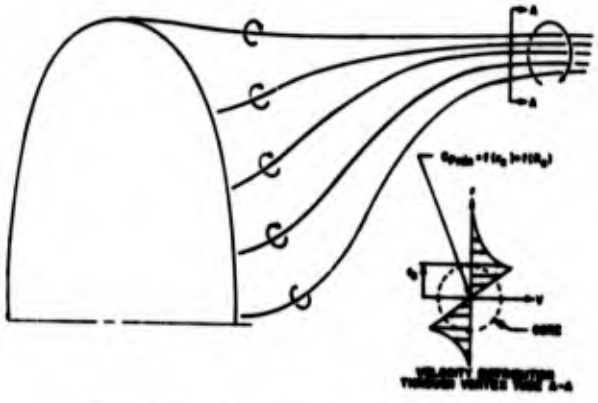

FIGURE 2-10 - TIP VORTEX CHARACTERISTICS

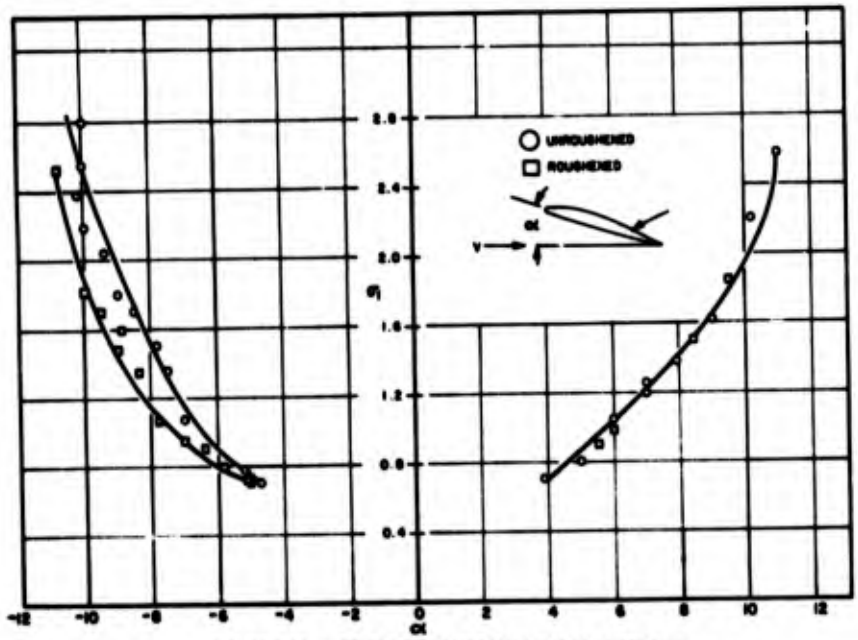

FIGURE 2-11 - EFFECT OF ROUGHNESS ON PROPELLER TIP σ_i (McCORMICK)

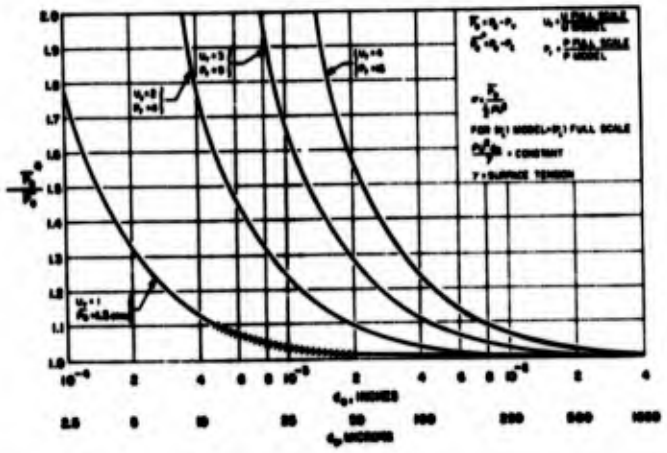

FIGURE 2-12 - THE EFFECT OF GAS BUBBLE SIZE ON CAVITATION INCEPTION

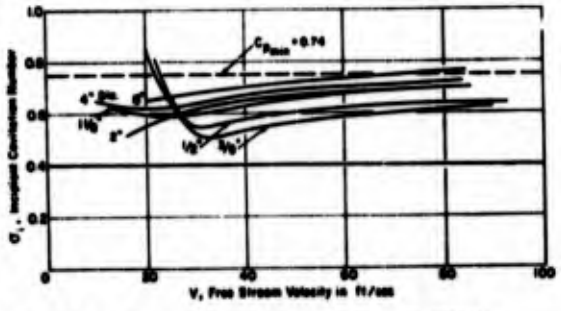

FIGURE 2-13 - INCIPIENT CAVITATION NUMBER VERSUS FREE-STREAM VELOCITY FOR HEMISPHERICAL NOSED BODIES (McMORMICK (21))

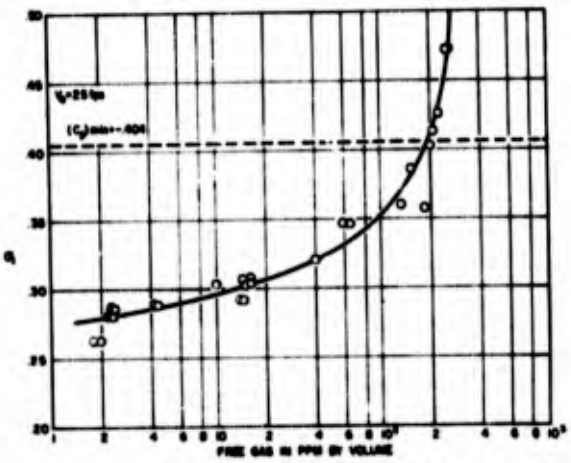

FIGURE 2-14 - EFFECT OF FREE GAS ON σ_i FOR 1.5 CALIBER OGIVE OF 0.625 INCH DIAMETER (RIPKEN AND KILLEN (18))

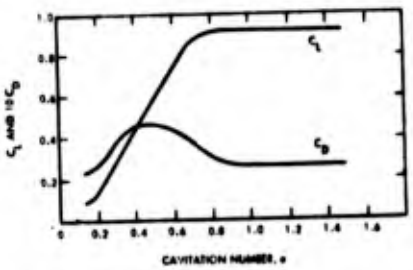

FIGURE 3-1 - LIFT AND DRAG COEFFICIENTS AS FUNCTIONS OF CAVITATION NUMBER FOR THE WALCHNER PROFILE 7 HYDROFOIL AT AN ANGLE OF ATTACK OF 4 DEGREES

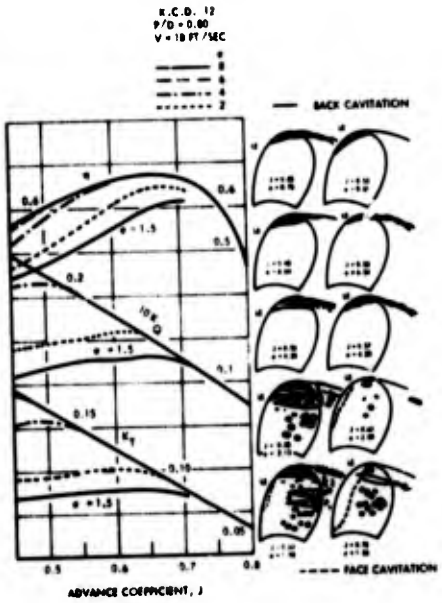

FIGURE 3-2 - EFFECT OF CAVITATION ON THE PERFORMANCE OF A PROPELLER

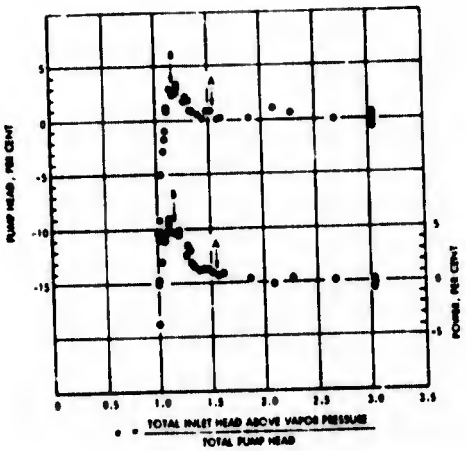

FIGURE 3-3 - CAVITATION TEST RESULTS OF AN AXIAL-FLOW PUMP OF SPECIFIC SPEED Ω = 6.75 Point A would be regarded as inception point, and it is interesting to note that a higher head is generated at Point B in the cavitating region. However a further inlet pressure reduction soon completely chokes the machine (after Wislicenus).

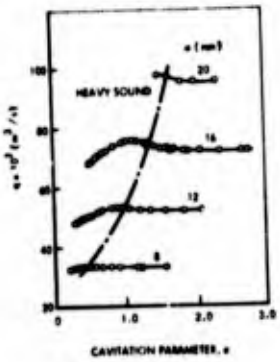

FIGURE 3-4 - THE RELATIONSHIP BETWEEN THE DISCHARGE THROUGH THE TURBINE AND THE CAVITATION PARAMETER (REF. 20)

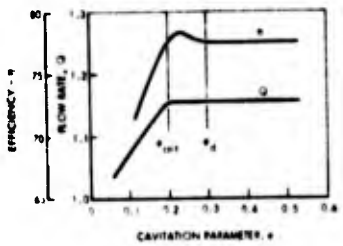

FIGURE 3-5 - CAVITATION REDUCES THE DISCHARGE THROUGH THE TURBINE THUS REDUCING THE POWER GENERATED AND THE EFFICIENCY

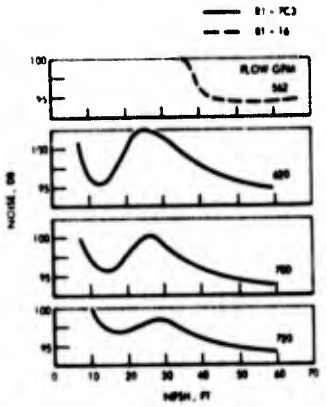

FIGURE 3-6 - NOISE CHARACTERISTICS FOR CAVITATING IMPELLERS TESTED IN WATER

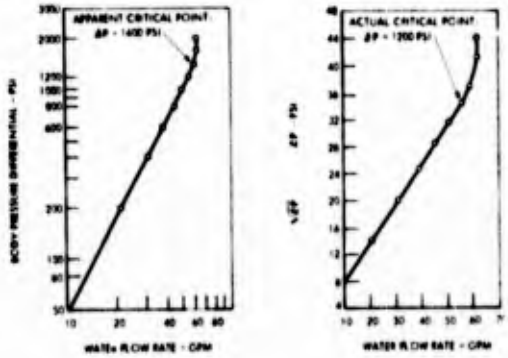

FIGURE 3-7 - WATER FLOW RATE DOES NOT INCREASE ANY FURTHER IN SPITE OF A LARGE INCREASE IN PRESSURE DIFFERENTIAL. THIS IS DUE TO CAVITATION (REF. 31)

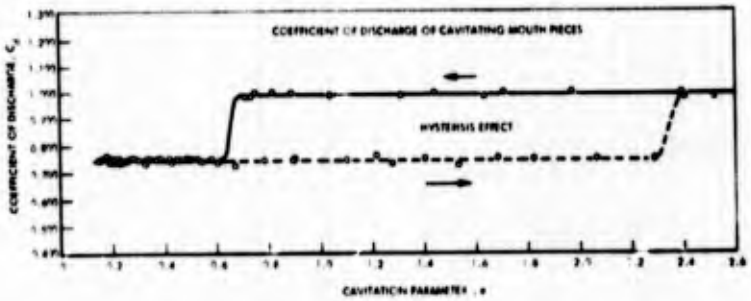

FIGURE 3-8 HYSTERESIS EFFECT CAUSED BY CAVITATION ON THE COEFFICIENT OF DISCHARGE OF A MOUTH PIECE. (Thoma-Livingston, 1958)

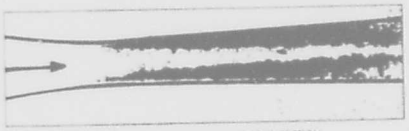

FIGURE 4-1 – CAVITATION IN A VENTURI SECTION (ROTTINGER [93])

FIGURE 4-2 – CAVITATION ON A MODEL PROPELLER SHOWING "STEADY" CAVITATION NEAR THE TIP OF THE UPPERMOST BLADE (DTMB, U.S. NAVY)

FIGURE 4-3 – "TRANSIENT" CAVITATION ON A MODEL PROPELLER (DTMB, U.S. NAVY)

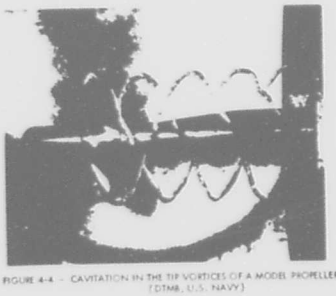

FIGURE 4-4 – CAVITATION IN THE TIP VORTICES OF A MODEL PROPELLER (DTMB, U.S. NAVY)

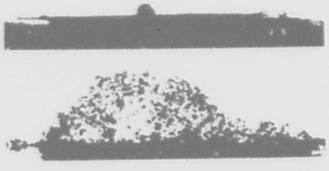

FIGURE 4-5 – CAVITATION CLOUD AT TWO DIFFERENT POINTS OF A PRESSURE CYCLE IN A BARIUM TITANATE APPARATUS (ELLIS [33])

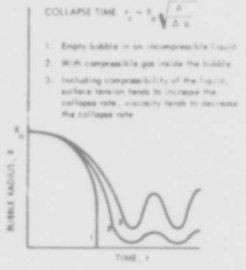

FIGURE 4-6 – SPHERICAL COLLAPSE OF A BUBBLE (RALEIGH 1917, AND OTHERS)

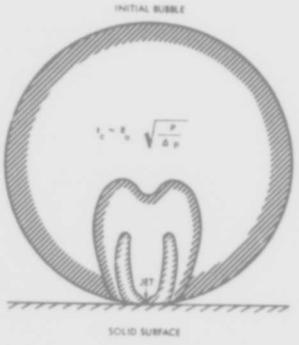

FIGURE 4-7 – COLLAPSE OF BUBBLE IN THE NEIGHBORHOOD OF A SOLID BOUNDARY (PLESSET AND CHAPMAN [56])

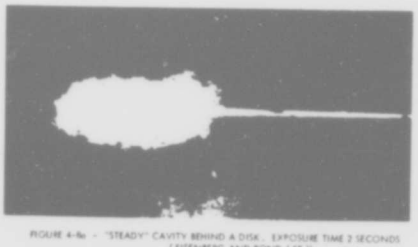

FIGURE 4-8a – "STEADY" CAVITY BEHIND A DISK. EXPOSURE TIME 2 SECONDS (EISENBERG AND POND [58])

FIGURE 4-8b – "STEADY" CAVITY BEHIND A DISK. EXPOSURE TIME 1/10,000 SECOND (EISENBERG AND POND [58])

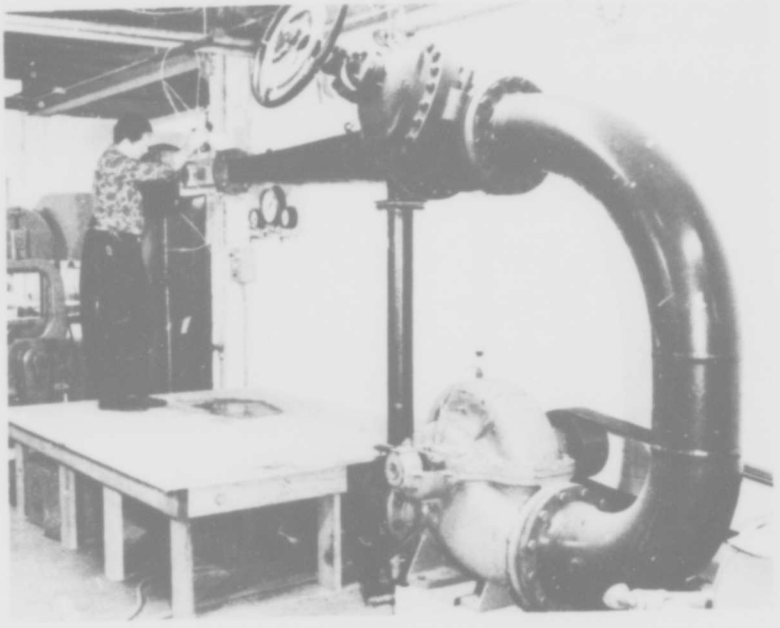

OVERALL VIEW

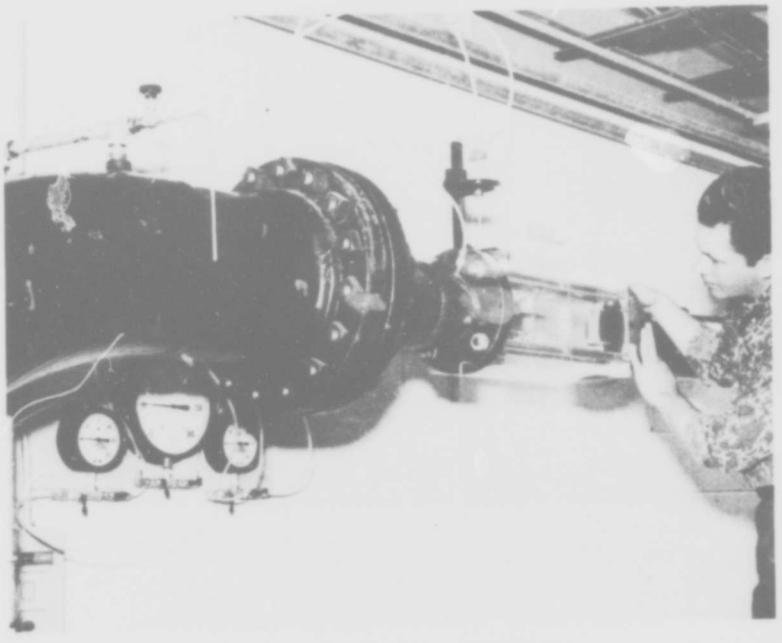

CLOSE-UP OF TEST SECTION

FIGURE 6-1 - ULTRA HIGH SPEED CAVITATION-EROSION CHANNEL

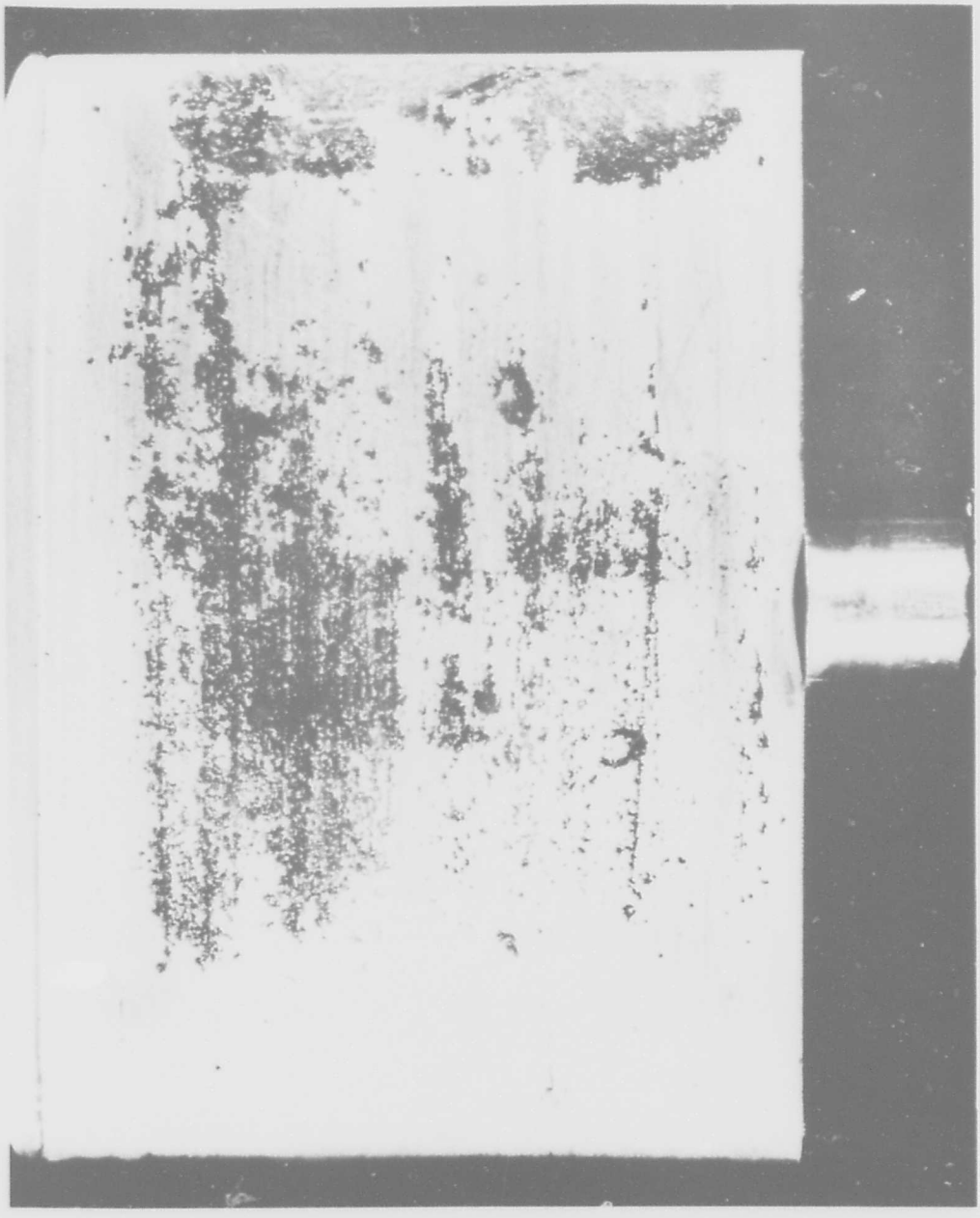

FIGURE 6-2 - CAVITATION DAMAGE OF COATING ON HYDROFOIL

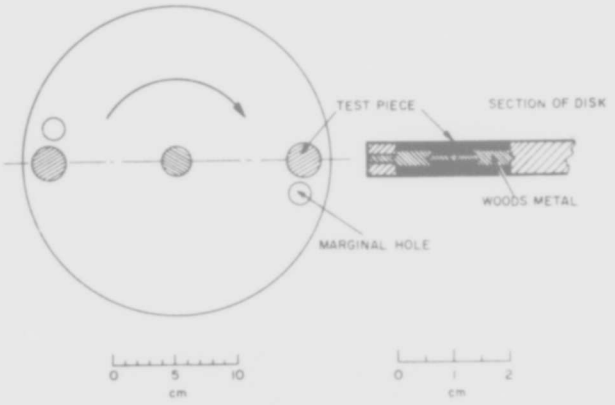

FIGURE 6-3 - ROTATING DISK FOR CAVITATION DAMAGE EXPERIMENTS
(RASMUSSEN (86))

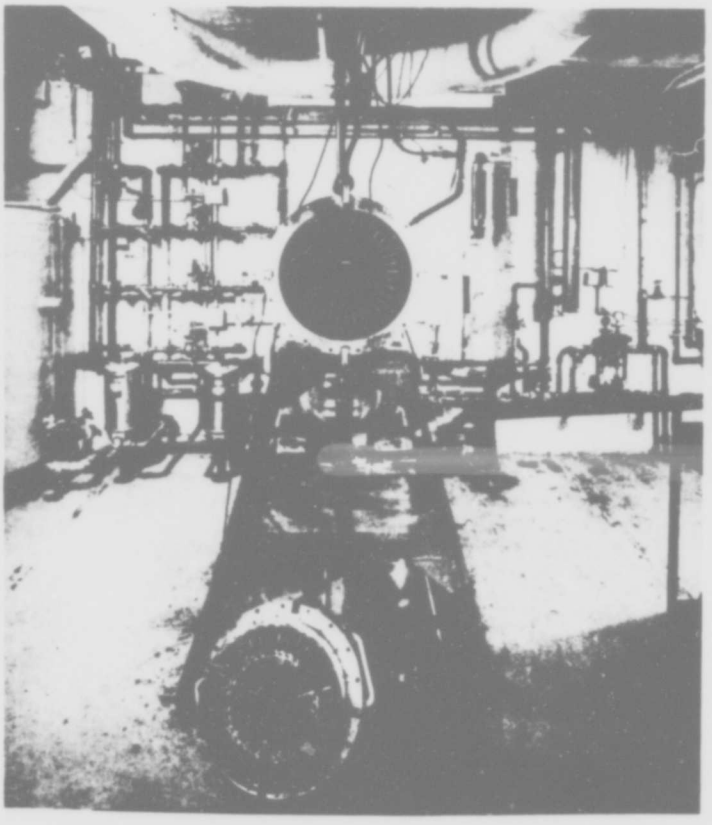

FIGURE 6-4 - FRONT VIEW OF ROTATING DISK CHAMBER ON NAVAPLSCIENLAB
ROTATING DISK CAVITATION EROSION APPARATUS
(LICHTMAN AND WEINGRAM (132))

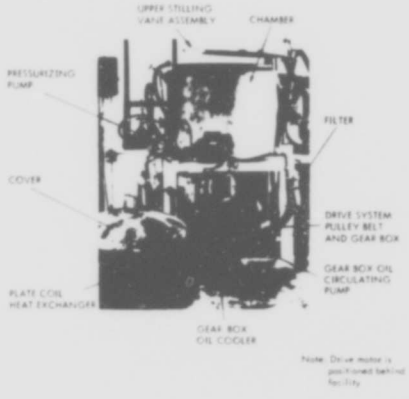

FIGURE 6-5a - ROTATING FOIL APPARATUS

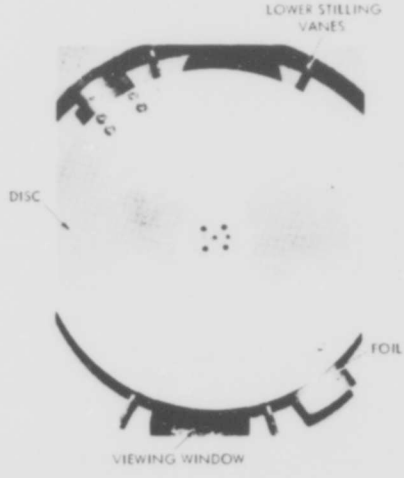

FIGURE 6-5b - ROTATING FOIL APPARATUS DISC ASSEMBLY

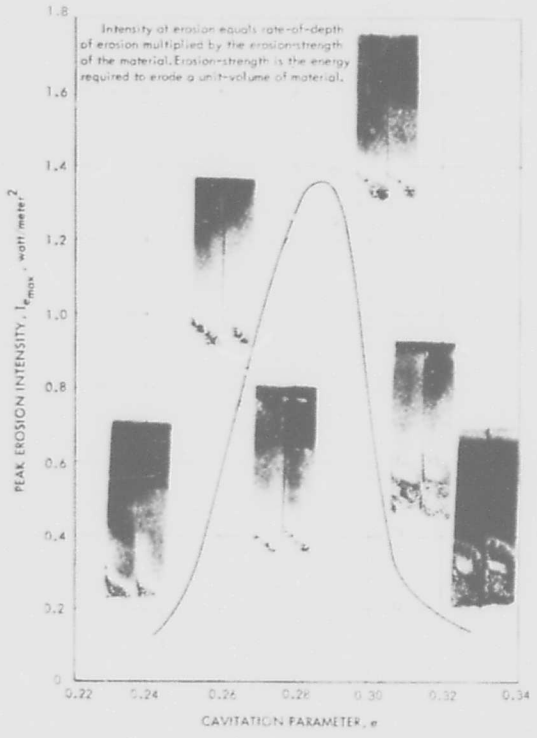

FIGURE 6-6 - PEAK INTENSITY OF EROSION VS. CAVITATION PARAMETER

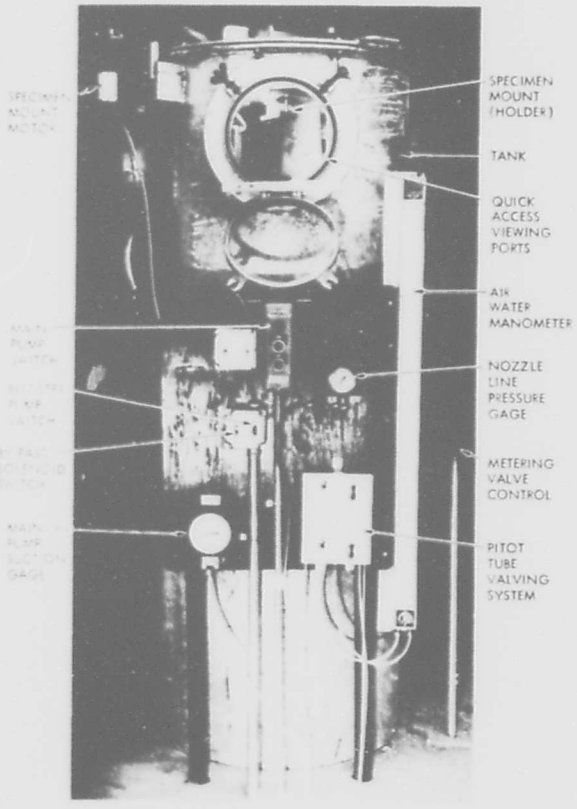

FIGURE 6-7 - CAVITATING WATER JET FACILITY

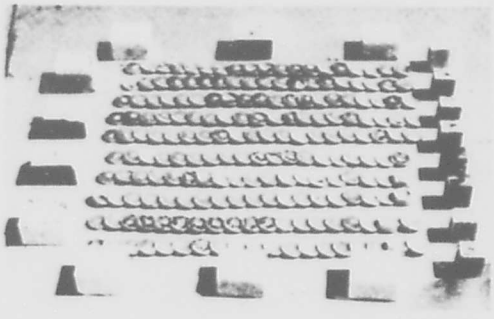

FIGURE 6-8 - SPECIMENS TESTED IN THE CAVITATING WATER JET TEST FACILITY

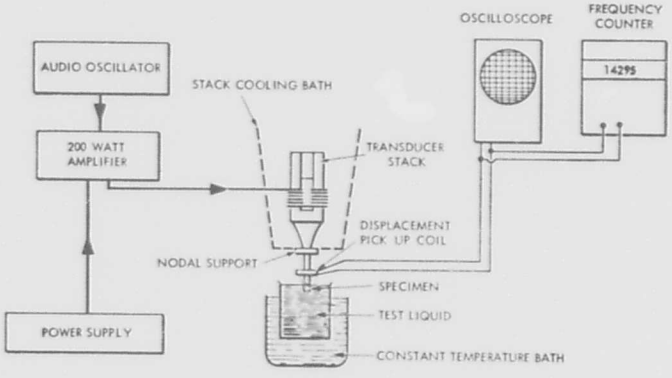

FIGURE 6-9 - SCHEMATIC OF VIBRATORY CAVITATION EROSION APPARATUS

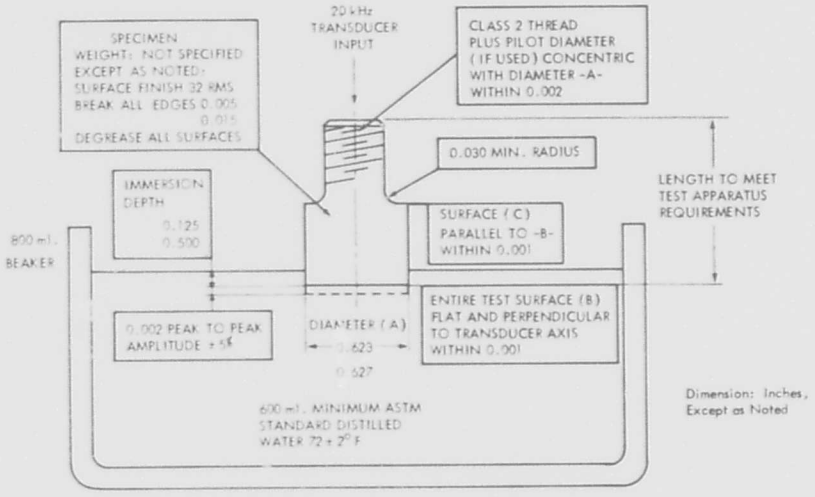

FIGURE 6-10 - IMPORTANT PARAMETERS OF VIBRATORY TEST FACILITY

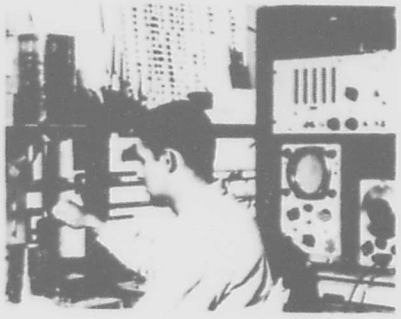

FIGURE 6-11 - PHOTOGRAPH OF A TYPICAL VIBRATORY CAVITATION EROSION TEST FACILITY

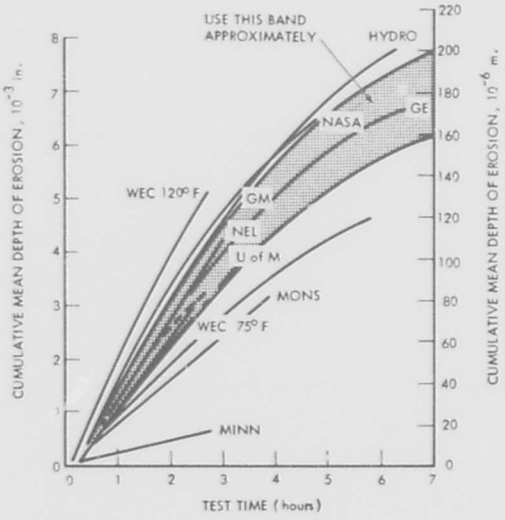

FIGURE 6-12 - RANGE OF TEST RESULTS TO BE EXPECTED WITH ANNEALED NICKEL 270 AT THE SPECIFIED TEST CONDITIONS

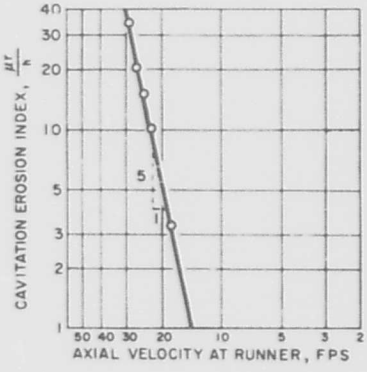

FIGURE 6-13 - CAVITATION EROSION AS MEASURED BY CHANGE IN RADIOACTIVITY IN MICRO-CURIES PER HOUR, AS A FUNCTION OF AXIAL VELOCITY AT A TURBINE RUNNER (KERR AND ROSENBERG (103))

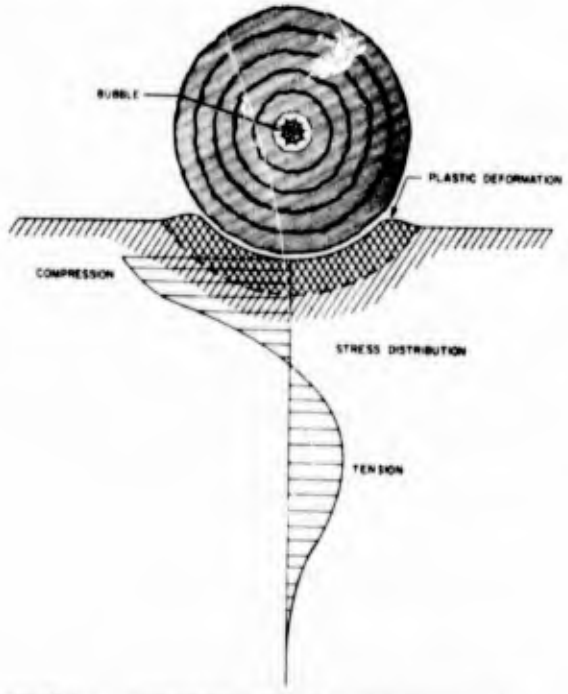

FIGURE 7-1 - DEFINITION SKETCH FOR DEFORMATION DUE TO CAVITATION BUBBLE COLLAPSE (THIRUVENGADAM, (61))

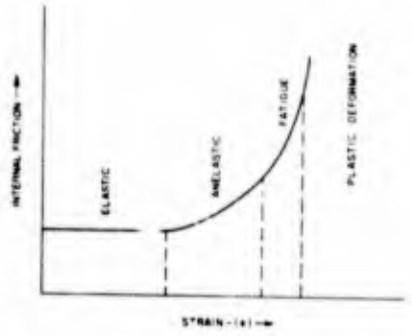

FIGURE 7-2 - SCHEMATIC REPRESENTATION OF THE RESPONSE OF METALS TO REPEATED STRAINING

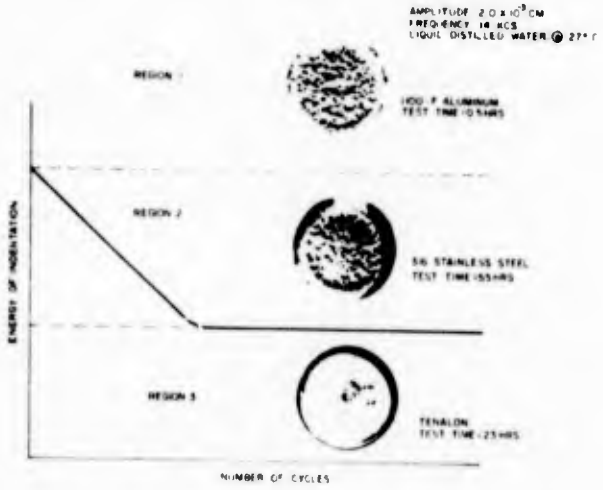

FIGURE 7-3 - SCHEMATIC INDENTATION FATIGUE DIAGRAM SHOWING THREE REGIONS (THIRUVENGADAM AND WARING (110))

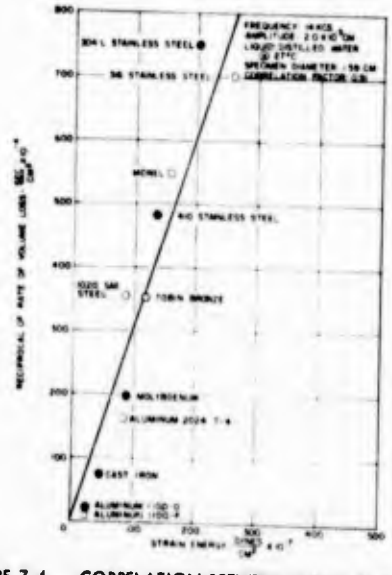

FIGURE 7-4 - CORRELATION BETWEEN STRAIN ENERGY AND RECIPROCAL OF RATE OF VOLUME LOSS (THIRUVENGADAM AND WARING, (110))

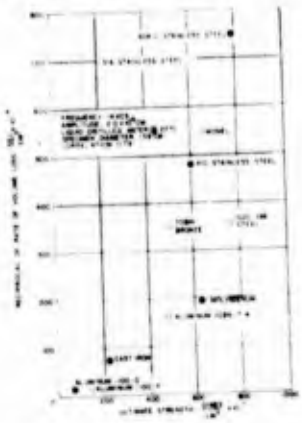

FIGURE 7-5 - CORRELATION BETWEEN ULTIMATE STRENGTH AND RECIPROCAL OF RATE OF VOLUME LOSS

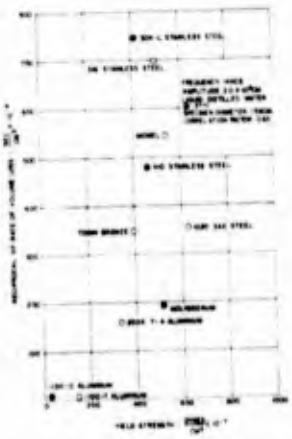

FIGURE 7-6 - CORRELATION BETWEEN YIELD STRENGTH AND RECIPROCAL OF RATE OF VOLUME LOSS

FIGURE 7-7 - CORRELATION BETWEEN BRINELL HARDNESS AND RECIPROCAL OF RATE OF VOLUME LOSS

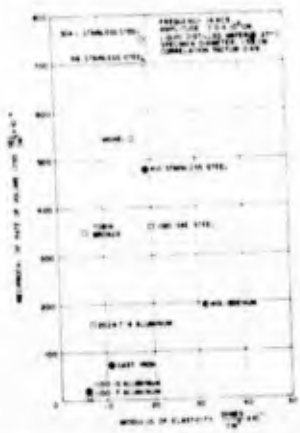

FIGURE 7-8 - CORRELATION BETWEEN MODULUS OF ELASTICITY AND RECIPROCAL OF RATE OF VOLUME LOSS

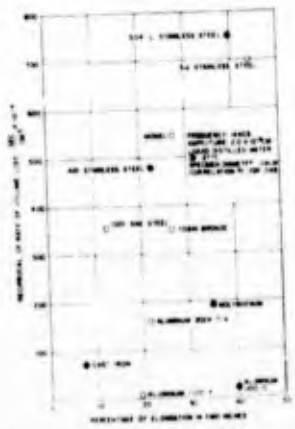

FIGURE 7-9 - CORRELATION BETWEEN ULTIMATE ELONGATION AND RECIPROCAL OF RATE OF VOLUME LOSS

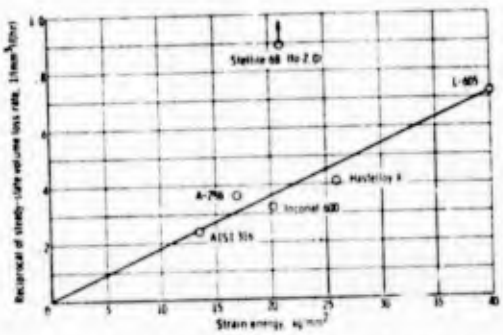

FIGURE 7-10 - RELATION OF CAVITATION DAMAGE IN SODIUM WITH STRAIN ENERGY PARAMETER (REF. 111)

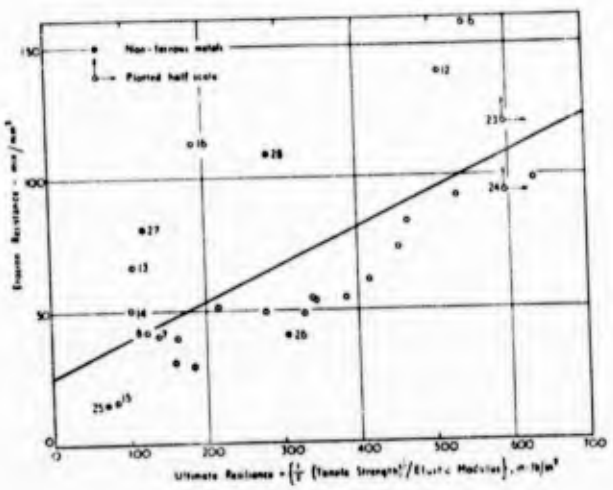

FIGURE 7-11 - EROSION RESISTANCE VERSUS ULTIMATE RESILIENCE (REF. 114)

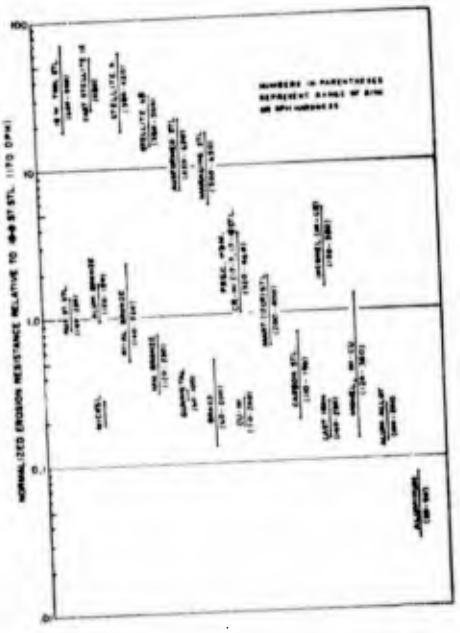

FIGURE 7-12 - NORMALIZED EROSION RESISTANCE RELATIVE TO 18-8 STAINLESS STEEL (170 DPH). HARDNES OF VARIOUS MATERIALS (IN PARENTHESES) IS IN BRINELL OR VICKERS HARDNESS NUMBERS.

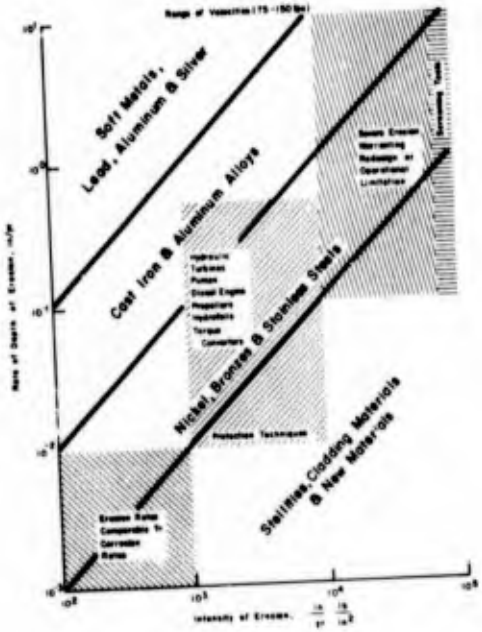

FIGURE 7-13 - MASTER CHART FOR CAVITATION EROSION

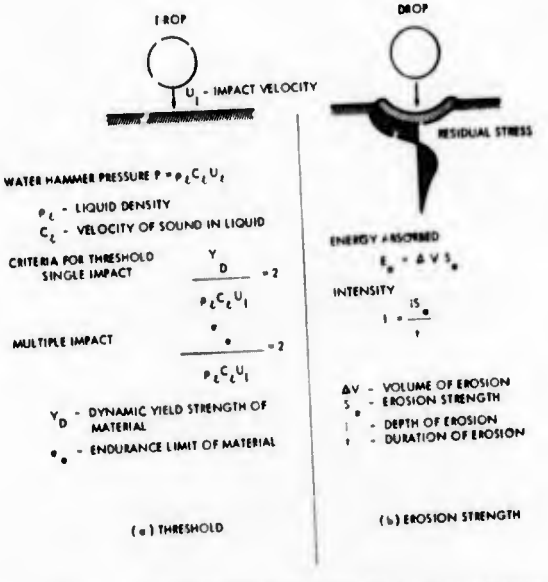

FIGURE 7-14 - DEFINITION SKETCH OF THE MATERIAL RESPONSE TO EROSIVE FORCES

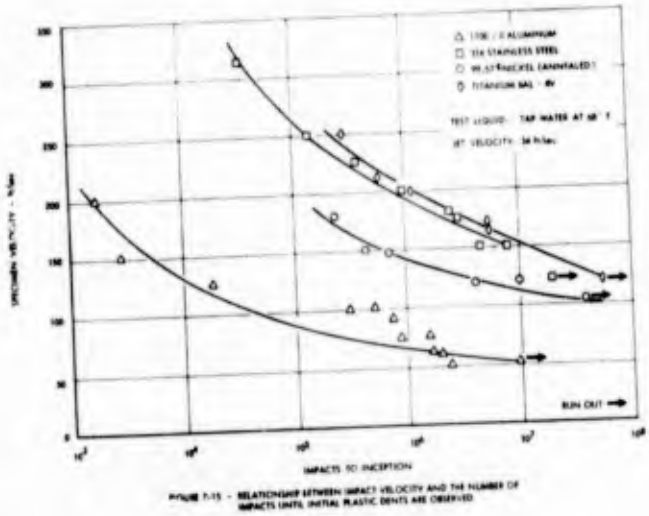

FIGURE 7-15 - RELATIONSHIP BETWEEN IMPACT VELOCITY AND THE NUMBER OF IMPACTS UNTIL INITIAL PLASTIC DENTS ARE OBSERVED

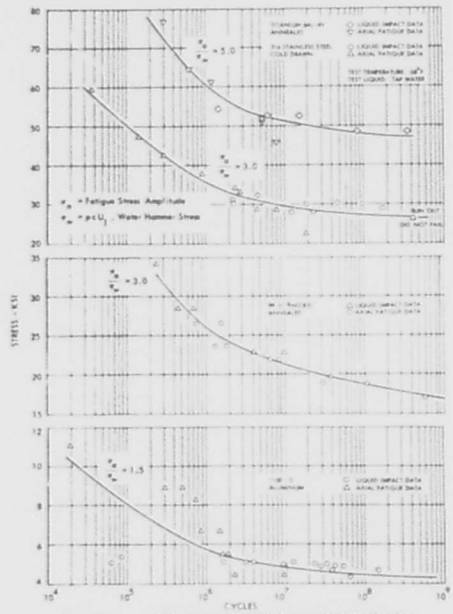

FIGURE 7-16 - CORRELATION OF WATER HAMMER STRESSES WITH FATIGUE ENDURANCE LIMITS

IN WATER TUNNEL

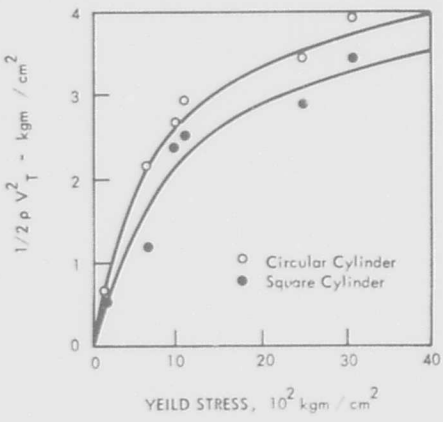

FIGURE 7-17 - HYDRODYNAMIC PRESSURE AT THRESHOLD OF EROSION VERSUS YIELD STRESS

INCEPTION OF DAMAGE NUMBER Di

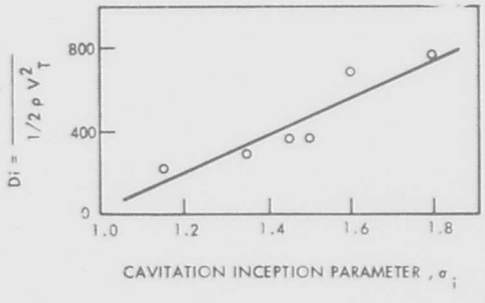

FIGURE 7-18 - RATIO OF YIELD STRESS TO THRESHOLD PRESSURE VERSUS CAVITATION INCEPTION PARAMETER

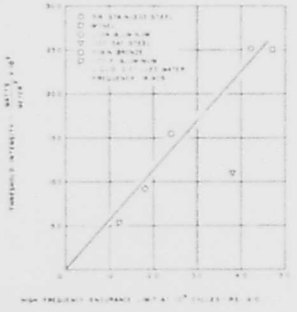

FIGURE 7-19 - THRESHOLD INTENSITY OF CAVITATION DAMAGE AS A FUNCTION OF HIGH-FREQUENCY ENDURANCE LIMIT OF METALS

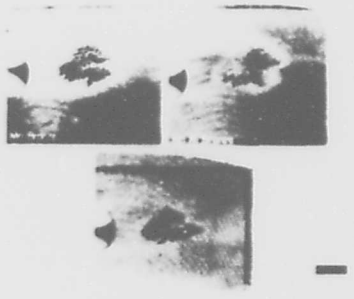

FIGURE 7-20 - IN A ROTATING DISK SCREENING TEST, COMMON PROPELLER MATERIALS SUCH AS MANGANESE BRONZE, MANGANESE NICKEL BRONZE AND NICKEL ALUMINUM BRONZE ERODE AT A RATE OF 1.76 INCH IN 72 HOURS AT 50 fps. THIS CORRESPONDS TO 8 INCHES PER YEAR RATE OF EROSION.

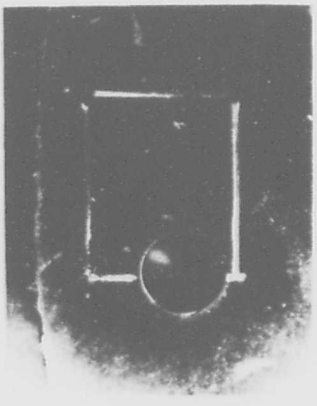

FIGURE 7-21 - ELASTOMERIC COATINGS SUCH AS NEOPRENE AND POLYURETHANE OFFER REMARKABLE EROSION RESISTANCE. THIS FIGURE SHOWS THE PERFORMANCE OF NEOPRENE COATING AT 150 fps AFTER 72 HOURS EXPOSURE IN THE ROTATING DISK APPARATUS.

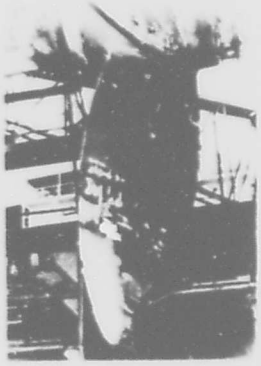

FIGURE 7-22 - ALTHOUGH ELASTOMERIC COATINGS OFFER EXCELLENT RESISTANCE TO EROSION, ADHESION FAILURE OF THESE COATINGS IN SERVICE IS STILL A MYSTERIOUS PROBLEM. UNDERSTANDING OF THE MECHANISM OF ADHESION FAILURES AND THE DEVELOPMENT OF COATING SYSTEMS WITH ADEQUATE ADHESION STRENGTH WILL EVENTUALLY ENHANCE THE OPERATING LIFE OF NAVAL PROPELLERS TO A GREAT EXTENT.

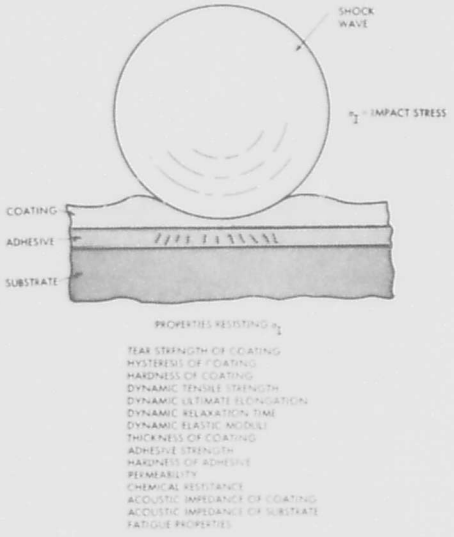

FIGURE 7-23 - RESPONSE OF A COATING-ADHESIVE-SUBSTRATE SYSTEM TO BUBBLE COLLAPSE IMPACT

FIGURE 7-24 - FAILURE OF ELASTOMERIC MATERIAL ALONG GRAIN DIRECTION (CHATTEN AND THIRUVENGADAM, (129))

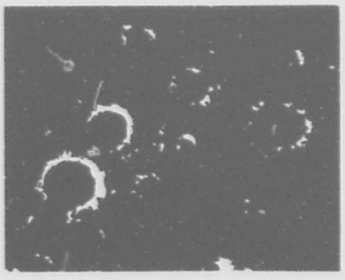

FIGURE 7-25 - INDENTATION DUE TO BUBBLE COLLAPSE ON LEAD (THIRUVENGADAM, (61))

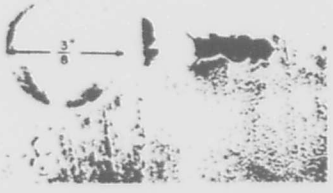

FIGURE 7-26 - GROSS REMOVAL OF LOW-TEAR STRENGTH ELASTOMERIC MATERIAL (CHATTEN AND THIRUVENGADAM, (129))

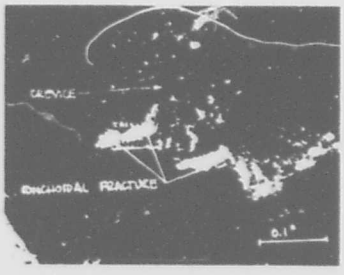

FIGURE 7-27 - CONCHOIDAL FRACTURE OF AN EPOXY-POLYSULFIDE COMPOUND (LICHTMAN, (130))

FIGURE 7-28 - TYPICAL ELASTOMERIC COATING PERFORMANCE OF FIRST ORDER OF MERIT
(LICHTMAN AND WEINGRAM (132))

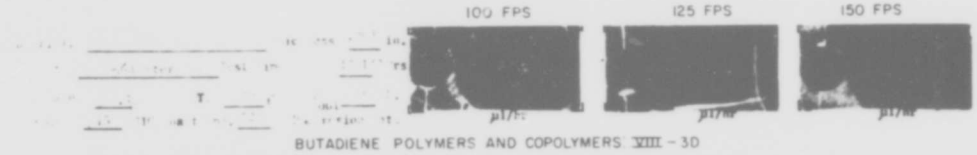

FIGURE 7-29 - TYPICAL ELASTOMERIC COATING PERFORMANCE OF SECOND ORDER OF MERIT
(LICHTMAN AND WEINGRAM (132))

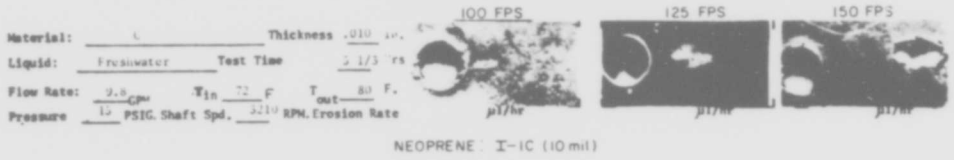

FIGURE 7-30 - TYPICAL ELASTOMERIC COATING PERFORMANCE OF THIRD ORDER OF MERIT
(LICHTMAN AND WEINGRAM (132))

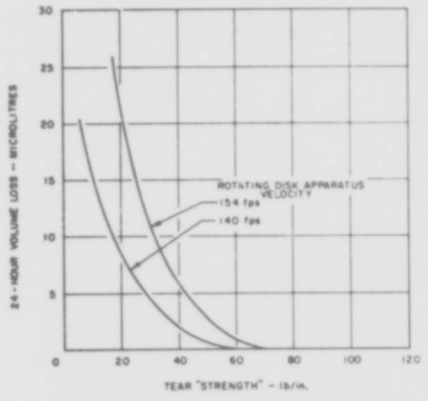

FIGURE 7-31 - RELATION BETWEEN TEAR STRENGTH AND
CAVITATION DAMAGE RESISTANCE
(CHATTEN AND THIRUVENGADAM (129))

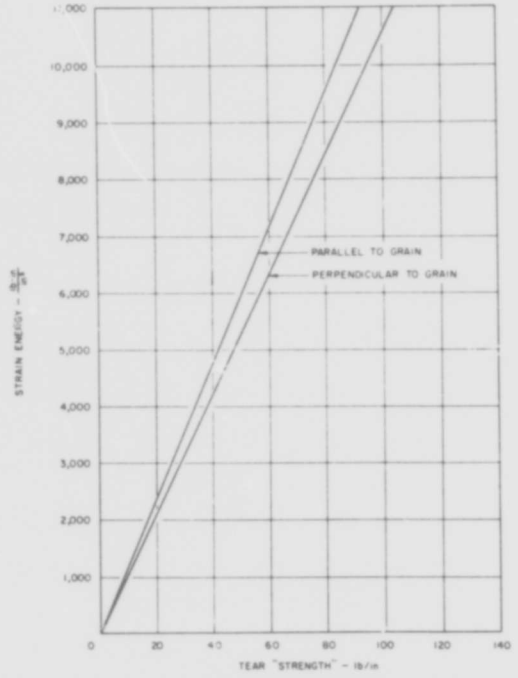

FIGURE 7-32 - RELATION BETWEEN TEAR STRENGTH AND STRAIN ENERGY
(CHATTEN AND THIRUVENGADAM (129))

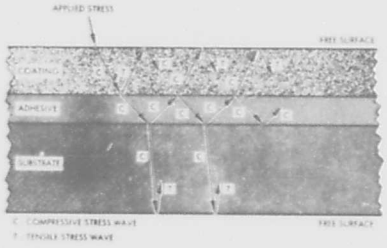

FIGURE 7-33 - STRESS WAVE INTERACTION IN A COATING-ADHESIVE-SUBSTRATE SYSTEM

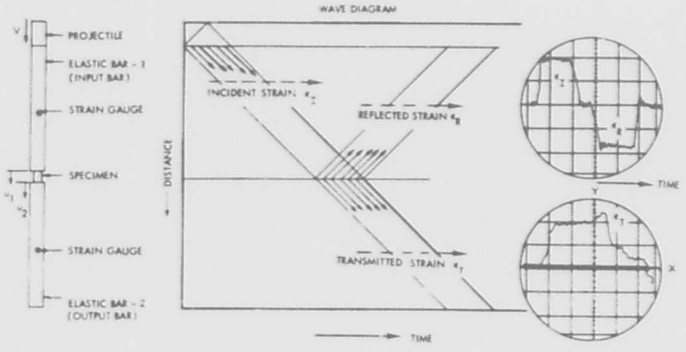

FIGURE 7-34 - PRINCIPLE OF SPLIT HOPKINSON PRESSURE BAR APPARATUS FOR OBTAINING HIGH TEMPERATURE STRESS-STRAIN DATA AT HIGH STRAIN RATES

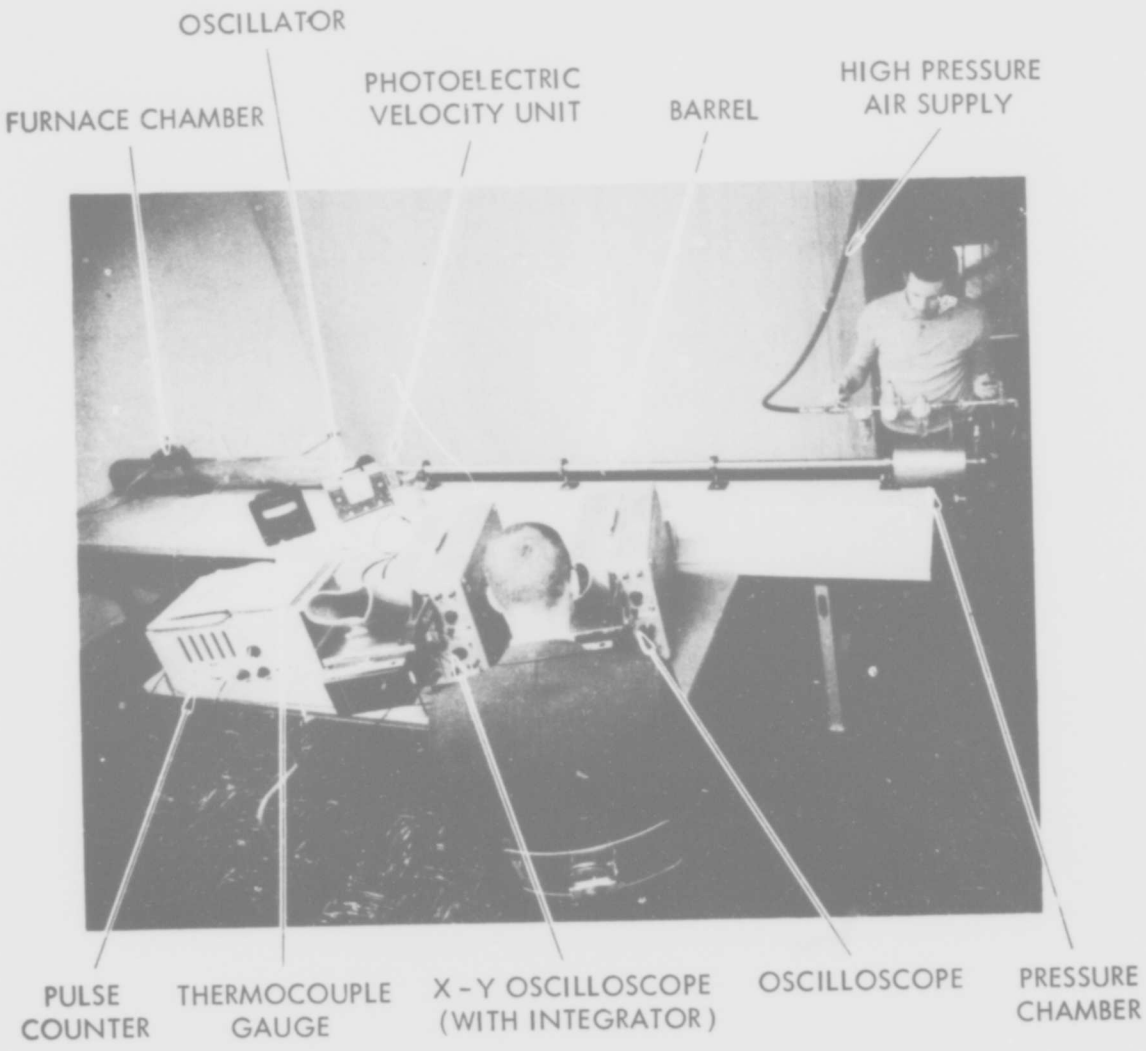

FIGURE 7-35 - SPLIT HOPKINSON PRESSURE BAR TEST FACILITY WITH HIGH TEMPERATURE FURNACE

HYDRONAUTICS, INCORPORATED

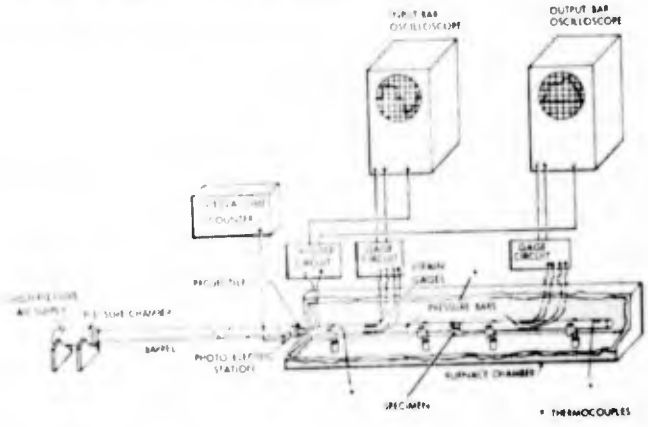

FIGURE 7-36 - SCHEMATIC OF SPLIT HOPKINSON PRESSURE BAR TEST FACILITY

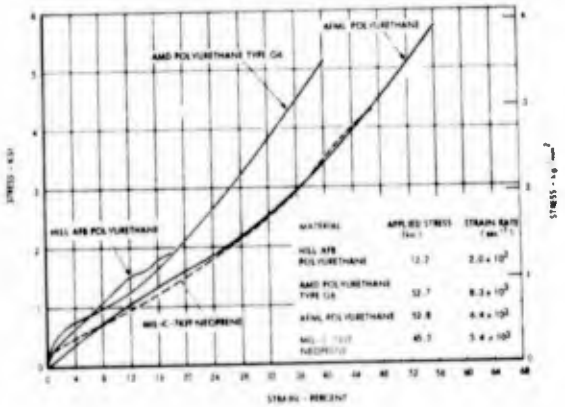

FIGURE 7-37 COMPARISONS OF DYNAMIC STRESS-STRAIN RESPONSE OF ELASTOMERS, ROOM TEMPERATURE, APPLIED PULSE 100 μsec DURATION

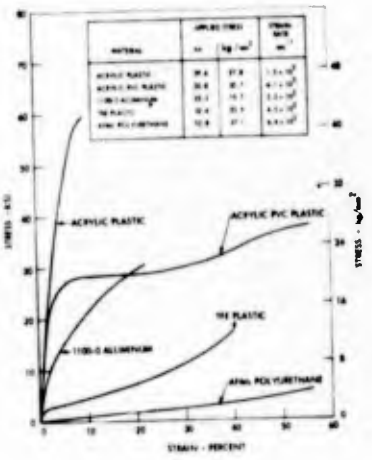

FIGURE 7-38 COMPARISON OF DYNAMIC STRESS - STRAIN BEHAVIOR, ROOM TEMPERATURE, APPLIED PULSE 150 μsec DURATION

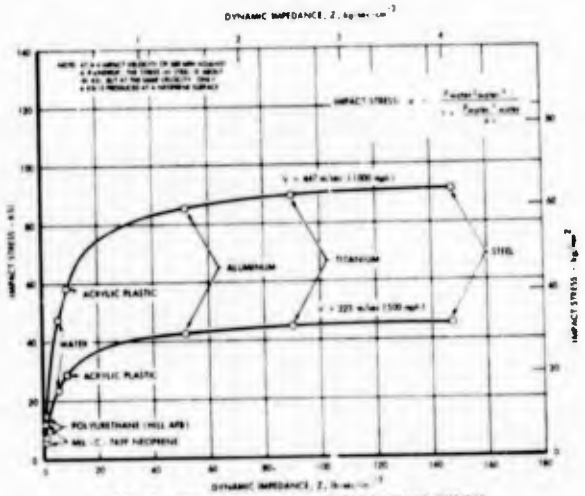

FIGURE 7-39 DEPENDENCE OF RAINDROP IMPACT STRESS ON DYNAMIC IMPEDANCE OF COATING AND SUBSTRATE

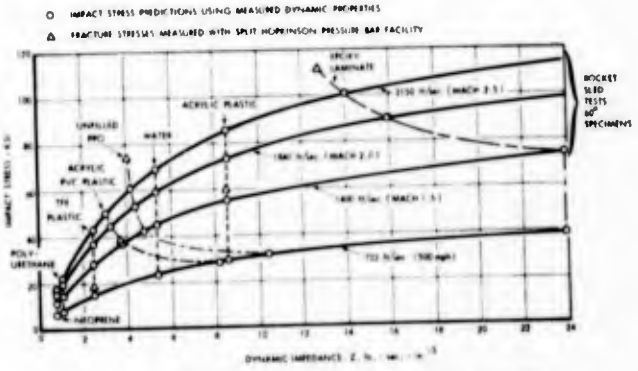

FIGURE 7-40 COMPARISON OF IMPACT STRESS PREDICTIONS WITH SINGLE IMPACT FRACTURE STRESS

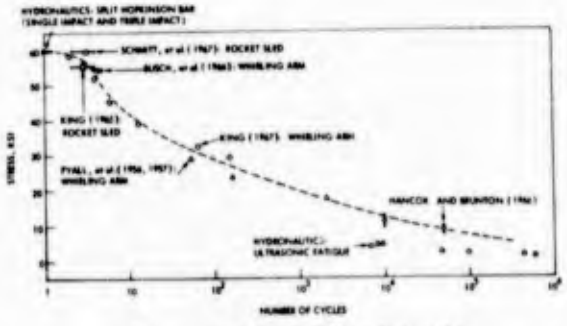

FIGURE 7-41 - RESPONSE OF AN ACRYLIC PLASTIC TO REPETITIVE LOADING,

SPECIMEN TESTED IN MULTIPLE IMPACT EROSION FACILITY
SUBSTRATE : Epoxy resin with glass fiber lamination
COATING : White AFML polyurethane, 8.6 mils thick
IMPACT VELOCITY : 650 ft/sec
NUMBER OF IMPACTS : 200

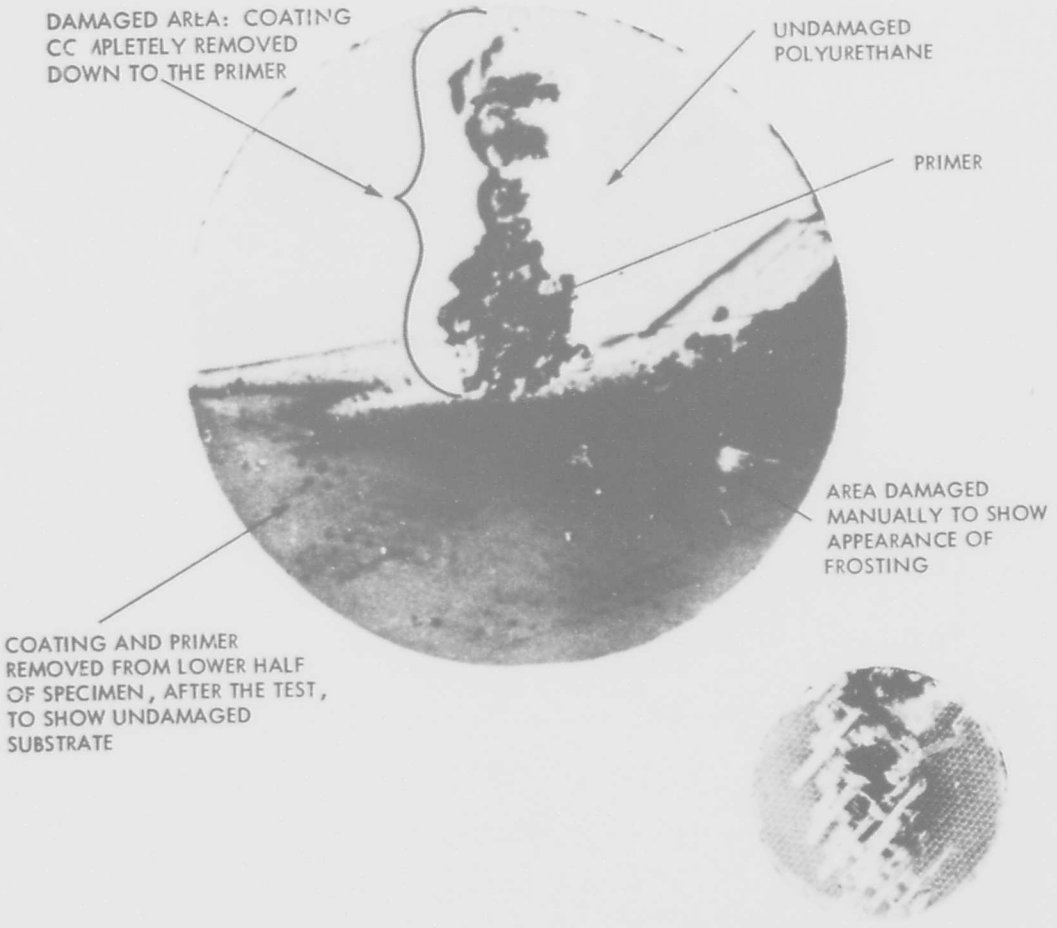

FIGURE 7-42 - AN EXPERIMENTAL DEMONSTRATION OF THE APPLICABILITY OF THE UNIAXIAL STRESS, ELASTIC-PLASTIC STRESS WAVE THEORY TO DESCRIBE RAIN EROSION OBSERVATIONS. This observed absence of substrate damage shows the lack of validity of the shock wave, uniaxial strain theory, which predicts stresses in a coated substrate that are larger than the stresses predicted for direct water impact on bare substrate.

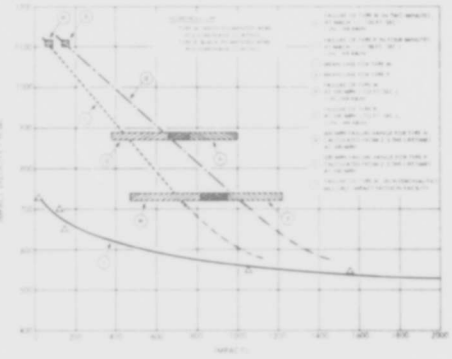

ORDER OF MERIT: 2

ORDER OF MERIT: 7

FIGURE 7-44 - TYPICAL DAMAGE ON STRUCTURAL PLASTICS
(LICHTMAN AND WEINGRAM (132))

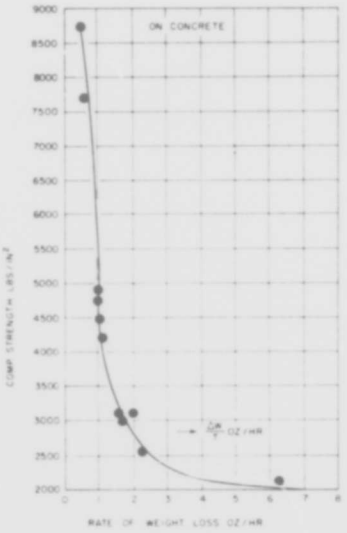

FIGURE 7-45 - RELATION BETWEEN COMPRESSIVE STRENGTH AND CAVITATION DAMAGE FOR CONCRETE
(THIRUVENGADAM (143))

MATERIAL: ANTI-CORROSIVE AND ANTI-FOULING, ORDER OF MERIT: 1

MATERIAL: ZINC RICH, ORDER OF MERIT: 4

FIGURE 7-46 - TYPICAL PERFORMANCE OF NON-ELASTOMERIC COATINGS
(LICHTMAN AND WEINGRAM (132))

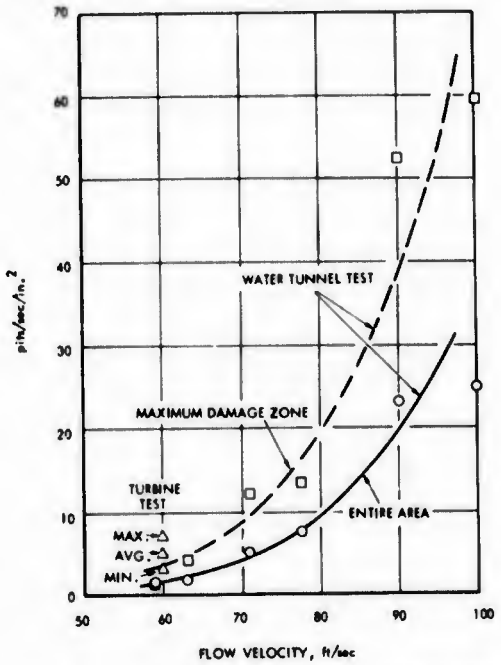

FIGURE 8-1 - COMPARISON OF TURBINE PITTING RATE WITH WATER TUNNEL TEST RESULTS (KNAPP, (60))

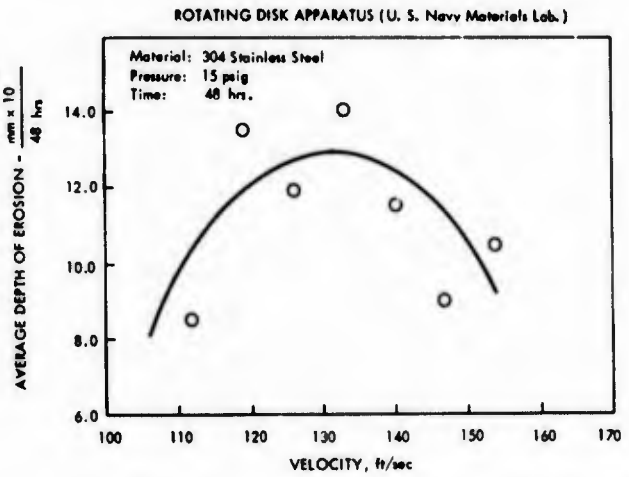

FIGURE 8-2 - EFFECT OF VELOCITY ON RATE OF DEPTH OF EROSION (149)

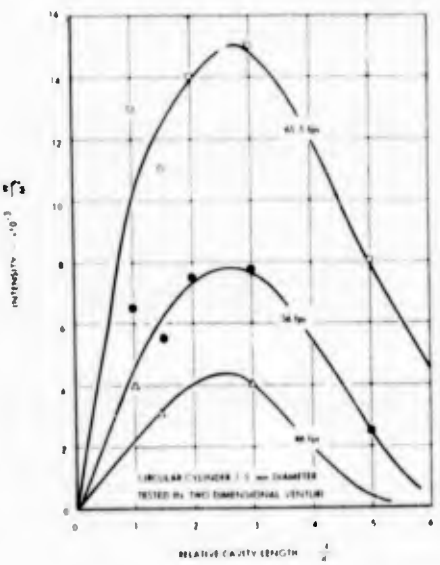

FIGURE 8-3 - INTENSITY OF EROSION AS A FUNCTION OF RELATIVE CAVITY LENGTH (SHALNEV (151))

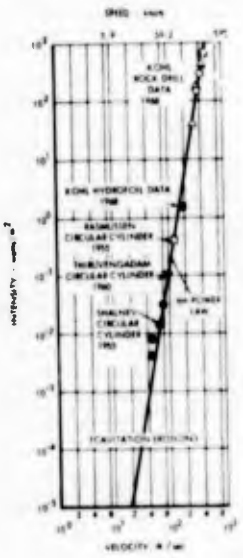

FIGURE 8-4 - INTENSITY OF CAVITATION EROSION AS A FUNCTION OF VELOCITY

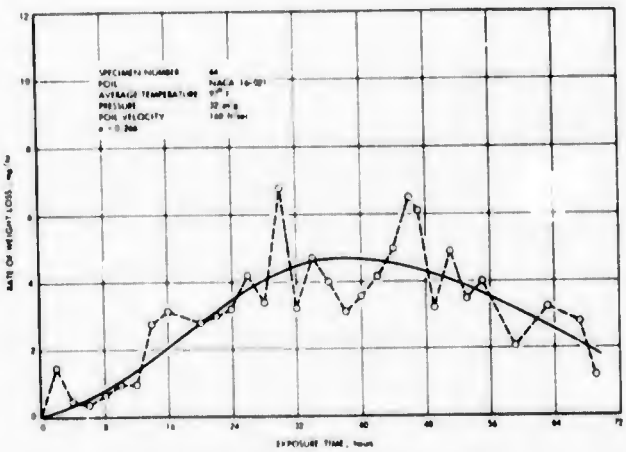

FIGURE 8-5 - RATE OF WEIGHT LOSS VS. TESTING TIME FOR THE FULL SIZE (3" CHORD LENGTH) HYDROFOIL.

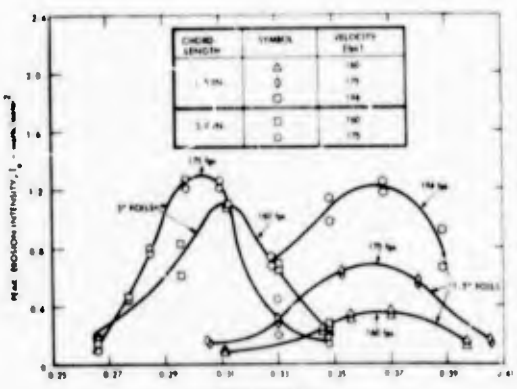

FIGURE 8-6 - RELATIONSHIP BETWEEN PEAK INTENSITY OF EROSION AND CAVITATION PARAMETER FOR NACA-16-021 FOILS

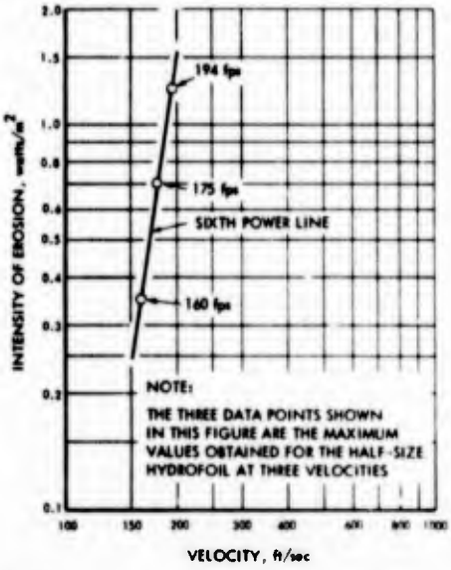

FIGURE 8-7 - DATA FOR 18 in. NACA-16-021 HYDROFOIL AT THREE VELOCITIES COMPARED WITH SIXTH POWER LAW

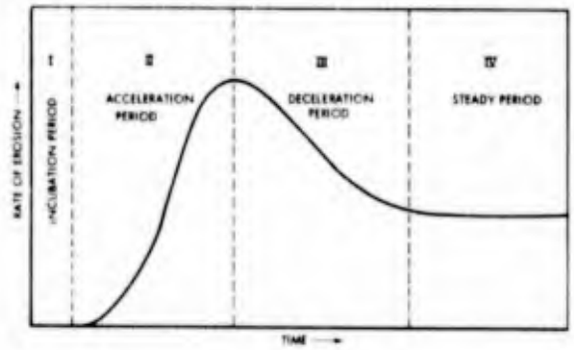

FIGURE 8-8 - CLASSIFICATION OF EROSION PERIODS

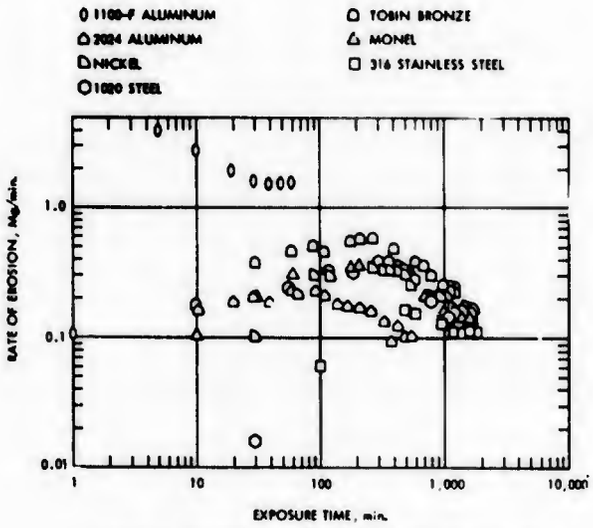

FIGURE 8-9 - EROSION RATE AND EXPOSURE TIME RELATIONS FOR SEVEN MATERIALS

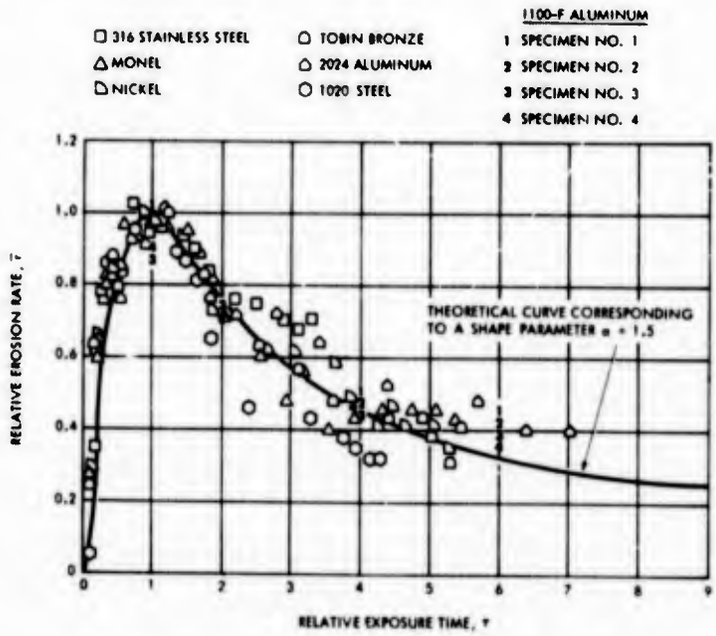

FIGURE 8-10 - RELATIVE EROSION RATE AS A FUNCTION OF RELATIVE EXPOSURE TIME FOR THE SEVEN MATERIALS

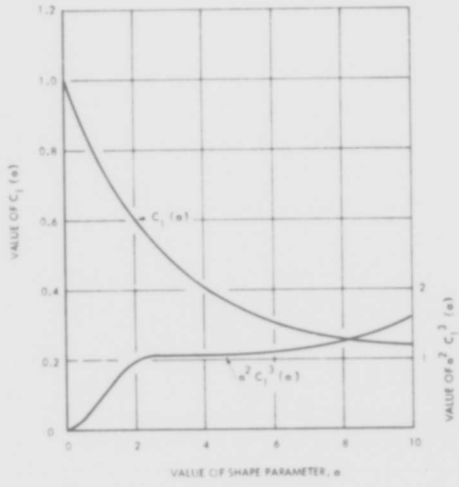

FIGURE 8-11 - FUNCTIONS $C_1(\alpha)$ AND $\alpha^2 C_1^2(\alpha)$

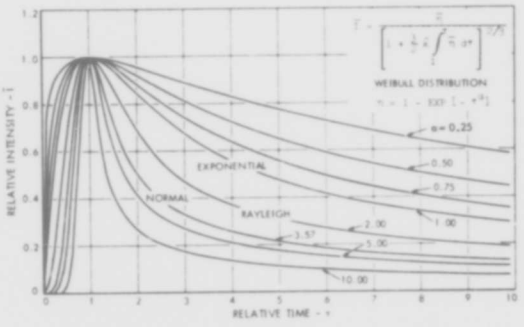

FIGURE 8-12 - THEORETICAL PREDICTION OF THE EFFECT OF TIME ON INTENSITY OF EROSION WHEN $n = 2$

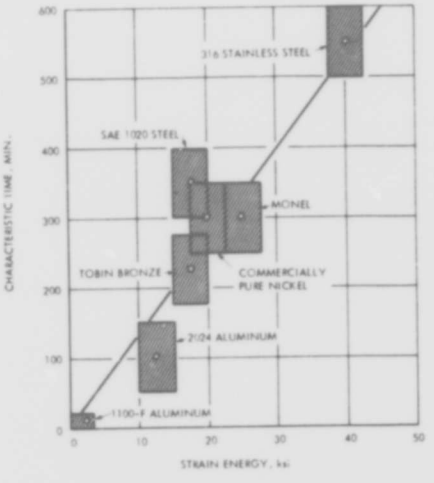

FIGURE 8-13 - RELATION BETWEEN CHARACTERISTIC TIME AND STRAIN ENERGY

$R^2 \cdot P_i = d^2 \cdot S_e$, and $d^2 = \Delta\gamma' \cdot R$ (approximately)

Hence $\Delta\gamma' \cdot S_e = P_i \cdot R$ (for Single Impact)

$N \cdot \Delta\gamma' = P_i \cdot R \cdot f \cdot \Delta t$ (for Multiple Impact), where $N = f \cdot \Delta t$

Then $\frac{\Delta\gamma}{\Delta\gamma} \cdot S_e = P_i \cdot R \cdot f$, where $N \cdot \Delta\gamma' = \Delta\gamma$

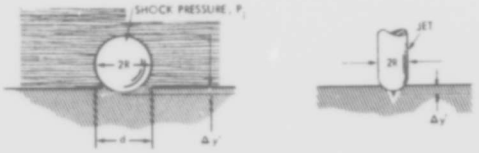

	STAGNATION PRESSURE (Macrojet)	WATER-HAMMER PRESSURE (Microjet)
SPHERICAL COLLAPSE		
$P_i = P_o (R_o / R_c)^2$	$P_i = \frac{1}{2} \rho V_j^2$	$P_i = \rho C V_j$
For example:	$P_i = \frac{1}{2} \rho \cdot P_o / \rho$	$P_i = \rho C (P_o / \rho)^{\frac{1}{2}}$
$R_o / R_c = \exp (P_o / Q_o)$	$P_i = P_o$	$P_i = C (\rho P_o)^{\frac{1}{2}}$

FIGURE 8-14 - PARAMETERS GOVERNING INDENTATION AND RATE OF EROSION

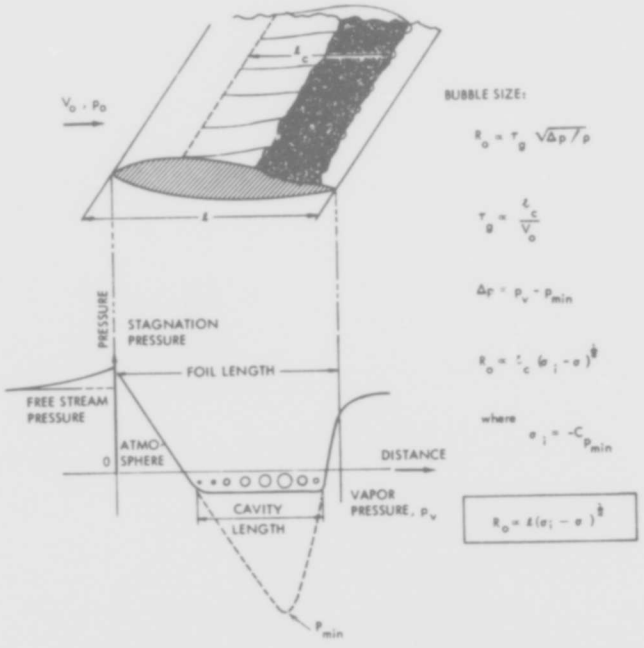

FIGURE 8-15 - PARAMETERS GOVERNING THE MAXIMUM SIZE OF THE BUBBLES

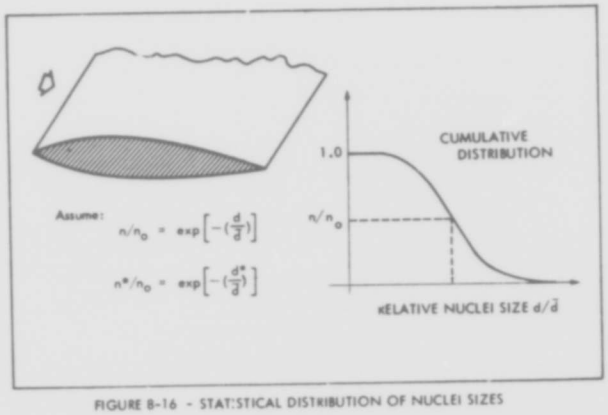

FIGURE 8-16 - STATISTICAL DISTRIBUTION OF NUCLEI SIZES

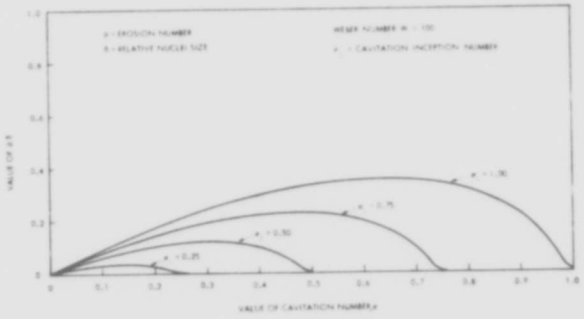

FIGURE 8-17 - EFFECT OF CAVITATION NUMBER ON THE EROSION NUMBER

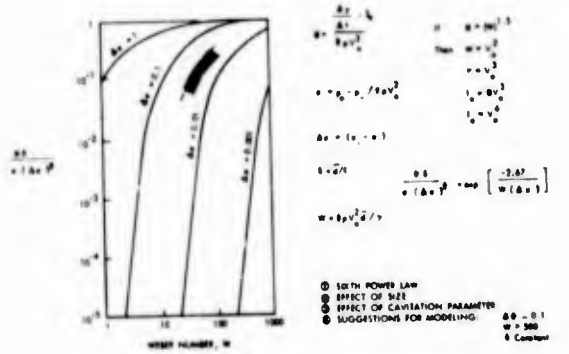

FIGURE 8-18 - EFFECT OF WEBER NUMBER ON CAVITATION EROSION

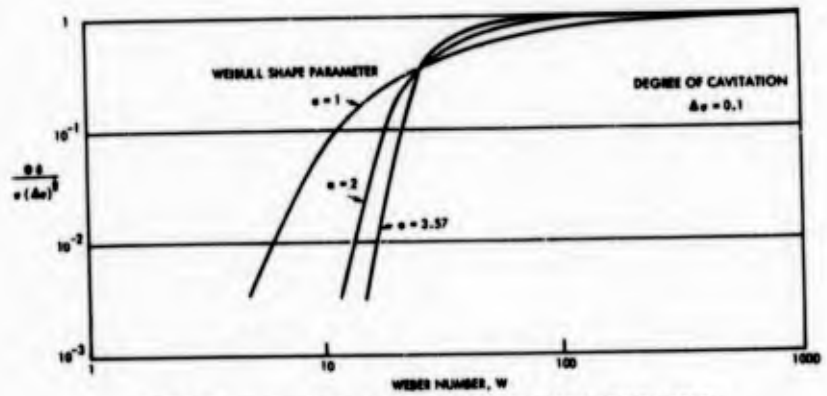

FIGURE 8-19 - INFLUENCE OF DIFFERENT NUCLEI DISTRIBUTIONS ON CAVITATION EROSION

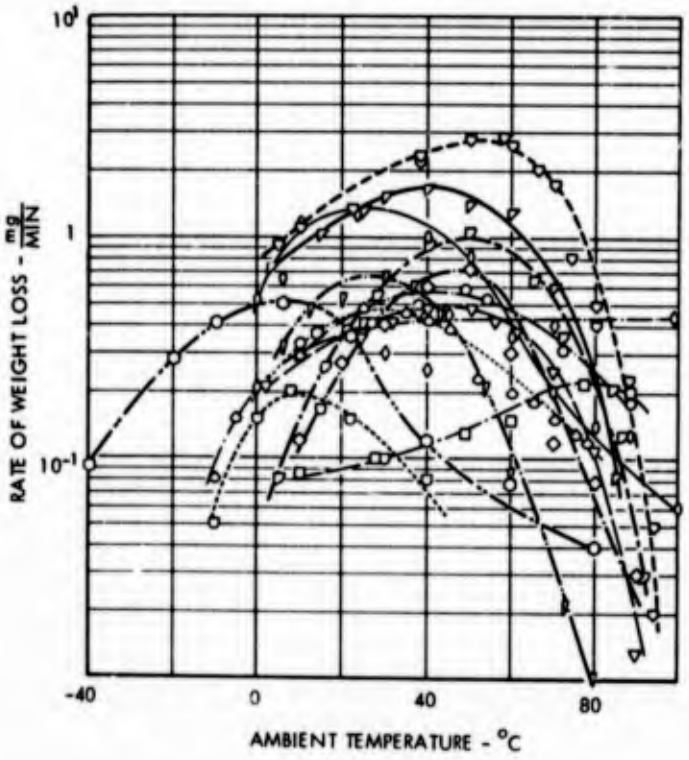

INVESTIGATOR	TEST MATERIAL	TEST LIQUID	FREQUENCY (kcs)	AMPLITUDE (mils)	PRESSURE ATMOSPHERES	DATA SYMBOL
SCHUMB, PETERS AND MILLIGAM	ALUMINUM 51 - ST	WATER	8.7	1.[illegible]	1.0	▽
NOWOTNY	MAGNESIUM	WATER	9.0	1.18	1.0	◇
KERR AND LEITH	CAST IRON	WATER	6.5	1.71	1.0	○
	CAST IRON	WATER	6.5	1.71	2.4	□
BEECHUCK	ALUMINUM	WATER	8.0	—	1.0	▽
	ALUMINUM	BENZENE	8.0	—	1.0	□
	ALUMINUM	KEROSENE	8.0	—	1.0	○
WILSON AND GRAHAM	WROUGHT ALUMINUM	ANILINE	12.0	—	1.0	◇
DEVINE AND PLESSET	ALUMINUM 7 /H 129	WATER	15.0	1.00	1.0	▽
WHITE	ALUMINUM	WATER	14.0	0.69	1.0	▽
	ALUMINUM	BENZENE	14.0	0.69	1.0	7
	ALUMINUM	TOLUENE	14.0	0.69	1.0	○
	ALUMINUM	ANILINE	14.0	0.69	1.0	0

* DATA OBTAINED BY MRS. S. W. WHITE WITH THE HYDRONAUTICS' MAGNETOSTRICTION APPARATUS

LIQUID PROPERTY RANGE COVERED BY CAVITATION DAMAGE					
LIQUID	VAPOR PRESSURE dynes/cm²	VISCOSITY Centipoises	SURFACE TENSION dynes/cm	DENSITY g/cm³	VELOCITY OF SOUND m/sec
WATER	8.13×10^3 - 8.14×10^4	1.79 - 0.284	75.6 - 59.8	0.9998 - 0.9584	1431 - 1552
ANILINE	1.46×10^3 - 6.09×10^4	10.2 - 1.27	44.1 - 39.4	1.03893 - 0.97787	1643
BENZENE	6.06×10^3 - 7.27×10^4	0.758 - 0.329	30.2 - 25.0	0.88936 - 0.82466	1317
TOLUENE	1.37×10^3 - 3.86×10^4	0.772 - 0.354	27.7 - 25.0	0.92393 - 0.80913	1318

FIGURE 9-1 - SUMMARY OF RESULTS OF VIBRATORY TESTS

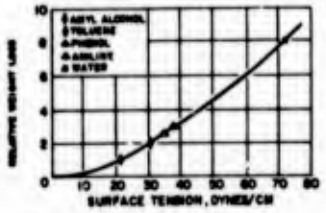

FIGURE 9-2 - DEPENDENCE OF WEIGHT LOSS OF ALUMINUM SPECIMEN ON SURFACE TENSION (REF. NOWOTNY (11))

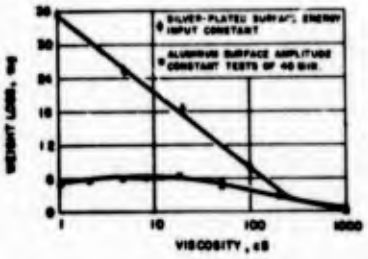

FIGURE 9-4 - EFFECT OF VISCOSITY OF LIQUID ON CAVITATION DAMAGE (REF. WILSON AND GRAHAM (180))

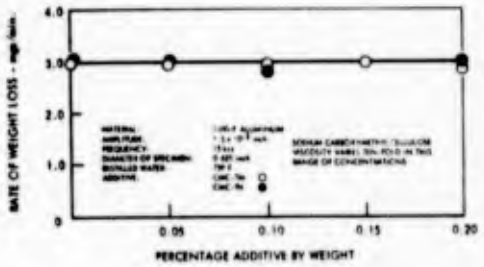

FIGURE 9-5 - EFFECT OF NON-NEWTONIAN ADDITIVE ON CAVITATION DAMAGE RATE

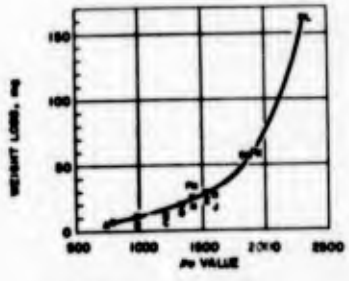

FIGURE 9-6 - CORRELATION OF CAVITATION DAMAGE WITH PRODUCT OF LIQUID DENSITY AND SOUND VELOCITY (WILSON AND

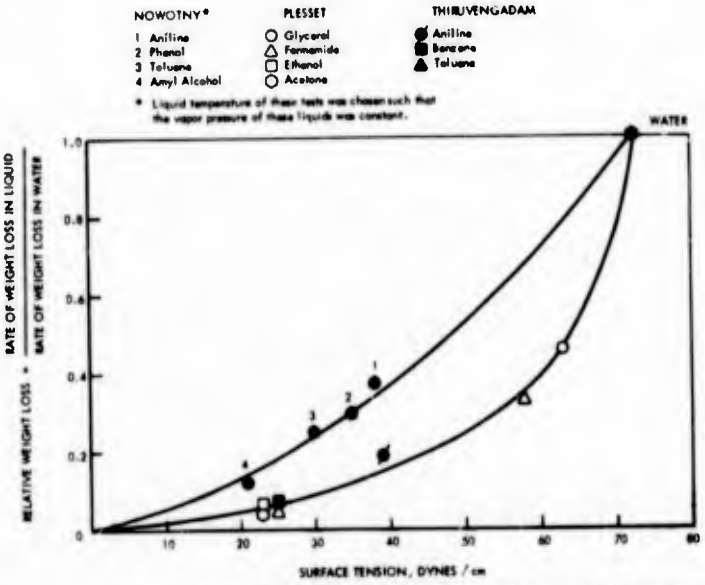

FIGURE 9-3 - RELATION BETWEEN RATE OF EROSION AND SURFACE TENSION OF VARIOUS LIQUIDS (THIRUVENGADAM)

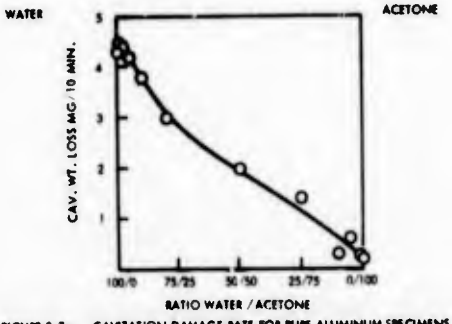

FIGURE 9-7a - CAVITATION DAMAGE RATE FOR PURE ALUMINUM SPECIMENS IN SOLUTIONS OF WATER AND ACETONE. THE SOLUTION RATIOS ARE VOLUME RATIOS WATER TO ACETONE (PLESSET (184))

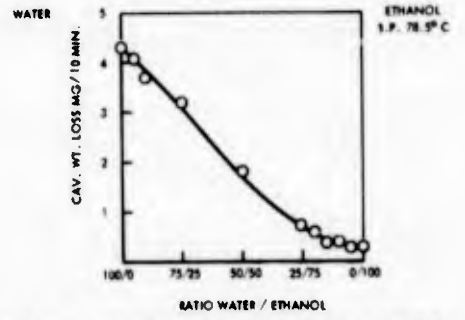

FIGURE 9-7b - CAVITATION DAMAGE RATE FOR PURE ALUMINUM SPECIMENS IN SOLUTIONS OF WATER AND ETHANOL. THE SOLUTION RATIOS ARE VOLUME RATIOS WATER TO ETHANOL (PLESSET (184))

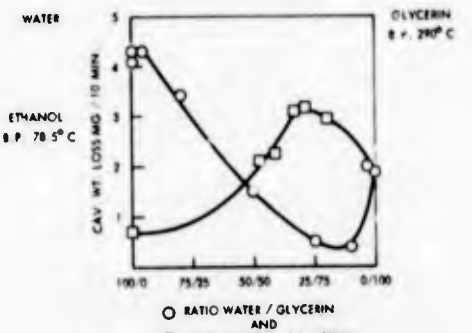

FIGURE 9-7c - CAVITATION DAMAGE RATES ARE SHOWN FOR SOLUTIONS OF WATER AND GLYCEROL (CIRCLES) AND FOR SOLUTIONS OF ETHANOL AND GLYCEROL

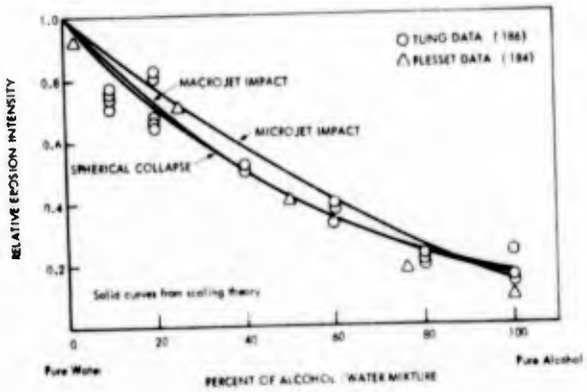

FIGURE 9-8 - COMPARISON OF THEORETICAL EROSION INTENSITY WITH EXPERIMENTAL DATA (186)

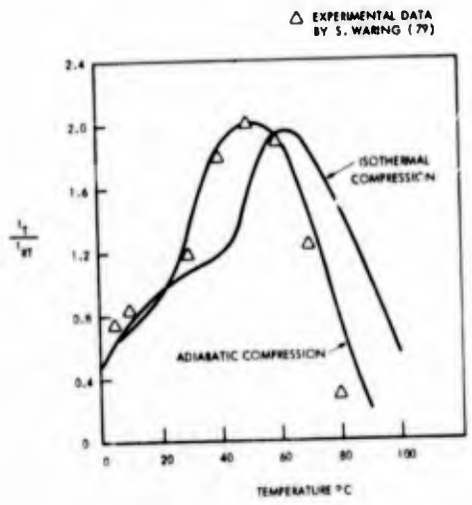

FIGURE 9-9 - TEMPERATURE EFFECTS IN CAVITATION EROSION

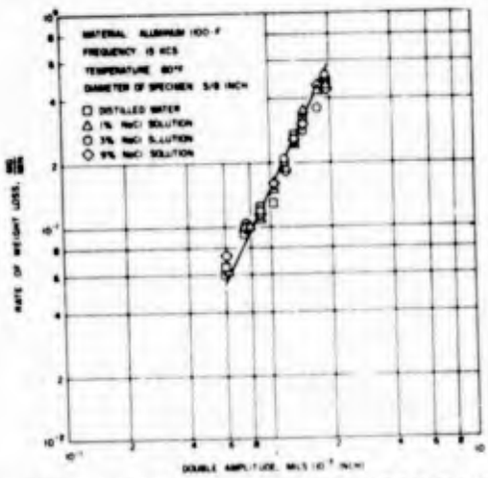

FIGURE 9-10 - EFFECT OF NaCl CONCENTRATION ON THE AMPLITUDE VERSUS DAMAGE RATE RELATIONSHIP FOR ALUMINUM 1100-F (WARING (79))

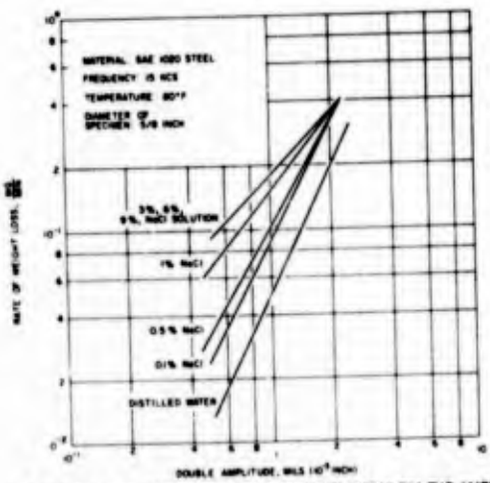

FIGURE 9-11 - EFFECT OF NaCl CONCENTRATION ON THE AMPLITUDE VERSUS DAMAGE RATE RELATIONSHIP FOR SAE 1020 STEEL (WARING (79))

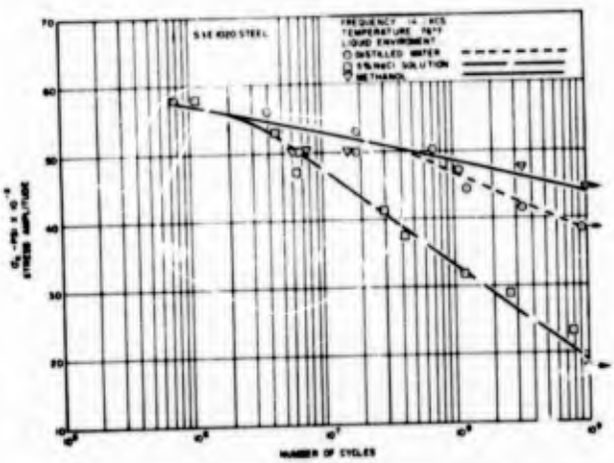

FIGURE 9-12 - HIGH FREQUENCY CORROSION FATIGUE OF SAE 1020 STEEL (THIRUVENGADAM (123))

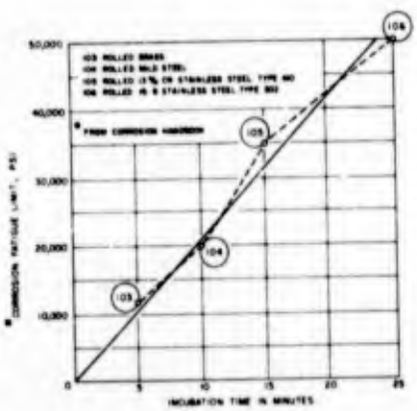

FIGURE 9-13 - CORROSION FATIGUE LIMIT AND INCUBATION TIME (LEITH (69))

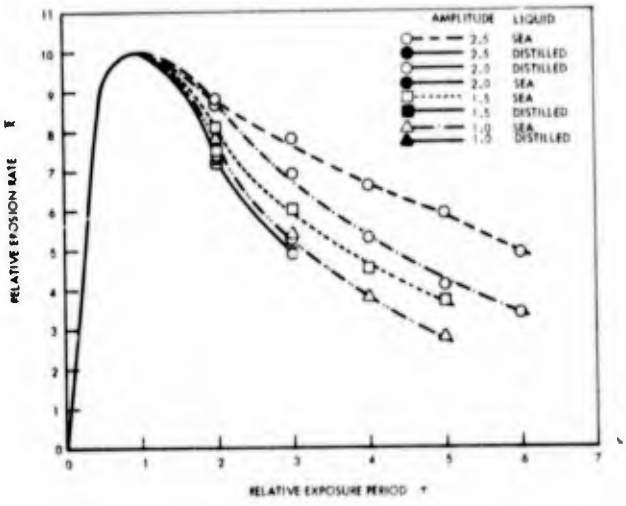

FIGURE 9-14 - RELATIVE EROSION RATE CURVES FOR HY-130 STEEL

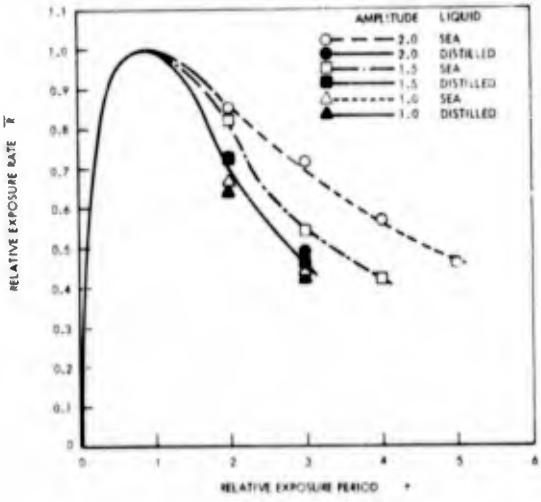

FIGURE 9-15 - RELATIVE EROSION RATE CURVES FOR HY-80 STEEL

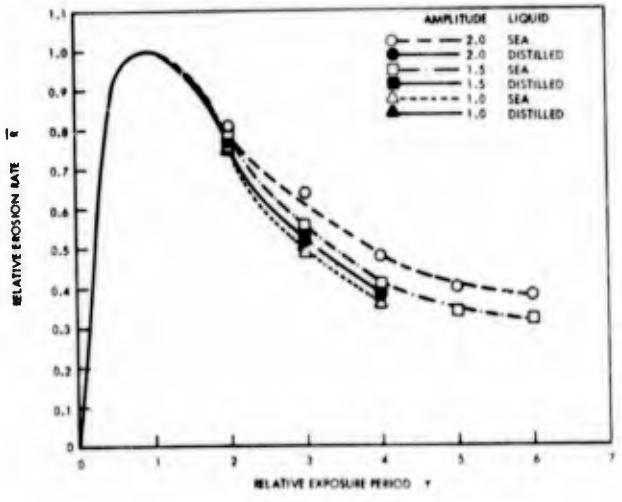

FIGURE 9-16 - RELATIVE EROSION RATE CURVES FOR SAE 1020 STEEL

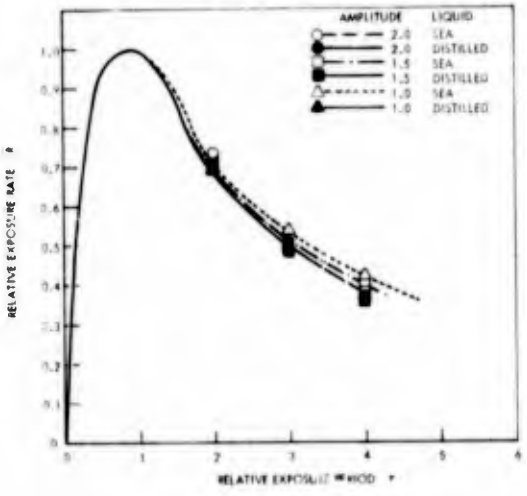

FIGURE 9-17 - EROSION RATE CURVES FOR 5086 H117 ALUMINIUM

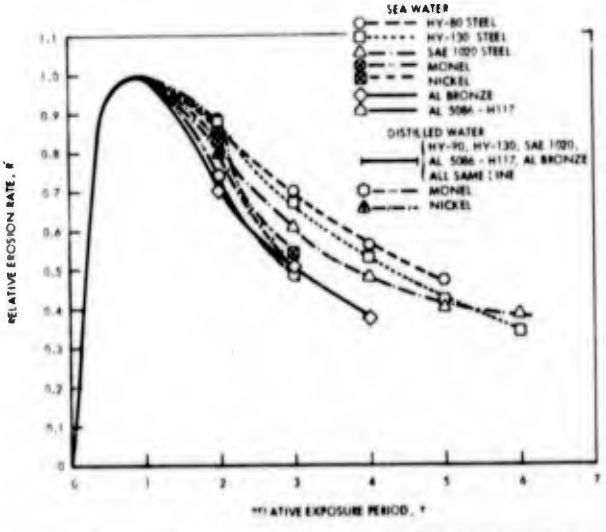

FIGURE 9-18 - COMPARISON OF RELATIVE EROSION RATE CURVES FOR VARIOUS MATERIALS TESTED AT 2.0 MIL AMPLITUDE

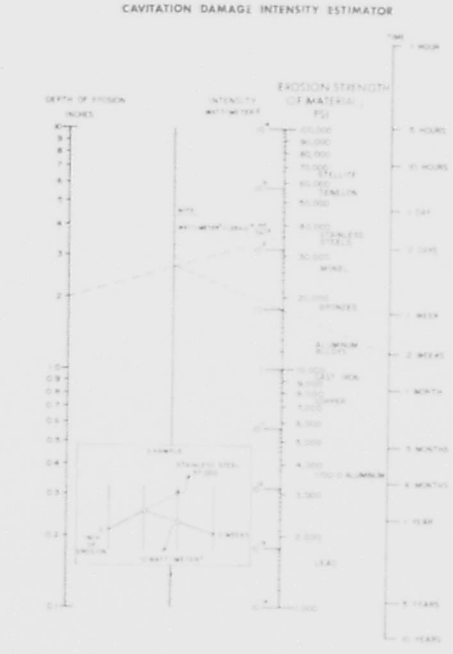

FIGURE 10-1 - NOMOGRAM FOR ESTIMATING THE INTENSITY OF CAVITATION DAMAGE (THIRUVENGADAM (125))

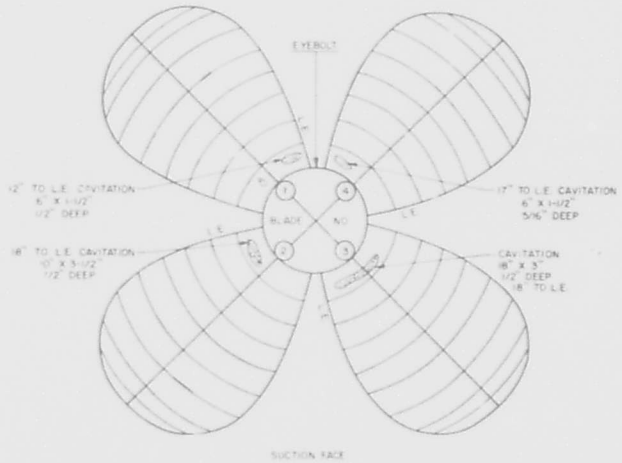

FIGURE 10-2 - TYPICAL FIELD INSPECTION RECORD OF THE PROPELLER OF DESTROYER, USS HIGBEE (J. HILL, U.S. BUREAU OF SHIPS (212))

FIGURE 10-3 - TYPICAL DAMAGE ON THE SUCTION FACE OF BLADE NO. 3 OF A PROPELLER ON THE USS HIGBEE (J. HILL, U.S. BUREAU OF SHIPS (212))

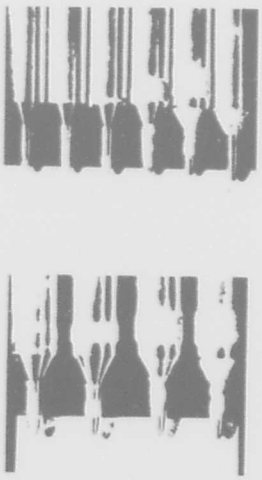

FIGURE 10-4 - CAVITATION DAMAGE ON NEEDLE VALVES (BORLAND AND STILES (31))

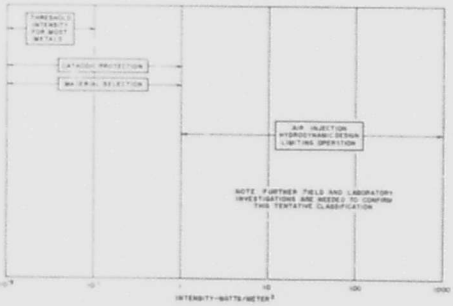

FIGURE 10-5 - RANGE OF INTENSITIES FOR THE POSSIBLE APPLICATION OF KNOWN PROTECTION METHODS (THIRUVENGADAM (125))

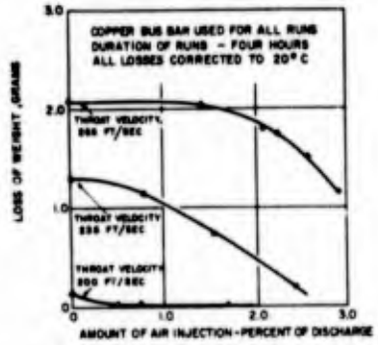

FIGURE 11-1a - COPPER BUS BARS IN VENTURI APPARATUS (MOUSSON (67))

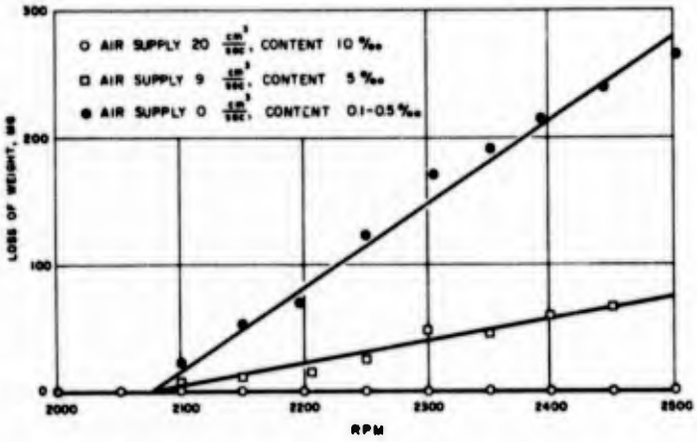

FIGURE 11-1b - ALUMINUM ALLOYS IN ROTATING DISK APPARATUS (RASMUSSEN (86))

FIGURE 11-1 - EFFECT OF AIR INJECTION ON CAVITATION

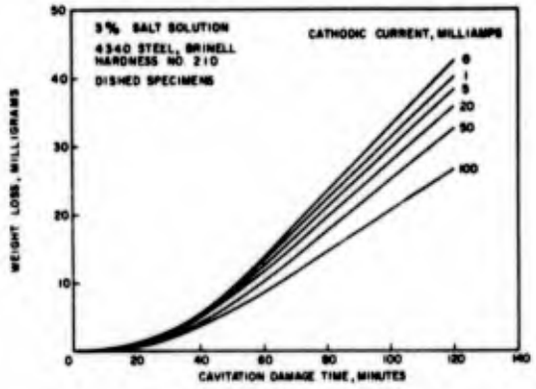

FIGURE 11-2a - 4340 STEEL

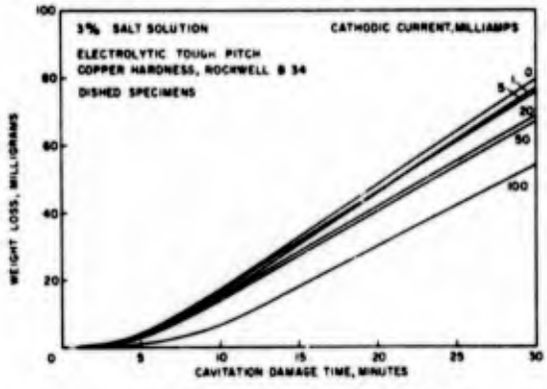

FIGURE 11-2b - PURE COPPER

FIGURE 11-2 - AVERAGE CURVES OF CAVITATION DAMAGE LOSSES OF STEEL AND COPPER SPECIMENS IN 3% SALT SOLUTIONS AS A FUNCTION OF CATHODIC CURRENT (PLESSET (196))

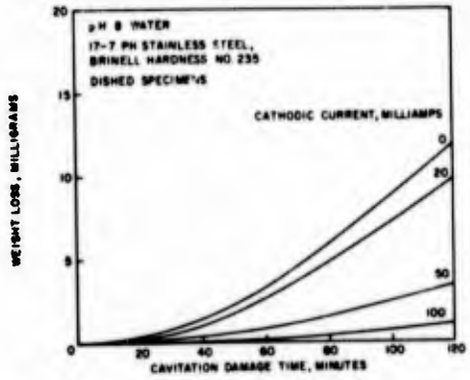

FIGURE 11-3a - SPECIMEN CATHODIC

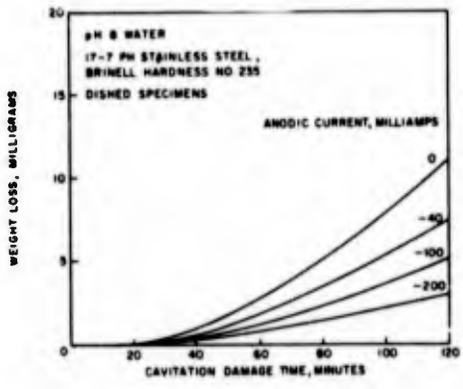

FIGURE 11-3b - SPECIMEN ANODIC

FIGURE 11-3 - AVERAGE CAVITATION DAMAGE LOSSES OF 17-7 STAINLESS STEEL SPECIMENS AS CATHODES AND ANODES IN BUFFERED DISTILLED WATER (PLESSET (196))

FIGURE 12-1 - USS STORMES (DD780) FITTING IF SRA INLAY IN RECESS OF STARBOARD PROPELLER BLADE (SUCTION FACE) (LICHTMAN (132))

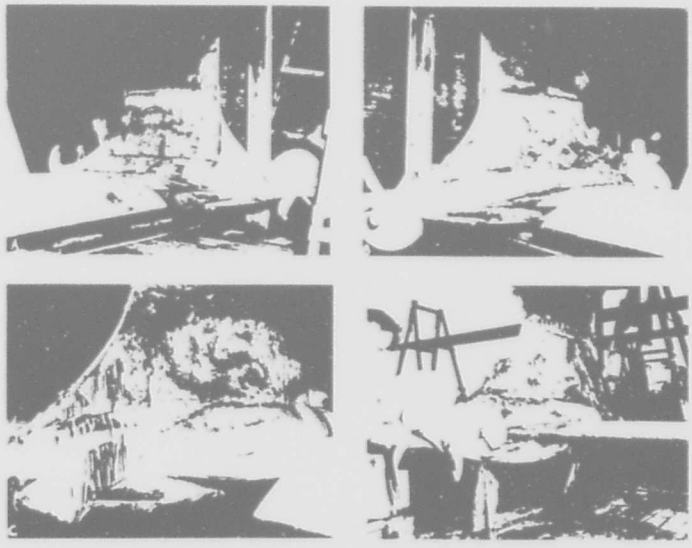

FIGURE 12-2 - PC(H) - 1 - ADHESION SEPARATION OF NEOPRENE COATING OCCURRING DURING MAY 1963 TRIALS (LICHTMAN (132))

A - STBD. STRUT, INBD. B - PORT STRUT, INBD.
C - STBD. STRUT & NACELLE, OUTBD. D - PORT NACELLE, OUTBD.

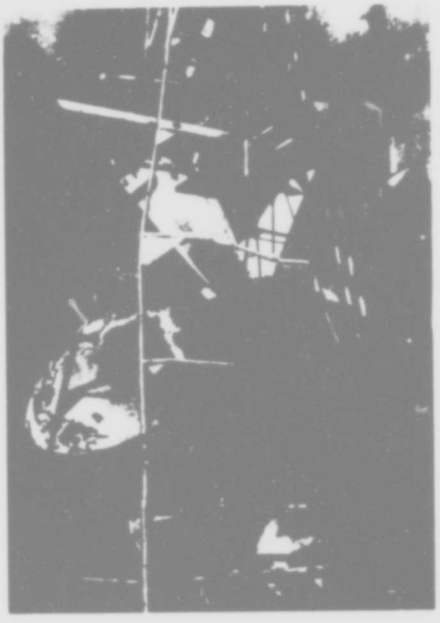

FIGURE 12 - 3 - USNS AMERICAN EXPLORER (T-AG 165) PRESSURE FACES OF NEOPRENE COATED PROPELLER (VIEWED FROM PORT SIDEAFTER SERVICE (LIGHTMAN (132))

FIGURE 12 -4 - USS STORMES (DD 780) PORT PROPELLER, SBR INLAY, BLADE 3 (DSR 39505) (LIGHTMAN (132))

FIGURE 12-5 - USS STORMES (DD 780) STARBOARD PROPELLER, NEOPRENE INLAY (DSR 39516) (LIGHTMAN (132))